UNIVERSIDADE FEDERAL DE UBERLÂNDIA
FACULDADE DE ENGENHARIA QUÍMICA
PROGRAMA DE PÓS-GRADUAÇÃO EM ENGENHARIA QUÍMICA

ANALYTICAL CATALYTIC PYROLYSIS OF SOYBEAN RESIDUE AND COCOA BEAN SHELL

PIRÓLISE ANALÍTICA DE RESÍDUO DE SOJA E CASCA DE CACAU EM LEITO CATALÍTICO

Rodolfo Sapata Gonzalez
Uberlândia
Janeiro/2024

UNIVERSIDADE FEDERAL DE UBERLÂNDIA
FACULDADE DE ENGENHARIA QUÍMICA
PROGRAMA DE PÓS-GRADUAÇÃO EM ENGENHARIA QUÍMICA

ANALYTICAL CATALYTIC PYROLYSIS OF SOYBEAN RESIDUE AND COCOA BEAN SHELL

PIRÓLISE ANALÍTICA DE RESÍDUO DE SOJA E CASCA DE CACAU EM LEITO CATALÍTICO

Rodolfo Sapata Gonzalez

Dissertação de Mestrado apresentada ao Programa de Pós-Graduação em Engenharia Química da Universidade Federal de Uberlândia como parte dos requisitos necessários à obtenção do título de Mestre em Engenharia Química na área de concentração em Processos Químicos.

Uberlândia
Janeiro/2024

“The Art of Living consists in bringing the greatest good out of the greatest evil.”
Machado de Assis

To my wife Raíssa, who knows that ignorance is a bliss, but still wants to learn everything along with me.

Ficha Catalográfica Online do Sistema de Bibliotecas da UFU
com dados informados pelo(a) próprio(a) autor(a).

G643 Gonzalez, Rodolfo Sapata, 1990-
2024 PIRÓLISE ANALÍTICA DE RESÍDUO DE SOJA E CASCA DE CACAU EM LEITO CATALÍTICO [recurso eletrônico] / Rodolfo Sapata Gonzalez. - 2024.

Orientadora: Carla Eponina Hori.
Coorientador: Luiz Gustavo Martins Vieira.
Dissertação (Mestrado) - Universidade Federal de Uberlândia, Pós-graduação em Engenharia Química.
Modo de acesso: Internet.
Disponível em: http://doi.org/10.14393/ufu.di.2024.16
Inclui bibliografia.

1. Engenharia química. I. Hori, Carla Eponina,1965-, (Orient.). II. Vieira, Luiz Gustavo Martins,1976-, (Coorient.). III. Universidade Federal de Uberlândia. Pós-graduação em Engenharia Química. IV. Título.

CDU: 66.0

Bibliotecários responsáveis pela estrutura de acordo com o AACR2:

Gizele Cristine Nunes do Couto - CRB6/2091
Nelson Marcos Ferreira - CRB6/3074

UNIVERSIDADE FEDERAL DE UBERLÂNDIA
Coordenação do Programa de Pós-Graduação em Engenharia Química
Av. João Naves de Ávila, 2121, Bloco 1K, Sala 206 - Bairro Santa Mônica, Uberlândia-MG, CEP 38400-902
Telefone: (34)3239-4249 - www.ppgeq.feq.ufu.br - secppgeq@feq.ufu.br

ATA DE DEFESA - PÓS-GRADUAÇÃO

Programa de Pós-graduação em:	Engenharia Química				
Defesa de:	Mestrado Acadêmico, 1/2024, PPGEQ				
Data:	30 de janeiro de 2024	Hora de início:	14:00	Hora de encerramento:	15:35
Matrícula do Discente:	12122EQU010				
Nome do Discente:	Rodolfo Sapata Gonzalez				
Título do Trabalho:	Analytical catalytic pyrolysis of soybean residue and cocoa bean shell				
Área de concentração:	Desenvolvimento de Processos Químicos				
Linha de pesquisa:	Processos de Separação				
Projeto de Pesquisa de vinculação:	Influência do uso de catalisadores na pirólise rápida de biomassas para produção de bicombustíveis e/ou matérias-primas para indústria química				
ODS-ONU:	ODS 7 – Energia Limpa e Acessível, ODS 9 – Indústria, Inovação e Infraestrutura e ODS 13 – Ação contra a mudança global do clima				

Reuniu-se por meio de webconferência, a Banca Examinadora designada pelo Colegiado do Programa de Pós-graduação em Engenharia Química, assim composta: Professores Doutores: Cássia Regina Cardoso - DEA/UFTM, Laiane Alves de Andrade - CPNA/UFMS, Luiz Gustavo Martins Vieira - PPGEQ/UFU, coorientador, e Carla Eponina Hori - PPGEQ/UFU, orientadora do candidato.

Iniciando os trabalhos a presidente da mesa, Profª Drª Carla Eponina Hori, apresentou a Comissão Examinadora e o candidato, agradeceu a presença do público, e concedeu ao discente a palavra para a exposição do seu trabalho. A duração da apresentação do discente e o tempo de arguição e resposta foram conforme as normas do Programa.

A seguir, a presidente concedeu a palavra, pela ordem sucessivamente aos examinadores, que passaram a arguir o candidato. Ultimada a arguição, que se desenvolveu dentro dos termos regimentais, a Banca, em sessão secreta, atribuiu o resultado final, considerando o candidato:

Aprovado

Esta defesa faz parte dos requisitos necessários à obtenção do título de Mestre.

O competente diploma será expedido após cumprimento dos demais requisitos, conforme as normas do Programa, a legislação pertinente e a regulamentação interna da UFU.

Nada mais havendo a tratar foram encerrados os trabalhos. Foi lavrada a presente ata que após lida e achada conforme foi assinada pela Banca Examinadora.

Documento assinado eletronicamente por **Carla Eponina Hori**, **Professor(a) do Magistério Superior**, em 30/01/2024, às 15:36, conforme horário oficial de Brasília, com fundamento no art. 6º, § 1º, do Decreto nº 8.539, de 8 de outubro de 2015.

Documento assinado eletronicamente por **Luiz Gustavo Martins Vieira**, **Professor(a) do Magistério Superior**, em 30/01/2024, às 15:37, conforme horário oficial de Brasília, com fundamento no art. 6º, § 1º, do Decreto nº 8.539, de 8 de outubro de 2015.

Documento assinado eletronicamente por **Laiane Alves De Andrade**, **Usuário Externo**, em 30/01/2024, às 15:42, conforme horário oficial de Brasília, com fundamento no art. 6º, § 1º, do Decreto nº 8.539, de 8 de outubro de 2015.

Documento assinado eletronicamente por **CÁSSIA REGINA CARDOSO**, **Usuário Externo**, em 30/01/2024, às 15:43, conforme horário oficial de Brasília, com fundamento no art. 6º, § 1º, do Decreto nº 8.539, de 8 de outubro de 2015.

A autenticidade deste documento pode ser conferida no site https://www.sei.ufu.br/sei/controlador_externo.php?acao=documento_conferir&id_orgao_acesso_externo=0, informando o código verificador **5142759** e o código CRC **3A4A8AA1**.

Referência: Processo nº 23117.006972/2024-81 SEI nº 5142759

AGRADECIMENTOS

À minha esposa que caminha ao meu lado nos dias mais claros e mais escuros. Minha amiga e minha alma gêmea. Ela que me motivou e ajudou a continuar a perseguir mais essa conquista.

Ao meu pai que sempre me incentivou a continuar estudando e me profissionalizando. Ele que já revisou muitos trabalhos e textos meus, mas infelizmente não pôde revisar este.

À minha mãe por toda a educação que é a base do que sou hoje e à minha irmã com quem sei que sempre posso contar.

Aos meus professores orientadores Carla Eponina Hori e Luiz Gustavo Martins Vieira pelo suporte, compreensão, conhecimento compartilhado e parceria aos longos desses anos.

À banca examinadora, pelo tempo dedicado para revisar e avaliar este trabalho.

Ao Lucas Gomes por gentilmente ceder uma quantidade de seus catalisadores para serem utilizados neste estudo.

À Cargill Agrícola pela doação das biomassas utilizadas nos estudos de pirólise analítica.

Às equipes de técnicos, núcleos de pesquisa e assistentes administrativos da Faculdade de Engenharia Química da Universidade Federal de Uberlândia por todo suporte no desenvolvimento e finalização desse trabalho.

Ao CNPq (Conselho Nacional de Desenvolvimento Científico e Tecnológico), à CAPES (Coordenação de Aperfeiçoamento de Pessoal de Nível Superior) e à FAPEMIG (Fundação de Amparo à Pesquisa do Estado de Minas Gerais) pelo incentivo à pesquisa e desenvolvimento.

A todos aqui não citados que, direta ou indiretamente, contribuíram para a realização deste trabalho.

SUMMARY

FIGURES CONTENT i
TABLES CONTENT v
ACRONYMS vii
ABSTRACT viii
RESUMO ix
CHAPTER 1 1
1. INTRODUCTION 1
1.1. Objectives 4
1.2. References 1
CHAPTER 2 3
2. LITERATURE REVIEW 3
2.1. Renewable Energy 3
2.1.1. An Outline 3
2.2. Biomass Energy 6
2.2.1. Waste-to-energy 9
2.3. Agricultural waste 12
2.3.1. Soybean Residue 13
2.3.2. Cocoa Bean Shell 15
2.4. Thermochemical Processes 18
2.4.1. Fast Pyrolysis 19
2.4.2. Analytical Pyrolysis 20
2.4.3. Operating parameters 23
2.5. Catalysts' use 25
2.5.1. Hydrotalcite (HTC) 27
2.5.2. Zeolite 28
2.5.3. Catalysts derived from niobic acid 29
2.5.4. Thermochemical studies developed by the Faculty of Chemical Engineering at the Federal University of Uberlândia (FEQ-UFU) - A synthesized timeline 30
2.6. References 31
CHAPTER 3 45

3. MATERIALS AND METHODS 45
3.1. Biomasses 45
3.2. Biomass Characterization 46
3.2.1. Cocoa Bean Shell (CBS) and Soybean Residue (SR) Proximate Analysis 46
Moisture Content 46
Volatile Content 47
Ash Content 48
Fixed Carbon Content 48
3.2.2. Elemental Analysis and Higher Heat Value of CBS and SR 48
3.2.3. Chemical Composition Analysis of CBS and SR 49
Protein Content 49
Lipid Content 50
Crude Fiber Content 50
Carbohydrate Content 51
3.2.4. Lignocellulosic composition of the CBS and SR 51
3.2.5. Thermogravimetric Analysis (TGA) of CBS and SR 52
3.2.6. Fourier Transform Infrared Spectroscopy (FTIR) Analysis of CBS and SR 52
3.2.7. X-ray fluorescence analysis (XRF) of Analysis of CBS and SR 52
3.2.8. Scanning Electron Microscopy (SEM) Analysis of CBS and SR 53
3.3. Catalysts 53
3.3.1. Zeolite 54
3.3.2. Hydrotalcite [$Mg_6Al_2(OH)16CO_3.4H_2O$] (HTC) 54
3.3.3. Catalysts Derived from Niobic Acid (Ni/Nb_2O_5 and $Ni\text{-}Re/Nb_2O_5$) 54
3.4. Analytical pyrolysis (micro-pyrolysis) 55
3.4.1. Analytical pyrolysis (micro-pyrolysis) 55
3.4.2. Analytical pyrolysis (micro-pyrolysis) in a catalytic bed 56
3.4.3. Design of experimental 57
3.5. References 60
CHAPTER 4 66
4. RESULTS AND DISCUSSIONS – BIOMASS CHARACTERIZATION 66
4.1. Immediate Analyzes and Higher Heat Value (HHV) of the SR and CBS 66

4.2. Ultimate Analyzes of the SR and CBS 67
4.3. Chemical Composition of the SR and CBS 68
4.4. Thermogravimetric Analysis (TGA) of the SR and CBS 70
4.5. Fourier Transform Infrared Spectroscopy (FTIR), Scanning Electron Microscopy (SEM) and X-ray Fluorescence (XRF) Analysis of CBS and SR 72
4.6. References 76
CHAPTER 5 81
5. RESULTS AND DISCUSSIONS – ANALYTICAL PYROLYSIS 81
5.1. Catalyst Effect 81
5.1.1. Non-Catalytic Pyrolysis 85
5.1.2. Catalytic Pyrolysis with Hydrotalcite Precursor (HTC) 89
5.1.3. Catalytic Pyrolysis with Zeolite HZSM-5 94
5.1.4. Catalytic Pyrolysis with Ni-Re/Nb_2O_5 100
5.1.5. Catalytic Pyrolysis with Ni/Nb_2O_5 104
5.1.6. Catalyst Effect Conclusions 107
5.2. Temperature Effect 108
5.2.1. Non-Catalytic Pyrolysis with temperature variation from 350°C to 750°C 112
5.2.2. Catalytic Pyrolysis with Hydrotalcite (HTC) with temperature variation from 450°C to 750°C 116
5.2.3. Catalytic Pyrolysis with Zeolite HZSM-5 with temperature variation from 450°C to 750°C 120
5.2.4. Temperature Effect Conclusions 124
5.3. Catalyst-to-biomass Ratio (C:B) Effect 125
5.4. References 134
CHAPTER 6 143
6. CONCLUSIONS 143
6.1. Recommendations for Future Work 144
APPENDIX A 146
ANALYTICAL PYROLYSIS CHROMATOGRAMS AND COMPOUNDS' TABLES 146

FIGURES CONTENT

Figure 1.1. Alternative pathways to reduce GHG emissions. 1
Figure 2.1. Global primary energy consumption by source (OWD, 2022). 3
Figure 2.2. Schematic drawing of the crucible used in the analytical pyrolysis (IPCC, 2018). 4
Figure 2.3. Total primary energy supply globally (GBS, 2022). 5
Figure 2.4. Total primary energy supply globally (IEA, 2021). 6
Figure 2.5. Global production of major crops in 2021 (GBS, 2022). 7
Figure 2.6. Supply of biomass globally (GBS, 2022). 8
Figure 2.7. Schematic view of the variety of commercial and developing bioenergy routes from biomass feedstocks (Chum et al., 2011)..... 9
Figure 2.8. Framework of environment, waste-to-energy (WTE) supply chains and circular economy system (Pan et al., 2015). 11
Figure 2.9. Energy from waste in 2019 (GBS, 2022). 12
Figure 2.10. Soybean residue..... 15
Figure 2.11. Cocoa beans and their processing by-products (Rojo-poveda et al., 2020)..... 16
Figure 2.12. Typical product yields from different types of pyrolysis (Bridgwater, 2018). 19
Figure 2.13. Conceptual fast pyrolysis process (Bridgwater, 2018). 20
Figure 2.14. Schematic diagram of the different types of pyrolyzers currently used. (A) Filament type, (B) Currie-point type, and (C) micro-furnace type (Kumagai et al., 2020)..... 21
Figure 2.15. Schematic representation of the hydrotalcite structure (Dębek et al., 2017). 27
Figure 2.16. Examples of zeolites structures and their micropore systems (Nazir et al., 2020). . 29
Figure 2.17. Thermochemical studies developed by the FEQ-UFU - A synthesized timeline. ... 31
Figure 3.1. Soybean residue. 46
Figure 3.2. Dried cocoa bean shell..... 46
Figure 3.3. Schematic drawing of the crucible used in the analytical pyrolysis. 55
Figure 3.4. Schematic drawing of an analytical pyrolysis system. Adapted from (Li et al., 2022). 56
Figure 3.5. Schematic drawing of the crucible used in the analytical pyrolysis (*ex-situ* catalytic bed)..... 57

Figure 3.6. Schematic drawing of the experimental design. 58
Figure 4.1. Immediate Analysis Results for: (a) SR; (b) CBS. 66
Figure 4.2. Chemical Composition Results for: a) SR; b) CBS. 69
Figure 4.3. TGA and DTG Results for: a) SR; b) CBS. 71
Figure 4.4. FTIR spectrums for a) SR; b) CBS. 73
Figure 4.5. Soybean Residue SEM – a) magnitude of 1.00 K X; b) magnitude of 10.00 K X. ... 75
Figure 4.6. Cocoa Bean Shell SEM – a) magnitude of 1.00 K X; b) magnitude of 5.00 K X. 76
Figure 5.1. Categorization of catalytic and non-catalytic pyrolysis products of (a) SR and (b) CBS; temperature of 550°C and 3:1 catalyst-to-biomass ratio 83
Figure 5.2. Pyrolysis products categorization by organic functional groups for (a) SR and (b) CBS; temperature of 550°C and 3:1 catalyst proportion 84
Figure 5.3. Non-Catalytic Pyrolysis products categorization by organic functional groups for (a) SR and (b) CBS; temperature of 550°C 86
Figure 5.4. Non-Catalytic Pyrolysis products from other biomasses (Wang et al., 2017)..... 87
Figure 5.5. Size of chains based on number of carbons in the organic structure for the non-catalytic pyrolysis of (a) SR and (b) CBS; temperature of 550°C 88
Figure 5.6. Categorization of non-catalytic and catalytic (HTC) pyrolysis products of (a) SR and (b) CBS; temperature of 550°C and 3:1 catalyst proportion 90
Figure 5.7. Keto-enol tautomerism: The interconversion between the two forms can be catalyzed by an acid or a base. (Higginbotham, 2021)..... 91
Figure 5.8. Size of chains based on number of carbons in the organic structure for the non-catalytic pyrolysis and pyrolysis with HTC of (a) SR and (b) CBS; temperature of 550°C and 3:1 catalyst proportion 92
Figure 5.9. Categorization of non-catalytic and catalytic (HZSM-5) pyrolysis products of (a) SR and (b) CBS; temperature of 550°C and 3:1 catalyst proportion 96
Figure 5.10. Size of chains based on number of carbons in the organic structure for the non-catalytic pyrolysis and pyrolysis with HZSM-5 of (a) SR and (b) CBS; temperature of 550°C and 3:1 catalyst proportion 97
Figure 5.11. Xylene formation pathway from Diels-Alder cycloaddition of dimethylfuran and ethylene over Lewis acid zeolite catalyst (adapted from Chang et al., 2016. 97

Figure 5.12. Reaction pathways for the catalytic pyrolysis of lignocellulosic biomass with HZSM-5 (Wang et al., 2014)..... 99
Figure 5.13. Categorization of non-catalytic and catalytic (Ni-Re/Nb_2O_5) pyrolysis products of (a) SR and (b) CBS; temperature of 550°C and 3:1 catalyst proportion 102
Figure 5.14. Size of chains based on number of carbons in the organic structure for the non-catalytic pyrolysis and pyrolysis with Ni-Re/Nb_2O_5 of (a) SR and (b) CBS; temperature of 550°C and 3:1 catalyst proportion 103
Figure 5.15. Categorization of non-catalytic and catalytic (Ni/Nb_2O_5) pyrolysis products of (a) SR and (b) CBS; temperature of 550°C and 3:1 catalyst proportion.....105
Figure 5.16. Size of chains based on number of carbons in the organic structure for the non-catalytic pyrolysis and pyrolysis with Ni/Nb_2O_5 of (a) SR and (b) CBS; temperature of 550°C and 3:1 catalyst proportion 106
Figure 5.17. Categorization of pyrolysis products of SR for (a) non-catalytic, (b) catalytic with HTC, (c) HZSM-5; and of CBS for (d) non-catalytic, (e) catalytic with HTC, (f) HZSM-5 111
Figure 5.18. Categorization of non-catalytic pyrolysis products of (a) Soybean Residue and (b) Cocoa Bean Shell; temperature varying from 350 to 750°C.....113
Figure 5.19. Size of chains based on number of carbons in the organic structure for the non-catalytic pyrolysis of (a) SR and (b) CBS; temperature varying from 350 to 750°C.....114
Figure 5.20. Categorization of HTC-catalytic pyrolysis products of (a) SR and (b) CBS; temperature varying from 450 to 750°C and 3:1 catalyst proportion 117
Figure 5.21. Size of chains based on number of carbons in the organic structure for the HTC-catalytic pyrolysis of (a) SR and (b) CBS; temperature varying from 450 to 750°C and 3:1 catalyst proportion 118
Figure 5.22. Categorization of HZSM-5 catalytic pyrolysis products of (a) Soybean Residue and (b) Cocoa Bean Shell; temperature varying from 450 to 750°C and 3:1 catalyst proportion 121
Figure 5.23. Size of chains based on number of carbons in the organic structure for the HZSM-5 catalytic pyrolysis of (a) SR and (b) CBS; temperature varying from 450 to 750°C and 3:1 catalyst proportion 122
Figure 5.24. Categorization of pyrolysis products at different catalyst:biomass proportion for (a) SR at 550°C, (b) SR at 750°C, (c) CBS at 550°C and (d) CBS at 750°C.....126

Figure 5.25. Organic groups categorization of pyrolysis products at different catalyst:biomass proportion for (a) SR at 550°C, (b) SR at 750°C, (c) CBS at 550°C and (d) CBS at 750°C.....129
Figure 5.26. Size of chains based on number of carbons in the organic structure for the pyrolysis products at different catalyst:biomass proportion for (a) SR at 550°C, (b) SR at 750°C, (c) CBS at 550°C and (d) CBS at 750°C.....130
Figure 5.27. Reaction pathways for the catalytic pyrolysis of SR and CCBS with HZSM-5 (adapted from Yang et al., 2023).....133
Fig. A1. Chromatogram for the non-catalytic analytical pyrolysis of SR at 550 °C.....146
Fig. A2. Chromatogram for the non-catalytic analytical pyrolysis of CBS at 550 °C. 148
Fig. A3. Chromatogram for the catalytic analytical pyrolysis of SR at 550 °C. Performed using HZSM-5 at a catalyst-to-biomass ratio of 5:1. 150
Fig. A4. Chromatogram for the catalytic analytical pyrolysis of CBS at 550 °C. Performed using HZSM-5 at a catalyst-to-biomass ratio of 5:1. 152

TABLES CONTENT

Table 2.1. Recent studies involving coca byproducts. 17
Table 3.1. Stage 1 of the experimental design. 59
Table 3.2. Stage 2 of the experimental Design. 60
Table 3.3. Stage 3 of the experimental Design. 60
Table 4.1. Comparison of Immediate Analysis and HHV of some Solid Fuels. 67
Table 4.2. Comparison of Ultimate Analysis of some Solid Fuels. 68
Table 4.3. SR and CBS Lignocellulosic characterization. 70
Table 4.4. XRF results of SR and CBS. 74
Table 5.1. Main organic products from non-catalytic pyrolysis at the temperature of 550°C 89
Table 5.2. Main organic products from Catalytic pyrolysis with HTC at the temperature of 550°C and 3:1 catalyst proportion 93
Table 5.3. Main organic products from Catalytic pyrolysis with HZSM-5 at the temperature of 550°C and 3:1 catalyst proportion 98
Table 5.4. Main organic products from Catalytic pyrolysis with Ni-Re/Nb_2O_5 at the temperature of 550°C and 3:1 catalyst proportion 104
Table 5.5. Main organic products from Catalytic pyrolysis with Ni/Nb_2O_5 at the temperature of 550°C and 3:1 catalyst proportion 106
Table 5.6. Main organic products from non-catalytic pyrolysis of the Soybean Residue with temperatures from 350°C to 750°C. 115
Table 5.7. Main organic products from non-catalytic pyrolysis of the Cocoa Bean Shell with temperatures from 350°C to 750°C. 116
Table 5.8. Main organic products from catalytic pyrolysis with HTC of the Soybean Residue with temperatures from 450°C to 750°C and catalyst proportion of 3:1. 119
Table 5.9. Main organic products from catalytic pyrolysis with HTC of the Cocoa Bean Shell with temperatures from 450°C to 750°C and catalyst proportion of 3:1. 120
Table 5.10. Main organic products from catalytic pyrolysis with HZSM-5 of the Soybean Residue with temperatures from 450°C to 750°C and catalyst proportion of 3:1. 123

Table 5.11. Main organic products from catalytic pyrolysis with HZSM-5 of the Cocoa Bean Shell with temperatures from 450°C to 750°C and catalyst proportion of 3:1. 124
Table 5.12. Main organic products from catalytic pyrolysis with HZSM-5 of the SR with temperatures of 550°C and 750°C and catalyst:biomass proportion varying from 0:1 to 5:1. ...131
Table 5.13. Main organic products from catalytic pyrolysis with HZSM-5 of the CBS with temperatures of 500°C and 750°C and catalyst:biomass proportion varying from 0:1 to 5:1. ...132
Table A1. Compounds identified in the test non-catalytic analytical pyrolysis of SR at 550 °C. 147
Table A2. Compounds identified in the test non-catalytic analytical pyrolysis of CBS at 550 °C. 149
Table A3. Compounds identified in the catalytic analytical pyrolysis of SR at 550 °C. Performed using HZSM-5 at a catalyst-to-biomass ratio of 5:1. 151
Table A4. Compounds identified in the catalytic analytical pyrolysis of CBS at 550 °C. Performed using HZSM-5 at a catalyst-to-biomass ratio of 5:1.....153

ACRONYMS

AOAC: Association of Official Analytical Chemists
ASTM: American Society for Testing and Materials
BBOT:2.5-Bis(5-tert-butyl-2-benzo-oxazol-2-yl) thiophene
BE: Bioenergy
BET: Brunauer-Emmett-Teller
CBS: Cocoa Bean Shells
CES: Circular Economy System
DTG: Differential Thermogravimetry
EGR: Emissions Gap Report
FAOSTAT: Food and Agriculture Organization Statistics
FEQUI: Chemical Engineering Faculty
FTIR: Fourier Transform Infrared Spectroscopy
GBS: Global Bioenergy Statistics
GC: Gas Chromatography
GHG: Greenhouse Gas
HHV: Higher Heating Value
HTC: Hydrotalcite
IEA: International Energy Agency
IPCC: Intergovernmental Panel on Climate Change
NIST: National Institute of Standards and Technology
NUFISQ: Laboratory of the Nucleus of Physical-Chemical Processes
NZE: Net Zero Emissions
OWD: Our World in Data
PPM: Parts per Million
Py-GC/MS: pyrolysis-gas chromatography coupled with mass spectrometry
SDGR: Sustainable Development Goals Report
SDGs: Sustainable Development Goals
SEM: Scanning Electron Microscopy
SR: Soybean Residue
TGA: Thermogravimetric Analysis
UFU: University of Uberlandia
UN: United Nations
WTE: Waste-to-energy
XRD: X-ray Diffraction Patterns
XRF: X-ray fluorescence analysis

ABSTRACT

With the growing concern regarding the impacts of Climate Change, there is an increase in the exploration of technologies to replace fossil fuels with renewable sources. Among several alternatives, the pyrolysis process emerges as a promising solution to address the current challenges related to energy generation. Additionally, it can effectively tackle the escalating issue of waste generation, which rises (especially in the agricultural sector) with population growth. However, the efficiency of this thermochemical process requires enhancement, primarily concerning the quality of its resulting products. To delve into improving this alternative, analytical pyrolysis proves to be a crucial tool for investigating pyrolytic behavior, analyzing the composition of pyrolysis products, and studying effects during the pyrolysis of organic material. This study delves into the application of four different catalysts (zeolite HZSM-5, hydrotalcite, and catalysts derived from niobic acid: Ni-Re/Nb_2O_5 and Ni/Nb_2O_5) during the catalytic pyrolysis of two distinct agricultural wastes: soybean residue (SR) and cocoa bean shell (CBS), employing analytical pyrolysis under a helium atmosphere. Both residues share characteristics with other biomasses, boasting high volatiles (78 and 88%, respectively), carbon content of 49 and 45%, higher hydrogen levels than other biomasses (11 and 9%), and SR exhibiting a noteworthy nitrogen content of 6%. Thermogravimetric analysis (TGA) revealed that nearly all compounds are consumed around 450°C for both biomasses. The pyrolysis experiments involved 3 stages: assessing the effects of catalyst type, temperature, and catalyst proportion. Analytical pyrolysis tests were conducted on pure biomass at 350, 450, 550, 650, and 750°C, generating heterogeneous products with a prevalence of oxygenated compounds, including acids, aldehydes, ketones, phenols, alcohols, and ethers. The temperature demonstrated a minor impact on their thermal conversion, with the highest hydrocarbon content observed at 750°C (34 and 17%), primarily composed of propene and benzene derivatives. At 550°C, all four catalysts, with a catalyst-to-biomass (C:B) proportion of 3:1, displayed the ability to reduce oxygen compounds. Behaviors that were highly comparable between SR and CBS. However, niobic acid catalysts converted a substantial amount into nitrogenated compounds, mainly long-chain nitriles, constituting 42 and 24% with Ni/Nb_2O_5. HTC and HZSMS-5 exhibited superior potential for enhancing the quality of pyrolytic products. Further tests at 450, 650, and 750°C revealed that HTC's results improved at higher temperatures, producing 54 and 43% of hydrocarbons at 750°C. In contrast, the HZSM-5 catalyst proved to be more efficient, achieving values around 70% for both biomasses. Thus, HZSM-5 was selected for evaluating the catalyst proportion in the final stage of experiments, conducted at 550 and 750°C, with C:B ratios of 1:1 and 5:1 for comparison with previous results. In conclusion, HZSM-5 exhibited satisfactory results for enhancing the quality of pyrolytic products while also potentially minimizing the reaction temperatures. The best results were achieved at 550°C, where 95 and 90% of the compounds generated from SR and CBS, respectively, were hydrocarbons, with 74 and 82% being aromatics.

Keywords: soybean residue, cocoa bean shell, agro-industrial waste, analytical pyrolysis, catalytic pyrolysis, zeolite, hydrotalcite, niobium.

RESUMO

Com a crescente preocupação com os impactos das Mudanças Climáticas, há um aumento na exploração de tecnologias para substituição de combustíveis fósseis por fontes renováveis. Dentre diversas alternativas, o processo de pirólise surge como uma solução promissora para enfrentar os atuais desafios relacionados a geração de energia. Além disso, pode resolver eficazmente o problema crescente da produção de resíduos, que aumenta (especialmente no sector agrícola) com o crescimento populacional. Contudo, a eficiência deste processo termoquímico necessita de melhorias, principalmente no que diz respeito à qualidade dos produtos resultantes. Para aprofundar o aprimoramento desta alternativa, a pirólise analítica prova ser uma ferramenta essencial para investigar o comportamento pirolítico, analisar a composição dos produtos da pirólise e estudar os efeitos durante a pirólise do material orgânico. Este estudo investiga a aplicação de quatro catalisadores diferentes (zeólita HZSM-5, hidrotalcita e catalisadores derivados de ácido nióbico: Ni-Re/Nb_2O_5 e Ni/Nb_2O_5) durante a pirólise catalítica de dois resíduos agrícolas distintos: resíduo de soja (SR) e casca de grão de cacau (CBS), empregando a pirólise analítica sob uma atmosfera de hélio. Ambos os resíduos partilham características com outras biomassas, apresentando elevados voláteis 78 e 88%, respetivamente, teor de carbono de 49 e 45%, níveis de hidrogénio mais elevados do que outras biomassas (11 e 9%), e SR exibindo um notável teor de nitrogênio de 6%. A análise termogravimétrica (TGA) revelou que quase todos os componentes são consumidos em torno de 450°C para ambas as biomassas. Os experimentos de pirólise envolveram 3 etapas: avaliação dos efeitos do tipo de catalisador, temperatura e proporção do catalisador. Testes analíticos de pirólise foram realizados na biomassa pura a 350, 450, 550, 650 e 750°C, gerando produtos heterogêneos com prevalência de compostos oxigenados, incluindo ácidos, aldeídos, cetonas, fenóis, álcoois e éteres. A temperatura demonstrou um impacto menor na sua conversão térmica, com o maior teor de hidrocarbonetos observado a 750°C (34 e 17%), composto principalmente por derivados de propeno e benzeno. A 550°C, todos os quatro catalisadores, com uma proporção catalisador-biomassa (C:B) de 3:1, apresentaram a capacidade de reduzir compostos de oxigênio. Comportamentos que foram altamente semelhantes entre SR e CBS. No entanto, os catalisadores de ácido nióbico converteram uma quantidade substancial em compostos nitrogenados, principalmente nitrilos de cadeia longa, constituindo 42 e 24% com Ni/Nb_2O_5. HTC e HZSMS-5 exibiram potencial superior para melhorar a qualidade de produtos pirolíticos. Outros testes a 450, 650 e 750°C revelaram que os resultados do HTC melhoraram em temperaturas mais altas, produzindo 54 e 43% de hidrocarbonetos a 750°C. Em contrapartida, o catalisador HZSM 5 mostrou-se mais eficiente, atingindo valores em torno de 70% para ambas as biomassas. Assim, o HZSM-5 foi selecionado para avaliação da proporção de catalisador na etapa final dos experimentos, conduzidos a 550 e 750°C, com relações adicionais de C:B de 1:1 e 5:1 para comparação com resultados anteriores. Em conclusão, a zeólita HZSM-5 exibiu resultados satisfatórios em relação a otimização da qualidade dos produtos pirolíticos e, ao mesmo tempo, pode minimizar potencialmente as temperaturas de reação. Os melhores resultados foram alcançados a 550°C, onde 95 e 90% dos compostos gerados a partir de SR e CBS, respectivamente, eram hidrocarbonetos, sendo 74 e 82% aromáticos.

Keywords: resíduo de soja, casca de cacau, resíduo agroindustrial, pirólise analítica, pirólise catalítica, zeólita, hidrotalcita, nióbio.

CHAPTER 1

1. INTRODUCTION

In recent years, there has been a growing concern regarding the consumption of fossil fuels and the resulting greenhouse gas (GHG) emissions (Usman et al., 2021). Replacing conventional fossil fuels with renewable energy sources is one of the priorities for all nations globally. Furthermore, limiting climate change requires increasing clean and renewable energy capacities to satisfy the global energy demand (Liu et al., 2022). Figure 1.1 shows some alternative pathways to reduce GHG emissions. One of the promising categories of renewable energy resources is biomass waste. The utilization of waste for energy production plays a crucial role in waste management. It not only addresses the issue of biomass waste itself but also contributes to renewable energy generation due to the abundance of agro-industrial waste (Sobek et al., 2020).

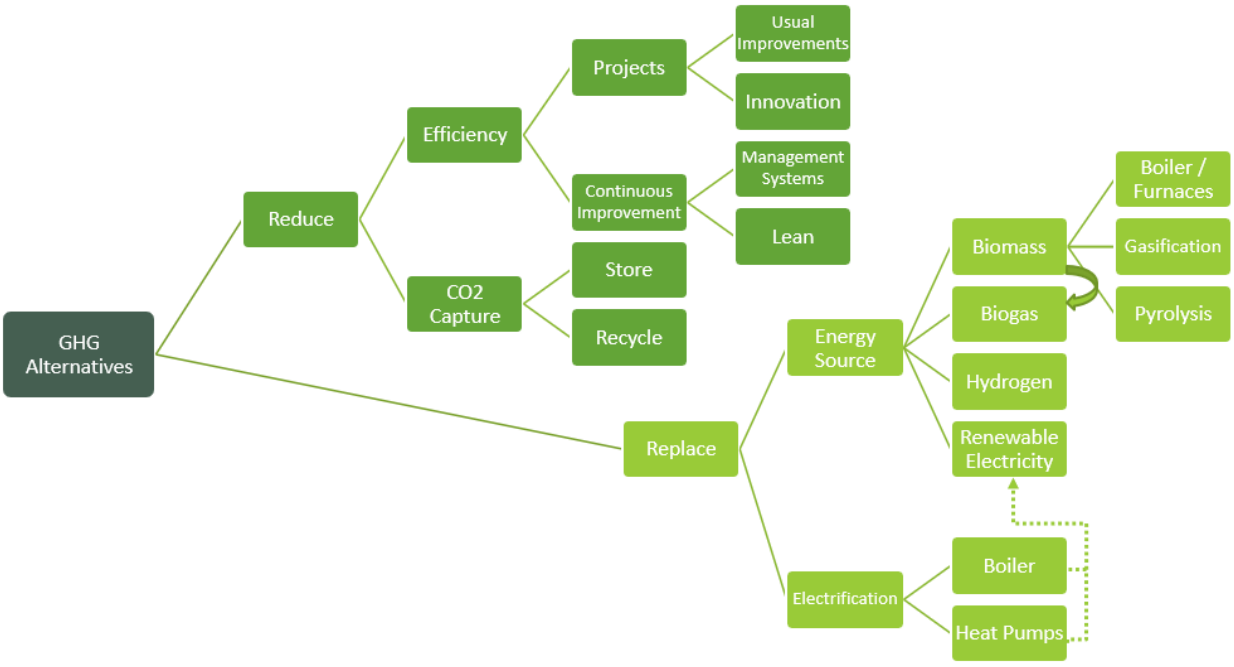


Figure 1.1. Alternative pathways to reduce GHG emissions.

Moreover, waste-to-energy processes have the potential to be carbon neutral and offer employment opportunities while also providing flexibility and significant contributions to

mitigating climate change. Various technologies are employed to convert different types of waste into gas or liquid fuels for energy production. These technologies encompass physical, thermal, chemical, and biological conversion processes. Among these approaches, thermochemical conversion stands out as a promising method for transforming waste (Jha et al., 2022). Thermochemical waste conversion technologies, such as incineration, gasification, and pyrolysis, are categorized based on the type of product they generate, namely gas, liquid, or solid. Researchers have focused on biomass and biomass waste conversion through thermochemical processes to produce renewable value-added products (Seo et al., 2022; Bridgwater, 2018). Furthermore, the energy generated from waste through thermochemical pathways can contribute to meeting Brazil's renewable portfolio standards. One particular process that has garnered significant interest is pyrolysis, whose products can be considered an efficient and sustainable alternative to fossil fuels (Leng et al., 2019). Pyrolysis is a simple technique where organic material is heated in the absence of oxygen, leading to its decomposition. It is widely considered as one of the most promising thermochemical technologies for converting biomass into high-value products. These products with more energy content could represent a great solution in renewable energy systems and be an option to address the challenge of climate change. Thermochemical systems could reuse biomass waste and offer advantages such as increased energy storage capacity, reduced energy generation costs, and enhanced overall energy efficiency (Lee et al., 2022; Lee et al., 2023). Different organic materials and process conditions, including heating rate, temperature, reaction time, and sweeping gas, can influence the distribution and characteristics of pyrolytic products (Sekar et al., 2021). Employing chemical and structural characterization techniques makes evaluating organic materials' thermal degradation behavior possible to assist a satisfactory pyrolysis setup choice (Bridgwater, 2018; Rossi et al., 2021a). Pyrolysis has been applied to various types of biomasses, and agro-industrial residues are particularly appealing due to Brazil's position as one of the largest producers and exporters of agricultural commodities. Brazil ranks as the 7th largest cocoa producer globally in addition to being considered a potential market for expanding production due to its climate and the organization and strength of agribusiness in the country, generating an estimated 6 million tons of cocoa (Ministério da Agricultura, Pecuária e Abastecimento, 2021). Similarly, soybean production in Brazil reached approximately 135 million tons in the 2020/21 harvest, making Brazil the world's largest grain producer and a significant generator of agricultural waste (EMBRAPA Soja, 2021). Exploring the energy conversion potential of these agro-industrial residues can yield

substantial advancements in the country's energy sector while efficiently managing these waste materials and enhancing their value. Therefore, studies that establish correlations between pyrolysis operating conditions and the quantity and quality of the obtained products can contribute to improving the efficiency of agro-industrial waste management in the country.

Analytical pyrolysis, also known as micro-pyrolysis, is a rapid and reliable technique to obtain preliminary information for biofuel production. It allows for investigating process parameters such as reaction temperature and catalytic reactions for producing hydrocarbons and other desired chemicals before conducting experiments on larger-scale equipment (Mariyam et al., 2022). Analytical catalytic pyrolysis of biomass waste offers the opportunity to obtain compounds that can be directly used as fuel or raw materials in the chemical industry (Nardella et al., 2022). The utilization of catalysts aims to modify the product composition, promoting the formation of desirable compounds, particularly hydrocarbons while mitigating undesirable characteristics like high acidity and low calorific value. Solid acid catalysts, such as zeolites, are commonly employed in catalytic pyrolysis, as they enable the integration of biorefinery systems into the pyrolysis process (Kim et al., 2019; Wang et al., 2020). Additionally, catalysts with basic and acid-basic (bifunctional) functions, such as calcium oxide (CaO) and hydrotalcite-type precursors, have also been investigated. Catalysts containing noble metals (Pd, Pt, Rh, and Ru), transition metals (Fe, Co, Mo, Ni), or niobium-based supports (represented by Nb^{4+}/Nb^{5+} cations) can facilitate deoxygenation reactions and hinder coke formation (Jafarian et al., 2018; Moura et al., 2022). Different catalysts can act on different routes and promote the removal of oxygenated and nitrogenous compounds depending on the process settings and the chosen biomass. The choice of catalyst should consider its activity, selectivity, and stability (critical properties that can influence the generation of desirable compounds and the yield of bio-products) (Guedes et al., 2018). Developing renewable energy generation technologies by thermochemical processes can reduce environmental impacts and increase the population's quality of life by addressing contemporary challenges related to energy security, waste management, and environmental sustainability. (Pang, 2019).

In terms of research development, ongoing efforts are directed towards understanding the fundamental mechanisms of pyrolysis reactions, optimizing catalytic setups, and exploring novel feedstocks. Additionally, advancements in analytical techniques, such as spectroscopy and chromatography, have enabled a more detailed characterization of pyrolytic products, contributing

to a deeper understanding of the process. Thus, this study investigated the catalytic analytical pyrolysis employing zeolite HZSM-5, hydrotalcite, and catalysts derived from niobic acid: Ni-Re/Nb_2O_5 and Ni/Nb_2O_5 of two agro-industrial residues generated on a large scale in Brazil: cocoa bean shells (CBS) and soybean residue (SR). This present study not only addresses the challenge of waste management but also harnesses the potential of agro-industrial by-products for valuable resource recovery. By employing cutting-edge catalytic processes, this transformative thermochemical technique opens new avenues for efficient and eco-friendly utilization of agricultural residues, marking a significant stride towards a more sustainable and resource-efficient future. Furthermore, suggested reaction pathways are proposed, aiming to contribute to this dynamic and rapidly evolving field. Consequently, the catalysts studied in this paper may be further investigated for their selectivity and quality in generating specific desired pyrolytic products.

To our knowledge, no study on using SR and CBS with niobic acid and hydrotalcite has been reported. This catalytic setup could be a groundbreaking approach to sustainable resource utilization, specifically for agro-industrial residues that take center stage in large-scale applications.

1.1. Objectives

The main objective of this work is to perform analytical pyrolysis of two agro-industrial residues that are generated on a large scale in Brazil: (i) cocoa bean shells, (ii) and soybean residue using different catalysts (hydrotalcite, zeolite, and catalysts derived from niobic acid).

Specifically, the objectives are:

- perform the biomasses characterization;
- evaluate the effects of the reaction temperature using analytical pyrolysis;
- evaluate the influence the hydrotalcite catalyst $[M_{(1-x)}^{2+}\ M_x^{3+}(OH)_2]\bullet[A^{n-}]_{x/n}\bullet mH_2O$ on pyrolytic products;
- evaluate the influence of zeolite (HZSM-5) catalyst on pyrolytic products;
- evaluate the influence of the catalysts derived from niobic acid (Ni/Nb_2O_5 and Ni-Re/Nb_2O_5) on pyrolytic products;
- identify the conditions to optimize hydrocarbon content generation.

1.2.References

Bridgwater, B.T. (2018), Challenges and Opportunities in Fast Pyrolysis of Biomass: Part I, Johnson Matthey Technology Review, 62, 118–130. https://doi.org/10.1595/205651318X696693

EMBRAPA Soja. (2021), https://www.embrapa.br/soja/cultivos/soja1/dados-economicos, [on-line accessed 18-07-2022].

Guedes, R.E., Luna, A.S., Torres, A.R. (2018), Operating Parameters for Bio-Oil Production in Biomass Pyrolysis: A Review, Journal of Analytical and Applied Pyrolysis, 129, 134–149. https://doi.org/10.1016/j.jaap.2017.11.019

Jafarian, S., Tavasoli, A. (2018), A comparative study on the quality of bioproducts derived from catalytic pyrolysis of green microalgae Spirulina (Arthrospira) plantensis over transition metals supported on HMS-ZSM5 composite, International Journal of Hydrogen Energy, 43, 19902–19917. https://doi.org/10.1016/j.ijhydene.2018.08.171

Jha, S., Nanda, S., Acharya, B., Dalai, A. K. (2022), A Review of Thermochemical Conversion of Waste Biomass to Biofuels, Energies, 15 (17), 1–23. https://doi.org/10.3390/en15176352

Kim, Y. M., Jeong, J., Ryu, S., Lee, H. W., Jung, J. S., Siddiqui, M. Z. (2019), Catalytic pyrolysis of wood polymer composites over hierarchical mesoporous zeolites, Energy Convers Manage, 195, 727–37. https://doi.org/10.1016/j.enconman.2019.05.034

Lee, D., Nam, H., Won Seo, M., Hoon Lee, S., Tokmurzin, D., Wang, S, Park, Y.K. (2022), Recent progress in the catalytic thermochemical conversion process of biomass for biofuels, Chemical Engineering Journal, 447, 137501. https://doi.org/10.1016/j.cej.2022.137501

Lee, J, Lin, K.Y.A., Jung, S., Kwon, E.E. (2023), Hybrid renewable energy systems involving thermochemical conversion process for waste-to-energy strategy, Chemical Engineering Journal 452, 139218. https://doi.org/10.1016/j.cej.2022.139218

Leng, L., Huang, H., Li, H., LI, J., Zhou, W. (2019), Biochar stability assessment methods: A review, Science of the Total Environment, 647, 210–222. https://doi.org/10.1016/j.scitotenv.2018.07.402

Liu, Z., Saydaliev, H.B., Lan, J., Ali, S., Anser, M.K. (2022), Assessing the effectiveness of biomass energy in mitigating CO2 emissions: Evidence from Top-10 biomass energy consumer countries, Renewable Energy, 191, 842–851. https://doi.org/10.1016/j.renene.2022.03.053

Mariyam, S., Alherbawi, M., Rashid, N., Al-Ansari, T., McKay, G. (2022), Bio-Oil Production from Multi-Waste Biomass Co-Pyrolysis Using Analytical Py–GC/MS, Energies, 15 (19). https://doi.org/10.3390/en15197409

Ministério da Agricultura, Pecuária e Abastecimento. (2021), https://www.gov.br/agricultura/pt-br/assuntos/noticias/producao-nacional-de-cacau-pode-crescer-60-mil-toneladas-em-quatro-anos, [on-line accessed 18-07-2022].

Moura, L.G. (2022), Study of hydrodeoxygenation reaction of phenolic compounds using niobium-based catalysts, Tese de Doutorado, Faculdade de Engenharia Química, Universidade Federal de Uberlândia.

Nardella, F., Bellavia, S., Mattonai, M., Ribechini, E. (2022), Co-pyrolysis of biomass and plastic: Synergistic effects and estimation of elemental composition of pyrolysis oil by analytical pyrolysis–gas chromatography/mass spectrometry, Bioresource Technology, 354, 127170. https://doi.org/10.1016/j.biortech.2022.127170

Pang, S. (2019), Advances in thermochemical conversion of woody biomass to energy, fuels and chemicals, Biotechnology Advances, 37 (4), 589–597. https://doi.org/10.1016/j.biotechadv.2018.11.004

Rossi, R.A.S., Barbosa, J.M., Barrozo, M.A.S., Vieira, L.G.M. (2021a), Catalytic solar hydropyrolysis of the Chlamydomonas reinhardtii microalgae, Biomass and Bioenergy, 152, 106183. https://doi.org/10.1016/j.biombioe.2021.106183

Sekar, M., Mathimani, T., Alagumalai, A., Chi, N.T.L., Duc, P.A., Bhatia, S.K., Brindhadevi, K., Pugazhendhi, A. (2021), A review on the pyrolysis of algal biomass for biochar and bio-oil – Bottlenecks and scope, Fuel, 283,119190. https://doi.org/10.1016/j.fuel.2020.119190

Seo, M.W., Lee, S.H., Nam, H., Lee, D., Tokmurzin, D., Wang, S., Park, Y.K. (2022), Recent advances of thermochemical conversieon processes for biorefinery. Bioresource Technology, 343, 126109. https://doi.org/10.1016/j.biortech.2021.126109

Sobek, S., Werle, S. (2020), Kinetic modelling of waste wood devolatilization during pyrolysis based on thermogravimetric data and solar pyrolysis reactor performance, Fuel, 261, 116459. https://doi.org/10.1016/j.fuel.2019.116459

Usman, M., Makhdum, M.S.A. (2021), What abates ecological footprint in BRICS-T region? Exploring the influence of renewable energy, non-renewable energy, agriculture, forest area and financial development, Renewable Energy, 179, 12–28. https://doi.org/10.1016/j.renene.2021.07.014

Wang, Y., Ke, L., Peng, Y., Yang, Q., Du, Z., Dai, L. (2020), Characteristics of the catalytic fast pyrolysis of vegetable oil soapstock for hydrocarbon-rich fuel, Energy Convers Management, 213, 112860. https://doi.org/10.1016/j.enconman.2020.112860

CHAPTER 2

2. LITERATURE REVIEW

Within this chapter, the theoretical foundations that underpin this work development are presented.

2.1.Renewable Energy

2.1.1. An Outline

Over the past decade, there has been a noticeable upward trend in global energy demand and consumption, consequently leading to an increase in global greenhouse gas (GHG) emissions. Figure 2.1 indicates the increase in global primary energy consumption by source, which has doubled in the last 40 years.

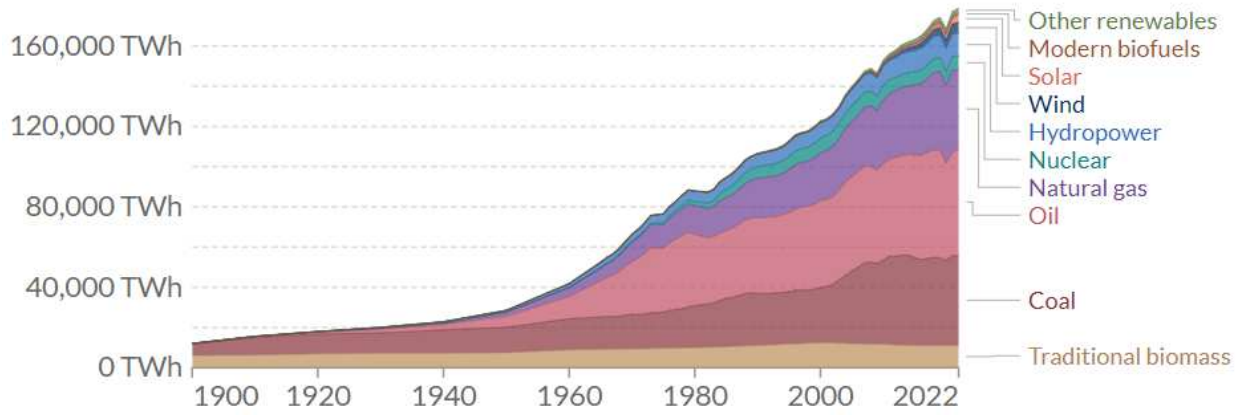


Figure 2.1. Global primary energy consumption by source (OWD, 2022).

The Emissions Gap Report (EGR, 2022) reveals that if current policies remain unchanged, emissions are expected to reach 58 $GtCO^2e$ by 2030. The projected emissions in 2030 are three times higher than the estimated emissions calculated for 2021, indicating a significant increase in GHG emissions. If no additional action is taken, these current policies could result in global warming of 2.8°C over this century. Therefore, it is imperative to implement revised policies that reflect each country's national efforts to align with the long-term temperature goal of the Paris

Agreement. These amended policies are essential to mitigate the expected warming and strive to limit it to at least 2.6°C (EGR, 2022; IEA, 2022). Figure 2.2 shows the global temperature change and modeled responses to anthropogenic emission.

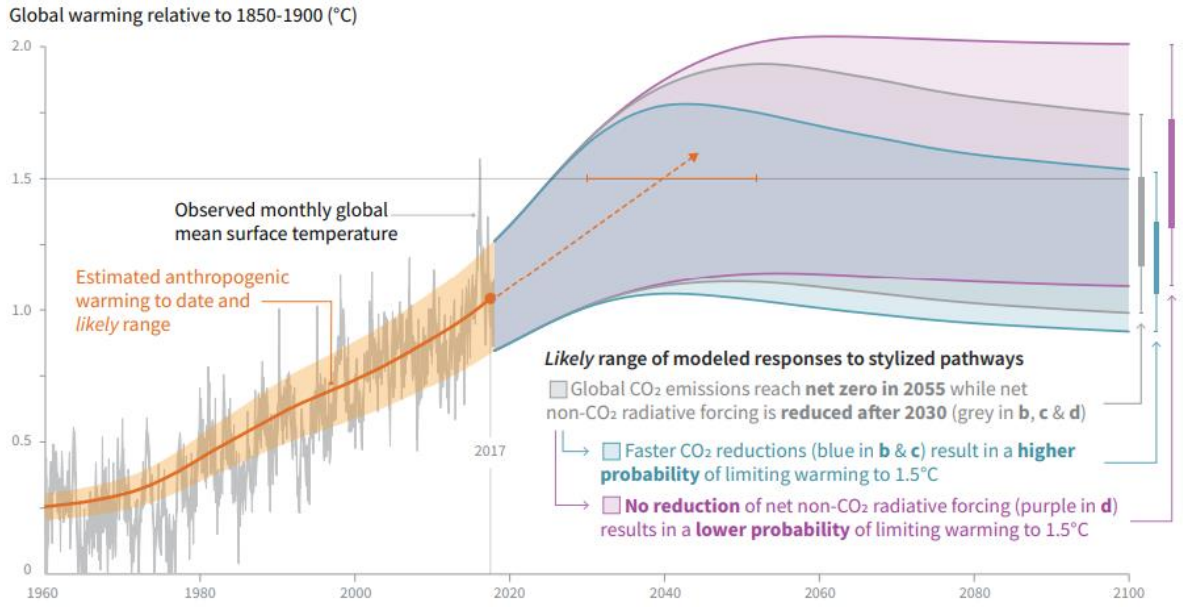


Figure 2.2. Schematic drawing of the crucible used in the analytical pyrolysis (IPCC, 2018).

In the realm of global sustainable development, it is vital to acknowledge the significance of the Sustainable Development Goals (SDGs). These 17 interconnected goals were adopted by all 193 member countries of the United Nations General Assembly in 2015. They are an integral part of the 2030 Agenda for Sustainable Development and aim to be achieved on a global scale by 2030 (SDGR UN, 2022). While SDG 7, Affordable and Clean Energy, is the goal directly linked to the energy system, it is important to recognize that the SDGs are interconnected. Many of the other goals also encompass aspects that are relevant to the energy system. The Sustainable Development Goals (SDGs) form a comprehensive framework to address environmental challenges and foster a more sustainable future (SDGR UN, 2022; DNV, 2022). They encompass a wide range of objectives, including: (a) the substantial increase in the utilization of renewable energy sources in the global energy mix and the strengthening of international collaboration to facilitate access to clean energy research and technologies, as part of SDG 7; (b) modernizing infrastructure and industries to ensure their sustainability, which involves enhancing resource efficiency and adopting cleaner and more environmentally friendly technologies and industrial

practices, as part of SDG 9; (c) the creation of favorable policy environment for promoting industrial diversification and value addition to commodities, as part of SDG 9; (d) sustainable management and efficient use of natural resources that involves the reduction in waste generation, as part of SDG 12; and (e) education and awareness enhancement regarding climate change mitigation, as part of SDG 13 (SDGR UN, 2022). This highlights the interdependence of various SDGs and emphasizes the need for a comprehensive and integrated approach to address sustainable development challenges. When considering the actual global energy supply (Figure 2.3), fossil fuels play a dominant role. In 2020, the total primary energy supply reached 585 EJ, with fossil fuels accounting for a significant 80% share. Among the fossil fuels, coal constituted 27%, oil accounted for 29%, and gas held 24%. In contrast, renewable energy technologies such as solar, wind, hydro, biomass, and geothermal comprised only 15% of the primary energy supply in 2020. This represents a 0.9% increase compared to the previous year (GBS, 2022). Although a gradual shift toward renewable sources can be highlighted, more efforts are necessary to reach the 2030 goals, as was exposed by the Emissions Gap Report (EGR, 2022).

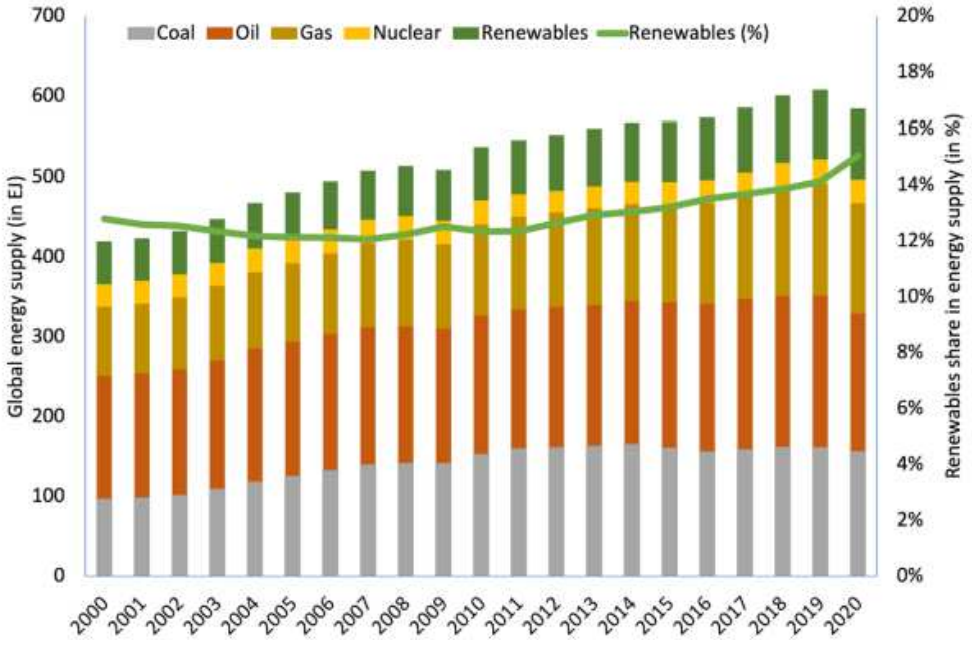


Figure 2.3. Total primary energy supply globally (GBS, 2022).

Figure 2.4 shows the total energy supply in the Net Zero Emissions (NZE) by 2050. From 2010 to 2020, the average annual energy intensity reduction was less than 2%. However, the increasing production of new fuels like advanced biofuels, hydrogen, and synthetic fuels tends to

offset these gains by driving up energy consumption. Consequently, the rate of decline in energy intensity is projected to slow down to 2.7% per year between 2030 and 2050, a period in which wind, solar, and modern bioenergy (solid or liquid) play an essential role in this scenario (IEA, 2021). In the Net Zero Emission (NZE) scenario, the total energy supply in 2050 will be close to the levels seen in 2010, despite a global population increase of nearly 3 billion people and a three-fold global economy expansion (IEA, 2022). Thus, focusing on developing technologies that can make renewable energies economically competitive is crucial. Sustainable alternatives are needed in various areas, and some promising options exist. For instance, using clean energy sources like solar, wind, and geothermal can make a significant difference (Amenaghawon et al., 2021; Potrč et al., 2021). Another path worth exploring is biomass thermal conversion, which has the potential to contribute to sustainable energy solutions as well, leading to a greener and more sustainable future by pushing forward with these innovations (Jha et al., 2022).

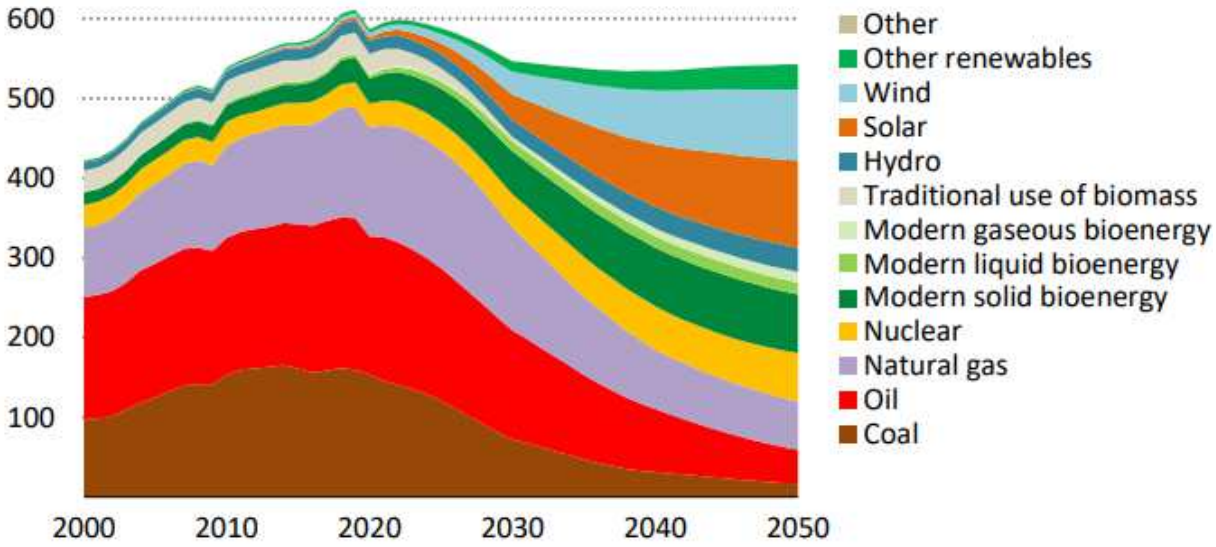


Figure 2.4. Total primary energy supply globally (IEA, 2021).

2.2.Biomass Energy

It is evident that the agricultural sector holds immense potential for the future utilization of bioenergy. Figure 2.5 indicates the global production of major crops. Surprisingly, even though it currently accounts for just around 10% of the global biomass supply, there's a lot of room for increasing its contribution (GBS, 2022). Not only focusing on improving the yields of major crops

but also improving the use of agricultural residues aiming a significant untapped potential in biomass energy (Gyamfi et al., 2021).

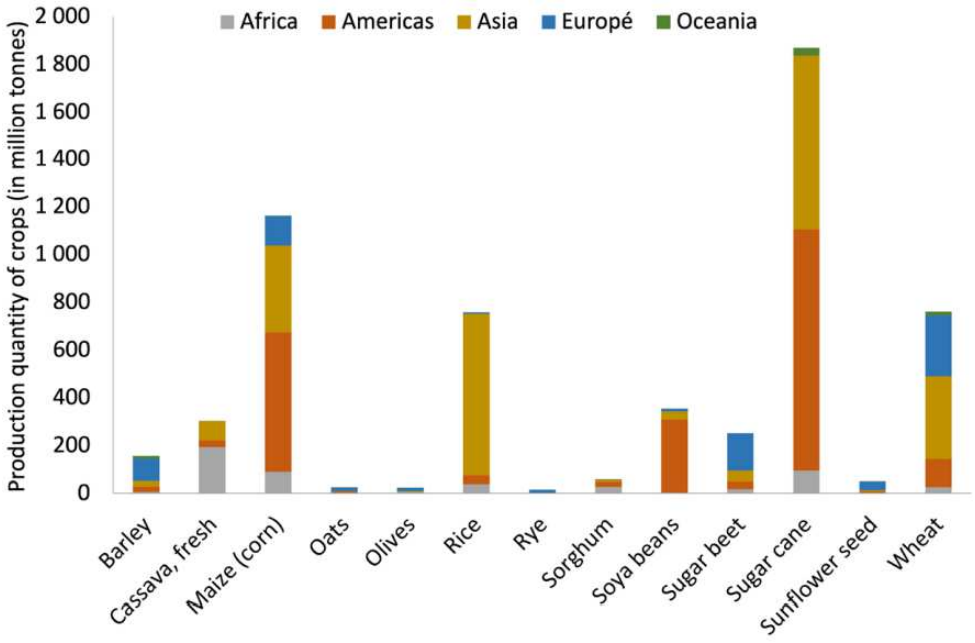


Figure 2.5. Global production of major crops in 2021 (GBS, 2022).

In the year 2021, 1.9 billion m^3 of wood fuel was produced across the globe. The wood pellet industry has witnessed remarkable growth in the bioenergy sector, with an estimated production of 44.3 million ton of pellets in the same year. An estimated 146 billion liters of biofuels were produced, with North and South America collectively contributing to 70% of the total output, while Europe accounted for 15% (GBS, 2022). Figure 2.6 shows the increase in the supply of biomass globally. In 2020, 5.3 EJ of biomass was utilized in electricity plants for power generation, while 3.4 EJ was used in combined heat and power plants. Additionally, approximately 38.1 billion m^3 of biogas was produced worldwide, corresponding to an energy content of 1.46 EJ. These numbers reflect the growing relevance of bioenergy in the global energy landscape. For instance, China has taken significant steps by launching a clean-heat initiative, which is anticipated to encourage using biomass and waste-fueled generation plants. Implementing this initiative is expected to be most widespread in regions with ample access to biomass resources and where regulations favor the reduction of coal-fired boilers to enhance environmental conditions (Destek et al., 2021). In Brazil, the government initiated the RenovaBio plan in 2020 to increase the production of transport biofuels. Consequently, this initiative has led to a rise in biogas-based

electricity generation, with both existing and new manufacturing firms contributing to this growth (Simões et al., 2021). In India, capital and fiscal subsidies have supported bioenergy (BE) capacity expansion. These incentives have facilitated the expansion of existing plants and encouraged the establishment of new manufacturing facilities. Such strategic investments have been crucial in advancing India's BE sector (Gao et al., 2021).

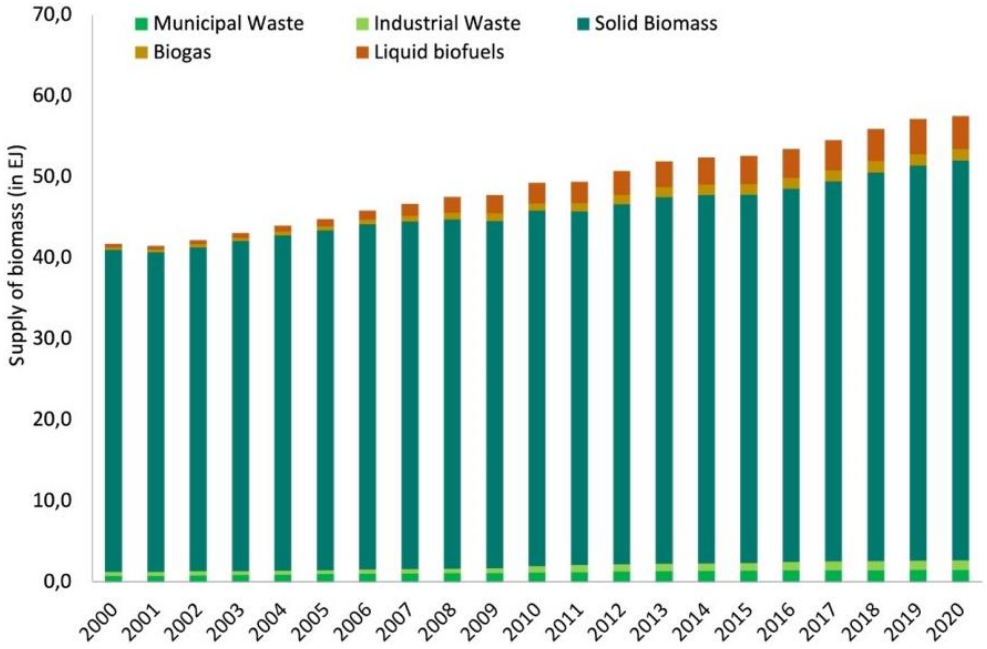


Figure 2.6. Supply of biomass globally (GBS, 2022).

However, the generation of bioenergy experienced a modest increase of approximately 5%, which fell below the average growth rate observed over the past five years since 2011, and did not align with the Sustainable Development Goals (SDGs) Scenario (GBS, 2020; IEA, 2022). Biomass energy is an important energy source, but it must be modernized in terms of efficiency, cost and supply-chain. Many bioenergy options, such as municipal solid waste, bioenergy cycles, and agro-residues, have significant capability to reduce CO_2 (Banja et al., 2019). The biomass energy development dynamics should encourage viable research to identify the role of the modern use of biomass in the mitigation of CO_2 and the environmental issues. Modern bioenergy has come a long way in terms of efficiency and convenience. The different forms of solids, liquids, and gases as secondary energy carriers to produce heat, electricity, combined heat and power, and transport fuels for various sectors could be one pathway to lessen GHG emissions. Liquid biofuels, like ethanol and biodiesel, have found their place in global road transport and some industrial

applications (Proskurina et al., 2019). Brazil is the world's second-largest ethanol supplier, contributing to approximately 30% of the global volume between the years 2019 to 2021 (Vidal, 2022). On the other hand, more development in the biomass market is needed, and larger-scale conversion units with better fuel flexibility needed to be deployed. This would lead to more energy-efficient conversion facilities and cost reduction. To achieve all this, different conversion technologies involving mechanical, thermochemical, biochemical, and chemical steps are employed to transform the diverse potential feedstocks into a broader range of secondary energy carriers (Shahbaz et al., 2019). The goal is to produce not just electricity and heat but also a variety of liquid and gaseous fuels, generating new energy carriers through more efficient biomass conversion methods as illustrated in Figure 2.7.

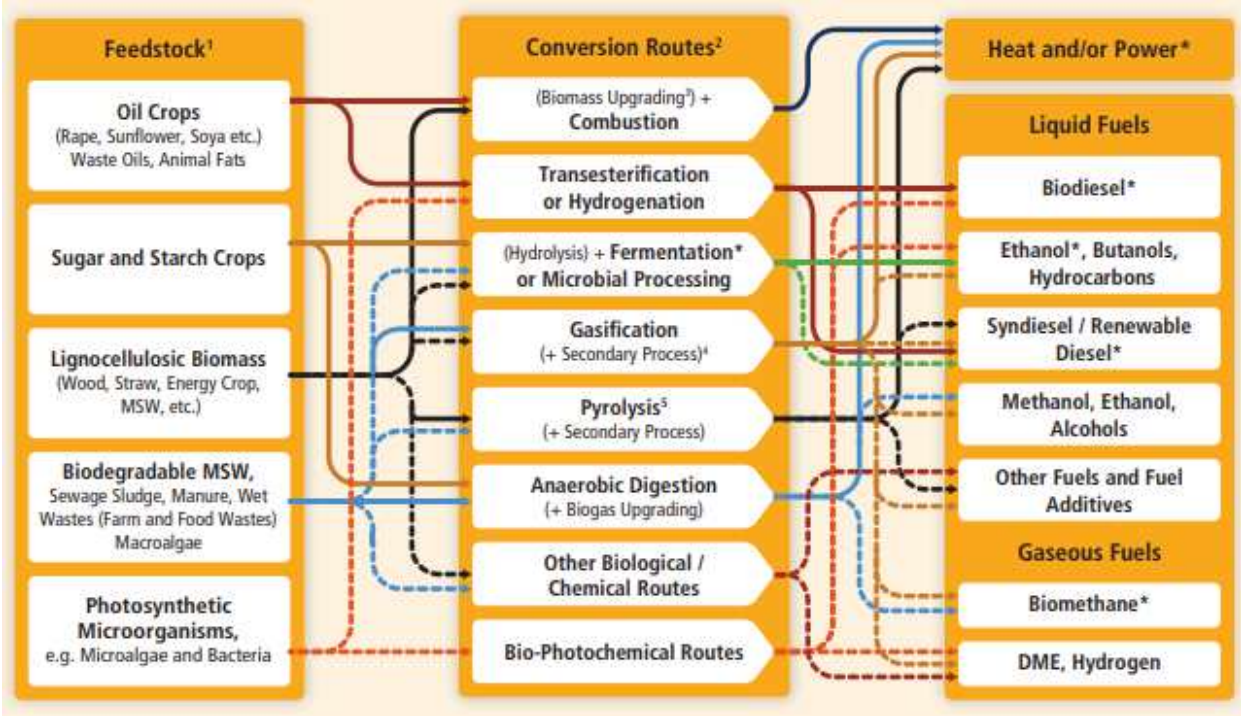


Figure 2.7. Schematic view of the variety of commercial and developing bioenergy routes from biomass feedstocks (Chum et al., 2011).

2.2.1. Waste-to-energy

Waste-to-energy (WTE) has gained international recognition as an effective means of curbing greenhouse gas emissions. According to the International Panel on Climate Change (IPCC), WTE stands out as a promising carbon-neutral technology that creates employment

opportunities and significantly contributes to mitigating climate change. Various models approximate that a WTE facility can save approximately 100-350 kg CO_2 equivalent per ton of waste processed (Rogoff et al., 2019). This variability stems from factors such as waste composition (specifically the percentage of biogenic materials), heat and electricity generated (as higher heat production translates to more significant CO_2 savings), and the country's energy substitution mix. In recent times, global markets have emerged to compensate WTE operators for their efforts in reducing CO_2 emissions. Notably, these carbon credits hold higher value in developing countries due to inadequate landfill practices in such regions. As such, WTE presents itself as a valuable and environmentally sound option for waste management and emission reduction on a global scale. (Ali et al., 2020; Rogoff et al., 2019). Effectively managing waste generation to harness resources such as heat, energy, and recyclable materials remains a significant challenge. The World Bank's report indicates that the annual global waste production reached approximately 1.3 billion tons in 2025, projected to increase to 2.2 billion tons annually. Consequently, properly disposing of and treating diverse waste worldwide is becoming increasingly crucial (Ali et al., 2020). The waste composition varies from region to region, influenced by economic conditions, cultural practices, climate, and energy sources. Generally, low-income countries tend to produce a substantial amount of organic waste, whereas high-income nations predominantly generate inorganic materials (Yarberry et al., 2019). As a result, it is imperative to establish advanced technologies that can effectively utilize the waste specific to a region for generating and producing heat, energy, fertilizers, and solid/liquid biofuels. Meeting this challenge will play a pivotal role in sustainable waste management and resource utilization on a global scale (Fellner et al., 2021; Majeed et al., 2022). Thus, addressing the prevailing issues of energy demand, greenhouse gas emissions, and waste management on a global scale, the integration of waste-to-energy supply chains into the energy system emerges as a crucial stride toward achieving an industrial circular economy solution (Figure 2.8) (Pan et al., 2015). Thermal waste recovery presents compelling arguments centered around two key aspects: (a) reducing the waste volume requiring disposal; and (b) offering an efficient means of energy recovery. Leveraging thermal power plants for waste utilization could result in a notable increase in energy output, including the production of high-density energy biofuel (Lee et al., 2023).

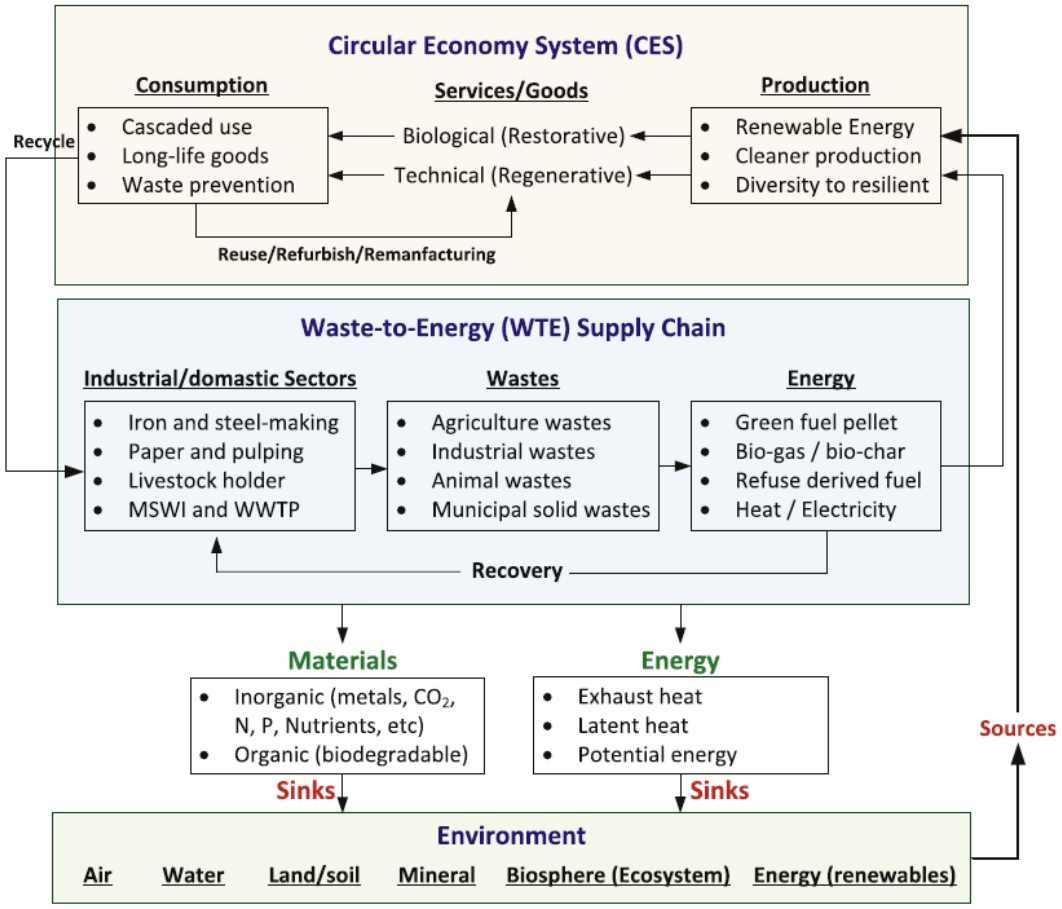


Figure 2.8. Framework of environment, waste-to-energy (WTE) supply chains and circular economy system (Pan et al., 2015).

In 2020, the domestic energy supply from municipal and industrial waste was 2.65 EJ, with 55% from municipal waste and the remaining from industrial waste. Europe is the world leader in the production of energy from waste. In 2019, the municipal and industrial waste supply was 1.44 EJ. Europe accounted for 54% of all global energy from waste, followed by the Americas at 32% (GBS, 2022). Figure 2.9. presents the energy from waste in 2019 by continent. Efforts are underway to repurpose these waste byproducts, aiming to enhance the overall efficiency of the production cycle. Nevertheless, several milestones must still be achieved to establish a genuinely circular economic system, particularly concerning waste-to-energy processes, to maximize the potential of residues in a sustainable manner and contribute to one's country's energy mix.

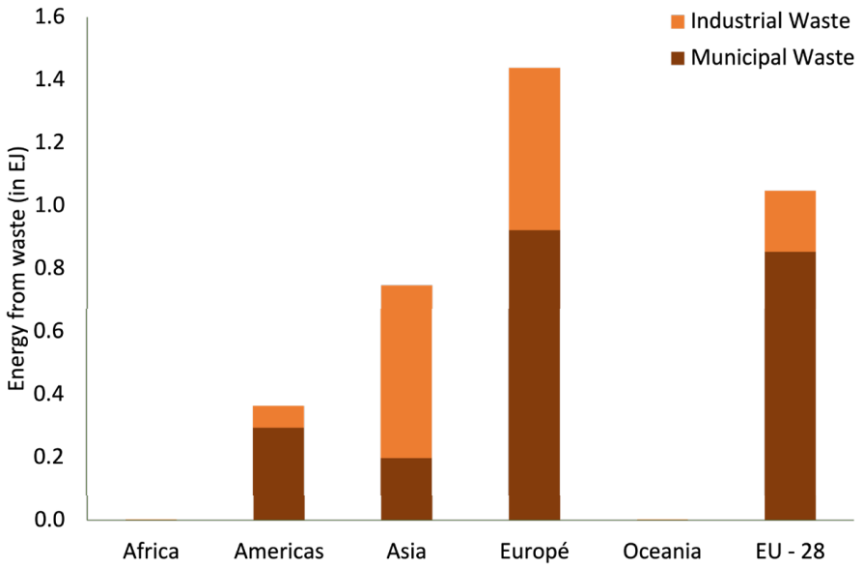


Figure 2.9. Energy from waste in 2019 (GBS, 2022).

2.3.Agricultural waste

Agro-industrial wastes encompass non-edible materials generated during diverse agricultural and agro-industrial activities. These waste materials originate from animal manure, field crop residues, harvest leftovers, and food consumption and processing remnants. The resulting wastes exhibit significant diversity and heterogeneity due to the vast array of products involved in the agricultural and livestock sectors. Consequently, agro-industrial wastes can be categorized into various types based on their material composition and management practices (AgroBioHeat, 2022). Agriculture-based industries generate substantial quantities of residues. Throughout the food production cycle, including transportation, storage, processing, distribution, and consumption, a significant volume of waste is produced. For instance, cereal, cane, and grain processing result in husks, bran, and bagasse, while nuts yield shells, cakes, and slurry after oil extraction. Moreover, during crop growth, various primary residues, and wastes, including stalks, stover, straw, leaves, stems, bagasse, and cobs, are produced (Saravanan et al., 2022). The sheer diversity and scale of waste production across these agriculture-based industries present significant challenges for waste management and recycling efforts (IEA, 2017).

The global agricultural residue has significant environmental potential since it can be recovered and transformed into more valuable products to generate revenue, considering economic, social, and political constraints. Globally, there is an estimated availability of approximately 731, 354, 204, 181, and 110 Mt of rice straw, wheat straw, corn straw, sugarcane bagasse, and rice husk, respectively. In addition, wood biomass waste was estimated to be 4.6 Gt/yr (Cho et al., 2020). Residues from cereal and sugarcane production account for 80 % of the total crop residues and represent the most harvestable biomass (IEA, 2017). Additionally, it was reported by Capanoglu et al. (2022) that approximately 1.3 billion tons of food, accounting for about one-third of the total food produced, is lost as waste either before or after reaching the consumer. This represents a significant concern regarding food wastage and its impact on sustainability. In summary, evaluating the global agricultural residue potential is a complex process involving different possibilities and considering various sources of biomass and waste, all of which have economic, environmental, and social sustainability implications (Pilafidis et al., 2022). To follow the increase of the major crops, various pathways to valorize bio waste into value-added products such as biofuel, biochar, and biomaterials need to emerge and be feasible for upscaling. This makes agriculture a vital enabler for promoting widespread bioenergy adoption worldwide, simultaneously boosting food and fuel production (Yaashikaa et al., 2022). The circular economy transition is gaining momentum and garnering more significant support from policymakers as a proactive response to the pressing global environmental challenges confronting our planet. This transformative approach entails converting waste streams into valuable products through bioconversion, enhancing sustainability and economically efficient waste management. Despite its potential benefits, the current reality shows that merely 25% of the vast agro-industrial waste, amounting to 138 million ton, is recycled annually (Kee et al., 2022).

2.3.1. Soybean Residue

Soybean, a leguminous crop, holds extensive cultivation across several countries, notably the United States, Brazil, Argentina, China, and parts of Europe. In 2021, global soybean production reached a staggering 380 million tons, with Brazil being a significant contributor, accounting for approximately 35% of this production (FAOSTAT, 2021). Soybean is a crucial crop cultivated worldwide that generates a significant by-product called soybean residue during oil extraction and meal manufacturing. These residues constitute approximately 1 to 3% of the whole

grain by mass during industrial processing (Santana et al., 2016). With a global soybean production of 380 million tons, the world's generation of soybean residue is substantial. Despite differences in soybean varieties, production areas, and conditions, the main components of its residues remain relatively consistent. Figure 2.10 shows the soybean residue removed in the early stage of soybean meal production. Notably, soybean boasts a crude protein content of about 30% and can be predominantly used for animal feed (Vong et al., 2018). However, soybean residues also hold the potential as a valuable feedstock for producing biofuels and chemicals. Although soybean residue is seldom considered for biofuel production, its sheer volume of the annual output makes it worthwhile to explore its utilization as feedstock for the conversion into biofuels and functional carbon materials (Lim et al., 2022). Soybean residue's richness in proteins opens up possibilities for preparing nitrogen-containing carbon materials, diversifying the applications of soybean residue, and paving the way for innovative uses in various fields. One viable option to address this surplus biomass is its thermochemical conversion, which can effectively harness this surplus for multiple purposes (Sun et al., 2021).

New alternatives to using soybean residues (SR) are rising, including techniques like adsorptive elimination of aqueous dyestuffs, bacterial biofilm inhibition, bioconversion, and thermochemical conversion to augment the value of this byproduct (Módenes et al., 2019; Ramos et al., 2021; Arpit Singh et al., 2022; Saravanan et al., 2022).

Boateng et al. (2010) studied the biofuel generation from soybean straw. Their research demonstrates an efficient production of high yields of pyrolysis liquids from soybean straws using fluidized-bed fast pyrolysis technology. The resulting bio-oil heating values exceed 20 MJ/kg, with yields reaching approximately 70 wt.%. Oliveira et al. (2015) examined the fast pyrolysis of soybean hulls across various temperatures, finding a bio-oil characterized by a diverse mixture abundant in phenols, cyclopentene derivatives, and tetradecane. The primary compounds identified were 1,3-pentadiene, acetic acid, and tetradecane. Sun et al. (2021) explored the product characteristics arising from the pyrolysis of SR under various temperatures and residence times. SR exhibited a lower presence of heavy organic components, leading to bio-oil with fewer heavy organics compared to bio-oil derived from the pyrolysis of cellulose and lignin-rich biomass. Nevertheless, alongside phenols, alcohols, acids, and esters, the resulting bio-oil from SR contained a significant amount of nitrogenous compounds attributed to the elevated content of proteins, amino acids, and other nitrogen-containing nutrients present in SR. Santana et al. (2016) evaluated the

impact of sodium, zinc, and magnesium chlorides as additives in soybean hull pyrolysis. Their results indicated a decrease in the decomposition temperature and a reduction in the maximum degradation rate for soybean hulls impregnated with $ZnCl_2$ and $MgCl_2$. The primary influence of $MgCl_2$ and $ZnCl_2$ addition was observed in the alteration of aldehyde content in the vapors, with furfural being the aldehyde exhibiting the highest concentration. A notable increase in aldehyde content was noted in materials treated with 10% and 20% $MgCl_2$.

Despite a growing number of studies on the thermal decomposition of soybean residues and the evolving understanding of this material, there is still a lack of sufficient research on the pyrolysis reaction pathways.



Figure 2.10. Soybean residue.

2.3.2. Cocoa Bean Shell

Cocoa was cultivated by the Mayans and Aztecs and held significant cultural value as a symbol of health, even serving as currency during ancient times. Figure 2.11 shows the cocoa beans and their processing by-products. Over the past four decades, cocoa production has witnessed continuous growth, mainly in developing nations, bringing about noteworthy benefits from sustainable practices, including increased yields, improved household income, better living, and working conditions, and enhanced environmental protection (Campos-Vega et al., 2018). Presently, cocoa bean production predominantly occurs in tropical regions with favorable climate

conditions, particularly in West African countries like Ivory Coast, Ghana, Nigeria, and Cameroon, as well as in Indonesia, Brazil, and Papua New Guinea.



Figure 2.11. Cocoa beans and their processing by-products (Rojo-poveda et al., 2020).

In 2021 global cocoa production was approximately 5.5 million tons. Africa accounts for 77% of global production, followed by Latin America and Asia, contributing 17% and 6%, respectively. Brazil accounts for about 3%. Among the top 10 cocoa bean producers, Côte d'Ivoire and Ghana emerge as leaders, producing 2,150,000 MT and 850,000 MT, respectively (FAOSTAT, 2021). Europe holds the largest share of global consumption at 45%, closely followed by the USA. These beans undergo various processing methods, yielding cocoa mass, cocoa butter, cocoa powder, chocolate, and other cocoa products (Vásquez et al., 2019). In the cocoa production chain, cocoa beans constitute nearly one-third of the fruit's weight, while the residual biomass, including cocoa shells, pod husks, skin, and other cocoa wastes, accounts for 67–76% by dry weight. Only cocoa bean shells (CBS) are one of the main by-products of the transformation of cocoa beans, representing 10–17% of the total cocoa bean weight. Considering the weight percentage of CBS and the cocoa production data, this would mean that more than 700 thousand tons of CBS waste is produced worldwide (Rojo-poveda et al., 2020). This significant volume necessitates efficient solutions for reuse, considering that it includes substantial energy content (4,060 kcal/kg for pod husk and 4,110 kcal/kg for bean shells), which could fulfill the energy demands of various industrial processes involved in cocoa processing. To explore this potential, energy models of cocoa processing are needed (Valladares-Diestra et al., 2022). To address these residue management challenges and environmental concerns, researchers have explored the valorization of

cocoa by-products by extracting various commercially valuable components and producing bioenergy and high-value biomolecules. These endeavors hold potential applications in the food, pharmaceutical, and cosmetic industries, presenting a promising pathway toward sustainable utilization of cocoa by-products (Vandenberghe et al., 2022). Cocoa bean shells (CBS) are commonly incorporated into food applications as ground cocoa flour or fiber extracts obtained through enzymatic treatment. In the food industry, researchers have harnessed the antioxidant properties of CBS to prevent lipid oxidation worldwide (Rojo-poveda et al., 2020). Recently, there has been a growing interest in the bioconversion of food processing residues into valuable products. Consequently, industrial countries are formulating strategic policies and strategies to address this aspect. Research and studies are being conducted in various fields to explore new applications for these byproducts. Notably, the food industry, livestock feed, and industrial utilization as a biofuel, absorbent, or composite are among the most common areas under investigation (Olatundun et al., 2020). This way, new alternatives to using cocoa bean shells (CBS) are being evaluated to help decrease their potentially harmful environmental aspects while generating value for this byproduct. Table 2.1 presents some recent studies involving cocoa byproducts. Pyrolysis is emerging to deal with cocoa byproducts. However, catalytic pyrolysis and reaction pathways remain insufficient and must be explored.

Table 2.1. Recent studies involving coca byproducts.

Biomass	Technique	Main discovery	Reference
Cocoa bean shell	Antioxidant activity determinations	significant antioxidant activity	Martínez et al. (2012)
Cocoa bean shell	densification into pellet	14.5 MJ/kg calorific value	Thompson et al. (2021)
Cocoa fruit shell	Pyrolysis	26% of acetic acid	Wijaya et al. (2020)
Cocoa bean shell	Pyrolysis	44% of acids, esters, and ketones	Grillo et al. (2019)
Cocoa shell	Pyrolysis	high-energy compounds generation	Mumbach et al. (2020)
Cocoa shell	Pyrolysis	biochar with satisfactory properties for CO_2 capture	Najafabadi et al. (2021)
Cocoa pod husks	Pyrolysis	53% of octadecadienoic acid	Adjin-Tetteh et al. (2018)
Cocoa pod husks	Combustion	41.7 GJ/year using cocoa pod husks from Uganda	Kilama et al. (2019)
Cocoa husks	Catalytic slow pyrolysis	bio-oil yield of 37%	Milian-Luperón et al. (2020)

2.4.Thermochemical Processes

The significance of renewable energy has been steadily increasing as environmental and energy supply concerns grow. Among renewable sources, biomass stands out as it provides the only replenishable fixed carbon source, a crucial element for fulfilling fuel and consumer goods demands (Lee et al., 2023). Primary renewable energy resources include wood, annual crops, agricultural and forestry residues, and biodegradable municipal solid and industrial waste components. Although converting residues into bio-energy is a substantial process, waste-to-energy remains insufficient worldwide (Ali et al., 2020). Moreover, biomass/waste-based energy from short-rotation forestry and energy crops can significantly contribute to achieving the Sustainable Development Goals (SDGs) by reducing greenhouse gas emissions and addressing climate change-related challenges. It can supply energy with high efficiency and low cost, besides avoiding the accumulation of CO_2 in the atmosphere (SDGR UN, 2022). Residues can be effectively converted into energy using thermal processes, wherein thermal decomposition occurs without oxygen (Arpit Singh et al., 2022). Different products can be obtained depending on the process parameters, such as temperature and residence time as shown in Figure 2.12. Charcoal production is favored at lower process temperatures and longer hot vapor residence times, while higher temperatures and longer residence times lead to increased biomass conversion into gas. Moderate temperatures and short residence times are ideal for producing liquids (Bridgwater, 2012). By adjusting these conditions, a wide range of product distributions can be achieved, providing considerable flexibility (Raza et al., 2021).

Thermal conversion often yields multiple and complex products in a short reaction time. Inorganic catalysts are frequently employed to enhance product quality or broaden their spectrum. Although combustion is a mature commercial technology widely adopted in industrialized and developing nations, extensive efforts are being directed toward addressing environmental concerns that combustion itself can not supply (Damartzis et al., 2011). Recently, pyrolysis at moderate temperatures around 500°C and terse reaction times of up to 2 seconds has gained significant interest. This process directly yields high liquid yields of up to 75 wt.%, making it attractive for various applications or as an efficient energy carrier (Bridgwater, 2018). On the other hand, gasification has been in practice for numerous years. Although there has been a more established technology, the number of fully operational and successful units remains limited (Li et al., 2021).

Mode	Conditions	Liquid	Solid	Gas
Fast	~500°C Short hot vapour residence time <2 s Short solid residence time up to 10 s	75 wt% (bio-oil)	12 wt% char	13 wt%
Intermediate	~400°C Moderate hot vapour residence time 5–20 s Moderate solid residence time up to 20 minutes	40 wt% in two phases	40 wt% char	20 wt%
Slow pyrolysis (Carbonisation)	~400°C Long hot vapour residence time up to hours depending on technology Long solid residence time depending on technology	30 wt% in two phases	35 wt% char	35 wt%
Gasification (allothermal)	~750–900°C Short hot vapour residence time 5 s Short solid residence time	Minimal	Up to 2 wt% char	Up to 98 wt%
Torrefaction (slow)	~250–300°C Solids residence time up to 30 mins	0 wt% unless vapours are condensed, then up to 15 wt%	70–80 wt% solid	15 wt%

Figure 2.12. Typical product yields from different types of pyrolysis (Bridgwater, 2018).

2.4.1. Fast Pyrolysis

Fast pyrolysis is a rapid biomass decomposition process that predominantly produces vapors and aerosols, along with some charcoal and gas. A dark brown liquid with a heating value of approximately half that of conventional fuel oil is obtained upon cooling and condensation (Balagurumurthy et., 2014). Fast pyrolysis proves particularly effective in yielding a substantial amount of liquid from low-ash biomass feeds. The key features of a fast pyrolysis process for liquid production include: (a) employment of finely ground biomass feed to facilitate very high heating and heat transfer rates at the biomass particle reaction interface, as biomass generally possesses low thermal conductivity; (b) precise control of the pyrolysis reaction temperature, usually around 500°C to maximize the liquid yield for most biomass types; (c) short residence times of the hot vapors to minimize secondary reactions; (d) swift removal of product char to prevent vapor cracking; and (e) rapid cooling of the pyrolysis vapors to obtain more significant liquid yield (Bridgwater, 2003; Bridgwater, 2006; Amutio et al., 2015). Fast pyrolysis involves processes occurring within a few seconds or less, where heat and mass transfer phenomena, phase transitions, and chemical reaction kinetics significantly influence the outcomes. It is a process that can be applied with different types of reactors such as fixed bed, fluidized bed, spouted bed, rotating cone,

microwave pyrolysis reactor, among others (Elordi et al., 2011). A critical challenge is ensuring the reacting biomass particles reach the optimal process temperature while minimizing exposure to lower temperatures that favor charcoal formation. This objective can be achieved using small particles and fluidized bed reactors or by rapidly transferring heat only to the particle surface (Guedes et al., 2018). A typical fast pyrolysis process (Figure 2.13) could contain the following stages: (a) pre-treatment of biomass to reduce its moisture content to typically less than 10%; (b) conversion of solid biomass into liquid energy (bio-oil) through fast pyrolysis; and (c) further processing and/or refining of primary liquid product to produce marketable end-products such as biofuels and chemicals (Bridgwater, 2018). Fast pyrolysis can be applied to any form of biomass, offering a versatile approach to bio-oil production with potential applications in various energy and chemical industries (Dai et al., 2020).

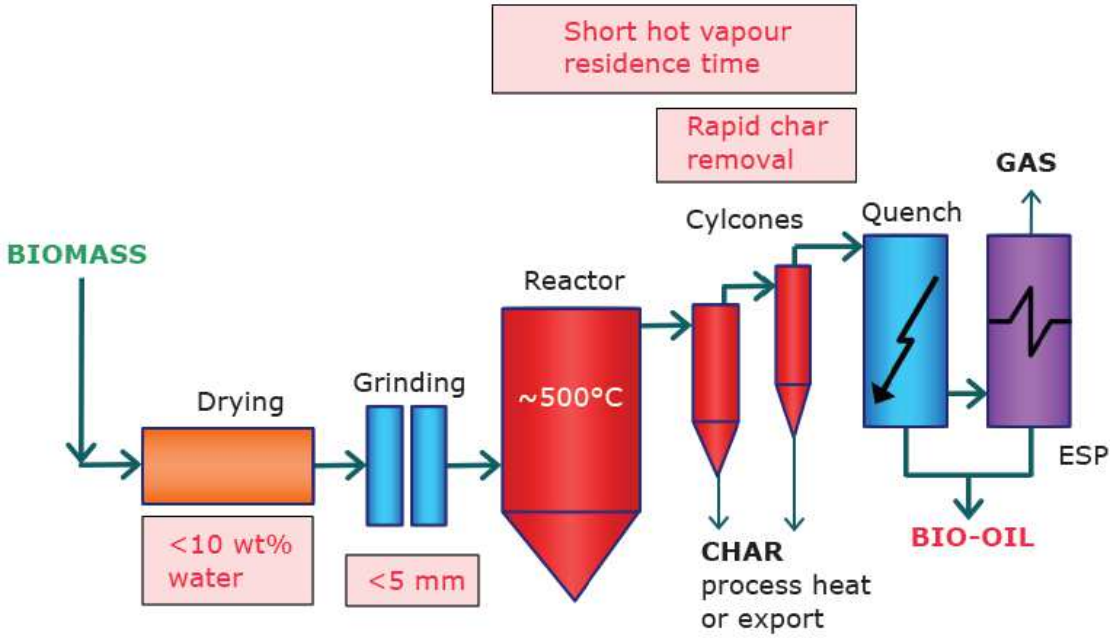


Figure 2.13. Conceptual fast pyrolysis process (Bridgwater, 2018).

2.4.2. Analytical Pyrolysis

Analytical pyrolysis-gas chromatography coupled with mass spectrometry (Py-GC/MS) serves as a robust tool for exploring the pyrolytic behavior, analyzing the composition of pyrolysis products, and studying synergistic effects during the pyrolysis of organic material. In this process, the material is pyrolyzed in a micro-pyrolyzer, and the resulting products are then analyzed using

gas chromatography (GC) (Mariyam et al., 2022). Capillary columns and mass spectrometers (MS) are commonly employed in Py-GC, with the detection system selected based on the specific analysis objectives (Li et al., 2022). The innovative Py-GC method for in-depth microstructural analysis using analytical pyrolysis was developed to significantly improve the reproducibility of data obtained through Py-GC. There are three main types of pyrolyzers: filament-type, Curie-point-type, and micro-furnace-type, all enabling rapid and precise heating with broad temperature control (Figure 2.14.) (Kumagai et al., 2020).

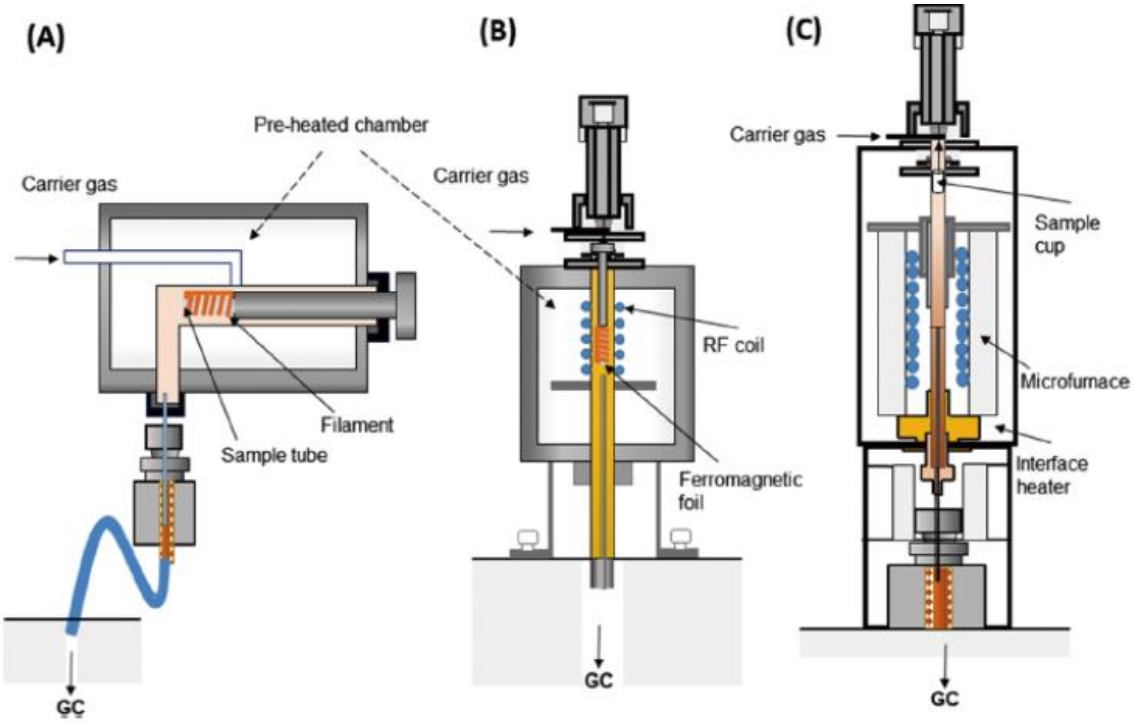


Figure 2.14. Schematic diagram of the different types of pyrolyzers currently used. (A) Filament type, (B) Currie-point type, and (C) micro-furnace type (Kumagai et al., 2020).

Analytical pyrolysis systems are designed with specific characteristics to ensure rapid decomposition of biomass macromolecules and accurate product analysis (Tamburini, 2021). These systems feature high heating rates (typically over 100°C/s) in micro-pyrolyzers, enabling fast heating to the target temperature. The retention time of pyrolysis vapors is kept short. Usually, less than 1/10 s and quick coupling with analytical equipment prevents secondary reactions. Additionally, good reproducibility is vital, and some systems achieve a relative standard deviation of 2% or less for the programs. Py-GC/MS is employed to examine the composition of pyrolysis

oil obtained from organic samples subjected to varying percentages of catalysts (Kumagai et al., 2020; Li et al., 2022; Yu et al., 2018). Semi-quantitative data is utilized to conduct principal component analysis, revealing notable distinctions in the composition of biomass pyrolysis oil. Moreover, the method involves investigating changes in the molecular composition of pyrolysis oils. The data processing typically relies on estimating chromatographic peak areas and utilizing brute formulas of identified pyrolysis products (Nardella et al., 2022).

Py-GC offers the advantage of investigating various materials and catalysts without any pretreatment, providing essential compositional and structural information straightforwardly. Analytical pyrolysis finds applications in multiple fields, such as environmental, biological, medical, forensic, cultural heritage, food, geochemical, polymer, and materials science, using new instrumentation and analytical methods based on pyrolysis reactions (Tamburini, 2021). Various feedstocks, such as woody biomass, herbaceous biomass, algal biomass, solid waste, and specific biomass components (cellulose, hemicellulose, lignin), are commonly employed in analytical pyrolysis systems (Kumagai et al., 2020; Ghysels et al., 2022; Santana Junior et al., 2019). Over time, the development of these systems has allowed the inclusion of liquid and gaseous samples as feedstocks, expanding their applications to other biomass thermochemical technologies like catalytic pyrolysis, oxidative pyrolysis, and gasification (Akalin et al., 2014). Applied pyrolysis involves developing pyrolytic processes for producing valuable chemicals, energy carriers (gas, liquid, and solid), materials from fossils, renewable feedstock, or waste, and material recycling and disposal of toxic substances. In both analytical and applied pyrolysis, Py-GC proves to be a promising technique for rapid and accurate analysis of pyrolyzates, aiding in understanding the pyrolysis reaction mechanism and facilitating the efficient screening of pyrolysis conditions (Šimkovic et al., 2023). Analytical pyrolysis is essential in studying biomass thermochemical conversion mechanisms and optimal reaction conditions that would assist technology developments in pyrolysis systems and their applications (Coralli et al., 2023). However, despite its significance, the application of analytical pyrolysis in various biomass thermochemical technologies still faces challenges. Although numerous quantitative methods have been reported for analyzing pyrolysis systems, improving the online analysis of heavy compounds remains a priority (Li et al., 2022).

Analytical and pilot scales represent distinct stages in developing and testing processes or products, particularly in research. The primary purpose of analytical experiments is to explore and

understand the fundamental principles of a process or to try a new concept. It is often the initial phase where researchers investigate feasibility and gather basic data (Kumagai et al., 2020). Experiments at this scale use smaller quantities of materials, which makes the process less costly. The environment can be well-controlled, enabling it to study specific variables in detail since the conditions can be easily manipulated for in-depth analysis (Li et al., 2022). The equipment and apparatus used are designed for minimal quantities, making the process more versatile and designed for flexibility in experimentation. However, setups that work well under the analytical pyrolysis may encounter unforeseen challenges when scaled up. This makes the analytical pyrolysis essential to test different setups before going to larger-scale operations (Ghysels et al., 2022).

A pilot-scale operation aims to validate and optimize processes that have shown promise in the analytical process. The focus is on replicating and refining the conditions observed in the laboratory on a larger scale. Operations at the pilot scale involve larger quantities and are often conducted in environments that mimic the conditions of full-scale production (Bird et al., 2022). The equipment used is more robust and designed to handle increased volumes. While still controlled, conditions at the pilot scale are closer to real-world scenarios. This allows for a more realistic assessment of factors influencing the process. Costs increase at the pilot scale due to the larger quantities of materials involved (Karmee et al., 2020). The pilot scale helps identify and address challenges associated with scaling up. It serves as an intermediate step before full-scale production, reducing the risks associated with direct scale-up from the laboratory (Fortuna et al., 1997).

In summary, the transition from analytical to pilot pyrolysis involves moving from exploring and understanding fundamental principles to validating and optimizing processes in a more realistic setting. Each scale serves a specific purpose in the research and development.

2.4.3. Operating parameters

The yield and composition of pyrolysis products can be significantly influenced by both process operating parameters and design configurations. This is primarily attributed to the complexity and diversity of chemical reactions involved, many of which remain largely unknown. Consequently, specific conditions may promote certain reactions over others (Barbosa et al., 2021). Key parameters and configurations impacting the process include the heating rate, pyrolysis temperature, the size of the pyrolyzed particle, biomass composition, the sweeping gas, retention

time of the vapors, type of reactor, and the presence or absence of a catalyst (Guedes et al., 2018). In the pyrolysis process, temperature plays a crucial role as it provides the necessary heat for breaking down the bonds present in biomass. As the temperature increases, the biomass conversion efficiency also improves due to the additional energy available for bond breakage. Various experimental studies have examined the influence of temperature on bio-oil yield, and it has been found that higher liquid yields are typically obtained within the temperature range of 450 to 550°C (Bridgwater, 2018). However, these optimal values may vary depending on the specific biomass used and other process variables. While an increase in temperature generally leads to a positive effect on liquid yield, extremely high temperatures can have the opposite effect, resulting in an increased gas yield. This phenomenon occurs because very high temperatures cause secondary cracking of the volatiles, leading to higher gas production. The optimal pyrolysis temperature for maximum liquid yield differs among different biomasses (Andrade et al., 2020). Additionally, the liquid's quality is affected by temperature variations. At lower temperatures, the bio-oil mainly consists of species such as long-chain fatty acids and esters, aliphatic nitriles, and amides. As the pyrolysis temperature increases, lower-molecular-weight compounds of alcohols, ketones, and their derivatives are formed due to subsequent decomposition reactions. The heating rate of the biomass decomposition process is a critical factor to consider. It can significantly impact the oxygen content of the resulting liquid phase (Akhtar et al., 2012; Wang et al., 2017). Higher heating rates tend to reduce the presence of oxygenates, leading to more outstanding production of gases like CO or CO_2 (Resende, 2016). During the pyrolysis process of biomass, a significant amount of vapor is generated. These pyrolysis vapors can undergo secondary reactions, including thermal cracking, repolymerization, and recondensation of the char residue, which ultimately leads to a decrease in bio-oil yield (Venderbosch et al., 2010). To mitigate these undesirable secondary reactions, rapidly removing the vapors from the reaction zone is crucial. For this purpose, nitrogen gas is commonly employed due to its inert nature, cost-effectiveness, and easy availability (Tripathi et al., 2016). Increasing the gas flow in the process results in a shorter residence time of the vapors in the hot pyrolysis zone. Numerous studies examining the impact of nitrogen flow in pyrolysis have indicated that higher inert gas flow enhances the bio-oil yield. However, extremely high gas flow rates can reduce the liquid yield because the vapors may not completely condense. Consequently, this increases the gas yield in the process (Sulaiman et al., 2011). The reaction time denotes the duration the biomass is exposed to the specific pyrolysis temperature. In batch process

operations, it is crucial to ensure that the reaction time is adequate to achieve the desired outcomes in the process. However, longer reaction times can lead to undesired secondary reactions of pyrolysis vapors, such as carbonization, gasification, and thermal cracking, ultimately reducing bio-oil production (Rossi et al., 2021b). Additionally, the reaction time significantly influences the design of the reactor. Prolonging the reaction time increases the secondary cracking reactions of the pyrolysis vapors. This can lead to the accumulation of char fines within the reactor tube and transfer line, which can be problematic (Pattiya et al., 2012). The composition of biomass used is another critical parameter influencing the pyrolysis process. Even the same type of biomass can exhibit variations in composition due to differences in soil, age, or planting conditions (Leng et al., 2020). These composition variations play a vital role in determining the composition and yield of the pyrolysis products. Biomasses containing more significant amounts of volatile material exhibit higher volatility and reactivity, favoring bio-oil production (Xie et al., 2015). Additionally, the ash content in biomass significantly impacts the proportions of pyrolysis products. A high ash content leads to a decrease in bio-oil yield while increasing the production of char and gases (Fakayode et al., 2020). In addition to biomass composition, particle size plays a significant role in determining the bio-oil yield during pyrolysis. Biomass is a poor heat conductor, making particle size a crucial factor in the process. Generally, smaller particles are preferred for pyrolysis because they heat up more quickly and uniformly, improving bio-oil production (Chagas et al., 2016; Akhtar et al., 2012).

2.5.Catalysts' use

Biomass fast pyrolysis involves a complex combination of simultaneous reactions, including dehydration, depolymerization, re-polymerization, fragmentation, and rearrangement. As a result, the bio-oil contains several different compounds, including various oxygenates, that contribute to undesirable properties such as low higher heating value (HHV), high corrosiveness, viscosity, and instability (Wang et al., 2015). These properties pose significant limitations on bio-oil application, especially as a transportation liquid fuel. To overcome these limitations, crude bio-oil must undergo upgrading before it can be used as a viable liquid biofuel (Ansah et al., 2018). Bio-oil upgrading aims to refine crude bio-oil into fine chemical or hydrocarbons that can integrate into petroleum refineries, enabling the production of green gasoline and diesel. This upgrading process involves the removal of oxygenated compounds from bio-oil through the formation of H_2O,

CO, and CO_2 while simultaneously reducing molecular weight and modifying chemical structures (Resende, 2016). Typically, bio-oil upgrading may involve multiple catalytic reactions like cracking, hydrodeoxygenation, decarbonylation, decarboxylation, denitrification, hydrocracking, or hydrogenation (Aniza et al., 2021). Specific catalysts are employed to produce targeted products, and each component in bio-oil may play a role in bio-oil upgrading reactions. The efficiency of bio-oil upgrading heavily relies on the catalysts' activity, selectivity, and energy efficiency. However, catalyst deactivation poses a significant challenge in developing active and stable catalysts. Among various methods, catalytic cracking and hydrodeoxygenation have shown great promise in upgrading crude bio-oils into liquid hydrocarbon biofuels (Fan et al., 2018). These techniques effectively reduce the content of oxygenated compounds while producing high yields of hydrocarbons (Barbosa et al., 2021). Heterogeneous catalysts, which have been successful in petroleum refining, also hold considerable promise for bio-oil upgrading. High-quality liquid products should have elevated carbon and hydrogen levels, while excessive oxygen content decreases the calorific value of bio-oil (He et al., 2018). Catalysts can be employed in two different configurations during the pyrolysis process: *in-situ* and *ex-situ*. In the *in-situ* configuration, the catalyst is mixed directly with the biomass inside the same reactor. This arrangement is more convenient to implement. However, it may hinder heat and mass transfers. Moreover, this configuration prevents the catalyst from operating at its optimal temperature as it needs to function under the pyrolysis temperature conditions (Huo et al., 2018). In contrast, in the *ex-situ* configuration, the catalyst is placed in a separate bed within the pyrolysis reactor. The volatiles generated during pyrolysis percolate through this bed, enabling the catalyst to function at its optimal temperature, which may differ from the pyrolysis temperature. This setup allows the catalyst to perform more efficiently (Guo et al., 2020). Furthermore, in *ex-situ* catalysis, unlike in the in-situ process, the catalyst can be recovered through regeneration processes, reducing the cost of bio-oil production (Wan et al., 2014). Catalysts of different natures have been tested to enhance bio-oil quality generated during the biomass pyrolysis process. Among these catalysts are acidic ones like y-Al_2O_3, silica-alumina, zeolites, and catalysts derived from niobic acid. Additionally, investigations have been conducted on noble metals, supported sulfides, and natural minerals such as bentonite as potential catalysts (Navarro et al., 2018).

2.5.1. Hydrotalcite (HTC)

Hydrotalcites are double hydroxides arranged in layers. They are derived from layers of brucite (MgOH) and have the formula $[M_{(1-x)}^{2+}\ M_x^{3+}(OH)_2]\bullet[A^{n-}]_{x/n}\bullet mH_2O$, where M^{2+} and M^{3+} occupy the six-coordinate octahedral interstitial sites for hydroxyl groups forming brucite-like compounds in sheets that stack up to create a layered structure. Consequently, charge-balancing anions (typically CO_3) and water molecules reside between these layers (Figure 2.15) (Lebedeva et al., 1999; Dębek et al., 2017).

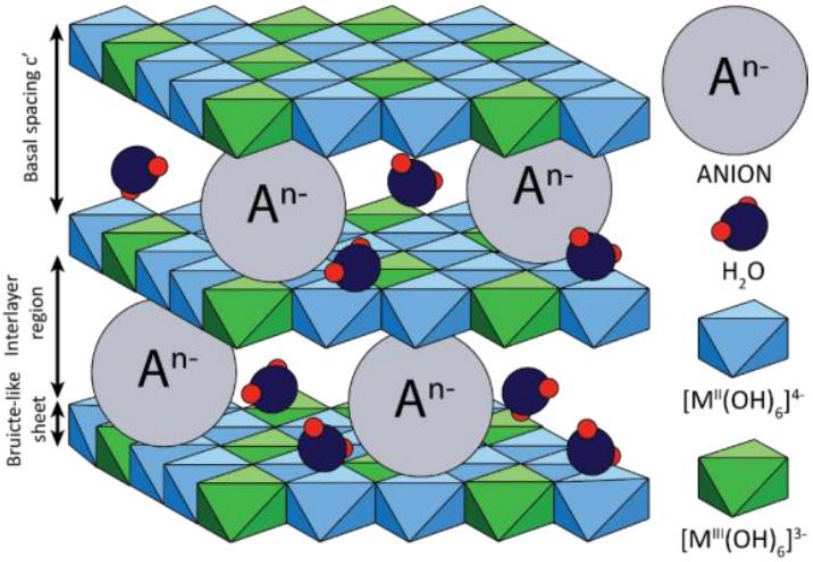


Figure 2.15. Schematic representation of the hydrotalcite structure (Dębek et al., 2017).

Subjecting hydrotalcite to high-temperature calcination breaks it down into Mg-Al mixed oxides, which control this catalyst's bifunctional (acid-basic) character (Xie et al., 2006). The versatility of hydrotalcite extends to various processes, including ion exchange, CO_2 capture, hosting bioactive molecules, serving as an adsorbent, and catalyst support. This adaptability is attributed to its advantages: notable surface area, structural stability, robust thermal stability, and the ability to regulate its basicity (Wiyantoko et al., 2015). The mixed oxides derived from hydrotalcite exhibit a dual nature with both acidic and basic sites. They make them conducive to deoxygenation reactions while concurrently curbing gas formation by controlling cracking reactions at acidic sites. For Mg-Al oxides, the catalyst's basicity hinges on the Mg/Al ratio, the composition of anions in between layers, and the applied heat treatment (Gholami et al., 2020;

Navarro et al., 2018). Several studies have probed the impact of varying Mg/Al ratios on oxide basicity, with findings indicating an elevation in basicity as the Mg/Al ratio rises (Goh et al., 2008; Díez et al., 2003). The bifunctional character might assist in eliminating nitrogen from bio-oil through the Hofmann elimination mechanism (Andrade et al., 2018; Prado et al., 2017). Within this mechanism, the acidic site protonates a heterocyclic nitrogen molecule's -NH- group, forming a nucleophilic amino -NH_2- species. Concurrently, the adjacent basic site attracts the β-H, leading to the cleavage of the C-N bond and subsequent nitrogen expulsion (Andrade et al., 2018; Prado et al., 2017).

2.5.2. Zeolite

The research engaged in catalysts to enhance the stability of bio-oil (preventing polymerization and condensation reactions), reducing its acidity, and elevating both energy density and the hydrogen-to-carbon effective ratio emerges primarily due to the lower-pressure and temperature operational required in catalytic pyrolysis (Zhang et al., 2017). To fulfill these objectives, applying catalytic pyrolysis employing diverse heterogeneous catalysts has been extensively explored (Lorenzetti et al., 2016; Ma et al., 2016). The selection of catalysts significantly influences the direct conversion of biomasses into high-quality bio-oil. Notably, zeolites are recognized as effective agents for bio-oil upgrading due to their uniform pore structure and appropriate acidity (Li et al., 2017; Vincent et al., 2017). Zeolites represent a category of microporous alumino-silicate materials which present exceptional selectivity and are widely employed in thermochemical procedures due to their remarkable hydrothermal character and reactivity (Nazir et al., 2020). The three-dimensional intersecting pore structure of the HZSM-5 catalyst is characterized by well-defined 10-membered rings with straight and sinusoidal channels, in which oxygenated organic compounds are removed (Olsbye et al., 2012; Zhang et al., 2015). Figure 2.16. shows the examples of zeolites structures and their micropore systems. Zeolites' diverse acid strengths and varying pore dimensions facilitate aromatic hydrocarbons' synthesis and catalyze bio-oil deoxygenation. These catalysts' pronounced acidity enables the breakdown of large molecules into smaller ones, promoting the oligomerization of ethylene and propylene, followed by cyclization within the catalyst's pores to generate aromatic compounds (Lazdovica et al., 2016). Further research on microporous zeolites HZSM-5, HBETA, and HY revealed the necessity to moderate the abundance of these acid sites, as an excess can lead to coke formation. Thus,

achieving a balance in these acid sites is crucial in catalyst design, as it directly impacts the selectivity of product formation (Aho et al., 2007; Bulushev et al., 2011).

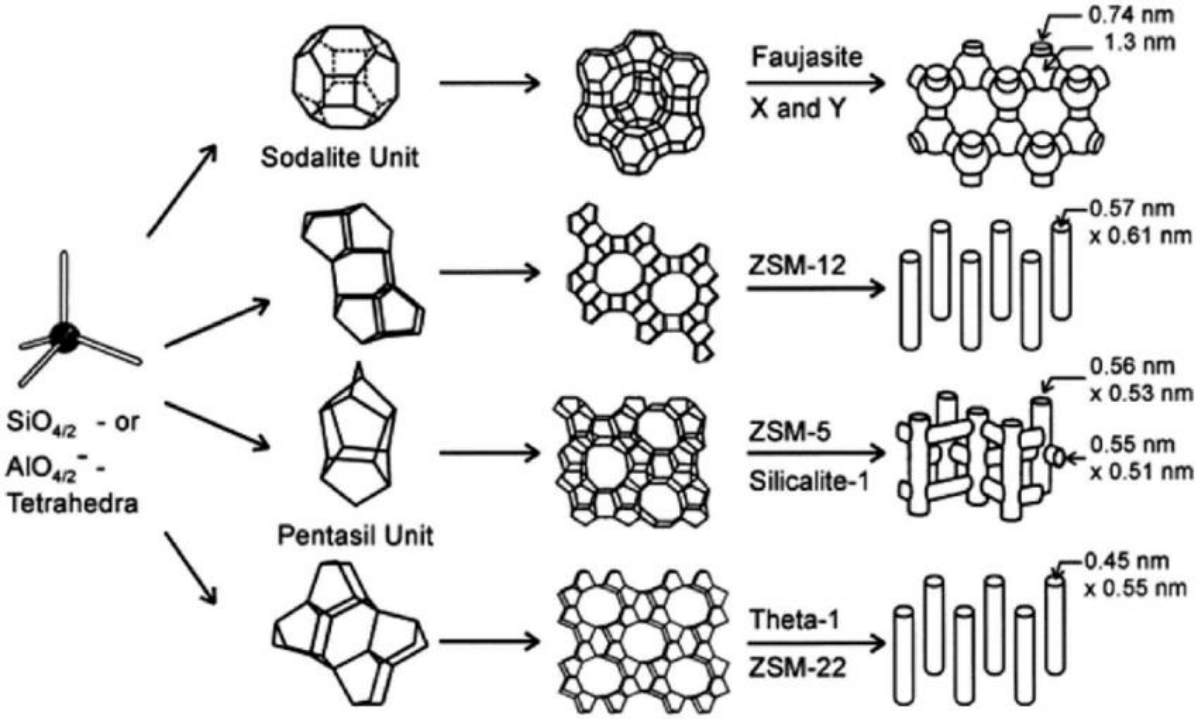


Figure 2.16. Examples of zeolites structures and their micropore systems (Nazir et al., 2020).

2.5.3. Catalysts derived from niobic acid

Over the past two decades, niobium has emerged as an interesting component in numerous catalytic systems with its incorporation into catalyst formulations. Contemporary catalytic research involving niobium materials encompasses various forms, including compounds/complexes, mixed bulk oxides, oxide supports, and surface niobium oxide phases (Ziolek et al., 2017). The niobium-containing mesoporous silicates have captivated researchers due to their well-ordered structures, substantial surface areas, and narrow pore size distributions (Wawrzynczak et al., 2018). Niobium oxide is renowned for its distinct capacity as a supportive matrix for metal and metal oxide catalysts due to its tendency to readily interact with numerous other oxides. Consequently, extensive exploration has been undertaken into various mixed metal oxides encompassing niobium, particularly within selective hydrocarbon oxidation (Ushikubo, 2000; Ziolek, 2003). Beyond its role as a catalyst component, niobium is increasingly recognized as an essential promoter in various applications. The intricate chemistry of niobium gives rise to its propensity to react with numerous

elements from the periodic table, resulting in an array of compounds and oxide phases with complex structures. Furthermore, this characteristic has fostered considerable expectations regarding their potential for a wide range of applications as constituents of industrial catalysts (Guerrero-Pérez et al., 2009). Niobium oxide (Nb_2O_5) is a highly efficient support material for metallic catalysts. A multitude of niobium-containing materials such as $NbCl_5$, NbF_5, NbH, NbS_2, NbN, NbC, NbOx, and niobium organometallic compounds have found catalytic utility. Furthermore, niobic acid can catalyze hydration, esterification, and condensation reactions (Guerrero-Pérez et al., 2009). In recent years, several reactions using niobium-based catalysts have been investigated, such as fatty acid esterification, glycerol and methanol dehydration, selective cyclohexene oxidation, and glycerol acetalization (García-Sancho et al., 2011; Ziolek et al., 2017). The role of niobium as a promoter significantly enhancing catalyst activity and selectivity is noteworthy. Equally significant is niobium's role in robust niobium-metal species interactions that facilitate electron transfer between transition metals, thus altering catalyst surface properties (Ziolek et al., 2017). In addition, niobium minerals have great importance in Brazil since it is one of the largest producers worldwide, producing around 40,000 metric tons annually (SoCientifica, 2002).

2.5.4. Thermochemical studies developed by the Faculty of Chemical Engineering at the Federal University of Uberlândia (FEQ-UFU) - A synthesized timeline

Figure 2.17 illustrates some essential research endeavors conducted by the Faculty of Chemical Engineering at the Federal University of Uberlândia (FEQ-UFU). Exploring thermochemical processes within the realm of renewable energy has emerged as a promising avenue, and FEQ-UFU has been notably active in this domain. Since 2012, the faculty has dedicated efforts to developing and optimizing pyrolysis processes, encompassing diverse reactor types (fixed and spouted beds), and employing various energy sources, including conventional, analytical, solar, and microwave methods.

This comprehensive research extends to evaluating a range of biomasses, spanning from commonly generated agro-industrial residues in Brazil to more esteemed biomasses such as microalgae. A pivotal aspect of the investigation involves using catalysts to enhance biofuels' physicochemical characteristics. FEQ-UFU's exploration includes both commercially available

catalysts like zeolite as well as catalysts synthesized in-house, such as hydrotalcite. Additionally, the faculty delves into catalysts derived from locally abundant metals, such as niobium.

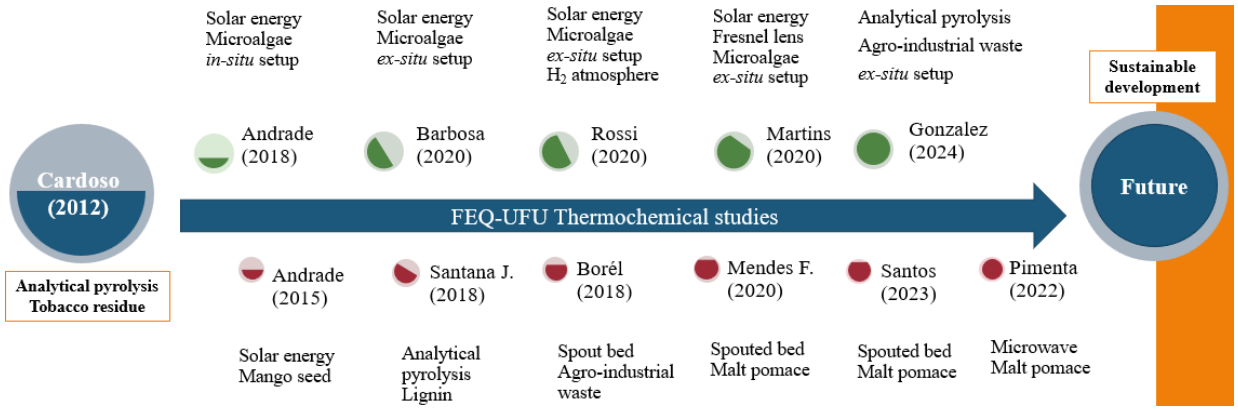


Figure 2.17. Thermochemical studies developed by the FEQ-UFU - A synthesized timeline.

These research endeavors significantly contribute to advancing scientific knowledge aligned with the United Nations' sustainable objectives, particularly in pursuing sustainable development in energy usage and generation.

2.6.References

Adjin-Tetteh, M., Asiedu, N., Dodoo-Arhin, D., Karam, A., Amaniampong, P.N. (2018). Thermochemical conversion and characterization of cocoa pod husks a potential agricultural waste from Ghana. Industrial Crops and Products, 119, 304–312. https://doi.org/10.1016/j.indcrop.2018.02.060

AgroBioHeat (2022). A guide for agro-industrial residues to energy, Promoting the penetration of agro-biomass in European rural areas. Grant Agreement No. 818369

Aho, A., Kumar, N., Eränen, K., Salmi, T., Hupa, M., Murzin, D.Y. (2007), Catalytic pyrolysis of biomass in a fluidized bed reactor: influence of the acidity of H-beta zeolite, Process Saf Environ Prot, 85, 473–80. https://doi.org/10.1205/psep07012

Akalin, M.K., Karagöz, S. (2014), Analytical pyrolysis of biomass using gas chromatography coupled to mass spectrometry, TrAC - Trends in Analytical Chemistry, 61, 11–16. https://doi.org/10.1016/j.trac.2014.06.006

Akhtar, J., Saidina Amin, N. (2012), A review on operating parameters for optimum liquid oil yield in biomass pyrolysis, Renew. Sustain. Energy Rev., 16, 5101–5109. https://doi.org/10.1016/j.rser.2012.05.033

Ali, J., Rasheed, T., Afreen, M., Anwar, M. T., Nawaz, Z., Anwar, H., Rizwan, K. (2020), Modalities for conversion of waste to energy — Challenges and perspectives, Science of the Total Environment, 727, 138610. https://doi.org/10.1016/j.scitotenv.2020.138610

Amenaghawon, A.N., Anyalewechi, C.L., Okieimen, C.O., Kusuma, H.S. (2021), Biomass pyrolysis technologies for value-added products: a state-of-the-art review, In Environment, Development and Sustainability, 23, 10. https://doi.org/10.1007/s10668-021-01276-5

Amutio, M., Lopez, G., Alvarez, J., Olazar, M., Bilbao, J. (2015), Fast pyrolysis of eucalyptus waste in a conical spouted bed reactor, Bioresource Technology, 194, 225–232. https://doi.org/10.1016/j.biortech.2015.07.030

Andrade, L.A., Barbosa, J.M., Barrozo, M.A.S., Vieira, L.G.M. (2020), A comparative study of the behavior of Chlamydomonas reinhardtii and Spirulina platensis in solar catalytic pyrolysis, Energy Research, 1–15. https://doi.org/10.1002/er.5289

Andrade, L.A., Barrozo, M.A.S, Vieira, L.G.M. (2018), Catalytic solar pyrolysis of microalgae Chlamydomonas reinhardtii, Solar Energy, 173, 928–938. https://doi.org/10.1016/j.solener.2018.08.035

Aniza, R., Chen, W.H., Lin, Y.Y., Tran, K.Q., Chang, J.S., Lam, S.S., Park, Y.K., Kwon, E.E., Tabatabaei, M. (2021), Independent parallel pyrolysis kinetics of extracted proteins and lipids as well as model carbohydrates in microalgae, Applied Energy, 300, 117372. https://doi.org/10.1016/j.apenergy.2021.117372

Ansah, E., Wang, L., Zhang, B., Shahbazi, A. (2018), Catalytic pyrolysis of raw and hydrothermally carbonized Chlamydomonas debaryana microalgae for denitrogenation and production of aromatic hydrocarbons, Fuel, 228, 234–242. https://doi.org/10.1016/j.fuel.2018.04.163

Arpit Singh, T., Sharma, M., Sharma, M., Dutt Sharma, G., Kumar Passari, A., Bhasin, S. (2022), Valorization of agro-industrial residues for production of commercial biorefinery products, Fuel, 322, 124284. https://doi.org/10.1016/j.fuel.2022.124284

Balagurumurthy, B, Bhaskar, T. (2014), Hydropyrolysis of lignocellulosic biomass: state of the art review, Biomass Conversion and Biorefinery, 4, 67-75, https://doi.org/10.1007/s13399-013-0086-2.

Banja, M., Sikkema, R., Jégard, M., Motola, V., Dallemand, J.F. (2019), Biomass for energy in the EU – The support framework. Energy Policy, 131, 215–228. https://doi.org/10.1016/j.enpol.2019.04.038

Barbosa, J.M., Rossi, R.A.S., Vieira, L.G.M., Barrozo, M.A.S. (2021), A study of optimization of solar pyrolysis and catalyst recovery and reuse, Energy Conversion and Management, 237, 114094. https://doi.org/10.1016/j.enconman.2021.114094

Bird, H., Heidrich, E.S., Leicester, D.D., Theodosiou, P. (2022). Pilot-scale Microbial Fuel Cells (MFCs): A meta-analysis study to inform full-scale design principles for optimum wastewater treatment. Journal of Cleaner Production, 346, 131227. https://doi.org/10.1016/j.jclepro.2022.131227

Boateng, A.A., Mullen, C.A., Goldberg, N.M., Hicks, K.B., Devine, T.E., Lima, IM., McMurtrey, J.E. (2010). Sustainable production of bioenergy and biochar from the straw of high-biomass soybean lines via fast pyrolysis. Environmental Progress & Sustainable, 29, 2. https://doi.org/10.1002/ep.10446

Bridgwater, A.V. (2003), Renewable fuels and chemicals by thermal processing of biomass, Chemical Engineering Journal, 91, 87–102. https://doi.org/10.1016/S1385-8947(02)00142-0

Bridgwater, A.V. (2012), Review of fast pyrolysis of biomass and product upgrading, Biomass and Bioenergy, 38, 68–94. https://doi.org/10.1016/j.biombioe.2011.01.048

Bridgwater, B.T. (2018), Challenges and Opportunities in Fast Pyrolysis of Biomass: Part I, Johnson Matthey Technology Review, 62, 118–130. https://doi.org/10.1595/205651318X696693

Bridgwater, T. (2006), Review Biomass for energy, Journal of the Science of Food and Agriculture, https://doi.org/10.1002/jsfa.2605

Bulushev, D.A., Ross, J.R. (2011), Catalysis for conversion of biomass to fuels via pyrolysis and gasification: a review, Catal. Today, 171, 1–13. https://doi.org/10.1016/j.cattod.2011.02.005

Campos-Vega, R., Nieto-Figueroa, K.H., Oomah, B.D. (2018), Cocoa (Theobroma cacao L.) pod husk: Renewable source of bioactive compounds, Trends in Food Science and Technology, 81, 172–184. https://doi.org/10.1016/j.tifs.2018.09.022

Capanoglu, E., Nemli, E., Tomas-Barberan, F. (2022), Novel Approaches in the Valorization of Agricultural Wastes and Their Applications, Journal of Agricultural and Food Chemistry, 70(23), 6787–6804. https://doi.org/10.1021/acs.jafc.1c07104

Chagas, B.M.E., Dorado, C., Serapiglia, M.J., Mullen, C.A., Boateng, A.A., Melo, M.A F., Ataíde, C.H. (2016), Catalytic pyrolysis-GC/MS of Spirulina: Evaluation of a highly proteinaceous

biomass source for production of fuels and chemicals, Fuel, 179, 124–134. https://doi.org/10.1016/j.fuel.2016.03.076

Chagas, P., Oliveira, H.S., Mambrini, R., Le Hyaric, M., Almeida, M.V., Oliveira, L.C.A. (2013), A novel hydrofobic niobium oxyhydroxide as catalyst: Selective cyclohexene oxidation to epoxide, Appl. Catal. A: Gen., 454, 88–92. https://doi.org/10.1016/j.apcata.2013.01.007

Cho, E.J., Trinh, L.T.P., Song, Y., Lee, Y.G., Bae, H.J. (2020), Bioconversion of biomass waste into high value chemicals. Bioresource Technology, 298, 122386. https://doi.org/10.1016/j.biortech.2019.122386

Chum, H., Faaij, J., Moreira, G., Berndes, P., Dhamija, H., Dong, B., Gabrielle, A., Goss Eng, W., Lucht, M., Mapako, O., Masera Cerutti, T., McIntyre, T., Minowa, K. (2011), Bioenergy. In IPCC Special Report on Renewable Energy Sources and Climate Change Mitigation, Cambridge University Press, Cambridge, United Kingdom and New York, NY, USA.

Coralli, I., Fabbri, D., Facchin, A., Torri, C., Stevens, L. A., Snape, C.E. (2023), Analytical pyrolysis of polyethyleneimines, Journal of Analytical and Applied Pyrolysis, 169, 105838. https://doi.org/10.1016/j.jaap.2022.105838

Dai, L., Wang, Y., Liu, Y., He, C., Ruan, R., Yu, Z., Jiang, L., Zeng, Z., Wu, Q. (2020), A review on selective production of value-added chemicals via catalytic pyrolysis of lignocellulosic biomass, Science of the Total Environment, 749, 142386. https://doi.org/10.1016/j.scitotenv.2020.142386

Damartzis, T., Zabaniotou, A. (2011), Thermochemical conversion of biomass to second generation biofuels through integrated process design-A review, Renewable and Sustainable Energy Reviews, 15(1), 366–378. https://doi.org/10.1016/j.rser.2010.08.003

Dębek, R., Motak, M., Grzybek, T., Galvez, M. E., Da Costa, P. (2017), A short review on the catalytic activity of hydrotalcite-derived materials for dry reforming of methane, Catalysts, 7(1), 1–25. https://doi.org/10.3390/catal7010032

Destek, M.A., Sarkodie, S.A., Asamoah, E.F. (2021), Does biomass energy drive environmental sustainability? An SDG perspective for top five biomass consuming countries, Biomass Bioenergy 149, 106076. https://doi.org/10.1016/j.biombioe.2021.106076

Díez, V.K., ApesteguiA, C.R., Cosimo, D.I. (2003), Effect of the acid-base propertirs of MgAl mixed oxides on the catalyst deactivation during aldol condensation reactions, Latin Amerian Applied Research, 33, 79-86. https://doi.org/10.1016/j.apcata.2011.03.053

DNV. (2022), Energy Transition Outlook, A global and regional forecast to 2050, DNV_Energy_Transition_Outlook_Executive_summary_2022.pdf

EGR. (2022), Emissions Gap Report, The Closing Window Climate crisis calls for rapid transformation of societies, file:///C:/Users/raiss/Documents/Ra%C3%ADssa/Material%20Estudo/Artigos/Climate%20change/EGR2022.pdf

Elordi, G., Olazar, M., Lopez, G., Artetxe, M., Bilbao, J. (2011), Product yields and compositions in the continuous pyrolysis of high-density polyethylene in a conical spouted bed reactor, Industrial and Engineering Chemistry Research, 50(11), 6650–6659. https://doi.org/10.1021/ie200186m

Fakayode, O.A., Aboagarib, E.A.A., Zhou, C., Ma, H. (2020), Co-pyrolysis of lignocellulosic and macroalgae biomasses for the production of biochar – A review, Bioresource Technology, 297, 122408. https://doi.org/10.1016/j.biortech.2019.122408

Fan, L., Chen, P., Zhou, N., Liu, S., Zhang, Y., Liu, Y., Wang, Y., Omar, M.M., Peng, P., Addy, M., Cheng, Y., Ruan, R. (2018), In-situ and ex-situ catalytic upgrading of vapors from microwave-assisted pyrolysis of lignin, Bioresource Technology, 247, 851–858. https://doi.org/10.1016/j.biortech.2017.09.200

FAOSTAT. (2021), Food and agriculture organization of the United Nation, https://www.fao.org/faostat/en/#home , [on-line accessed 01-08-2022, 13:30h].

Fellner, J., Schwarzböck, T. (2021), Performance impairment of Waste to Energy plants during waste delivery times – An analysis of relevant operating parameter, Waste Management, 124, 303–313. https://doi.org/10.1016/j.wasman.2021.02.022

Fortuna, F., Cornacchia, G., Mincarini, M., Sharma, V.K. (1997). Pilot-scale experimental pyrolysis plant: Mechanical and operational aspects. Journal of Analytical and Applied Pyrolysis, 40–41, 403–417. https://doi.org/10.1016/S0165-2370(97)00026-0

Gao, J., Zhang, L. (2021), Does biomass energy consumption mitigate CO2 emissions? The role of economic growth and urbanization: evidence from developing Asia, J. Asia Pac. Econ., 26 (1) 96-115. https://doi.org/10.1080/13547860.2020.1717902

García-Sancho, C., Moreno-Tost, R., Mérida-Robles, J.M., Santamaría-González, J., Jiménez-López, A., Maireles-Torres, P. (2011), Niobium-containing MCM-41 silica catalysts for biodiesel production, Applied Catalysis B: Environmental, 108, 161–167. https://doi.org/10.1016/j.apcatb.2011.08.025

GBS. (2020), Global Bioenergy Statistics, World Bioenergy Association, https://worldbioenergy.org/uploads/201210%20WBA%20GBS%202020.pdf

GBS. (2022). Global Bioenergy Statistics, World Bioenergy Association. https://www.worldbioenergy.org/uploads/221223%20WBA%20GBS%202022.pdf

Gholami, Z., Tišler, Z., Velvarská, R., Kocík, J. (2020), Comn catalysts derived from hydrotalcite-like precursors for direct conversion of syngas to fuel range hydrocarbons, Catalysts, 10(8). https://doi.org/10.3390/catal10080813

Ghysels, S., Rathnayake, D., Maziarka, P., Mašek, O., Sohi, S., Ronsse, F. (2022), Biochar stability scores from analytical pyrolysis (Py-GC-MS), Journal of Analytical and Applied Pyrolysis, 161. https://doi.org/10.1016/j.jaap.2021.105412

Goh, K.H., Lim, T.T., Dong, Z. (2008), Application of layered double hydroxides for the removal of oxyanions, Water Res., 42, 1343-1368. https://doi.org/10.1016/j.watres.2007.10.043

Grillo, G., Boffa, L., Binello, A., Mantegna, S., Cravotto, G., Chemat, F., Dizhbite, T., Lauberte, L., Telysheva, G. (2019). Cocoa bean shell waste valorisation; extraction from lab to pilot-scale cavitational reactors. Food Research International, 115, 200–208. https://doi.org/10.1016/j.foodres.2018.08.057

Guedes, R.E., Luna, A.S., Torres, A.R. (2018), Journal of analytical and applied pyrolysis operating parameters for bio-oil production in biomass pyrolysis: a review, J. Anal. Appl. Pyrol., 129, 134-149, https://doi.org/10.1016/j.jaap.2017.11.019

Guerrero-Pérez, M.O., Bañares, M.A. (2009), Niobium as promoting agent for selective oxidation reactions, Catalysis Today, 142, 245–251. https://doi.org/10.1016/j.cattod.2008.10.041

Guo, F., Jia, X., Liang, S., Zhou, N., Chen, P., Ruan, R. (2020), Development of biochar-based nanocatalysts for tar cracking/reforming during biomass pyrolysis and gasification, Bioresource Technology, 298, 122263. https://doi.org/10.1016/j.biortech.2019.122263

Gyamfi, B.A., Ozturk, I, Bein, M.A., Bekun, F.V. (2021), An investigation into the anthropogenic effect of biomass energy utilization and economic sustainability on environmental degradation in E7 economies, Biofuels, Bioproducts and Biorefining, 15(3), 840-851. https://doi.org/10.1002/bbb.2206

He, Z., Jiao, Q., Fang, Z., Li, T., Feng, C., Li, H., Zhao, Y. (2018), Light olefin production from catalytic pyrolysis of waste tires using nano-HZSM-5/Γ-Al2O3 catalysts, Journal of Analytical and Applied Pyrolysis, 129, 66–71. https://doi.org/10.1016/j.jaap.2017.12.002

Huo, X., Xiao, J., Song, M., Zhu, L. (2018), Comparison between in-situ and ex-situ catalytic pyrolysis of sawdust for gas production, Journal of Analytical and Applied Pyrolysis, 135, 189–198. https://doi.org/10.1016/j.jaap.2018.09.003

IEA. (2017), (International Energy Agency), Mobilization of agricultural residues for bioenergy and higher value bio-products: Resources, barriers and sustainability, IEA Bioenergy Task, 43:1.

IEA. (2021), Net Zero by 2050, A Roadmap for the Global Energy Sector, https://iea.blob.core.windows.net/assets/deebef5d-0c34-4539-9d0c-10b13d840027/NetZeroby2050-ARoadmapfortheGlobalEnergySector_CORR.pdf

IEA. (2022), International Energy Agency, World Energy Outlook, https://iea.blob.core.windows.net/assets/830fe099-5530-48f2-a7c1-11f35d510983/WorldEnergyOutlook2022.pdf

IPCC. (2018), Summary for Policymakers. In: Global Warming of 1.5°C. An IPCC Special Report on the impacts of global warming of 1.5°C above pre-industrial levels and related global greenhouse gas emission pathways, in the context of strengthening the global response to the threat of climate change, sustainable development, and efforts to eradicate poverty [Masson-Delmotte, V., P. Zhai, H.-O. Pörtner, D. Roberts, J. Skea, P.R. Shukla, A. Pirani, W. Moufouma-Okia, C. Péan, R. Pidcock, S. Connors, J.B.R. Matthews, Y. Chen, X. Zhou, M.I. Gomis, E. Lonnoy, T. Maycock, M. Tignor, and T. Waterfield (eds.)]. Cambridge University Press, Cambridge, UK and New York, NY, USA, pp. 3-24. https://doi.org/10.1017/9781009157940.001.

Jha, S., Nanda, S., Acharya, B., Dalai, A.K. (2022), A Review of Thermochemical Conversion of Waste Biomass to Biofuels, Energies, 15 (17), 1–23. https://doi.org/10.3390/en15176352

Karmee, S.K., Kumari, G., Soni, B. (2020). Pilot scale oxidative fast pyrolysis of sawdust in a fluidized bed reactor: A biorefinery approach. Bioresource Technology, 318, 124071. https://doi.org/10.1016/j.biortech.2020.124071

Kee, S.H., Ganeson, K., Rashid, N.F.M., Yatim, A.F.M., Vigneswari, S., Amirul, A.A.A., Ramakrishna, S., Bhubalan, K. (2022), A review on biorefining of palm oil and sugar cane agro-industrial residues by bacteria into commercially viable bioplastics and biosurfactants, Fuel, 321, 124039. https://doi.org/10.1016/j.fuel.2022.124039

Kilama, G., Lating, P.O., Byaruhanga, J., Biira, S. (2019). Quantification and characterization of cocoa pod husks for electricity generation in Uganda. Energy, Sustainability and Society, 9 (1). https://doi.org/10.1186/s13705-019-0205-4

Kley Valladares-Diestra, K., Porto de Souza Vandenberghe, L., Ricardo C. (2022), A biorefinery approach for pectin extraction and second-generation bioethanol production from cocoa pod husk, Bioresource Technology, 346, 126635. https://doi.org/10.1016/j.biortech.2021.126635

Kumagai, S., Yoshioka, T. (2020), Latest Trends in Pyrolysis Gas Chromatography for Analytical and Applied Pyrolysis of Plastics, Analytical Sciences, 37(1), 145–157. https://doi.org/10.2116/ANALSCI.20SAR04

Lazdovica K, Liepina L, Kampars V. (2016), Catalytic pyrolysis of wheat bran for hydrocarbons production in the presence of zeolites and noble-metals by using TGA-FTIR method, Bioresour. Technol., 207, 26–33. https://doi.org/10.1016/j.biortech.2016.01.117

Lebedeva, O., Tichit, D., Coq, B. (1999), Influence of the compensating anions of Ni/Al and Ni/Mg/Al layered double hydroxides on their activation under oxidising and reducing atmospheres, Applied Catalysis A: General, 183(1), 61–71. https://doi.org/10.1016/S0926-860X(99)00039-3

Lee, J., Lin, K.Y.A., Jung, S., Kwon, E.E. (2023), Hybrid renewable energy systems involving thermochemical conversion process for waste-to-energy strategy, Chemical Engineering Journal, 452, 139218. https://doi.org/10.1016/j.cej.2022.139218

Leng, L., Yang, L., Chen, J., Leng, S., Li, H., Li, H., Yuan, X., Zhou, W., Huang, H. (2020), A review on pyrolysis of protein-rich biomass: Nitrogen transformation, Bioresource Technology, 315, 123801. https://doi.org/10.1016/j.biortech.2020.123801

Li, H., Wang, Y., Zhou, N., Dai, L., Deng, W., Liu, C., Cheng, Y., Liu, Y., Cobb, K., Chen, P., Ruan, R. (2021), Applications of calcium oxide–based catalysts in biomass pyrolysis/gasification – A review, Journal of Cleaner Production, 291, 125826. https://doi.org/10.1016/j.jclepro.2021.125826

Li, N., Bi, Y., Xia, X., Chen, H., Hu, J. (2017). H,drodeoxygenation of methyl laurate over ni catalysts supported on hierarchical HZSM-5 zeolite, Catalysts, 7(12). https://doi.org/10.3390/catal7120383

Li, T., Su, J., Wang, C., Watanabe, A., Teramae, N., Ohtani, H., Wang, K. (2022), Advances in the development and application of analytical pyrolysis in biomass research: A review, Energy Conversion and Management, 271, 116302. https://doi.org/10.1016/j.enconman.2022.116302

Lim, K.Y., Foo, K.Y. (2022), One-step synthesis of carbonaceous adsorbent from soybean bio-residue by microwave heating: Adsorptive, antimicrobial and antifungal behavior, Environmental Research, 204, 112044. https://doi.org/10.1016/j.envres.2021.112044

Lorenzetti, C., Conti, R., Fabbri, D., Yanik, J. (2016), A comparative study on the catalytic effect of H-ZSM5 on upgrading of pyrolysis vapors derived from lignocellulosic and proteinaceous biomass, Fuel, 166, 446-452. https://doi.org/10.1016/j.fuel.2015.10.051

Ma, C., Yu, J., Wang, B., Song, Z., Zhou, F., Xiang, J., Hu, S., Sun, L. (2016), Influence of Zeolites and Mesoporous Catalysts on Catalytic Pyrolysis of Brominated Acrylonitrile–Butadiene–Styrene (Br-ABS), Energy Fuels, 30(6), 4635-4643. https://doi.org/10.1021/acs.energyfuels.6b00460

Majeed, M.T., Luni, T., Tahir, T. (2022), Growing green through biomass energy consumption: the role of natural resource and globalization in a world economy, Environmental Science and Pollution Research, 29(22), 33657–33673. https://doi.org/10.1007/s11356-021-18017-w

Marc, J., Rogoff, F.S. (2019), Waste-to-Energy, Technologies and Project Implementation, 3rd Edition - March 9, 2019, William Andrew, Oxford, UK. ISBN: 9780128160800

Mariyam, S., Alherbawi, M., Rashid, N., Al-Ansari, T., McKay, G. (2022), Bio-Oil Production from Multi-Waste Biomass Co-Pyrolysis Using Analytical Py–GC/MS, Energies, 15(19). https://doi.org/10.3390/en15197409

Martínez, R., Torres, P., Meneses, M.A., Figueroa, J.G., Pérez-Álvarez, J.A., Viuda-Martos, M. (2012). Chemical, technological and in vitro antioxidant properties of cocoa (Theobroma cacao L.) co-products. Food Research International, 49 (1), 39–45. https://doi.org/10.1016/j.foodres.2012.08.005

Milian-Luperón, L., Hernández-Rodríguez, M., Falcón-Hernández, J., Otero-Calvis, A. (2020). Obtaining bioproducts by slow pyrolysis of coffee and cocoa husks as suitable candidates for being used as soil amendment and source of energy. Revista Colombiana de Quimica, 49 (2), 23–29. https://doi.org/10.15446/rev.colomb.quim.v49n2.83231

Módenes, A.N., Hinterholz, C.L., Neves, C.V., Sanderson, K., Trigueros, D.E.G., Espinoza-Quiñones, F.R., Borba, C.E., Steffen, V., Scheufele, F.B., Kroumov, A.D. (2019). A new alternative to use soybean hulls on the adsorptive removal of aqueous dyestuff. Bioresource Technology Reports, 6, 175–182. https://doi.org/10.1016/j.biteb.2019.03.004

Mumbach, G.D., Alves, J.L.F., Silva, J.C.G., Domenico, M., Sena, R.F., Marangoni, C., Machado, R.A.F., Bolzan, A. (2020). Pyrolysis of cocoa shell and its bioenergy potential: evaluating the kinetic triplet, thermodynamic parameters, and evolved gas analysis using TGA-FTIR. Biomass Conversion and Biorefinery, 12, 723–739. https://doi.org/10.1007/s13399-020-01058-5

Najafabadi, H.A., Ozalp, N., Davis, R.A. (2021). Biochar from Cocoa Shell Pyrolysis: Potential Sorbent for CO2 Capture. Journal of Energy Resources Technology, Transactions of the ASME, 143 (2), 1–8. https://doi.org/10.1115/1.4047765

Nardella, F., Bellavia, S., Mattonai, M., Ribechini, E. (2022), Co-pyrolysis of biomass and plastic: Synergistic effects and estimation of elemental composition of pyrolysis oil by analytical pyrolysis–gas chromatography/mass spectrometry, Bioresource Technology, 354, 127170. https://doi.org/10.1016/j.biortech.2022.127170

Navarro, R.M., Guil-Lopez, R., Fierro, J.L.G., Mota, N., Jiménez, S., Pizarro, P., Serrano, D.P. (2018), Catalytic fast pyrolysis of biomass over Mg-Al mixed oxides derived from hydrotalcite-like precursors: Influence of Mg/Al ratio, J. of Analytical and Ap. Pyrolysis, 134, 362–370. https://doi.org/10.1016/j.jaap.2018.07.001

Nazir, L.S.M., Yeong, Y.F., Chew, T.L. (2020), Methods and synthesis parameters affecting the formation of FAU type zeolite membrane and its separation performance: a review, Journal of Asian Ceramic Societies, 8(3), 553–571. https://doi.org/10.1080/21870764.2020.1769816

Olatundun, E.A., Borokini, O.O., Betiku, E. (2020), Cocoa pod husk-plantain peel blend as a novel green heterogeneous catalyst for renewable and sustainable honne oil biodiesel synthesis: A case

of biowastes-to-wealth, Renewable Energy, 166, 163–175. https://doi.org/10.1016/j.renene.2020.11.131

Oliveira, T.J.P., Cardoso, C.R., Ataíde, C.H. (2015). Fast pyrolysis of soybean hulls: Analysis of bio-oil produced in a fluidized bed reactor and of vapor obtained in analytical pyrolysis. Journal of Thermal Analysis and Calorimetry, 120 (1), 427–438. https://doi.org/10.1007/s10973-015-4600-6

Olsbye, U., Svelle, S., Bjorgen, M., Beato, P., Janssens, T.V.W., Joensen, F., Bordiga, S., Lillerud, K.P. (2012), Conversion of methanol to hydrocarbons: how zeolite cavity and pore size controls product selectivity, Angew. Chem. Int., 51, 5810–5831. https://doi.org/10.1002/anie.201103657

OWD. (2022), Our World in Data is a project of the Global Change Data Lab., https://ourworldindata.org/grapher/global-energy-substitution?time=1900..latest&facet=none, [on-line accessed, 21-07-2023, 10:00h].

Pan, S.Y., Du, M.A., Huang, I.T., Liu, I.H., Chang, E.E., Chiang, P.C. (2015), Strategies on implementation of waste-to-energy (WTE) supply chain for circular economy system: a review, Journal of Cleaner Production, 108, 409–421. https://doi.org/10.1016/j.jclepro.2015.06.124

Pattiya, A., Sukkasi, S., Goodwin, V. (2012), Fast pyrolysis of sugarcane and cassava residues in a free-fall reactor, Energy, 44, 1067-1077. https://doi.org/10.1016/j.energy.2012.04.035

Pilafidis, S., Diamantopoulou, P., Gkatzionis, K., Sarris, D. (2022), Valorization of Agro-Industrial Wastes and Residues through the Production of Bioactive Compounds by Macrofungi in Liquid State Cultures: Growing Circular Economy, Applied Sciences (Switzerland), 12(22). https://doi.org/10.3390/app122211426

Porto de Souza Vandenberghe, L., Kley Valladares-Diestra, K., Amaro Bittencourt, G., Fátima Murawski de Mello, A., Sarmiento Vásquez, Z., Zwiercheczewski de Oliveira, P., Vinícius de Melo Pereira, G., Ricardo, C. (2022), Added-value biomolecules' production from cocoa pod husks: A review, Bioresource Technology, 344. https://doi.org/10.1016/j.biortech.2021.126252

Potrč, S., Čuček, L., Martin, M., Kravanja, Z. (2021), Sustainable renewable energy supply networks optimization – The gradual transition to a renewable energy system within the European Union by 2050, Renewable and Sustainable Energy Reviews, 146. https://doi.org/10.1016/j.rser.2021.111186

Prado, G.H.C., Rao, Y., De Klerk, A. (2017), Nitrogen removal from oil: A review, Energy and Fuels, 31 (1), 14–36. https://doi.org/10.1021/acs.energyfuels.6b02779

Proskurina, S., Junginger, M., Heinimö, J., Tekinel, B., Vakkilainen, E. (2019), Global biomass trade for energy— Part 2: Production and trade streams of wood pellets, liquid biofuels, charcoal, industrial roundwood and emerging energy biomass, Biofuels, Bioproducts and Biorefining, 13(2), 371–387. https://doi.org/10.1002/bbb.1858

Ramos, F.S., Martins, D.M., Nunes Sagini, J.P., Quines, C.B., de Oliveira Pereira, F.S., de Ávila, D.S., Zanzarin, D., Pilau, E.J., de Lima Postiga, I.A., Tostes, J., Seixas, A., Zimmer, A.R., Zimmer, K.R. (2021). Soybeans agroindustrial residues as Staphylococcus epidermidis and S. aureus biofilm inhibitors. Industrial Crops and Products, 170. https://doi.org/10.1016/j.indcrop.2021.113713

Raza, M., Inayat, A., Abu-Jdayil, B. (2021), Crude glycerol as a potential feedstock for future energy via thermochemical conversion processes: A review, Sustainability (Switzerland), 13(22), 1–27. https://doi.org/10.3390/su132212813

Resende, F.L.P. (2016), Recent advances on fast hydropyrolysis of biomass: Transformations of Biomass and its derivatives to Fuels and Chemicals, Catalysis Today, 269, 148–155. https://doi.org/10.1016/j.cattod.2016.01.004

Rojo-poveda, O., Barbosa-pereira, L., Zeppa, G., St, C. (2020), Cocoa Bean Shell — A By-Product with Nutritional, Mdpi, 1–29. https://doi.org/10.3390/nu12041123

Rossi, R.A.S., Barbosa, J.M., Barrozo, M.A.S., Vieira, L.G.M. (2021b), Solar assisted catalytic thermochemical processes: pyrolysis and hydropyrolysis of Chlamydomonas reinhardtii microalgae, Renewable Energy, 170, 669-682. https://doi.org/10.1016/j.renene.2021.02.034

Santana Junior, J.A., Menezes, A.L., Ataíde, C.H. (2019), Catalytic upgrading of fast hydropyrolysis vapors from industrial Kraft lignins using ZSM-5 zeolite and HY-340 niobic acid, Journal of Analytical and Applied Pyrolysis, 144, 104720. https://doi.org/10.1016/j.jaap.2019.104720

Santana, J.A., Sousa, N.G., Cardoso, C.R., Carvalho, W.S., Ataíde, C.H. (2016), Sodium, zinc and magnesium chlorides as additives for soybean hulls pyrolysis: Influence on the temperature range of reactions and product selectivity, Journal of Thermal Analysis and Calorimetry, 125(1), 471–481. https://doi.org/10.1007/s10973-016-5381-2

Saravanan, A., Kumar, P.S., Mat Aron, N.S., Jeevanantham, S., Karishma, S., Yaashikaa, P.R., Chew, K.W., Show, P.L. (2022), A review on bioconversion processes for hydrogen production from agro-industrial residues, International Journal of Hydrogen Energy, 47(88), 37302–37320. https://doi.org/10.1016/j.ijhydene.2021.08.055

SDGR UN. (2022), The Sustainable Development Goals Report, United Nations, https://unstats.un.org/sdgs/report/2022/The-Sustainable-Development-Goals-Report-2022.pdf

Shahbaz, M., Balsalobre-Lorente, D., Sinha, A. (2019), Foreign direct Investment–CO2 emissions nexus in Middle East and North African countries: Importance of biomass energy consumption, Journal of Cleaner Production, 217, 603–614. https://doi.org/10.1016/j.jclepro.2019.01.282

Šimkovic, I., Dlapa, P., Schwarzinger, C. (2023), Elucidating the composition of organic matter in water-repellent forest soils using analytical pyrolysis combined with gas chromatography–mass

spectrometry (Py-GC–MS), Organic Geochemistry, 179. https://doi.org/10.1016/j.orggeochem.2023.104586

Simões, A.F., Romeiro, L.K.J., Kurita, R.M. (2021), Interrelationships between policies to encourage biofuels, energy efficiency and climate change mitigation: a synergistic analysis focusing on the Brazilian RenovaBio Program, Latin American Journal of Energy Research, 8 (1), 46-58. https://doi.org/10.21712/lajer.2021.v8.n1.p46-58

SoCientifica, 2022, https://socientifica.com.br/paises-que-mais-produzem-niobio/#:~:text=Atualmente%2C%20a%20medida%20de%20ni%C3%B3bio,40.000%20toneladas%20m%C3%A9tricas%20por%20ano, [on-line accessed, 20-07-2023, 13:00h].

Sulaiman, F., Abdullah, N. (2011), Optimum conditions for maximizing pyrolysis liquids of oil palm empty fruit bunches, Energy, 36, 2352–2359. https://doi.org/10.1016/j.energy.2010.12.067

Sun, Y., Li, C., Zhang, S., Li, Q., Gholizadeh, M., Wang, Y., Hu, S., Xiang, J., Hu, X. (2021), Pyrolysis of soybean residue: Understanding characteristics of the products, Renewable Energy, 174, 487–500. https://doi.org/10.1016/j.renene.2021.04.063

Tamburini, D. (2021), Analytical pyrolysis applied to the characterisation and identification of Asian lacquers in cultural heritage samples – A review, Journal of Analytical and Applied Pyrolysis, 157, 105202. https://doi.org/10.1016/j.jaap.2021.105202

Thompson, S.O., Rough, S.L. (2021). The densification of cocoa bean shells for bioenergy purposes. Biomass and Bioenergy, 148, 106057. https://doi.org/10.1016/j.biombioe.2021.106057

Tripathi, M., Sahu, J.N., Ganesan, P. (2016), Effect of process parameters on production of biochar from biomass waste through pyrolysis: a review, Renew. Sustain. Energy Rev., 55, 467–481. https://doi.org/10.1016/j.rser.2015.10.122

Ushikubo, T. (2000), Recent topics of research and development of catalysis by niobium and tantalum oxides, Catalysis Today, 57, 331–338. https://doi.org/10.1016/S0920-5861(99)00344-2

V´asquez, Z.S., de Carvalho Neto, D.P., Pereira, G.V.M., Vandenberghe, L.P.S., de Oliveira, P.Z., Tiburcio, P.B., Rogez, H.L.G., G´oes Neto, A., Soccol, C.R. (2019), Biotechnological approaches for cocoa waste management: A review, Waste Manag., 90, 72–83. https://doi.org/10.1016/j.wasman.2019.04.030.

Venderbosch, R.H., Prins, W. (2010), Fast pyrolysis technology development. Biofuels, Bioprod. Biorefining, 4, 178–208. https://doi.org/10.1002/bbb.205

Vidal, M.F. (2022). Agroindústria - Etanol. Banco Do Nordeste, 1–16.

Vincent, L., Benoitl, M., Ruben, Y., Toshiyuki, A., Ken, P., Mellissa, C., Bilge, Y. (2017), Engineering zeolites for catalytic cracking to light olefins, ACS Catal., 7, 6542–6566. https://doi.org/10.1021/acscatal.7b02011

Vong, W.C., Liu, S.Q. (2018), Bioconversion of green volatiles in okara (soybean residue) into esters by coupling enzyme catalysis and yeast (Lindnera saturnus) fermentation, Applied Microbiology and Biotechnology, 102(23), 10017–10026. https://doi.org/10.1007/s00253-018-9396-4

Wan, S., Wang, Y.A. (2014), Review on ex situ catalytic fast pyrolysis of biomass, Frontiers of Chemical Science and Engineering, 8, 280–294. https://doi.org/10.1016/j.biortech.2012.08.016

Wang, S., Cai, Q., Chen, J., Zhang, L., Zhu, L., Luo, Z. (2015), Co-cracking of bio-oil model compound mixtures and ethanol over different metal oxide-modified HZSM-5 catalysts, Fuel, 160, 534–543. https://doi.org/10.1016/j.fuel.2015.08.011

Wang, X., Tang, X., Yang, X. (2017), Pyrolysis mechanism of microalgae Nannochloropsis sp. based on model compounds and their interaction, Energy Conversion and Management, 140, 203-210. https://doi.org/10.1016/j.enconman.2017.02.058

Wawrzynczak, A., Nowak, I., Feliczak-Guzik, A. (2018), Toward exploiting the behavior of niobium-containing mesoporous silicates vs. polyoxometalates in catalysis, Frontiers in Chemistry, 6. https://doi.org/10.3389/fchem.2018.00560

Wijaya, M., Wiharto, M. (2020). Synthesis and characterization of bioactive compound from Cocoa fruit shell by pyrolysis process. Journal of Physics: Conference Series, 1567 (2). https://doi.org/10.1088/1742-6596/1567/2/022025

Wiyantoko, B., Kurniawati, P., Purbaningtias, T.E., Fatimah, I. (2015), Synthesis and Characterization of Hydrotalcite at Different Mg/Al Molar Ratios, Procedia Chem, 17, 21–26. https://doi.org/10.1016/j.proche.2015.12.115

Xie, Q., Addy, M., Liu, S., Zhang, B., Cheng, Y., Wan, Y., Li, Y., Liu, Y., Lin, X., Chen, P., Ruan, R. (2015), Fast microwave-assisted catalytic co-pyrolysis of microalgae and scum for bio-oil production, Fuel, 160, 577–582. https://doi.org/10.1016/j.fuel.2015.08.020

Xie, W., Peng, H., Chen, L. (2006), Calcined Mg-Al hydrotalcites as solid base catalysts for methanolysis of soybean oil, Journal of Molecular Catalysis A: Chemical, 246, 24–32. https://doi.org/10.1016/j.molcata.2005.10.008

Yaashikaa, P.R., Senthil Kumar, P., Varjani, S. (2022), Valorization of agro-industrial wastes for biorefinery process and circular bioeconomy: A critical review, Bioresource Technology, 343, 126126. https://doi.org/10.1016/j.biortech.2021.126126

Yarberry, A., Lansing, S., Luckarift, H., Diltz, R., Mulbry, W., Yarwood, S. (2019), Effect of anaerobic digester inoculum preservation via lyophilization on methane recovery, Waste Management, 87, 62–70. https://doi.org/10.1016/j.wasman.2019.01.033

Yu, Z., Dai, M., Huang, M., Fang, S., Xu, J., Lin, Y., & Ma, X. (2018). Catalytic characteristics of the fast pyrolysis of microalgae over oil shale: Analytical Py-GC/MS study. Renewable Energy, 125, 465–471. https://doi.org/10.1016/j.renene.2018.02.136

Zhang, B., Zhong, Z.P., Min, M., Ding, K., Xie, Q.L., Ruan, R. (2015), Catalytic fast copyrolysis of biomass and food waste to produce aromatics: analytical Py-GC/MS study, Bioresour. Technol., 189, 30–35. https://doi.org/10.1016/j.biortech.2015.03.092

Zhang, H., Shao, S., Luo, M., Xiao, R. (2017), The comparison of chemical liquid deposition and acid dealumination modified ZSM-5 for catalytic pyrolysis of pinewood using pyrolysis-gas chromatography/mass spectrometry, Bioresour. Technol., 244, 726-732. https://doi.org/10.1016/j.biortech.2017.08.036

Ziolek, M. (2003), Niobium-containing catalysts - The state of the art, Catalysis Today, 78, 47–64. https://doi.org/10.1016/S0920-5861(02)00340-1

Ziolek, M., Sobczak, I. (2017), The role of niobium component in heterogeneous catalysts, Catalysis Today, 285, 211–225. https://doi.org/10.1016/j.cattod.2016.12.013

CHAPTER 3

3. MATERIALS AND METHODS

This chapter details the materials utilized and the methodologies employed during the analytical pyrolysis experiments. Additionally, the characterization techniques of the biomasses and their pyrolytic products are described.

3.1.Biomasses

In the analytical pyrolysis studies, two types of biomasses were employed as raw materials: soybean residue (Figure 3.1) and cocoa bean shell (Figure 3.2). These biomasses were provided by *Cargill Agricola SA*. The soybean residue and the cocoa bean shells were both sampled directly from industrial receiving process as it is usually collected. Having mentioned this, it is worth noting that the soybean residue sample mostly contained stalks and pods with uneven maturation, probably because the period of the year it was collected, and also contained a small amount of soybeans and soybean hulls. Visually, it was identified that the cocoa product was much more homogeneous, containing practically only the bean shells.

To prepare them for experimentation, the biomasses underwent a series of steps. Initially, they were dried in an oven at 60°C for 10 hours (Houghton et al., 2009). Subsequently, the dried biomasses were macerated, homogenized, and sieved. In general, smaller particles are preferred for pyrolysis due to their faster and uniform heating, which is critical in minimizing heat transfer problems (Guedes et al., 2018). Thus, the experiment's selected material had an average particle diameter ranging from 0.177 to 0.297 mm.



Figure 3.1. Soybean residue.



Figure 3.2. Dried cocoa bean shell.

3.2.Biomass Characterization

3.2.1. Cocoa Bean Shell (CBS) and Soybean Residue (SR) Proximate Analysis

The proximate analysis was conducted in triplicate, adhering to the American Society for Testing and Materials (ASTM) guidelines.

Moisture Content

To determine the moisture content, the reference standard utilized was ASTM E871-82. For each biomass, approximately 2.0 ± 0.1 g was carefully placed in a Petri dish and subjected to

an oven temperature of 105°C for 2 hours. The sample was removed from the oven and cooled naturally within a desiccator. After one hour, the sample was reweighed. This process was repeated until the weight difference between consecutive dried samples was less than 0.2%. The moisture content was then calculated using Equation 3.1.

$$Moisture = \frac{mi - mf}{mi - mp} 100\% \tag{3.1}$$

where *mi* corresponds to the initial mass of the sample plus the plate mass, *mf* to the final mass and *mp* refers to the mass of the Petri dish.

Volatile Content

The ASTM E872-82 standard served as the reference to determine the volatile content. Around 1.0 ± 0.1 g of the sample was carefully transferred to a pre-weighed melting pot with a lid. The assembled set was then placed in a muffle set at 950°C for 7 minutes. Following this heating period, the sample was retrieved from the muffle and cooled naturally within a desiccator. After one hour, the set was reweighed. The volatile content was subsequently calculated using Equations 3.2 and 3.3.

$$Weight\ loss = \frac{mi - mf}{mi - mc} 100\% \tag{3.2}$$

$$Volatile\ content = Weight\ loss - Moisture \tag{3.3}$$

where *mi* corresponds to the initial mass of the sample plus the melting pot with lid mass, *mf* to the final mass and *mc* refers to the mass of the melting pot.

Ash Content

To determine the ash content, the reference standard employed was the ASTM E1534-93. Around 2.0 ± 0.1 g of the biomass was carefully transferred to a pre-weighed melting pot. This assembly was then subjected to a muffle at a temperature of 600°C for 4 hours. After this time, the sample was removed from the muffle and cooled naturally within a desiccator. After an additional hour, the set was reweighed, and the ash content was calculated using Equation 3.4.

$$Ash\ content = \frac{mf - mc}{mi - mc} 100\% \tag{3.4}$$

where *mi* corresponds to the initial mass of the sample plus the melting pot mass, *mf* to the final mass and *mc* refers to the mass of the crucible.

Fixed Carbon Content

The reference standard utilized was the ASTM D3172 to determine the carbon content. The fixed carbon content was calculated using Equation 3.5, incorporating the previously obtained volatile and ash content results.

$$Fixed\ carbon\ content = 100\% - (Volatile\ content + Ash\ content) \tag{3.5}$$

3.2.2. Elemental Analysis and Higher Heat Value of CBS and SR

The elemental analysis (CHNS/O) was conducted in triplicate at the Chemical Institute of São Carlos, utilizing a Thermo-Scientific Flash-Smart analyzer. The analysis is based on the traditional Pregl-Dumas method. The samples are combusted in a pure oxygen environment. In the presence of excess oxygen and combustion reagents, samples are combusted entirely and reduced to the elemental gases CO_2, H_2O, N_2, and SO_2. The resultant gases are separated by a chromatography column and subsequently measured by a thermal conductivity detector (The

PerkinElmer® 2400 Series II CHNS/O Elemental Analyzer). Approximately 1.5 mg of the sample was employed for the analysis, maintaining the oven temperature at 950°C and the chromatogram run time at 720 s. External calibration curves using standards such as BBOT, methionine, cystine, and sulfanilamide were utilized to identify and quantify the percentage of carbon (C), hydrogen (H), nitrogen (N), and sulfur (S). The oxygen content (O) was calculated through the difference method, employing Equation 3.6 (Dittmann et al., 2022).

$$Oxigen\ content = 100\% - (C + H + N + S + Ash) \tag{3.6}$$

The Higher Heat Value (HHV) was determined in triplicate by the private laboratory, Labornutri Análises Bromatológicas. The HHV value was obtained using a calorimeter (IKA C 2600) following the guidelines outlined in the ASTM D240-09 standard. For the analysis, approximately 1.5 g of the biomass sample was utilized, and the combustion process occurred under a pressure of 30 bar.

3.2.3. Chemical Composition Analysis of CBS and SR

Protein Content

The protein content was determined using the Kjeldahl method (proposed by the Association of Official Analytical Chemists - A.O.A.C) by the private laboratory, Labornutri Análises Bromatológicas. Each biomass sample, weighing approximately 0.25 g, was mixed with sulfuric acid in micro-Kjeldahl digester tube. Once the digestion was complete, the ammonium sulfate obtained in the last step is treated with excess NaOH, which releases the ammonia. The sample's nitrogen is collected in an Erlenmeyer flask containing a boric acid solution through distillation. The process is finished when all the ammonia has been released. Finally, the titration is performed, in which the ammonium borate is titrated with an HCl solution until the indicator turns over. The organic nitrogen content was used to determine the protein contained in the biomasses (Barrins et al., 2007). This value was then multiplied by the conversion factor of 6.25, as shown in Equation 3.7 and 3.8.

$$Nitrogen\,content = \frac{C_{HCl}(V_{HCl} - V_{blank})f_{Hcl}1.4}{m_{sample}}100\% \quad (3.7)$$

$$Protein\ \ content\ = 6.25\,(Nitrogen\ \ \ content)\ \ 100\,\% \quad (3.8)$$

where C_{HCl} is the molar concentration of HCl, f_{HCl} is the hydrochloric acid correction factor, V_{HCl} is the volume spent in the titration of the sample (mL), V_{blank} is the volume spent on the titration of the blank (mL) and m_{sample} is the sample weight (g).

Lipid Content

The lipid analysis was conducted following the Soxhlet method, as the Association of Official Analytical Chemists (A.O.A.C) outlined. The analysis was performed by the private laboratory, Labornutri Análises Bromatológicas. The sample is placed inside a thimble, and the flask is heated. As the solvent evaporates, it passes through a condenser, and the liquid is collected in the sample's extraction chamber. During this process, the solvent passes through the sample, extracting the fats and carrying them into the flask. Typically, this extraction procedure takes approximately 6 to 24 hours. Once the extraction is completed, the solvent is evaporated, and the remaining mass of lipids is measured (Hewavitharana et al., 2020). The lipid content is found according to the Equation 3.9.

$$Lipid\,content = \frac{m_{organic\ phase}}{m_{sample}}100\% \quad (3.9)$$

Crude Fiber Content

The analysis was performed by the private laboratory, Labornutri Análises Bromatológicas. The Weende method was used to determine the crude fiber content. Approximately 1 g of biomass is weighed, and 1.25% sulfuric acid and 3-5 drops of n-octanol (antifoam agent) are added. The solution is boiled for 30 minutes. The solution is filtered, and the

remaining material is washed with hot deionized water. Finally, 150 mL of preheated potassium hydroxide (KOH) is added, and the solution is again boiled for 30 minutes, filtered, and washed. After drying in an oven at 105°C for at least 8 hours, the dry weight was naturally cooled in a desiccator. This weight represents the crude fiber plus ash content (m_{dry}). To remove the ash content, the sample is placed in a muffle, heated to 600°C for 4 h, and reweighed after cooling in a desiccator (m_{ash}) (Nduko et al., 2018). The crude fiber was calculated according to Equation 3.10.

$$Crude\,Fiber\ content = \frac{m_{dry} - m_{ash}}{m_{sample}} 100\% \tag{3.10}$$

where m_{dry} corresponds to the melting pot weight with fiber and ashes filtered and dried, m_{ash} to the mass of melting pot with the ashes and m_{sample} refers to the initial mass of sample.

Carbohydrate Content

Considering the mass balance described by Martínez et al. (2012), it was possible to calculate de carbohydrate content according to the Equation 3.11.

$$Carbohydrate\ content = 100\% - (Protein + Lipid + Crude\,Fiber + Ash) \tag{3.11}$$

3.2.4. Lignocellulosic composition of the CBS and SR

The chemical composition of the biomasses was analyzed to ascertain the cellulose, hemicellulose, and lignin content. Duplicate analyses were conducted following the methodology detailed by Morais et al. (2010). The evaluations of chemical composition were carried out at the LaborNutri Bromatological Analysis private laboratory in Uberlândia.

3.2.5. Thermogravimetric Analysis (TGA) of CBS and SR

Approximately 10 mg of biomass samples were subjected to the thermogravimetric analysis (TGA). The samples were subjected to a controlled heating regimen, initiated at a relatively mild temperature of 30°C and gradually ramped to a significantly high temperature of 900°C (ASTM E1131-20, 2020). This gradual temperature increase was executed maintaining a constant heating rate of 10°C/min under the protective atmosphere of helium (He). The experimental setup employed for this analysis was the Shimadzu TGA-50 thermogravimetric analyzer at the Laboratory of the Nucleus of Physical-Chemical Processes (NUFISQ) at FEQUI/UFU.

3.2.6. Fourier Transform Infrared Spectroscopy (FTIR) Analysis of CBS and SR

Potassium bromide (KBr) pellets were prepared at a mass ratio of 1/100 (sample/KBr) in a hydraulic press for each biomass and the Fourier transform infrared spectroscopy (FTIR) analysis was carried out in an infrared spectrometer model Equinox 55 from Bruker using wavelengths from 400 to 4500 cm^{-1}, with 32 scans at a resolution of 4 cm^{-1}, according to Barbosa et al (2020). The analysis was performed in the Multiuser Laboratory of the Institute of Chemistry of the Federal University of Uberlandia (IQ/UFU).

3.2.7. X-ray fluorescence analysis (XRF) of Analysis of CBS and SR

The investigation of the minerals contained within the biomasses underwent using the X-ray fluorescence (XRF) technique. To prepare the samples, pastilles were prepared, maintaining a precise mass ratio of 10 parts sample to 1 part wax. A hydraulic press was used to shape the pastilles. The analysis was performed using X-ray fluorescence equipment (model S8 Tiger Bruker) at the Multiuser Laboratory in Renewable Energy at the Faculty of Chemical Engineering, Federal University of Uberlândia (FEQUI/UFU). The Quant-Express method (Bruker AXS) calculates, according to the manufacturer, the concentration (mass fraction) of each element utilizing parameters stored for more than 500 reference samples covering the most typical samples for XRF: oils, aqueous solutions, rocks, metals, chemicals, and polymers (S8 Tiger Bruker AXS, 2009).

3.2.8. Scanning Electron Microscopy (SEM) Analysis of CBS and SR

The analysis was performed using an electronic acceleration of 5 kV in an electron microscope model EVO MA 10 Zeiss and the images were acquired with a magnification between 5 and 10 Kx. SEM analysis is based on a focused beam of electrons that scan the sample, which interacts with the atoms in the sample to provide three-dimensional surface topography (Lam et al., 2023). The samples were sputter coated with a 20 nm layer of gold. Gold is used for its high electron density, which increases electron scatter to give high contrast in dark spots. Thus, promoting the emission of secondary electrons so that the specimen conducts evenly and provides a homogeneous surface for analysis and imaging (Bogner et al., 2007). This analysis was performed at the Multiuser Laboratory of Scanning Electron Microscopy at FEQ/UFU to evaluate the morphology of each biomass.

3.3. Catalysts

The catalysts were selected based on the following factors: (a) zeolites are a prominent choice due to their extensive application in the oil and gas industry, making them well-established candidates for thermochemical conversion processes. Notably, their exceptional catalytic performance in deoxygenation and aromatization, specifically in generating aromatic compounds, has garnered significant attention (Azreena et al., 2021; Zainan et al., 2018). Their unique ability to crack large molecules and induce deoxygenation reactions for hydrocarbon production makes them highly sought after; (b) hydrotalcite, on the other hand, was chosen for its distinctive bifunctional (acid-base) character, setting it apart from the strongly acidic nature of zeolites. Its notable structural stability also adds to its appeal (Goh et al., 2008); (c) the niobium-containing mesoporous silicates have captured the interest of researchers due to their well-ordered structures, substantial surface areas, and narrow pore size distributions (Wawrzynczak et al., 2018). In recent years, thermochemical processes using layered double hydroxides such as hydrotalcite and niobium-derivative catalysts have been investigated (Rossi et al., 2021; Navarro et al., 2018; Batista et al., 2019; Li et al., 2023). In addition, the significant niobium reserve in Brazil, one of the largest worldwide, which produces around 40,000 metric tons annually (SoCientifica, 2002), making exploring this national resource for potential applications in thermochemical processes, such as enhancing pyrolysis products, a commendable pursuit.

3.3.1. Zeolite

The HZSM-5 zeolite catalyst (CBV 8014) was purchased from the Zeolyst International company (United Kingdom). The catalyst was acquired in its powdered state and exhibited an ammoniacal form, boasting a SiO_2/Al_2O_3 molar ratio of 80. Before being employed in the analytical pyrolysis process, the HZSM-5 catalyst was calcined at 550°C in a constant flow of synthetic air for 4 hours, according to Ding et al. (2018). The catalyst exhibited distinct diffraction peaks, indicative of its mordenite structure. The BET-specific area and acid site density were 419 m^2/g and 2.08 μmol/m^2, respectively. The detailed characterization can be found in Rossi et al. (2024).

3.3.2. Hydrotalcite [$Mg_6Al_2(OH)16CO_3.4H_2O$] (HTC)

The hydrotalcite catalyst [$Mg_6Al_2(OH)16CO_3.4H_2O$] used in the analytical pyrolysis was synthesized by the co-precipitation method at constant pH (pH=10) according to Cavani et al. (1991). Analogously to the zeolite, the hydrotalcite catalyst was calcined at 550°C in a constant synthetic air flow for 4 hours to decompose the nitrates into oxides (Barbosa et al., 2021). The XRD pattern showed the formation of the mixed oxides derived from hydrotalcite (MgO, $MgAl_2O_4$, and Al_2O_3). The BET-specific area and acid site density were 247 m^2/g and 1.05 μmol/m^2, respectively. The detailed synthesis method and characterization can be found in Rossi et al. (2021).

3.3.3. Catalysts Derived from Niobic Acid (Ni/Nb_2O_5 and $Ni\text{-}Re/Nb_2O_5$)

The catalysts derived from niobic acid were synthesized by Moura et al. (2022). The niobium oxide (Nb_2O_5) was produced from the calcination of niobic acid at 400°C in a constant flow of synthetic air for 4 h (Moura et al., 2022). The Ni/Nb_2O_5 (Ni/Nb) catalyst was prepared by incipient wetness impregnation of the support (Nb_2O_5) with an aqueous solution of nickel precursor. The catalyst was prepared with a nominal loading of 5 wt.% of Ni. The $Ni\text{-}Re/Nb_2O_5$ (NiRe/Nb) catalyst was prepared by incipient wetness co-impregnating the supports with an aqueous solution of nickel (Ni) and rhenium (Re). The latter catalyst was prepared with a nominal loading of 5 wt.% of Ni and a 5:1 molar ratio of Ni:Re. After the impregnation, the samples were

dried in the oven overnight at 110°C and then reduced at 500°C for 4 h with a heating rate of 2°C/min under an H_2 flow. After reduction, the samples were cooled at about -10°C and passivated under a 5% O_2/Ar mixture flow for 30 min. The XRD patterns obtained after the reduction showed the crystalline structure of the niobium oxide. Both catalysts exhibited a peak at $2\theta = 44.4°$ that corresponds to the metallic nickel phase. The Ni/Nb showed a BET surface area and total acidity of 45 m^2/g and 0.23 $mmolNH_3/g_{cat}$. The NiRe/Nb presented a BET surface area and total acidity of 49 m^2/g and 0.22 $mmolNH_3/g_{cat}$, respectively. The detailed synthesis method and characterization can be found in Moura et al. (2022).

3.4. Analytical pyrolysis (micro-pyrolysis)

3.4.1. Analytical pyrolysis (micro-pyrolysis)

The preparation for each experimental run consisted in weighing 1.00 ± 0.01 mg of the biomass (or the Cocoa Bean Shell or the Soybean Residue) and placing it in a metallic crucible with diameter of 4 mm and length of 8 mm with quartz wool placed above the material (Figure 3.3).

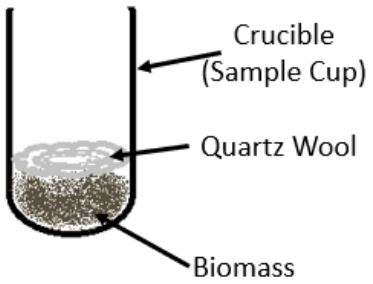


Figure 3.3. Schematic drawing of the crucible used in the analytical pyrolysis.

The crucible was then placed in the Frontier Lab Micropyrolyzer (EGA/PY-3030D) which is heated to the selected temperature by a resistance. The interface between the micropyrolyzer and the GC/MS was maintained at 250°C. Ultrapure helium (99.999%) was used as inert gas for pyrolysis, as well as carrier gas for volatiles. Pyrolytic vapors were introduced into the Mass Spectrometer (Shimadzu GCMS-QP2020 NX) along with helium, as the carrier gas, through a heating tube maintained at 280°C. The method programmed into the equipment was based on the Blasi method with solvent cut (Andrade, 2018; Barbosa, 2020). The vapors were separated by an

Rtx 1701 GC 195 capillary column (length = 60 m, I.D. = 0.25 mm, film thickness = 0.25 am). A Schematic drawing of the experiment apparatus is presented in the Figure 3.4. The column gas flow rate was set to 1 mL/min while the injector split ratio was 1:450. An initial oven temperature of 45°C was held for 4 min, and then a ramp rate of 3°C/min was implemented to reach the final oven temperature of 235°C (held for 8 min). The injector and interface temperatures were 250°C and 235°C, respectively. The analyzes were performed in duplicates. The ion chromatogram obtained was identified using the library database of the National Institute of Standards and Technology (NIST 14) with a similarity index of 80%. A semi-quantitative analysis was conducted using the area of chromatographic peaks to ascertain the compound distribution in pyrolysis products. This method is widely embraced by researchers in the field (Lee et al., 2022; Moogi et al., 2022; Prabhakara et al., 2022). The calculated values from this approach provide estimations of the quantity of a measured substance, as elucidated by Domínguez et al. (2003).

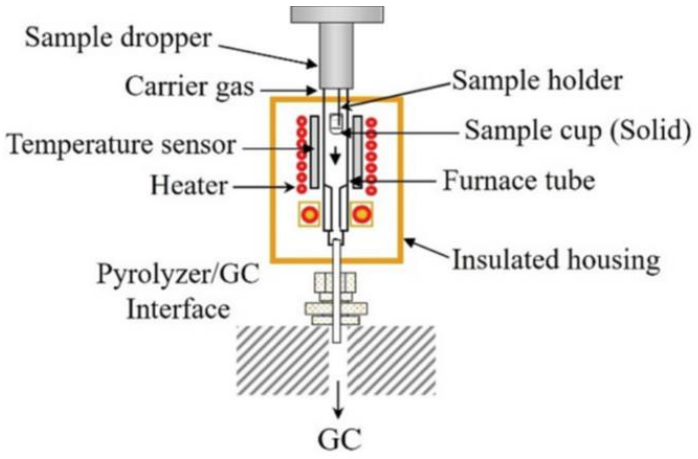


Figure 3.4. Schematic drawing of an analytical pyrolysis system. Adapted from (Li et al., 2022).

3.4.2. Analytical pyrolysis (micro-pyrolysis) in a catalytic bed

For the catalytic micropyrolysis, the methodology applied was the same with the difference in the crucible set preparation, which included each of the catalysts, weighted to achieve the desired proportion of biomass:catalyst, with addition in sequence of the quartz wool with another layer of

quartz wool above it as demonstrated in the Figure 3.5. This way the experiment was performed as an *ex-situ* catalytic pyrolysis. The rest of the methodology was repeated.

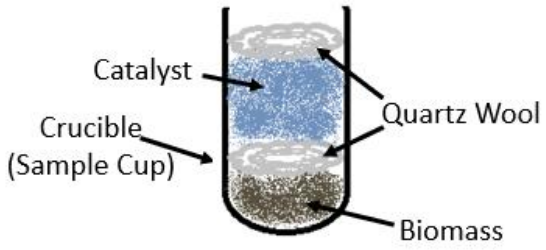


Figure 3.5. Schematic drawing of the crucible used in the analytical pyrolysis (*ex-situ* catalytic bed).

3.4.3. Design of experimental

The experiments were divided in three different stages, each one focusing on a different variable assessment. The three variables evaluated were: catalyst, temperature, and catalyst proportion. After performing the tests defined in each stage, the results were analyzed. After that, some alternatives were selected so that there was a narrowing of alternatives and greater detailing of those with greater potential to achieve the specific objectives of the work. A schematic drawing of the experimental design with its three stages is presented in the Figure 3.6.

Stage 1 - Definition of catalysts to be explored

The first stage defined consisted of the evaluation between non-catalytic pyrolysis against the four different types of catalyst selected. All the tests were performed at the same selected parameters, so it was possible to better evaluate only the effect of the catalysts and the non-catalyst alternative.

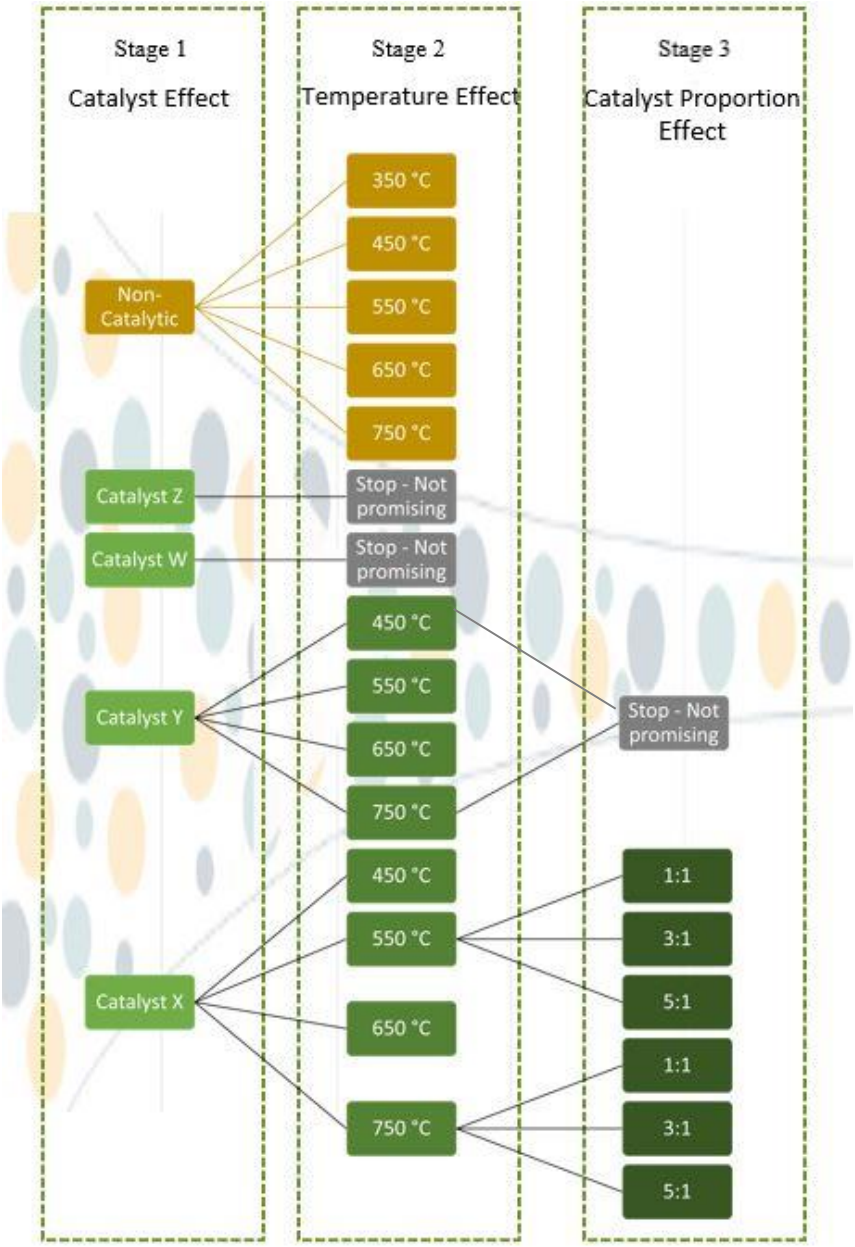


Figure 3.6. Schematic drawing of the experimental design.

The Table 3.1 presents the three variables considered for the study with the 5 tests: non-catalytic and the four different catalytic pyrolysis. The catalyst proportion was fixed at 3:1, proportion expected to be enough to guarantee a good contact between the gas produced by the thermochemical process and the catalysts. Balasundram et al. (2018), Zhou et al. (2018), and Muley et al. (2016) studied the effects of the catalyst-to-biomass ratio in pyrolysis. All of them varied the catalyst to biomass ratio from 0 to 2. Gautam et al. (2018) also investigated the variable catalyst-to-biomass ratio in pyrolysis, which was ranged from 0 to 3. The temperature fixed for all the tests were defined after the results of the TGA with the objective of having the total decomposition of the solids.

Table 3.1. Stage 1 of the experimental design.

Stage 1 - Definition of Catalysts to be explored					
Catalyst	**None**	**HTC**	**Zeolite**	**NiRe/Nb2O5**	**Ni/Nb2O5**
Catalyst Proportion		3:1	3:1	3:1	3:1
Temperature (°C)	550	550	550	550	550

Stage 2 - Temperature effect on catalytic and non-catalytic micropyrolysis

Main objective of the second stage is to evaluate the temperature effect of catalytic and non-catalytic micropyrolysis. The non catalytic test was performed between 350°C and 750°C with 100°C between each run. The catalytic tests were kept with catalyst proportion fixed at 3:1 and temperature variation started on 450°C and were increased by 100°C until 750°C. The temperature of 350°C was only performed without catalysts to evaluate possible impacts of performing the pyrolysis below the temperature identified in the TGA. All tests maximum temperature was 750°C so all the tests would stay below the threshold considered by literature between pyrolysis and gasification processes (Bridgwater, 2018).

As planned, this second stage already disregarded some alternatives evaluated in the first stage. This way, the catalytic process was performed only with the two most relevant catalysts for the study objective based on the results of the first tests, as presented in Table 3.2.

Table 3.2. Stage 2 of the experimental Design.

Stage 2 - Temperature effect on catalytic and non-catalytic micropyrolysis			
Catalyst	**None**	**Catalyst X**	**Catalyst Y**
Catalyst Proportion		3:1	3:1
Temperature (°C)	**[350 – 750]**	**[450 – 750]**	**[450 – 750]**

Stage 3 – Catalyst proportion effect

The third stage presented in Table 3.3 evaluated the last variable considered in the experimental design, the catalyst proportion. The catalytic tests were performed with the catalyst from stage 2 that presented more capability of having pyrolysis products rich in hydrocarbons. At this stage the proportion variation was 1:1, 3:1 and 5:1 (Guedes et al., 2018; Santana Júnior et al., 2019) and were performed at two different temperatures, 550°C and 750°C.

Table 3.3. Stage 3 of the experimental Design.

Stage 3 – Catalyst Proportion Effect	
Catalyst	Catalyst X
Catalyst Proportion	**[1:1, 3:1, 5:1]**
Temperature (°C)	**[550, 750]**

3.5. References

Andrade, L.A. (2018a). Pirólise Solar Catalítica De Microalgas. Universidade Federal de Uberlândia, Faculdade De Engenharia Química Programa De Pós-Graduação Em Engenharia Química – Tese de Doutorado.

ASTM D240-09. Standard Test Method for Heat of Combustion of Liquid Hydrocarbon Fuels by Bomb Calorimeter, ASTM International, 2009.

ASTM D3172. Standard Practice for Proximate Analysis of Coal And Coke, ASTM International, 2014.

ASTM E1131-20. (2020). Standard Test Method for Compositional Analysis by Thermogravimetry, ASTM International.

ASTM E1534-93. Standard Test Method for Determination of Ash Content of Particulate Wood Fuels, ASTM International, 2013.

ASTM E871-82. Standard Test Method for Moisture Analysis of Particulate Wood Fuels, ASTM International, 2019.

ASTM E872-82. Standard Test Method for Volatile Matter in the Analysis of Particulate Wood Fuels, ASTM International, 2019.

Azreena, I.N., Lau, H.L.N., Asikin-Mijan, N., Izham, S.M., Hassan, M.A., Kennedy, E., Stockenhuber, M., Taufiq-Yap, Y.H. (2021), Hydrodeoxygenation of oleic acid for effective diesel-like hydrocarbon production using zeolite-based catalysts, Reaction Kinetics Mechanisms and Catalysis, 134 (2), 1069–1083. https://doi.org/10.1007/s11144-021-02082-w

Balasundram, V., Ibrahim, N., Kasmani, R.M., Isha, R., Hamid, M.K.A., Hasbullah, H., Ali, R.R. (2018), Catalytic upgrading of sugarcane bagasse pyrolysis vapours over rare earth metal (Ce) loaded HZSM-5: Effect of catalyst to biomass ratio on the organic compounds in pyrolysis oil, Applied Energy, 220, 787–799. https://doi.org/10.1016/j.apenergy.2018.03.141

Barbosa, J.M. (2020). Pirólise solar catalítica *ex-situ* da microalga *Chlamydomonas reinhardtii*. Universidade Federal de Uberlândia, Faculdade De Engenharia Química Programa De Pós-Graduação Em Engenharia Química – Tese de Doutorado.

Barbosa, J.M., Rossi, R.A S., Vieira, L.G.M., Barrozo, M.A.S. (2021), A study of optimization of solar pyrolysis and catalyst recovery and reuse. Energy Conversion and Management, 237, 114094. https://doi.org/10.1016/j.enconman.2021.114094

Barrins, T., Bassompierre, M., Brodin, A., Brunsgaard, G., Burks, L.B., Butler, B.H., Ellefson, W., Gulden, J., Henriksen, J., Henry, M., Jin, L.N., Louviere, E., Opdebeeck, J., Pirozzola, P., Schulze, C.W., Soffia, E.O., Sorensen, H.O., Zaldivar, J., Miller, E.L., Sheridan, B. (2007), Repeatability and reproducibility of determination of the nitrogen content of fishmeal by the combustion (Dumas) method and comparison with the Kjeldahl method: interlaboratory study, Journal of AOAC International, 90 (1), 6–20. https://doi.org/10.1093/jaoac/90.1.6

Batista, L.M.B., Oliveira, J.L.F., Bezerra, F.A., Araújo, A.M.M., Fernandes Junior, V.J., Araujo, A.S., Alves, A.P.M., Gondim, A.D. (2019). Synthesis, characterization and evaluation of niobium catalysts in the flash pyrolysis of glycerol. Solid State Sciences, 97, 105977. https://doi.org/10.1016/j.solidstatesciences.2019.105977

Bogner, A.; Jouneau, P.H.; Thollet, G.; Basset, D.; Gauthier, C. (2007). A history of scanning electron microscopy developments: Towards "wet-STEM" imaging. Micron, 38 (4), 390–401. https://doi.org/10.1016/j.micron.2006.06.008

Bridgwater, T. (2018), Challenges and opportunities in fast pyrolysis of biomass: Part I, Johnson Matthey Technology Review, 62 (1), 118–130. https://doi.org/10.1595/205651318X696693

Cavani, F., Triffirò, F., Vaccari, A. (1991), Hydrotalcite-type Anionic Clays: Preparation, Properties and Applications, Catalysis Today, 11, 173-186. https://doi.org/10.1016/0920-5861(91)80068-K

Ding, K., Zhong, Z., Wang, J., Zhang, B., Fan, L., Liu, S., Wang, Y., Liu, Y., Zhong, D., Chen, P., Ruan, R. (2018). Improving hydrocarbon yield from catalytic fast co-pyrolysis of hemicellulose and plastic in the dual-catalyst bed of CaO and HZSM-5. Bioresource Technology, 261, 86-92. https://doi.org/10.1016/j.biortech.2018.03.138

Dittmann, D., Saal, L., Zietzschmann, F., Mai, M., Altmann, K., Al-Sabbagh, D., Schumann, P., Ruhl, A. S., Jekel, M., Braun, U. (2022). Characterization of activated carbons for water treatment using TGA-FTIR for analysis of oxygen-containing functional groups. Applied Water Science, 12 (8), 1–13. https://doi.org/10.1007/s13201-022-01723-2

Domínguez, A., Menéndez, J.A., Inguanzo, M., Bernad, P.L., Pis, J.J. (2003). Gas chromatographic-mass spectrometric study of the oil fractions produced by microwave-assisted pyrolysis of different sewage sludges. Journal of Chromatography A, 101, 193–206. https://doi.org/10.1016/S0021-9673(03)01176-2

Gautam, R., Vinu, R. (2018), Non-catalytic fast pyrolysis and catalytic fast pyrolysis of Nannochloropsis oculata using Co-Mo/γ-Al2O3 catalyst for valuable chemicals, Algal Research, 34, 12–24. https://doi.org/10.1016/j.algal.2018.06.024

Goh, K.H., Lim, T.T., Dong, Z. (2008), Application of layered double hydroxides for the removal of oxyanions, Water Res., 42, 1343-1368. https://doi.org/10.1016/j.watres.2007.10.043

Guedes, R.E., Luna, A.S., Torres, A.R. (2018), Journal of analytical and applied pyrolysis operating parameters for bio-oil production in biomass pyrolysis: a review, J. Anal. Appl. Pyrol., 129, 134-149, https://doi.org/10.1016/j.jaap.2017.11.019

Hewavitharana, G.G., Perera, D.N., Navaratne, S.B., Wickramasinghe, I. (2020), Extraction methods of fat from food samples and preparation of fatty acid methyl esters for gas chromatography: A review, Arabian Journal of Chemistry, 13 (8), 6865–6875. https://doi.org/10.1016/j.arabjc.2020.06.039

Houghton, T.P., Stevens, D.M., Pryfogle, P.A., Wright, C.T., Radtke, C.W. (2009). The effect of drying temperature on the composition of biomass. Applied Biochemistry and Biotechnology, 153 (1–3), 4–10. https://doi.org/10.1007/s12010-008-8406-x

Lee, D., Nam, H., Won Seo, M., Hoon Lee, S., Tokmurzin, D., Wang, S., Park, Y.K. (2022). Recent progress in the catalytic thermochemical conversion process of biomass for biofuels. Chemical Engineering Journal, 447, 137501. https://doi.org/10.1016/j.cej.2022.137501

Li, T., Su, J., Wang, C., Watanabe, A., Teramae, N., Ohtani, H., Wang, K. (2022), Advances in the development and application of analytical pyrolysis in biomass research: A review, Energy Conversion and Management, 271, 116302. https://doi.org/10.1016/j.enconman.2022.116302

Li, Z., Zhang, H., Yang, D., Hu, Z., Wang, F., Zhang, Z. (2023). Efficient Conversion of Lignin to Aromatics via Catalytic Fast Pyrolysis over Niobium-Doped HZSM-5. Molecules, 28 (10). https://doi.org/10.3390/molecules28104245

Martínez, R., Torres, P., Meneses, M.A., Figueroa, J.G., Pérez-Álvarez, J.A., Viuda-Martos, M. (2012), Chemical, technological and in vitro antioxidant properties of cocoa (Theobroma cacao L.) co-products, Food Research International, 49 (1), 39–45. https://doi.org/10.1016/j.foodres.2012.08.005

Moogi, S., Pyo, S., Farooq, A., Valizadeh, S., Jun Choi, Y., Hoon Rhee, G., Lee, J., Jae, J., Hussain, M., Ali Khan, M., Jeon, B.H., Andrew, L.K.Y., Chen, W.H., Park, Y.K. (2022). Enhancement of bioaromatics production from food waste through catalytic pyrolysis over Zn and Mo-loaded HZSM-5 under an environment of decomposed methane. Chemical Engineering Journal, 446, 137215. https://doi.org/10.1016/j.cej.2022.137215

Morais, J.P.S.; Rosa, M.F.; Marconcini, J.M. (2011). Procedimento para análise lignocelulósica. (Embrapa Agroindústria Tropical. Documentos, 236). Fortaleza: Embrapa Agroindústria Tropical, 54. http://ainfo.cnptia.embrapa.br/digital/bitstream/item/42211/1/DOC11003.pdf.

Moura, L.G. (2022), Study of hydrodeoxygenation reaction of phenolic compounds using niobium-based catalysts, Tese de Doutorado, Faculdade de Engenharia Química, Universidade Federal de Uberlândia.

Muley, P.D., Henkel, C.E., Aguilar, G., Klasson, K.T., Boldor, D. (2016), Ex situ thermo-catalytic upgrading of biomass pyrolysis vapors using a traveling wave microwave reactor, Applied Energy, 183, 995–1004. https://doi.org/10.1016/j.apenergy.2016.09.047

Navarro, R.M., Guil-Lopez, R., Fierro, J.G., Mota, N., Jiménez, S., Pizarro, P., Coronado, J.M., Serrano, D.P. (2018). Catalytic fast pyrolysis of biomass over Mg-Al mixed oxides derived from hydrotalcite-like precursors: Influence of Mg/Al ratio. Journal of Analytical and Applied Pyrolysis, 1–9. https://doi.org/10.1016/j.jaap.2018.07.001

Nduko, J.M., Maina, R.W., Muchina, R.K., Kibitok, S.K. (2018), Application of chia (Salvia hispanica) seeds as a functional component in the fortification of pineapple jam, Food Science and Nutrition, 6 (8), 2344–2349. https://doi.org/10.1002/fsn3.819

Prabhakara, H.M., Bramer, E.A., Brem, G. (2022). Hydrotalcite as a deoxygenation catalyst in fast pyrolysis of biomass for the production of high quality bio-oil. Journal of Analytical and Applied Pyrolysis, 161, 105431. https://doi.org/10.1016/j.jaap.2022.105431

Rossi, R.A.S. (2024). Microalgae Schizochytrium Limacinum Pyrolysis in A Tandem Catalytic Bed Composed by Hydrotalcite Precursor and HZSM-5 Zeolite in Three Different Process Configurations (Analytical, Solar and Microwave). Universidade Federal de Uberlândia, Faculdade De Engenharia Química Programa De Pós-Graduação Em Engenharia Química – Tese de Doutorado.

Rossi, R.A.S., Barbosa, J.M., Barrozo, M.A.S., Vieira, L.G.M. (2021), Catalytic solar hydropyrolysis of the Chlamydomonas reinhardtii microalgae, Biomass and Bioenergy, 152, 106183. https://doi.org/10.1016/j.biombioe.2021.106183

S8 Tiger Bruker AXS (2009). https://www.bruker.com/pt/products-and-solutions/elemental-analyzers/xrf-spectrometers/s8-tiger.html, [on- line accessed, 08-12-2023, 12:30h].

Santana Junior, J.A., Menezes, A.L., Ataíde, C.H. (2019). Catalytic upgrading of fast hydropyrolysis vapors from industrial Kraft lignins using ZSM-5 zeolite and HY-340 niobic acid. Journal of Analytical and Applied Pyrolysis, 144, 104720. https://doi.org/10.1016/j.jaap.2019.104720

SoCientifica. (2022), https://socientifica.com.br/paises-que-mais-produzem-niobio/#:~:text=Atualmente%2C%20a%20medida%20de%20ni%C3%B3bio,40.000%20toneladas%20m%C3%A9tricas%20por%20ano, [on-line accessed, 20-07-2023, 13:00h].

The PerkinElmer® 2400 Series II CHNS/O Elemental Analyzer. (2005). https://resources.perkinelmer.com/lab-solutions/resources/docs/bro_2400_seriesii_chnso_elemental_analysis.pdf, [on- line accessed, 08-12-2023, 17:00h].

Wawrzynczak, A., Nowak, I., Feliczak-Guzik, A. (2018), Toward exploiting the behavior of niobium-containing mesoporous silicates vs. polyoxometalates in catalysis, Frontiers in Chemistry, 6. https://doi.org/10.3389/fchem.2018.00560

Zainan, N.H., Srivatsa, S.C., Li, F.; Bhattacharya, S. (2018), Quality of bio-oil from catalytic pyrolysis of microalgae Chlorella vulgaris, Fuel, 223, 12–19. https://doi.org/10.1016/j.fuel.2018.02.166

Zhou, N., Liu, S., Zhang, Y., Fan, L., Cheng, Y., Wang, Y., Liu, Y., Chen, P., Ruan, R. (2018), Silicon carbide foam supported ZSM-5 composite catalyst for microwave-assisted pyrolysis of biomass, Bioresource Technology, 267, 257–264. https://doi.org/10.1016/j.biortech.2018.07.007

CHAPTER 4

4. RESULTS AND DISCUSSIONS – BIOMASS CHARACTERIZATION

This chapter discusses the outcomes acquired through characterizing the two biomasses under investigation.

4.1.Immediate Analyzes and Higher Heat Value (HHV) of the SR and CBS

Figure 4.1 displays the immediate analysis results for the two investigated biomasses. The analyses were conducted in triplicate, and the standard deviations for all results of both biomasses, namely soybean residue (a) and cocoa bean shell (b), were consistently below 0.40%. Both exhibit a notable quantity of volatiles, with soybean residue containing 78% and cocoa bean shell containing 88%, respectively. This high volatile content is advantageous for pyrolysis, which typically occurs within the temperature range of 450 to 750°C (Bridgwater et al., 2018).

a) b)



Figure 4.1. Immediate Analysis Results for: (a) SR; (b) CBS.

Table 4.1. provides a comparative analysis of the Higher Heating Value (HHV) and immediate analysis data for the two biomasses examined in this study compared with various solid fuels, primarily of biomass origin. Among the selected data, eight distinct biomasses are considered

agricultural residues, including cocoa bean shells, soybean residue, sugarcane bagasse, rice husk, almond shell, banana waste, tobacco residue, and soybean hulls.

Upon comparing these biomasses with the data collected from other studies, a striking similarity emerges in terms of volatile matter content, ranging between 69% and 92%. However, the ash content exhibited significant variation across these biomasses, with the majority containing more than 10% ash content. This variability poses a potential challenge when considering agricultural residues as a viable bioenergy source. Furthermore, this comparison underscores that the two biomasses investigated in our study also exhibited high ash content, which had a discernible impact on their higher heating value.

Table 4.1. Comparison of Immediate Analysis and HHV of some Solid Fuels.

	HHV (MJ/kg)	Volatiles	Fixed C	Ashes	Reference
Cocoa Bean Shell	**17.41 ±0.15**	**88% ±0.38**	**2% ±0.18**	**10% ±0.20**	**This Study**
Soybean Residue	**16.69 ±0.13**	**78% ±0.39**	**12% ±0.40**	**11% ±0.07**	**This Study**
Soybean Residue	-	60%	18%	16%	Sun et al. (2021)
Cocoa Bean Shell	17.21	71%	22%	7%	Mumbach et al. (2022)
Charcoal	31.00	25%	73%	2%	Massuque et al. (2023)
Eucalyptus Wood	17.60	86%	14%	1%	Telmo et al., (2010)
Sugarcane Bagasse	18.90	87%	9%	4%	Montoya et al. (2015)
Rice Husk	15.38	69%	18%	13%	Yuan et al. (2019)
Almond Shell	20.20	92%	6%	2%	Caballero et al. (1997)
Banana Waste	17.10	74%	15%	11%	Sellin et al. (2016)
Tobacco Residue	16.26	78%	2%	20%	Cardoso et al. (2013)
Bamboo Wood	18.89	81%	14%	5%	Onokwai et al. (2022)
Soybean Hulls	17.73	86%	8%	6%	Oliveira (2015)
Microalgae - *C. reinhardtii*	20.68	80%	12%	8%	Andrade et al. (2020)
Microalgae - *S. platensis*	18.77	87%	6%	7%	Andrade et al. (2020)

4.2.Ultimate Analyzes of the SR and CBS

Table 4.2. displays the findings from the ultimate analysis of the two biomasses under investigation, alongside a comparative examination with various solid fuels, predominantly of biomass origin. Notably, both studied biomasses contain a significant proportion of hydrogen, with cocoa bean shells at 9% and soybean residues at 11%. This hydrogen content exerts a detrimental

effect on the HHV values. The results also reveal elevated nitrogen levels in these biomasses, surpassing those found in other solid fuels, except for microalgae biomass. However, despite these distinctions, the overall outcomes remain consistent with the carbon, hydrogen, nitrogen, and sulfur (CHNS) profiles commonly observed in similar biomasses.

Table 4.2. Comparison of Ultimate Analysis of some Solid Fuels.

	C		H		N	S	O		Ashes		Reference
Cocoa Bean Shell	**45%**	**±0.35**	**9%**	**±0.55**	**3%**	**±0.05**	**0%**	**33%**	**±0.95**	**10%**	**±0.20**	**This Study**
Soybean Residue	**49%**	**±0.41**	**11%**	**±0.88**	**6%**	**±0.08**	**0%**	**24%**	**±1.38**	**11%**	**±0.07**	**This Study**
Soybean Residue	33%		3%		4%		0%	42%		16%		Sun et al. (2021)
Cocoa Bean Shell	42%		6%		1%		0%	44%		7%		Mumbach et al. (2022)
Charcoal	77%		3%		2%		0%	16%		2%		Massuque et al. (2023)
Eucalyptus Wood	46%		6%		0%		0%	47%		1%		Telmo et al. (2010)
Sugarcane Bagasse	47%		6%		0%		0%	43%		4%		Montoya et al. (2015)
Rice Husk	40%		5%		1%		0%	41%		13%		Yuan et al. (2019)
Almond Shell	55%		8%		0%		0%	35%		2%		Caballero et al. (1997)
Banana Waste	44%		6%		1%		1%	37%		11%		Sellin et al. (2016)
Tobacco Residue	41%		6%		2%		0%	30%		20%		Cardoso et al. (2013)
Bamboo Wood	45%		6%		0%		0%	44%		5%		Onokwai et al. (2022)
Soybean Hulls	39%		6%		2%		0%	47%		6%		Oliveira (2015)
Microalgae - *C. reinhardtii*	44%		7%		11%		2%	29%		8%		Andrade et al. (2020)
Microalgae - *S. platensis*	42%		6%		10%		1%	34%		7%		Andrade et al. (2020)

4.3.Chemical Composition of the SR and CBS

Figure 4.2. presents the results of the chemical composition analysis on a dry basis, categorizing the components into ashes, protein, lipids, carbohydrates, and crude fiber. The analyses were conducted in triplicate, and the standard deviations for all results of both biomasses, soybean residue (a) and cocoa bean shell (b), consistently remained below 0.60%.

As outlined in the materials section of this study, the soybean residue used in this study is heterogeneous and contains soybean seeds and hulls, likely stemming from inefficiencies in the screening industrial process during sample collection. This contamination is evident in the lipid content, which stood at 7 ± 0.06% in the sample. It deviates from the expected lipid content of hulls, pods, and stalks, generally below 2% since soybean seeds have a lipid content of

approximately 20% on a dry basis. Furthermore, the contamination from soybean seeds also contributed to an increase in the sample's protein content, given that soybeans are a plant-based protein source with an approximate protein content of 35 ± 0.12% on a dry basis (Nam et al., 2016; Liu et al., 2015).

The chemical composition of various cocoa bean shells was also evaluated by Okiyama et al. (2017). Their findings revealed variability influenced by factors such as origin and the specific processing methods employed. Lipid content in cocoa bean shells ranged from 2% to 18%, while fiber content typically approached nearly 50%. Additionally, ash content generally hovered around 10%, consistent with the results presented in this study's analysis.

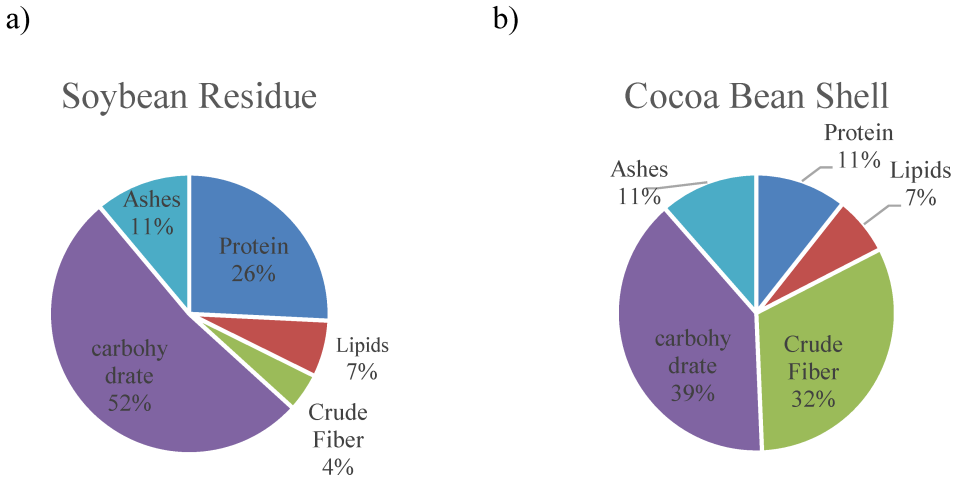


Figure 4.2. Chemical Composition Results for: a) SR; b) CBS.

Cellulose is the primary constituent in the composition of the plant cell wall. It represents a high molecular weight polysaccharide characterized by an extended linear arrangement of repetitive D-glucose units connected through glycosidic bonds. Hemicellulose, on the other hand, is a diverse amalgamation of polymerized monosaccharides (Hameed et al., 2019; Wang et al., 2017a).

Hemicelluloses exhibit branches with short side chains along the primary polymer chain, encompassing various sugars such as glucose, mannose, galactose, xylose, arabinose, and glucuronic acid, as detailed by Mohan et al. (2006). The presence of these carbohydrates can result in the formation of oxygen-containing compounds, as highlighted by Wang et al. (2017b).

Lignin has a polyphenolic structure characterized by extensive branching. Its chains are dispersed in multiple directions, creating a three-dimensional macromolecular configuration. This structure serves as a binding agent, facilitating the aggregation of fibrous cellulosic components. In this role, lignin provides structural support and impermeability, establishing an impervious barrier within the plant cell wall (Ilyas et al., 2021).

This investigation's combined cellulose and hemicellulose content reached approximately 48% and 70% for SR and CBS, respectively. These findings align with the total carbohydrate composition of the biomasses (carbohydrate and crude fiber), which accounted for 56% and 71% in SR and CBS, respectively. Moreover, the lignin content results were notably similar, hovering around 25% for both biomasses. This observation is consistent with the typical lignin content of angiosperm biomasses, which generally falls around 20% (Welker et al., 2015).

In comparison, Nguyen et al. (2018) reported approximately 48% carbohydrates in soybean residue, while Qing et al. (2017) found cellulose, hemicellulose, and lignin levels of 55%, 12.5%, and 27%, respectively. Additionally, Mumbach et al. (2020) characterized cocoa shell, revealing cellulose, hemicellulose, and lignin contents of 31%, 22%, and 32%, respectively. These results presented some discrepancies compared to the present study, which may be attributed to the heterogeneity of the SR and CBS biomasses that can also be based on the location where the product was sourced.

Table 4.3. SR and CBS Lignocellulosic characterization.

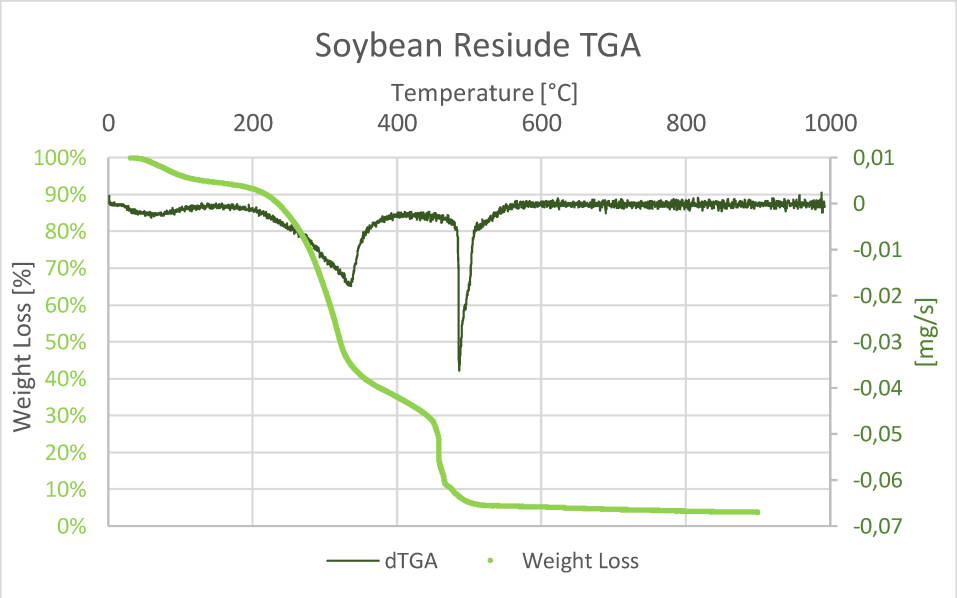
Lignocellulosic composition (%)		
	SR	**CBS**
Cellulose	27.94 ± 0.29	33.80 ± 0.35
Hemicellulose	19.87 ± 0.24	35.72 ± 0.50
Lignin	25.08 ± 0.45	25.10 ± 0.40

4.4.Thermogravimetric Analysis (TGA) of the SR and CBS

Figure 4.3. depicts the Thermal Gravimetric Analysis (TGA) and Differential Thermogravimetry (DTG) curves for the thermal conversion of biomass. Understanding this decomposition process is essential for determining the optimal temperature for thermal degradation and its connection to the formation of pyrolysis products. Previous studies have shown that the

degradation sequence is linked to the composition of carbohydrates, proteins, and lipids in that respective order (Li et al., 2019).

a)



b)

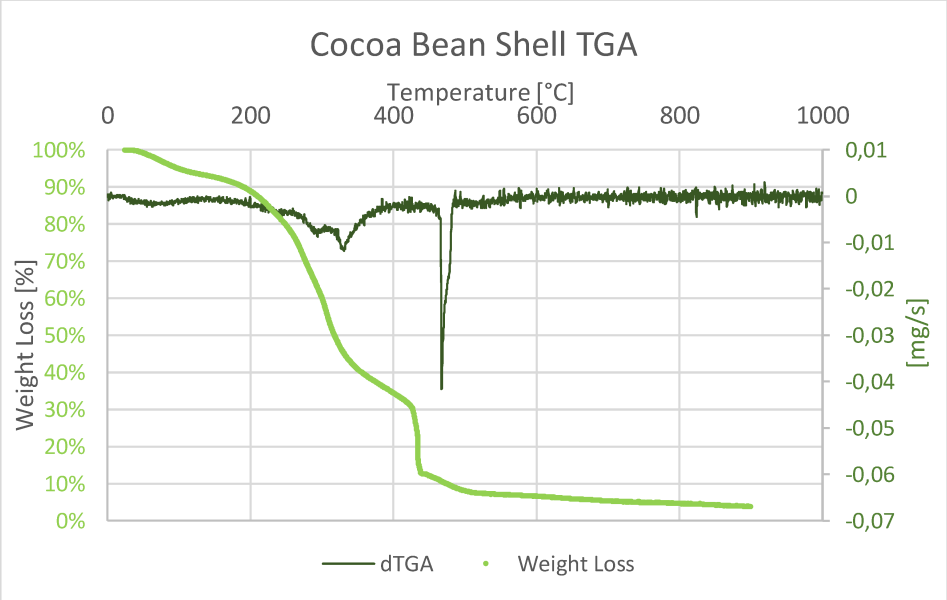


Figure 4.3. TGA and DTG Results for: a) SR; b) CBS.

As illustrated in Figure 4.3., both biomass analyses reveal three distinct zones. The first zone, from 50°C to approximately 150°C, corresponds to the drying process and the release of light volatiles, often called the pre-pyrolysis stage. The second zone, extending from roughly 180°C to 460°C, represents the active devolatilization or active pyrolysis phase, during which the most substantial mass loss typically occurs due to the breakdown of compounds such as hemicellulose and cellulose. The weight loss in this phase is closely tied to the hot volatile content in both biomasses. Lastly, the third phase is characterized as passive pyrolysis or char formation and occurs within the temperature range of 460°C to 600°C (Rojas et al., 2023; Mishra et al., 2023).

The observed similarities in both curves, as explained by Rojas et al. (2023), are a typical weight loss pattern exhibited by lignocellulosic biomass raw materials when subjected to thermal degradation processes. Lignin is characterized by its high stability and poses challenges in decomposition. One explanation is that the entire lignin content is degraded within a broad temperature range (Zhang et al., 2012). In the present study, lignin decomposition most likely happened between 200 and 500°C. In a study conducted by Bausch et al. (2021), the degradation of papyrus lignin was observed within a temperature range of 250 to 600°C. This behavior is consistent with findings from various sources, including corn brakes, wheat straw, hazelnut shell, sawdust, and chemically treated sawdust (Burhenne et al., 2013).

4.5.Fourier Transform Infrared Spectroscopy (FTIR), Scanning Electron Microscopy (SEM) and X-ray Fluorescence (XRF) Analysis of CBS and SR

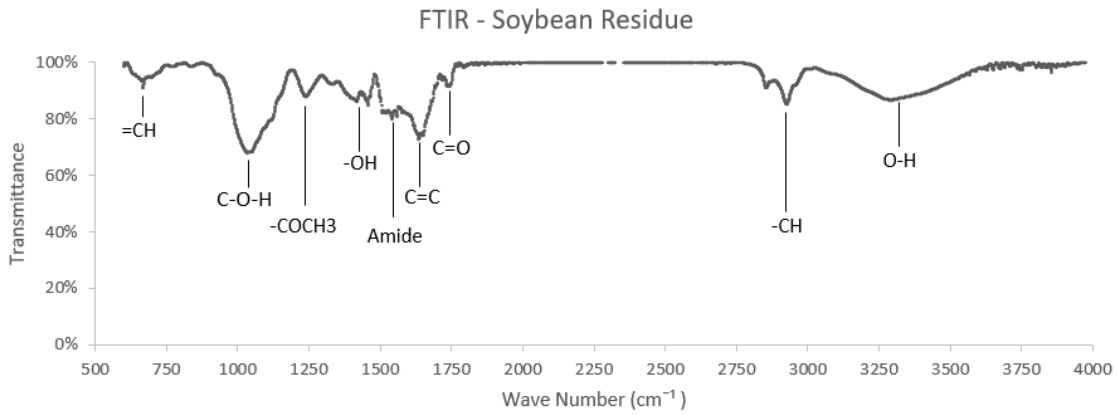
From The FTIR analysis, presented in Figure 4.4., there is a substantial resemblance between the two investigated biomasses. The spectra obtained from the dried materials unveil the most pertinent chemical bonds within their structures. Notably, the peaks for both soybean residue and cocoa bean shells occur in analogous regions, although with some variations in intensity.

The primary peak within the 1000-1200 cm^{-1} range indicates C-O stretching bands. These bands are likely associated with the presence of alcohols, phenols, ethers, and esters in the pyrolysis products following the biomass degradation. Additionally, the peak near 1250 cm^{-1} indicates acetyl groups and aromatic formations in the biomasses (Aboulkas et al., 2017). The band spanning 1320-1400 cm^{-1} corresponds to the bending vibration of alcoholic and phenolic hydroxyl (O-H) groups (Zhang et al., 2017). Furthermore, the peak at approximately 1500 cm^{-1} signifies the amide

functional group (Zainan et al., 2015), with higher intensity in the soybean residue, likely due to the nitrogen content observed in the ultimate analysis.

Another noteworthy peak, more prominent in the soybean residue but also present in the cocoa bean shell, occurs at 1656 cm^{-1}. This peak corresponds to C=C stretching vibrations and is indicative of alkenes, which are associated with lipids and proteins in the samples. The presence of methyl and methylene groups (alkanes and alkenes) is highlighted by the intense peak in the 2800-3000 cm^{-1} range, representing C-H stretching vibrations. The absorption peak between 3200 and 3400 cm^{-1} indicates the presence of oxygenated compounds (O-H groups). Finally, the last two, albeit smaller, peaks at 680 and 1770 cm^{-1} represent the presence of C=O, which might lead to alkanes and esters formation (Kassim et al., 2016).

a)



b)

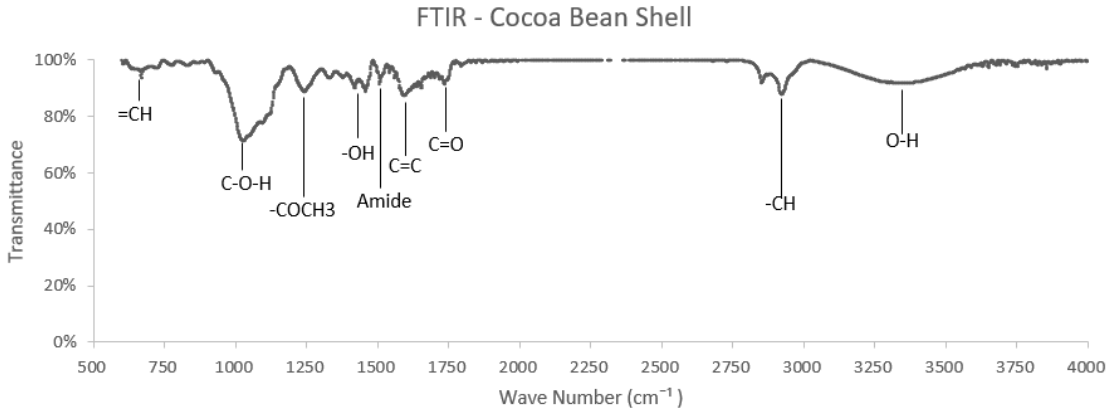


Figure 4.4. FTIR spectrums for a) SR; b) CBS.

Le et al. (2017) conducted a series of X-ray fluorescence analyses on a range of biomass samples, revealing the suitability of this technique for solid biomasses. As presented in Table 4.3., this study's findings highlight the predominant presence of elements falling within alkali, alkaline-earth metals, and non-metals groups. This outcome aligns with expectations, as phosphorus, sulfur, potassium, calcium, and magnesium are all integral components contributing to plant cell function and structure. In contrast, the presence of metals was relatively insignificant, with most of them registering below 60 parts per million (PPM). Iron exhibited a slightly more substantial presence, though its origin may not be from the plants but could be attributed to external mineral sources. A similar observation can be made regarding the presence of silicon, which stood at around 0.1% in both biomasses and could potentially come from sources such as sand (Le et al., 2017; Xing et al., 2016).

Table 4.4. XRF results of SR and CBS.

Element	Periodic table group	Soybean Residue Content	Cocoa Bean Shell Content
K	Alkali metal	2.09%	2.84%
Rb	Alkali metal	12 PPM	0.01%
Mg	Alkaline earth metal	0.39%	0.34%
Ca	Alkaline earth metal	0.54%	0.29%
Sr	Alkaline earth metal	35 PPM	31 PPM
P	Non-metal	0.52%	0.27%
S	Non-metal	0.28%	0.18%
Si	Non-metal	0.09%	0.11%
Cl	Halogen	0.04%	0.02%
Al	Other Metals	0.06%	0.05%
Fe	Metal	0.05%	0.04%
Zn	Metal	38 PPM	55 PPM
Mn	Metal	31 PPM	55 PPM
Ti	Metal	0.01%	47 PPM
Cu	Metal	24 PPM	40 PPM
Ru	Metal	27 PPM	30 PPM
Ni	Metal	38 PPM	15 PPM
Co	Metal	-	6 PPM
Zr	Metal	-	5 PPM

In Figure 4.5., we observe the soybean residue's scanning electron microscopy (SEM) image. Specifically, Figure 4.5. (a), the image portrays a material with distinct fibrous characteristics, likely originating from the soybean straw biomass, which has a lignocellulosic composition. This material exhibits a non-porous morphology devoid of any discernible pores or ridges, as depicted in the image (Jagtap et al., 2023; Bortolatto et al., 2022).

a) b)

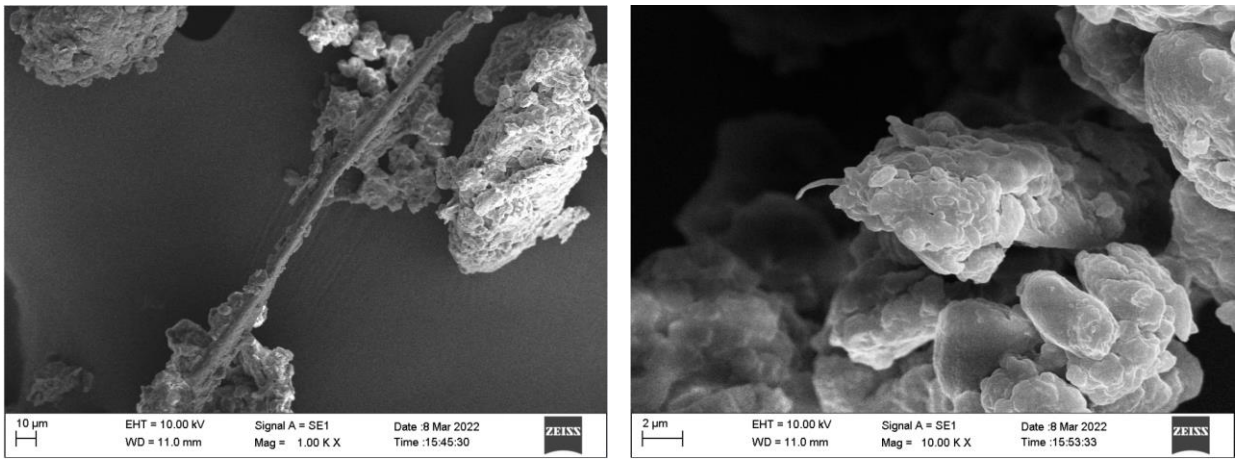


Figure 4.5. Soybean Residue SEM – a) magnitude of 1.00 K X; b) magnitude of 10.00 K X.

Figure 4.6. presents the scanning electron microscopy (SEM) image of the Cocoa Bean Shell (CBS). The micrographs of the raw CBS reveal an amorphous material characterized by a surface that appears cracked and crinkled while exhibiting a smooth and porous structure. Previous research has indicated the presence of components such as lignin, hemicellulose, and polysaccharides on the surface of CBS (Mellinas et al., 2020; Fioresi et al., 2017).

a) b)

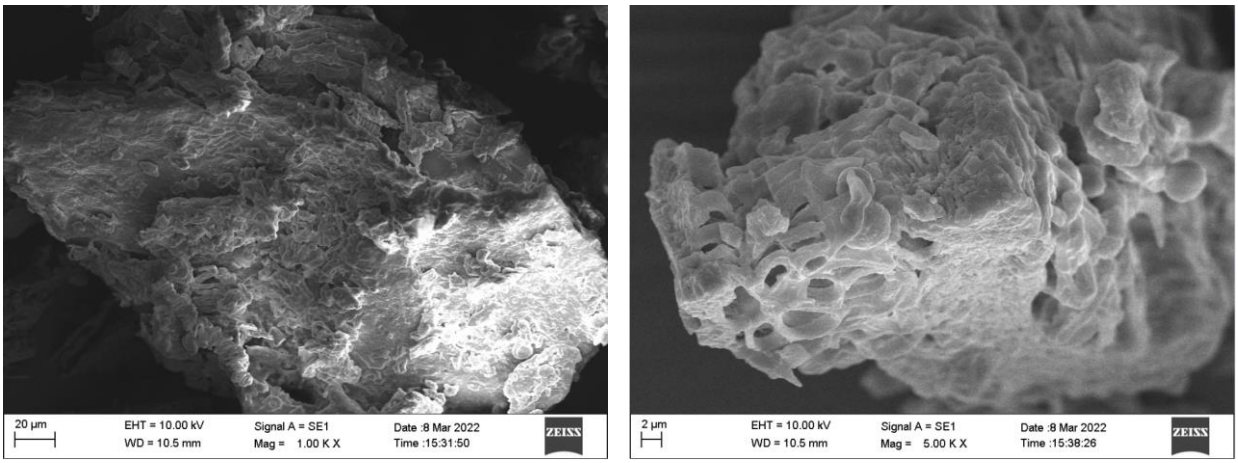


Figure 4.6. Cocoa Bean Shell SEM – a) magnitude of 1.00 K X; b) magnitude of 5.00 K X.

4.6.References

Aboulkas, A., Hammani, H., El Achaby, M., Bilal, E., Barakat, A., El harfi, K. (2017), Valorization of algal waste via pyrolysis in a fixed-bed reactor: Production and characterization of bio-oil and bio-char, Bioresource Technology, 243, 400–408. https://doi.org/10.1016/j.biortech.2017.06.098

Andrade, L A., Barbosa, J.M., Barrozo, M.A.S., Vieira, L.G.M. (2020), A comparative study of the behavior of Chlamydomonas reinhardtii and Spirulina platensis in solar catalytic pyrolysis, International Journal of Energy Research, 44 (7), 5397–5411. https://doi.org/10.1002/er.5289

Bausch, F., Owusu, D.D., Jusner, P., Rosado, M.J., Rencoret, J., Rosner, S., Del Río, J.C., Rosenau, T., Potthast, A. (2021). Lignin quantification of papyri by tga—not a good idea. Molecules, 26 (14). https://doi.org/10.3390/molecules26144384

Bortolatto, R., Bittencourt, P.R.S., Yamashita, F. (2022), Biodegradable starch / polyvinyl alcohol composites produced by thermoplastic injection containing cellulose extracted from soybean hulls (Glycine max L.), Industrial Crops and Products, 176, 114383. https://doi.org/10.1016/j.indcrop.2021.114383

Bridgwater, T. (2018), Challenges and Opportunities in Fast Pyrolysis of Biomass: Part I, Johnson Matthey Technology Review, 62, 118–130. https://doi.org/10.1595/205651318X696693

Burhenne, L., Messmer, J., Aicher, T., Laborie, M.P. (2013). The effect of the biomass components lignin, cellulose and hemicellulose on TGA and fixed bed pyrolysis. Journal of Analytical and Applied Pyrolysis, 101, 177–184. https://doi.org/10.1016/j.jaap.2013.01.012

Caballero, J.A., Conesa, J.A., Font, R., Marcilla, A. (1997), Pyrolysis kinetics of almond shells and olive stones considering their organic fractions, Journal of Analytical and Applied Pyrolysis, 42 (2), 159–175. https://doi.org/10.1016/S0165-2370(97)00015-6

Cardoso, C.R., Oliveira, T.J.P., Santana Junior, J.A., Ataíde, C.H. (2013), Physical characterization of sweet sorghum bagasse, tobacco residue, soy hull and fiber sorghum bagasse particles: Density, particle size and shape distributions, Powder Technology, 245, 105–114. https://doi.org/10.1016/j.powtec.2013.04.029

Fioresi, F., Vieillard, J., Bargougui, R., Bouazizi, N., Fotsing, P.N., Woumfo, E.D., Brun, N., Mofaddel, N., Le Derf, F. (2017), Chemical modification of the cocoa shell surface using diazonium salts, Journal of Colloid and Interface Science, 494, 92–97. https://doi.org/10.1016/j.jcis.2017.01.069

Hameed, S., Sharma A., Pareek V., Wu H., Yu, Y. (2019). A review on biomass pyrolysis models: Kinetic, network and mechanistic models. Biomass and Bioenergy, 123, 104-122. https://doi.org/10.1016/j.biombioe.2019.02.008

Ilyas, R.A., Atikah, M.S.N. (2021). Production of nanocellulose from sustainable algae marine biomass. Seminar on Advanced Bio- and Mineral Based Natural Fibre Composites (SBMC2021), January, 1–9. ISBN: 978-983-44426-9-9

Jagtap, A., Kalbande, S. (2023), Multiparametric optimization and statistical modelling of pelletization process: Effect of independent variables on physicochemical properties of soybean straw pellets, Bioresource Technology Reports, 23, 101527. https://doi.org/10.1016/j.biteb.2023.101527

Kassim, M.A., Bhattacharya, S. (2016), Dilute alkaline pretreatment for reducing sugar production from Tetraselmis suecica and Chlorella sp. Biomass, Process Biochemistry, 51 (11), 1757–1766. https://doi.org/10.1016/j.procbio.2015.11.027

Le, D.M., Sørensen, H.R., Meyer, A.S. (2017), Elemental analysis of various biomass solid fractions in biorefineries by X-ray fluorescence spectrometry, Biomass and Bioenergy, 97, 70–76. https://doi.org/10.1016/j.biombioe.2016.12.018

Li, F., Srivatsa, S.C., Bhattacharya, S. (2019), A review on catalytic pyrolysis of microalgae to high-quality bio-oil with low oxygeneous and nitrogenous compounds, Renewable and Sustainable Energy Reviews, 108, 481–497. https://doi.org/10.1016/j.rser.2019.03.026

Liu, Z., Cao, Y., Wang, Z., Ren, H., Amidon, T.E., Lai, Y. (2015), Soy straw. Pt. 1, characterization, Bioresources, 10 (2), 2266–2280. DOI: 10.15376/biores.10.2.2266-2280

Massuque, J., Roque Lima, M.D., Müller da Silva, P.H., de Paula Protásio, T., Trugilho, P.F. (2023), Potential of charcoal from non-commercial Corymbia and Eucalyptus wood for use in the steel industry, Renewable Energy, 211, 179–187. https://doi.org/10.1016/j.renene.2023.04.061

Mellinas, A.C., Jiménez, A., Garrigós, M.C. (2020), Optimization of microwave-assisted extraction of cocoa bean shell waste and evaluation of its antioxidant, physicochemical and functional properties, Lwt, 127, 109361. https://doi.org/10.1016/j.lwt.2020.109361

Mishra, R.K., Saini, R., Kumar, D.J.P., Sankannavar, R., Binnal, P., Dwivedi, N., Kumar, P. (2023), Thermo-catalytic pyrolysis of Azadirachta indica seeds over CaO and CuO: Pyrolysis kinetics, impact of catalysts on yield, fuel properties and its chemical compositions, Journal of the Energy Institute, 111, 101366. https://doi.org/10.1016/j.joei.2023.101366

Mohan, D., Pittman, C.U., Steele, P.H. (2006). Pyrolysis of Wood/Biomass for Bio-oil: A Critical Review. Energy & Fuels, 20, 848–889. https://doi.org/10.1021/ef0502397

Montoya, J.I., Valdés, C., Chejne, F., Gómez, C.A., Blanco, A., Marrugo, G., Osorio, J., Castillo, E., Aristóbulo, J., Acero, J. (2015), Bio-oil production from Colombian bagasse by fast pyrolysis in a fluidized bed: An experimental study, Journal of Analytical and Applied Pyrolysis, 112, 379–387. https://doi.org/10.1016/j.jaap.2014.11.007

Mumbach, G.D., Alves, J.L.F., Silva, J.C.G., Domenico, M., Sena, R.F., Marangoni, C., Machado, R.A.F., Bolzan, A. (2020). Pyrolysis of cocoa shell and its bioenergy potential: evaluating the kinetic triplet, thermodynamic parameters, and evolved gas analysis using TGA-FTIR. Biomass Conversion and Biorefinery, 12, 723–739. https://doi.org/10.1007/s13399-020-01058-5

Nam, K.H., Kim, D.Y., Pack, I.S., Park, J.H., Seo, J.S., Choi, Y. Do, Cheong, J.J., Kim, C.H., Kim, C.G. (2016), Comparative analysis of chemical compositions between non-transgenic soybean seeds and those from plants over-expressing AtJMT, the gene for jasmonic acid carboxyl methyltransferase, Food Chemistry, 196, 236–241. https://doi.org/10.1016/j.foodchem.2015.09.046

Nguyen, T.H., Ra, C.H., Sunwoo, I.Y., Sukwong, P., Jeong, G.T., Kim, S.K. (2018). Bioethanol Production from Soybean Residue via Separate Hydrolysis and Fermentation. Applied Biochemistry and Biotechnology, 184 (2), 513–523. https://doi.org/10.1007/s12010-017-2565-6

Okiyama, D.C.G., Navarro, S.L.B., Rodrigues, C.E.C. (2017), Cocoa shell and its compounds: Applications in the food industry, Trends in Food Science and Technology, 63, 103–112. https://doi.org/10.1016/j.tifs.2017.03.007

Oliveira, J.P. (2015), Pirólise rápida de casca de soja: desenvolvimento do reator de leito fluidizado, análise do bio-óleo produzido e do vapor obtido na pirólise analítica, Tese de Doutorado, Faculdade de Engenharia Química, Universidade Federal de Uberlândia.

Onokwai, A.O., Ajisegiri, E.S.A., Okokpujie, I.P., Ibikunle, R.A., Oki, M., Dirisu, J.O. (2022), Characterization of lignocellulose biomass based on proximate, ultimate, structural composition, and thermal analysis, Materials Today: Proceedings, 65, 2156–2162. https://doi.org/10.1016/j.matpr.2022.05.313

Qing, Q., Guo, Q., Zhou, L., Gao, X., Lu, X., Zhang, Y. (2017). Comparison of alkaline and acid pretreatments for enzymatic hydrolysis of soybean hull and soybean straw to produce fermentable sugars. Industrial Crops and Products, 109, 391–397. https://doi.org/10.1016/j.indcrop.2017.08.051

Rojas, M., Ruano, D., Orrego-Restrepo, E., Chejne, F. (2023), Non-isothermal kinetics of cellulose, hemicellulose, and lignin degradation during cocoa bean shell pyrolysis, Biomass and Bioenergy, 177, 106932. https://doi.org/10.1016/j.biombioe.2023.106932

Sellin, N., Krohl, D.R., Marangoni, C., Souza, O. (2016), Oxidative fast pyrolysis of banana leaves in fluidized bed reactor, Renewable Energy, 96, 56–64. https://doi.org/10.1016/j.renene.2016.04.032

Sun, Y., Li, C., Zhang, S., Li, Q., Gholizadeh, M., Wang, Y., Hu, S., Xiang, J., Hu, X. (2021), Pyrolysis of soybean residue: Understanding characteristics of the products, Renewable Energy, 174, 487–500. https://doi.org/10.1016/j.renene.2021.04.063

Telmo, C., Lousada, J., Moreira, N. (2010), Proximate analysis, backwards stepwise regression between gross calorific value, ultimate and chemical analysis of wood, Bioresource Technology, 101 (11), 3808–3815. https://doi.org/10.1016/j.biortech.2010.01.021

Xing, P., Mason, P.E., Chilton, S., Lloyd, S., Jones, J.M., Williams, A., Nimmo, W., Pourkashanian, M. (2016), A comparative assessment of biomass ash preparation methods using X-ray fluorescence and wet chemical analysis, Fuel, 182, 161–165. https://doi.org/10.1016/j.fuel.2016.05.081

Wang, S., Luo, Z. Pyrolysis of biomass. (2017a). Berlin: Walter de Gruyter GmbH, 268.

Wang, X., Tang, X., Yang, X. (2017b). Pyrolysis mechanism of microalgae Nannochloropsis sp. based on model compounds and their interaction. Energy Conversion and Management, 140, 203-210. https://doi.org/10.1016/j.enconman.2017.02.058

Welker, C.M., Balasubramanian, V.K., Petti, C., Rai, K.M., De Bolt, S., Mendu, V. (2015). Engineering plant biomass lignin content and composition for biofuels and bioproducts. Energies, 8 (8), 7654–7676. https://doi.org/10.3390/en8087654

Yuan, C., Wang, S., Cao, B., Hu, Y., Abomohra, A.E.F., Wang, Q., Qian, L., Liu, L., Liu, X., He, Z., Sun, C., Feng, Y., Zhang, B. (2019), Optimization of hydrothermal co-liquefaction of seaweeds

with lignocellulosic biomass: Merging 2nd and 3rd generation feedstocks for enhanced bio-oil production, Energy, 173, 413–422. https://doi.org/10.1016/j.energy.2019.02.091

Zainan, N.H., Srivatsa, S.C., Bhattacharya, S. (2015), Catalytic pyrolysis of microalgae Tetraselmis suecica and characterization study using in situ Synchrotron-based Infrared Microscop, Fuel, 161, 345–354. https://doi.org/10.1016/j.fuel.2015.08.030

Zhang, M., Resende, F.L.P., Moutsoglou, A., Raynie, D.E. (2012). Pyrolysis of lignin extracted from prairie cordgrass, aspen, and Kraft lignin by Py-GC/MS and TGA/FTIR. Journal of Analytical and Applied Pyrolysis, 98, 65–71. https://doi.org/10.1016/j.jaap.2012.05.009

Zhang, L., Li, K., Zhu, X. (2017), Study on two-step pyrolysis of soybean stalk by TG-FTIR and Py-GC/MS, Journal of Analytical and Applied Pyrolysis, 127, 91–98. https://doi.org/10.1016/j.jaap.2017.08.019

CHAPTER 5

5. RESULTS AND DISCUSSIONS – ANALYTICAL PYROLYSIS

In this chapter, the results and discussions from the experimental results of the catalytic and non-catalytic analytical pyrolysis process are presented.

The analytical pyrolysis technique assessed the feasibility of utilizing agricultural residues as the biomass source for biofuel production, achieved through examining pyrolytic vapors. The identified compounds were grouped in different ways for a better presentation and understanding of the results presented according to calculations referring to the percentage of the area of the chromatographic peak of each compound obtained by the ion chromatogram and identified using the library database of the National Institute of Standards and Technology (NIST 14). The most abundant 60 components with a similarity index greater than 80% were selected and then categorized in different manners. It is noteworthy that this represents a semi-quantitative analysis, as it establishes a linear relationship between the peak area of a specific compound and its quantity (Lee et al., 2022; Moogi et al., 2022; Domínguez et al., 2003). The identified compounds were classified and organized according to their organic functional groups, encompassing oxygenated species (e.g., ketones, alcohols, carboxylic acids), nitrogenated species (such as amines and nitriles), hydrocarbons, and other related compounds. Compounds featuring multiple functional groups, e.g., 2-Propanone, 1-hydroxy (ketone and alcohol organic groups), were categorized using the National Center for Biotechnology Information classification. In this instance, the compound is identified as functionally related to acetone, where one of the methyl hydrogens is substituted by a hydroxy group.

5.1. Catalyst Effect

The initial phase of this study involved the assessment of four distinct catalysts, seeking more effective alternatives to enhance the production of hydrocarbons while reducing the formation of undesirable byproducts such as acids and nitrogen-containing compounds. To achieve this, the outcomes of non-catalytic pyrolysis with those obtained through catalytic pyrolysis using four

catalysts: hydrotalcite, zeolite, Ni/Nb_2O_5 (Ni/Nb), and $Ni\text{-}Re/Nb_2O_5$ (NiRe/Nb) were compared. During this stage, all experiments were conducted at a temperature of 550°C, maintaining a catalyst-to-biomass ratio of 3:1.

A comprehensive comparison of these results was conducted using two distinct categorizations. The first categorization, illustrated in Figure 5.1, segregated the compounds into groups based on the number of oxygen atoms, distinguishing between those with one, two, and three or more oxygens. This classification would assist in discerning the potential cleavages involving C-O and C=O chemical bonds since oxygen removal is one of the primary routes to hydrocarbon formation in biomass pyrolysis.

The products categorization also encompasses aromatic and aliphatic hydrocarbons, nitrogen-containing, and oxygenated/nitrogenated compounds. Subsequently, (a) the results for soybean residue (SR) and (b) for cocoa bean shell (CBS) are presented.

In a broader context, the observations revealed that the catalysts exhibited consistent effects across the various biomass samples under study. Specifically, hydrotalcite and zeolites demonstrated a pronounced capacity for transforming oxygenated compounds into hydrocarbons. In the results of catalysts derived from niobic acid, a more significant generation of nitrogenates was observed while oxygenates were reduced. The following sections will address further discussions regarding the catalysts' effects.

When analyzing the main differences between the two residues, there was a notable increase in the production of nitrogenous compounds in all catalytic pyrolysis products derived from soybean residue (a). This is likely attributed to the higher nitrogen content in soybean residue (6%) compared to the cocoa shell (3%), as elucidated in the characterization results presented in Chapter 4. Andrade et al. (2020) investigated pyrolytic bio-oil from two distinct microalgae species, namely *Chlamydomonas reinhardtii* and *Spirulina platenses*, which contained approximately 10% nitrogen content. The production of nitrogen-containing compounds from these microalgae varied within a range of 15 to 50%, thus potentially halting the formation of hydrocarbons.

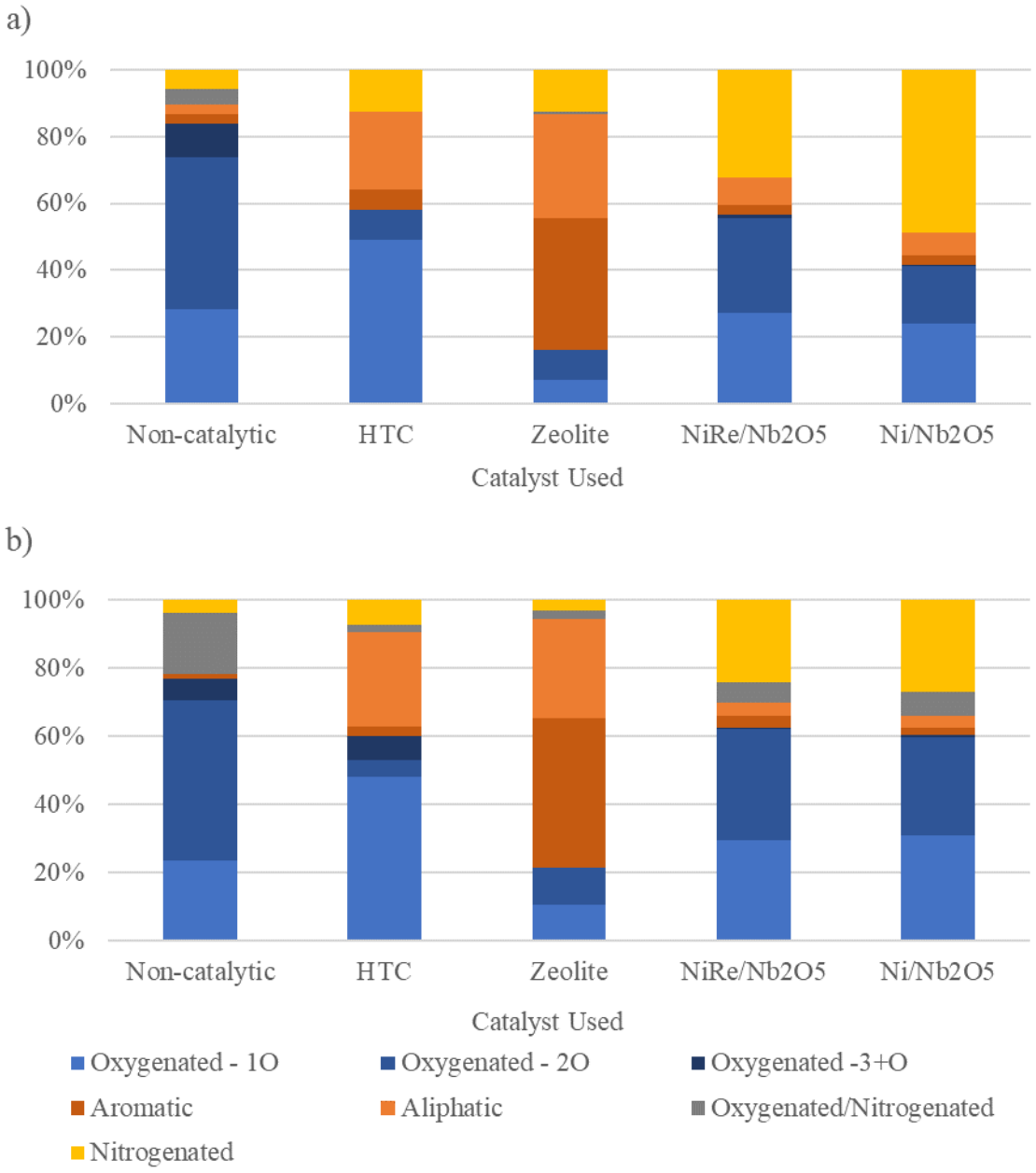


Figure 5.1. Categorization of catalytic and non-catalytic pyrolysis products of (a) SR and (b) CBS; temperature of 550°C and 3:1 catalyst-to-biomass ratio

The second broad comparison involved the classification of pyrolysis products into distinct organic functional groups, as shown in Figure 5.2. It is evident that non-catalytic pyrolysis exhibited a highly diverse composition, contrasting sharply with the catalytic outcomes obtained

with each of the four catalysts. This disparity underscores the potential for catalytic selectivity in product formation during chemical adsorption (Abelló et al., 2007; Danilina et al., 2011).

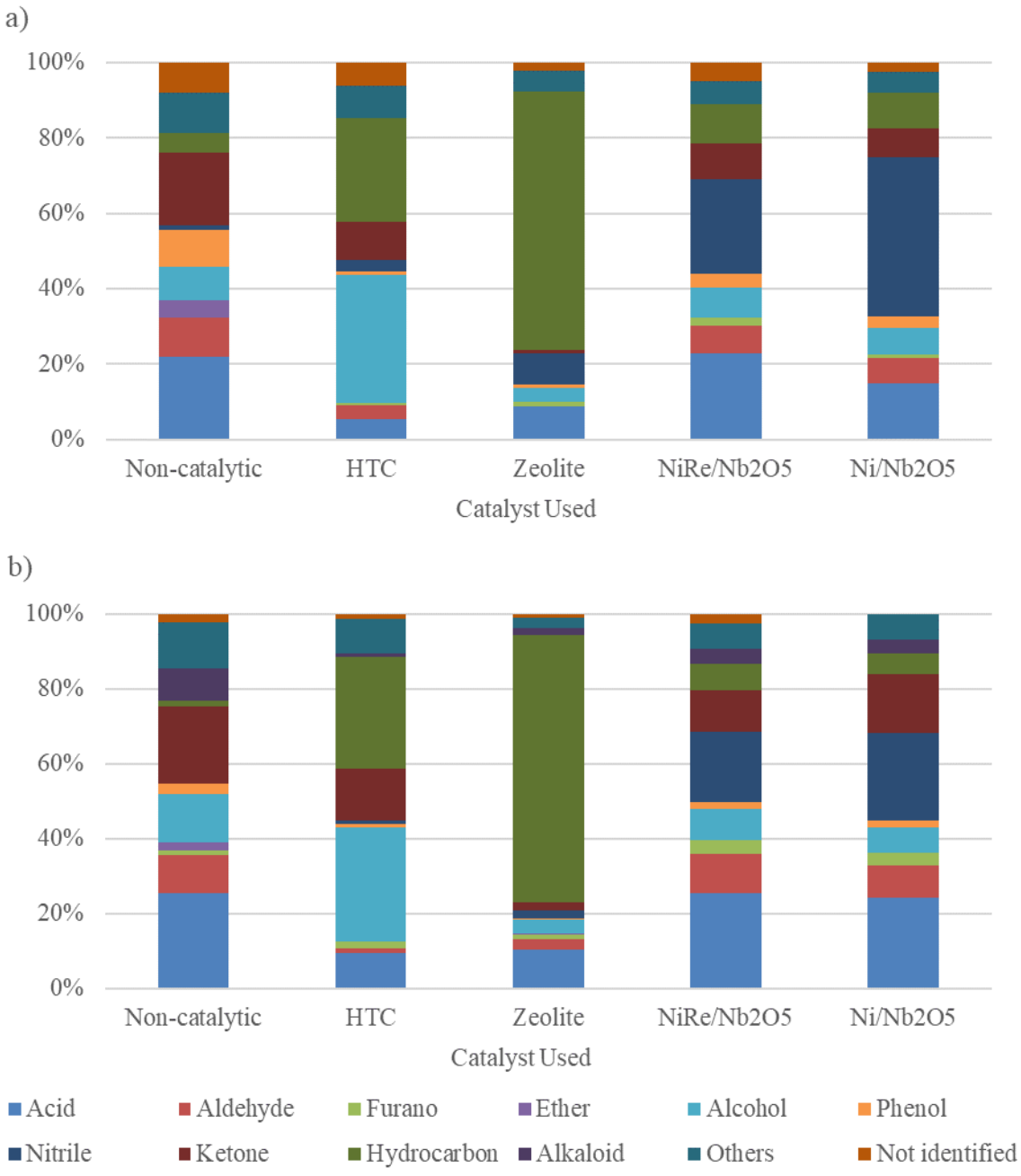


Figure 5.2. Pyrolysis products categorization by organic functional groups for (a) SR and (b) CBS; temperature of 550°C and 3:1 catalyst proportion

Similar behavior was again observed between soybean residue (a) and cocoa shell (b), with the primary distinction being the predominant formation of nitriles in soybean residue, which represents the main group of nitrogen-containing compounds, as indicated in Figure 5.1. Subsequent sections will delve into a comprehensive examination of each of the five micro-pyrolysis analyses at this stage of the study.

5.1.1. Non-Catalytic Pyrolysis

In non-catalytic pyrolysis, product heterogeneity arises from the intricate composition of the in natura biomass and the complex reaction mechanisms inherent to this thermochemical process (Silva, 2020). Figure 5.3 displays the organic functional groups derived from pyrolysis at 550°C of soybean residue (a) and cocoa shell (b).

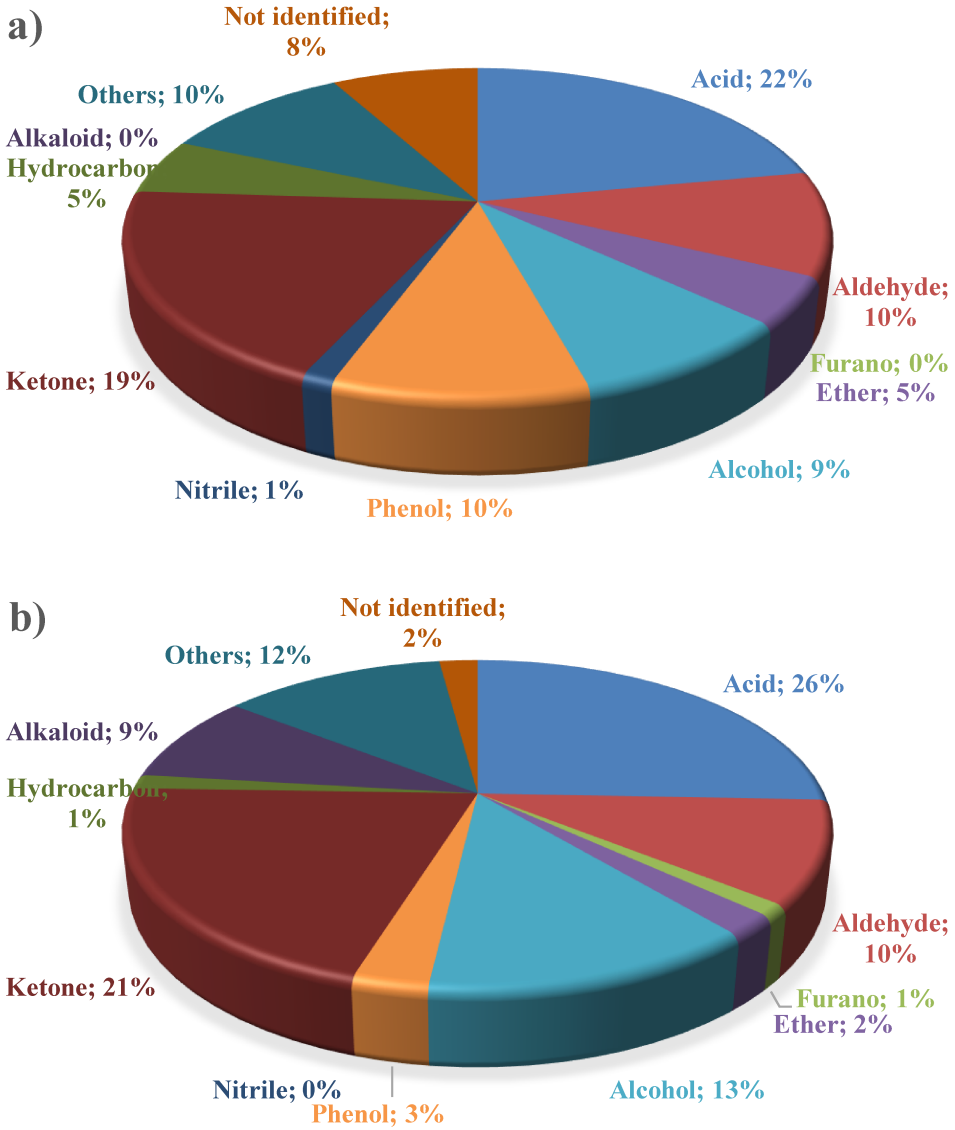


Figure 5.3. Non-Catalytic Pyrolysis products categorization by organic functional groups for (a) SR and (b) CBS; temperature of 550°C

It is observed that the components are a rich mixture of complex oxygenated hydrocarbons with an emphasis on the formation of carboxylic acids, aldehydes, ketones, phenolic compounds, and alcohols. The presence of these oxygenated compounds is attributable to the composition of the lignocellulosic fibers constituting the biomass. These results align with the literature, as documented in the Handbook of Biomass Downdraft Gasifier Engine Systems (1988) and are

consistent with the results reported by Wang et al. (2017) for various other biomass sources, as illustrated in Figure 5.4..

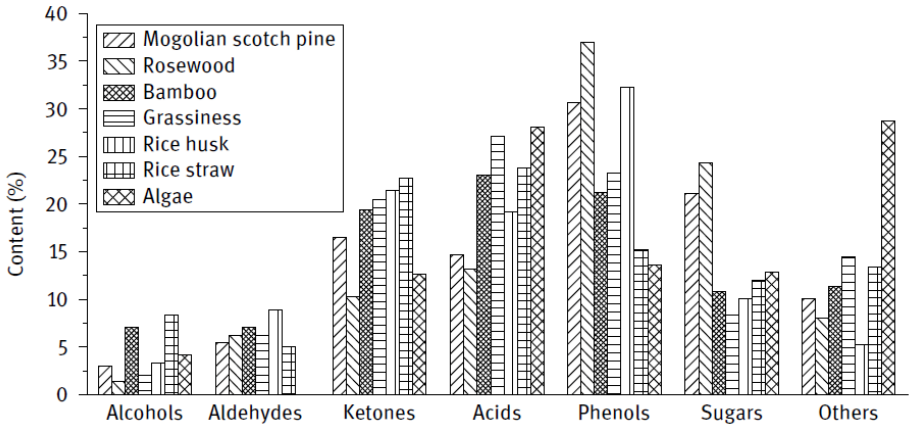


Figure 5.4. Non-Catalytic Pyrolysis products from other biomasses (Wang et al., 2017)

Another significant aspect of non-catalytic pyrolysis is the transformation of large and complex molecules into smaller and simpler ones (Morris, 2011). This behavior is evident when examining the size distribution of carbon chains, as depicted in Figure 5.5. Cellulose and hemicellulose that composed the biomasses used in this study are polymers formed by monomers of 5 and 6 carbons, such as pentose units (xylose and arabinose) and hexose units (glucose, galactose, mannose, rhamnose, and glucuronic and galacturonic acids) (Thompson, 2000; Väisänen et al., 2021). These large and complex polymeric structures were broken into smaller chains of up to 5 carbons through pyrolysis. In both biomass cases, approximately 70% of the product composition consisted of organic molecules with five carbons or fewer in their structure, while around 25% contained between six and ten carbons.

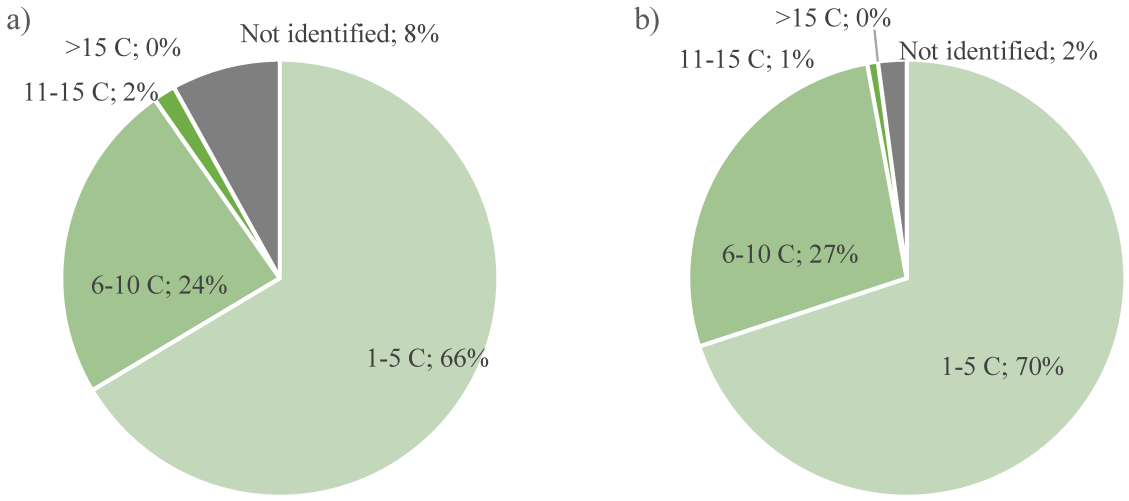


Figure 5.5. Size of chains based on number of carbons in the organic structure for the non-catalytic pyrolysis of (a) SR and (b) CBS; temperature of 550°C

The main compounds within each category are detailed in Table 5.1. and account for 45% of the identified organic compounds in the soybean residue pyrolysis and nearly 60% in the cocoa bean shell pyrolysis. Notably, four of these compounds represented approximately 40% of the organic products in the non-catalytic pyrolysis for both biomasses: acetic acid, acetaldehyde, methanol, and "2-Propanone, 1-hydroxy-metanol" These compounds are also categorized as "light oxygenates" and likely result from the aromatic ring opening and rearrangement processes occurring during the pyrolysis reactions of hemicellulose and cellulose (Liu et al., 2023). Acetic acid, the most representative product for both biomass, can be formed mainly during the thermal decomposition of hemicellulose (Wu et al., 2009), while the presence of methanol can be primarily due to the degradation of Xylane and, lastly, "2-Propanone, 1-hydroxy-" most likely comes from lignin and hemicellulose decomposition. (Güllü et al., 2001). In the case of cocoa bean shells, a notable presence of theobromine and caffeine was detected, which are inherent to the raw material. This fact implies that these compounds exhibit consistency either in solid or gaseous forms. They are released at temperatures higher than 500°C but do not undergo cleavage into different compounds, remaining in their original forms as theobromine and caffeine. Typically, these compounds account for approximately 4.7-11.6 mg/g and 1.1-2.1 mg/g of the cocoa bean, respectively (Cinar et al., 2021).

Table 5.1. Main organic products from non-catalytic pyrolysis at the temperature of 550°C

Compound	Formula	Soybean Residue	Cocoa Bean Shell
Acetic acid	$C_2H_4O_2$	18.0%	22.8%
2-Propanone, 1-hydroxy-	$C_3H_6O_2$	9.4%	8.5%
Methanol	CH_4O	7.5%	6.3%
Acetaldehyde	C_2H_4O	5.0%	3.7%
2,3,5-Trimethylanizole	$C_{10}H_{14}O$	1.9%	0.0%
DL-Proline, 5-oxo-	$C_5H_7NO_3$	3.2%	0.0%
Theobromine	$C_7H_8N_4O_2$	0.0%	13.6%
Caffeine	$C_8H_{10}N_4O_2$	0.0%	2.4%
Pyrrole	C_4H_5N	0.0%	3.7%
Total		**45.0%**	**61.1%**

As previously mentioned, oxygenated compounds impart unwanted features to the bio-oil in addition to being, in the majority, polar in nature, impairing it from being mixed with petroleum-derived fuels (Simão et al., 2018). The presence of catalysts can promote an increase in hydrocarbons and enhance the quality of pyrolytic products as oxygenated organic compounds are replaced or eliminated. The catalytic results will be presented for the four catalysts explored in this stage of the study.

5.1.2. Catalytic Pyrolysis with Hydrotalcite Precursor (HTC)

For catalytic pyrolysis with hydrotalcite, the product composition formed (% of chromatographic peak area) in analytical pyrolysis allows semiquantitative evaluation of deoxygenation and hydrocarbon production performance. Figure 5.6. presents the product composition in the pyrolysis at 550°C of soybean residue (a) and cocoa shell (b) with HTC in the catalyst-to-biomass ratio of 3:1 along with the non-catalytic control to facilitate the comparison.

Reduced heterogeneity of organic groups with more representative compositions is observed. Remarkably, the impact on the two biomass sources is quite similar, with a significant reduction in acids, aldehydes, ethers, phenols, ketones, and alkaloids (the latter only present in the CBS). In contrast, the production of hydrocarbons and alcohols was notably enhanced. These two groups together constitute slightly over 60% of the organic compounds generated under these specific conditions.

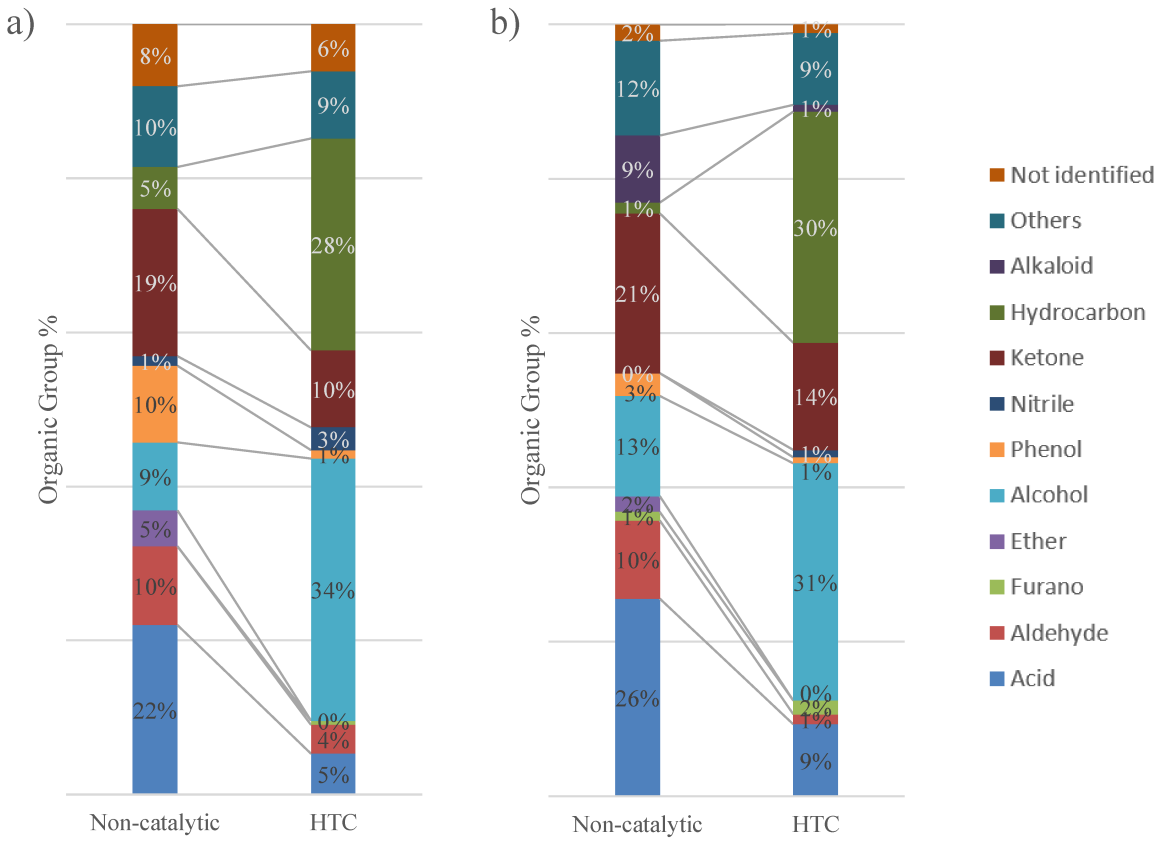


Figure 5.6. Categorization of non-catalytic and catalytic (HTC) pyrolysis products of (a) SR and (b) CBS; temperature of 550°C and 3:1 catalyst proportion

A study conducted by Prabhakara et al. (2022), employing HTC as the catalyst, performed beechwood pyrolysis at 500°C, yielding outcomes comparable to those observed in the present investigation for most functional groups. However, notable disparities were observed in the production of ketones and alcohols. Particularly, beechwood pyrolysis led to a more pronounced formation of cyclic ketones, while the soybean residue and cocoa bean shells generated cyclic alcohols. These distinctions suggest that similar mechanisms might be at play, but they likely initiate from different starting points, possibly influenced by the distinctive characteristics of the respective raw materials (Li et al., 2019; Lin et al., 2021; Prabhakara et al., 2022). It can be highlighted that ketones exist in an equilibrium with their corresponding enol forms, and this equilibrium is strongly thermodynamically controlled. At typical room temperature conditions, the keto form is favored and predominates. The interconversion between these forms can be catalyzed by the presence of either an acid or a base, as illustrated in Figure 5.7. (Higginbotham, 2021).

Therefore, the variation between these two studies could potentially be attributed to distinctive characteristics of the biomass materials, which might have shifted the equilibrium towards alcohol production instead of ketones, as observed in the research by Aleem et al. (2021) and Kumar et al. (2018).

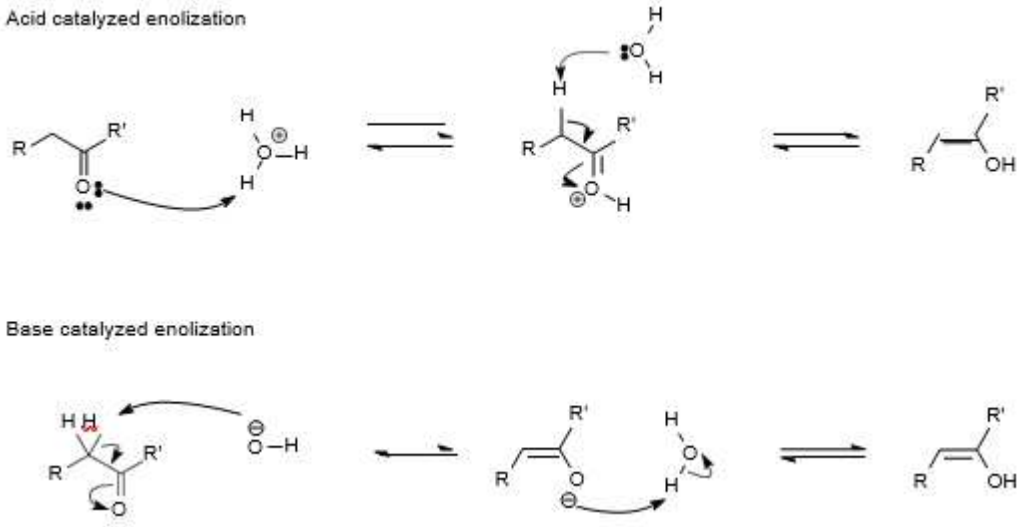


Figure 5.7. Keto-enol tautomerism: The interconversion between the two forms can be catalyzed by an acid or a base. (Higginbotham, 2021)

Another relevant aspect in understanding the reaction mechanisms when employing HTC as a catalyst is the examination of the organic chain sizes. Figure 5.8. presents the change observed in chain size, which includes a minor decrease in chains comprising 1 to 5 carbon atoms (reducing from 66% and 70% to 57% and 51% for SR and CBS, respectively). On the other hand, compounds within the 6 to 10 carbon group remained stable (24% and 27% to 28% and 30% for SR and CBS, respectively) regardless of the catalyst employment. Regarding the other two scrutinized groups, an increase is observed. Chains from 11 to 15 carbons escalated from 2% and 1% to 6% and 12%, and chains with more than 15 carbons went from non-significant values to 3% and 5%. Notably, most observed hydrocarbons comprised long chains with 11 or more carbon atoms, implying a polymerization mechanism during the catalytic process. Layered double hydroxides (LDHs), such as hydrotalcite, have been the subject of extensive research due to their potential applications in various significant fields, including catalysis, photochemistry, electrochemistry, and polymerization applications (Goh et al., 2008). Newman et al. (1998) reported the utilization of

LDHs to investigate the early phases of emulsifier-free emulsion polymerization of styrene. Evans et al. (2005) and Moujahid et al. (2002) propose that the polymerization of guest molecules might occur within the interlayer galleries of the LDHs. Gholami et al. (2020) studied the conversion of syngas using CoMn-HTC, finding 20 to 75% of hydrocarbons that ranged from 11 to 22 carbon atoms.

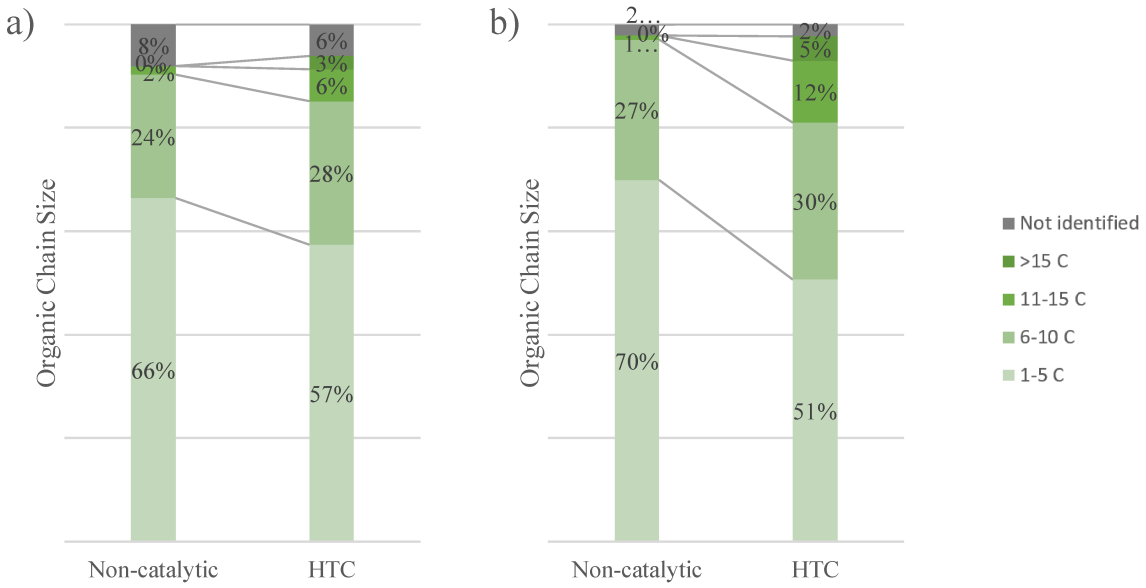


Figure 5.8. Size of chains based on number of carbons in the organic structure for the non-catalytic pyrolysis and pyrolysis with HTC of (a) SR and (b) CBS; temperature of 550°C and 3:1 catalyst proportion

The main compounds identified are outlined in Table 5.2., constituting nearly 60% of the organic compounds detected. Although there was a decrease in compounds with chains ranging from 1 to 5 carbon atoms, an enhanced homogeneity of compounds was observed, as shown in Table 5.2. with 8 compounds among the most significant products formed. In the case of alcohols, for instance, just three compounds, namely methanol, ethanol, and cyclobutanol, account for the vast majority of alcohol production. This uniformity exhibits an attractive character for HTC, potentially enhancing product selectivity in the pyrolysis reaction. Wang et al. (2020) examined ethanol transesterification using Mg/Al mixed oxide derived from hydrotalcite. They achieved a

selectivity of approximately 80% for ethyl methyl carbonate, resulting in an ethanol conversion rate ranging from 60 to 75%.

Comparing Tables 5.2. and 5.1., a significant decrease in acetic acid, "2-propanone, 1-hydroxy-," and acetaldehyde is evident for both biomass. Notably, acetaldehyde was eliminated from the formed compounds in the catalytic test using HTC.

In the case of CBS, there was also a decrease in the two distinctive compounds found in the raw material, theobromine and caffeine, which contain oxygen and nitrogen in their composition. This further underscores the deoxygenation and denitrification capabilities of the HTC catalyst, as these compounds remained unreacted during non-catalytic pyrolysis. Thus appearing in larger proportions in the resulting products. It's worth noting that, despite the reduction in the ketone group, a substantial production of acetone was observed, a characteristic feature of catalysts with basic metal oxide sites. Previous research has indicated that carboxylic acids can undergo conversion into ketones through ketonization on these basic metal oxide sites (Kumar et al., 2018).

Table 5.2. Main organic products from Catalytic pyrolysis with HTC at the temperature of 550°C and 3:1 catalyst proportion

Compound	Formula	Soybean Residue	Cocoa Bean Shell
Acetic acid	$C_2H_4O_2$	3.5%	2.4%
2-Propanone, 1-hydroxy-	$C_3H_6O_2$	2.3%	1.8%
Methanol	CH_4O	11.3%	9.5%
Acetaldehyde	C_2H_4O	0.0%	0.0%
Ethanol	C_2H_6O	13.2%	13.7%
1-Pentene, 4-methyl-	C_6H_{12}	5.8%	4.5%
Cyclobutanol	C_4H_8O	9.1%	6.0%
Toluene	C_7H_8	5.1%	2.7%
1-Heptene	C_7H_{14}	0.0%	3.5%
Acetonitrile	C_2H_3N	2.2%	1.0%
Acetone	C_3H_6O	2.3%	4.1%
Theobromine	$C_7H_8N_4O_2$	0.0%	0.7%
Caffeine	$C_8H_{10}N_4O_2$	0.0%	1.4%
Pyrrole	C_4H_5N	3.9%	4.6%
Total		**58.8%**	**56.0%**

The analytical pyrolysis revealed that hydrotalcite had a significant impact on the product composition, resulting in 58% and 60% oxygen-containing compounds and 29% and 30% hydrocarbons for SR and CBS residue, respectively. Although there remains a notable presence of

oxygen-containing compounds, hydrotalcite (HTC) demonstrated its catalytic potential for promoting selective reactions. HTC catalyst most likely favored decarbonylation that eliminates CO (Resende, 2016), therefore, reducing molecules with 2 atoms of oxygen. Under these conditions, HTC may have contributed to deacidification reactions, converting carboxylic acids into alcohols (molecules with 1 atom of oxygen). Ding et al. (2018) explored the catalytic pyrolysis of hemicellulose and confirmed the deacidification capability of CaO, which, like HTC, possesses active basic sites.

This positive influence extends to pyrolysis products' physical and chemical properties since just over half of these oxygenates are alcohols. These physical and chemical properties include the increase in calorific value, lower acidity, higher stability that can retard the aging and oxidation process of the bio-oil, and more excellent miscibility with other fuels (Bridgwater, 2018).

Navarro et al. (2018) studied the catalytic fast pyrolysis of biomass using Mg/Al mixed oxides obtained from hydrotalcite-like precursors. Their research indicated that the removal of oxygen from the bio-oil, achieved through decarbonylation and decarboxylation, exhibited a range between 20 and 25%. Consequently, their bio-oil had an approximate oxygen content of 35%.

5.1.3. Catalytic Pyrolysis with Zeolite HZSM-5

Similarly to the analysis conducted for hydrotalcite catalyst usage, Figure 5.9. illustrates the product composition resulting from pyrolyzing SR (a) and CBS (b) at 550°C, employing zeolite (HZSM-5) at a catalyst-to-biomass ratio of 3:1. These catalytic tests were also compared to the non-catalytic reaction.

In the case of the catalytic pyrolysis with HZSM-5, even greater uniformity in organic groups is evident when compared to hydrotalcite usage. Zeolites typically possess multi-dimensional microporous structures that facilitate the penetration of small molecular reactants into the internal acid sites within the zeolite framework. Pore structure, acid type, and strength are the crucial factors affecting aromatic formation (Wang et al., 2017b). Using HZSM-5, similar effects were observed for both biomass, with a pronounced increase in hydrocarbons from 5% and 1% to 69% and 71% for SR and CBS, respectively. Among the reduced functional groups, acids remained significant, accounting for 9% and 10% for SR and CBS, respectively. In contrast, nitrile groups

increased from 1% and 0% to 8% and 2% for SR and CBS, respectively. The SR presented a more significant increase in nitriles, most likely due to the greater nitrogen content in the raw material.

The hydrocarbon formation is due to the removal of oxygenates containing diverse functional groups, which leads to distinct deoxygenation pathways when using HZSM-5 as the catalyst. Alcohols and phenols predominantly release oxygen as H_2O, whereas aldehydes and carbohydrates primarily undergo oxygen removal in the form of CO_2 and H_2O, and carboxylic acids release oxygen as CO_2 and H_2O (Taarning et al., 2011). The pyrolysis of lignocellulosic biomass yields a substantial quantity of low-molecular-weight oxygenates, such as furans, ketones, and alcohols. These compounds have the potential to undergo Diels-Alder/aromatization reactions with light olefins when proper catalysts are employed, resulting in the formation of hydrocarbons (Dai et al., 2020).

For instance, the phenol content was significantly reduced from 10% and 3% to negligible levels in both SR and CBS biomasses. Typically, the decomposition of lignin initially results in mono-phenolic compounds (Zhou et al., 2016), which can undergo interactive reactions, including isomerization, transalkylation, and polymerization, when exposed to zeolite catalysts (Zhou et al., 2016; To et al., 2014). Subsequently, it is hypothesized that these intermediates are transformed into aromatic compounds through hydrogen transfer reactions, resulting in only a minor presence of phenolic compounds in the final product (Zhou et al., 2016; To et al., 2014; White, 2011).

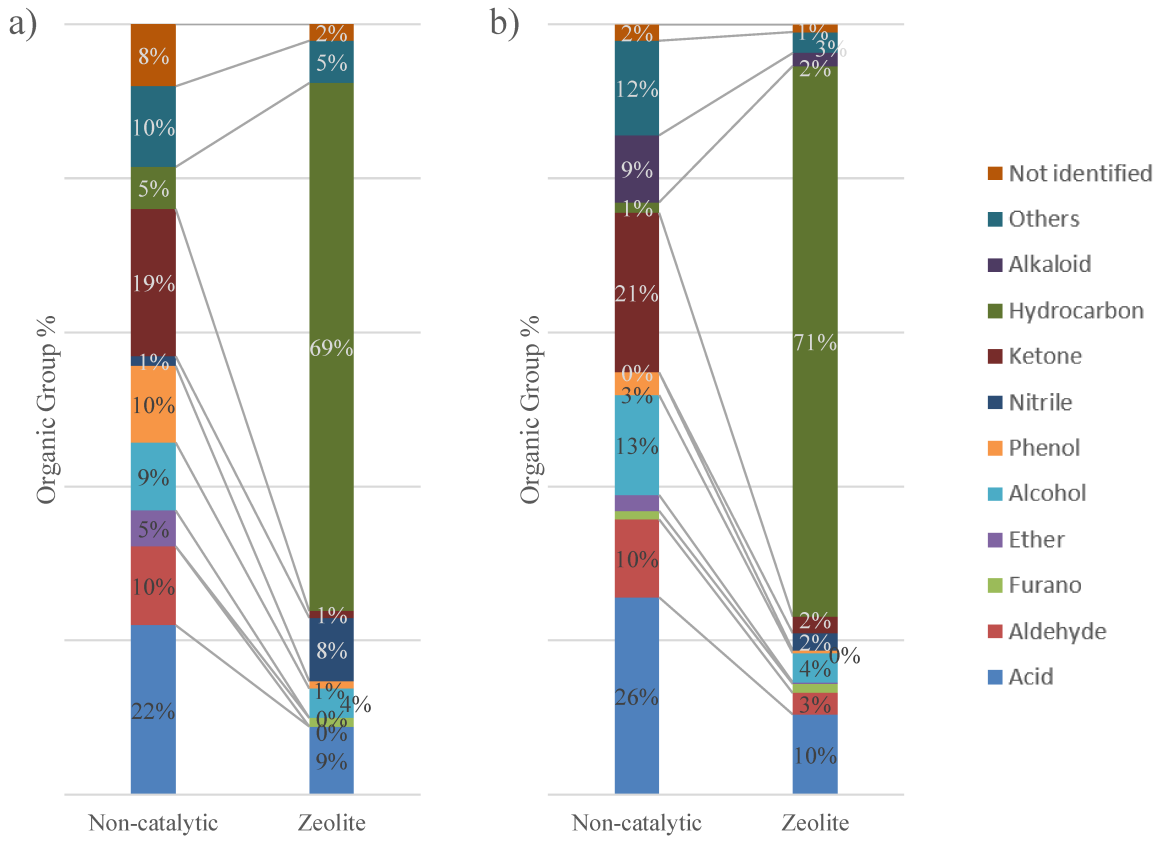


Figure 5.9. Categorization of non-catalytic and catalytic (HZSM-5) pyrolysis products of (a) SR and (b) CBS; temperature of 550°C and 3:1 catalyst proportion

Figure 5.10. illustrates the categorization of organic chain sizes, revealing a distinct shift for Zeolite. There is a noticeable transition from smaller chains containing 1 to 5 carbon atoms towards compounds with 6 to 10 carbons. A noteworthy presence of compounds derived from benzene is observed within this carbon chain category, constituting 30% for SR and 37% for CBS pyrolysis, as detailed in Table 5.3., which compiles the primary identified compounds. The Diels-Alder reaction pathway can be recognized as a pivotal process in the selective production of aromatic hydrocarbons from biomass pyrolysis, explaining the benzene formation. The Diels-Alder reaction entails the participation of a conjugated diene system and carbon-carbon double bonds, which are subsequently transformed into aromatic rings through further dehydrogenation. Notably, Chang et al. (2016) reported that H-BEA zeolite catalyzes Diels-Alder and dehydration reactions (Figure 5.11.), achieving a remarkable xylene selectivity of up to 90% in the liquid product.

Dai et al. (2019) studied bio-oil production from torrefied corncob pyrolysis using the hierachcal ZSM-5, finding around 46% of aromatic hydrocarbons.

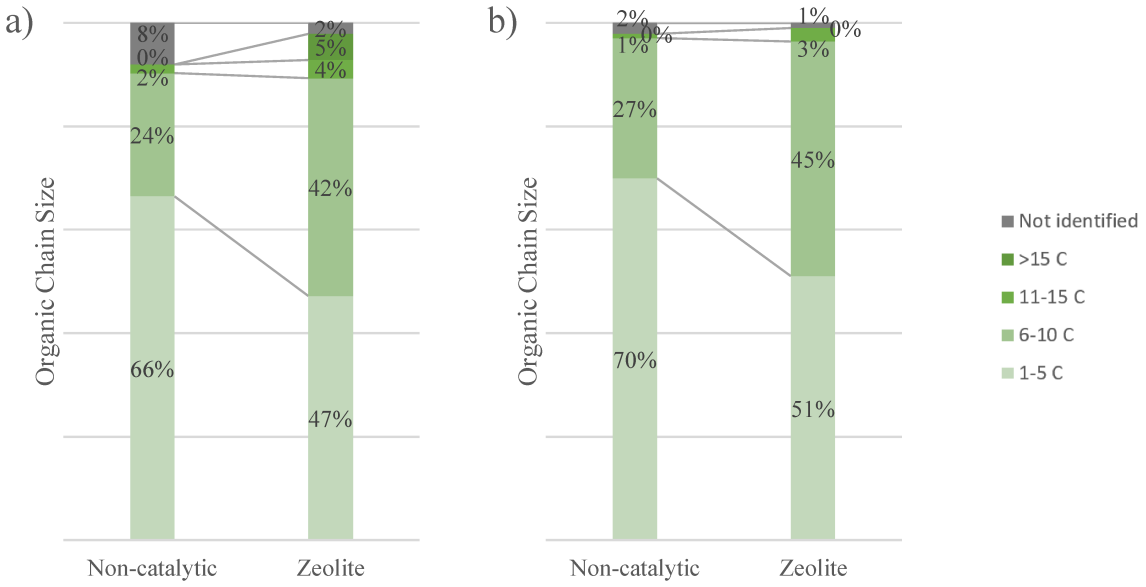


Figure 5.10. Size of chains based on number of carbons in the organic structure for the non-catalytic pyrolysis and pyrolysis with HZSM-5 of (a) SR and (b) CBS; temperature of 550°C and 3:1 catalyst proportion

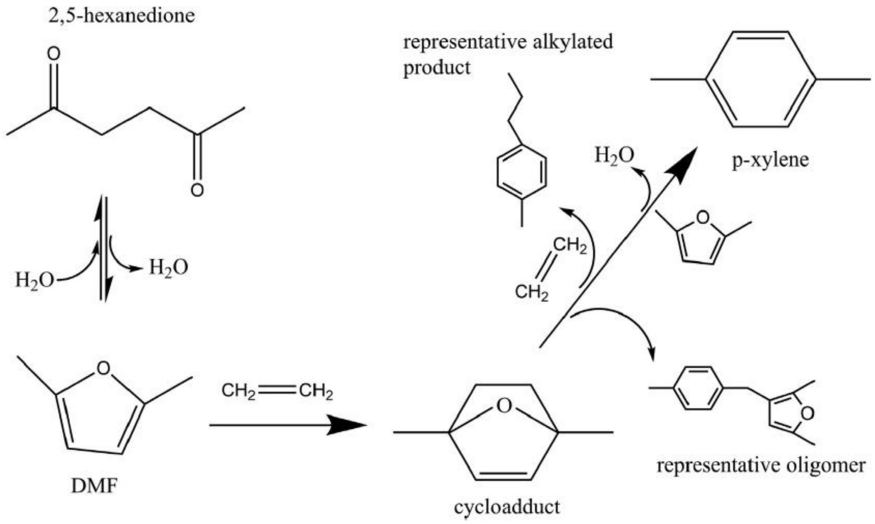


Figure 5.11. Xylene formation pathway from Diels-Alder cycloaddition of dimethylfuran and ethylene over Lewis acid zeolite catalyst (adapted from Chang et al., 2016.

Table 5.3. Main organic products from Catalytic pyrolysis with HZSM-5 at the temperature of 550°C and 3:1 catalyst proportion

Compound	Formula	Soybean Residue	Cocoa Bean Shell
Acetic acid	$C_2H_4O_2$	5.0%	8.4%
2-Propanone, 1-hydroxy-	$C_3H_6O_2$	0.0%	0.2%
Methanol	CH_4O	1.8%	2.0%
Acetaldehyde	C_2H_4O	0.0%	2.8%
Ethanol	C_2H_6O	0.0%	1.8%
2-Butene, (Z)- or (E)	C_4H_8	11.6%	8.7%
Propene	C_3H_6	10.0%	14.0%
Cycloprop, but and pent derivatives	-	5.0%	2.6%
Hydrocarbon Benzene Derivatives		30.6%	36.7%
Hydrocarbon Naphthalene Derivatives		0.0%	2.7%
Acetonitrile	C_2H_3N	3.8%	2.2%
Heptadecanenitrile	$C_{17}H_{33}N$	4.5%	0.0%
Theobromine	$C_7H_8N_4O_2$	0.0%	1.9%
Caffeine	$C_8H_{10}N_4O_2$	0.0%	0.5%
Total		**72.4%**	**84.3%**

Wang et al. (2014) investigated the catalytic pyrolysis of switchgrass using HZSM-5, and a mechanism was proposed for each of the primary constituents of lignocellulosic biomass (Figure 5.12.). This catalyst demonstrated a notable preference for producing alkenes and aromatic compounds during the initial pyrolysis in the presence of a high oxygenate concentration. The same behavior was observed in this present study, with the formation of alkenes and benzene derivatives constituting approximately 90% of all hydrocarbons generated from both biomasses. Aromatization is a significant pathway for aromatic compound formation, characterized by the prevailing processes of oligomerization and cyclization. This reaction transforms a substantial quantity of light oxygenates and olefins of the pyrolysis vapor into aromatic products (Fan et al., 2019).

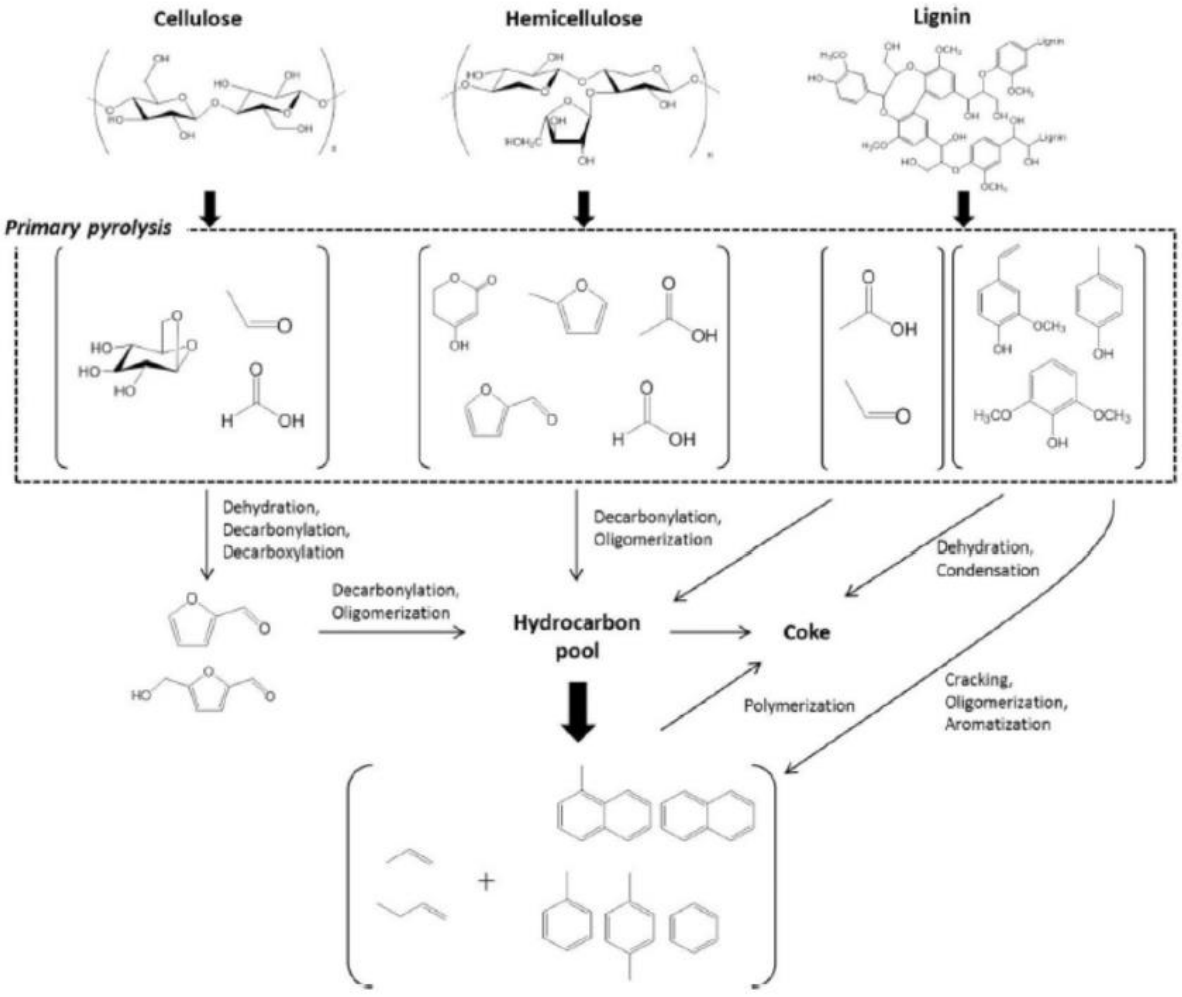


Figure 5.12. Reaction pathways for the catalytic pyrolysis of lignocellulosic biomass with HZSM-5 (Wang et al., 2014)

Additional findings from this study (Table 5.3.) highlight the reduced capacity of the HZSM-5 to diminish acetic acid when compared to the utilization of HTC as a catalyst. In contrast, an increase in nitrile compounds was observed when using zeolite, primarily in the form of acetonitrile.

Zeolites might display more excellent selectivity for oxygenated compounds (Hasegawa et al., 2002; Gu et al., 2005). In cases of a smaller catalyst quantity, nitrogenated substances are prone to remain untreated. The occupied sites of the zeolite can pose a challenge for nitrogen removal. As a result, nitrogen atoms are more likely to participate in pyrolysis reactions. The present study hypothesizes that nitrogen is involved in the polymerization reactions, generating long-chain

nitriles. Conversely, an increased catalyst load might assist in the elimination of both oxygenated and nitrogenated compounds (Gopakumara et al., 2012).

The long-chain nitriles formation was particularly pronounced in soybean residue, where there was also a relevant formation of heptadecanitrile. These results suggest the initiation of a polymerization process that involved nitrogen capture. This phenomenon is more pronounced in soybean residue, most likely due to its composition, as indicated in Table 4.2., which revealed a higher nitrogen content of 6%. According to Valle et al. (2010), elevated temperatures can promote and enhance the polymerization of phenolic derivatives contained in the bio-oil.

As demonstrated in prior research (Dai et al., 2019; Wang et al., 2017; Azreena et al., 2021; Liang et al., 2017), HZSM-5 zeolite has once again proven its potential as a catalyst with a remarkable ability to selectively produce hydrocarbons, making it a promising alternative for biofuel generation.

5.1.4. Catalytic Pyrolysis with Ni-Re/Nb_2O_5

Extending the analysis for analytical pyrolysis using a catalyst derived from niobic acid with Ni-Re impregnation, Figure 5.13. shows the product profiles obtained from the pyrolysis of SR (a) and CBS (b) at 550°C, employing Ni-Re/Nb_2O_5 compared with the non-catalytic pyrolysis. Notably, minimal changes are observed in most of the generated organic groups. The impact on both biomasses is rather similar, characterized by a reduction in ketones, phenols, ethers, and alkaloids (the latter only present in the cocoa bean shell). Simultaneously, there is a remarkable increase in the production of hydrocarbons, furans, and nitriles, with the latter being the most prominent. Nitrile production soared from 1% and 0% to 25% and 19% for SR and CBS, respectively. This trend aligns with observations made by Simão et al. (2018) and Moura (2022), who documented a consistent increase in nitrogen content when employing niobium-derived catalysts, highlighting the reproducibility of these results across different experiments.

Alcohols, aldehydes, and acids exhibited only marginal variations, which may indicate their limited interaction with the employed catalyst Ni-Re/Nb_2O_5. This observation suggests that the stability of acids (R-C(=O)OH), alcohols (R-COH), and aldehydes (R-CH=O) in catalytic pyrolysis is likely attributed to their polarity in comparison to other functional groups (Prusova et al., 2022). Additionally, their structural configuration, in which oxygen molecules are positioned at the end

of molecular chains, is distinct from ketones (R-C(=O)-R) and ethers (R-O-R), where oxygen atoms are bonded to two carbon atoms. One possible explanation is that when using a niobic acid-derived catalyst, a competitive series of reactions was favored, promoting ketone breakdown over the cleavage of alcohols, aldehydes, and acids. As a result, the breakage of ketones was more effectively achieved, leading to a halving of their content in both biomasses.

As elucidated in prior studies (Patwardhan et al., 2011; Shen et al., 2010), the pyrolysis of hemicellulose and cellulose can yield light oxygenates, such as water, acetone, methanol, acetic or formic acid, and furfural, either through competitive or sequential pathways.

Zhou et al. (2018) established mechanisms for hemicellulose pyrolysis. They categorized hemicellulose chain decomposition into two primary types of reactions: end-group and mid-group initiation reactions. Their findings highlighted a sequence of reactions encompassing end-chain initiation and mid-chain dehydration, which give rise to distinct chain species. Wang et al. (2015) compared the pyrolysis characteristics of hemicellulose derived from hardwood and softwood. The results indicated lower activation energy for hardwood hemicellulose, leading to higher concentrations of acids and furfural in the resulting bio-oil. Conversely, softwood hemicellulose primarily yielded HMF and anhydro sugars as the main pyrolysis products.

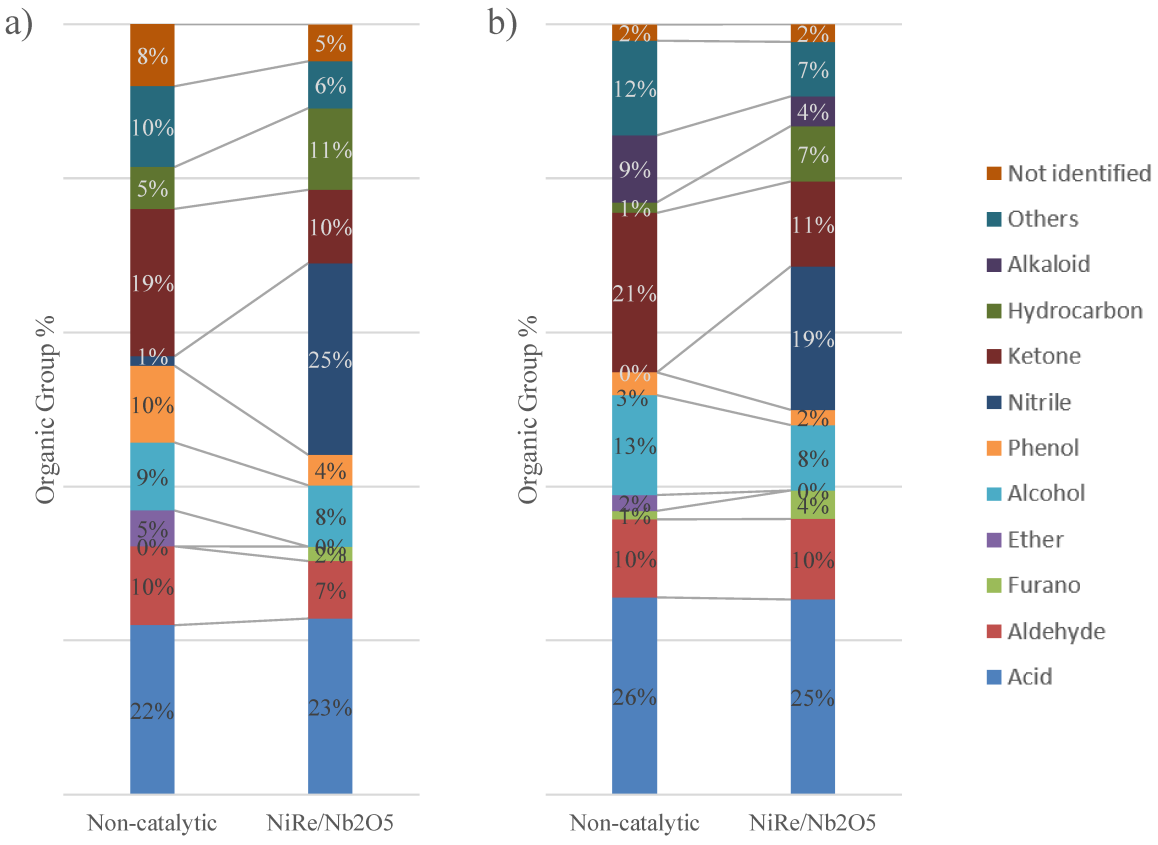


Figure 5.13. Categorization of non-catalytic and catalytic (Ni-Re/Nb_2O_5) pyrolysis products of (a) SR and (b) CBS; temperature of 550°C and 3:1 catalyst proportion

Figure 5.14. shows the classification of organic chains by size, revealing a noteworthy transition between groups of chains containing 6 to 10 carbon atoms and compounds with more than 15 carbons in their structure. This shift is accompanied by minimal changes in the other two groups (1-5 and 11-15 carbons). The larger chains substantially increased, rising from neglectable values to 26% and 16% for SR and CBS, predominantly represented by nitrogenous compounds (nitriles). The primary identified compounds within this category are detailed in Table 5.4..

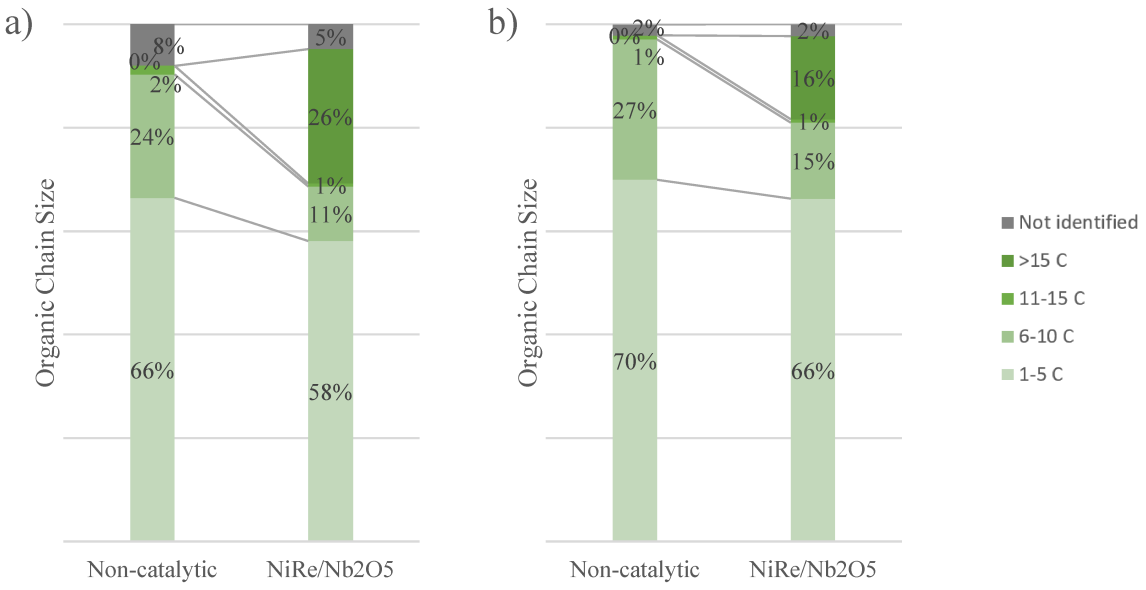


Figure 5.14. Size of chains based on number of carbons in the organic structure for the non-catalytic pyrolysis and pyrolysis with Ni-Re/Nb_2O_5 of (a) SR and (b) CBS; temperature of 550°C and 3:1 catalyst proportion

When examining Figures 5.13. and 5.14., as well as the primary compounds outlined in Table 5.4., it is possible to suggest that the niobium-derived catalyst plays a role in deoxygenating molecules of intermediate sizes and promoting polymerization with nitrogen capture occurring at the end of their chains, forming nitrile molecules. This hypothesis arises from the low occurrence of molecules containing more than 15 carbons in non-catalytic pyrolysis. This mechanism appears to be prioritized with the Ni-Re/Nb_2O_5 catalyst. Similar results involving the increase in nitrile compounds were also found for the zeolite catalyst.

Furthermore, another point to highlight in Table 5.4. is the minor variation in acetic acid, methanol, and acetaldehyde compared to the non-catalytic pyrolysis results in Table 5.1. This suggests that these compounds had limited interaction with the catalyst structure.

Table 5.4. Main organic products from Catalytic pyrolysis with Ni-Re/Nb_2O_5 at the temperature of 550°C and 3:1 catalyst proportion

Compound	Formula	Soybean Residue	Cocoa Bean Shell
Acetic acid	$C_2H_4O_2$	14.7%	20.6%
2-Propanone, 1-hydroxy-	$C_3H_6O_2$	1.1%	1.4%
Methanol	CH_4O	5.7%	7.0%
Acetaldehyde	C_2H_4O	4.8%	5.2%
Hydrocarbon Benzene Derivatives		3.0%	3.6%
Pyrrole	C_4H_5N	4.0%	3.5%
Acetonitrile	C_2H_3N	6.6%	3.5%
Methyl isocyanide	C_2H_3N	0.0%	2.4%
Heptadecanenitrile	$C_{17}H_{33}N$	6.5%	10.2%
9-Octadecynenitrile	$C_{18}H_{31}N$	1.4%	0.0%
Oleanitrile	$C_{18}H_{33}N$	9.7%	2.6%
1,8,11-Heptadecatriene	$C_{17}H_{30}$	4.0%	0.0%
Theobromine	$C_7H_8N_4O_2$	0.0%	3.8%
Caffeine	$C_8H_{10}N_4O_2$	0.0%	2.0%
Total		**61.3%**	**65.9%**

Using a niobium-derived catalyst impregnated with Ni-Re reinforces findings from previous studies, which indicate deoxygenation with a selectivity towards routes that yield nitrogenous compounds, as highlighted in a prior study (Simão et al., 2018). However, this outcome may not align with the specific objectives of this research, as it can negatively impact the characteristics of the bio-oil. The presence of these compounds in the bio-oil can have several adverse effects, including a reduction in calorific value, poor stability, and the liberation of NO_x substances during bio-oil combustion. These factors can pose challenges related to the miscibility of bio-oil in fuels and its storage (Bridgwater, 2018).

5.1.5. Catalytic Pyrolysis with Ni/Nb_2O_5

Regarding the niobic acid-derived catalyst with Ni impregnation, Figure 5.15. offers a comparative view of the products resulting from catalytic pyrolysis using Ni/Nb_2O_5 at 550°C for (a) SR and (b) CBS alongside a non-catalytic control. The outcomes resembled those obtained with the other niobium-derived catalyst (Ni-Re/Nb_2O_5), with a marginal reduction observed in the levels of aldehydes, alcohols, and acids. These levels remained relatively consistent with the Ni-Re-impregnated catalyst.

Notably, as previously mentioned, the characteristic rise in nitrogen content persisted, with nitrile compounds exhibiting the most significant increase. The increase was even more pronounced in this instance, escalating from 1 and 0% to 42 and 24% for SR and CBS, respectively.

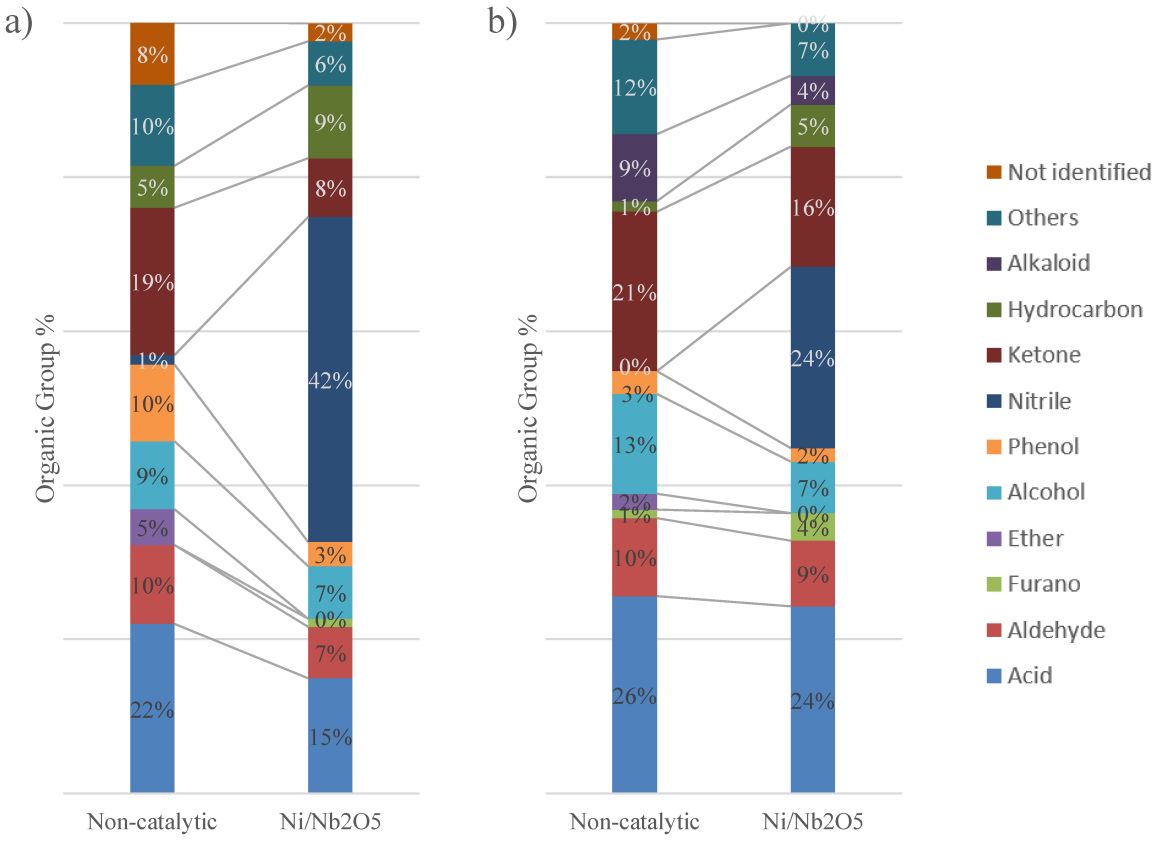


Figure 5.15. Categorization of non-catalytic and catalytic (Ni/Nb_2O_5) pyrolysis products of (a) SR and (b) CBS; temperature of 550°C and 3:1 catalyst proportion

This catalyst exhibited varying degrees of selectivity for each biomass, as evidenced by a distinct contrast in intensity. This is further elucidated by examining Figure 5.16., which analyzes organic chain sizes. There was a substantial increase in the proportion of chains containing more than 15 carbon atoms for SR, which rose from 0 to 44%. The increase was less pronounced for CBS, going from 0 to 20%. Most of these compounds predominantly comprise nitrogenous substances, as detailed in Table 5.5., which provides an overview of the primary identified compounds.

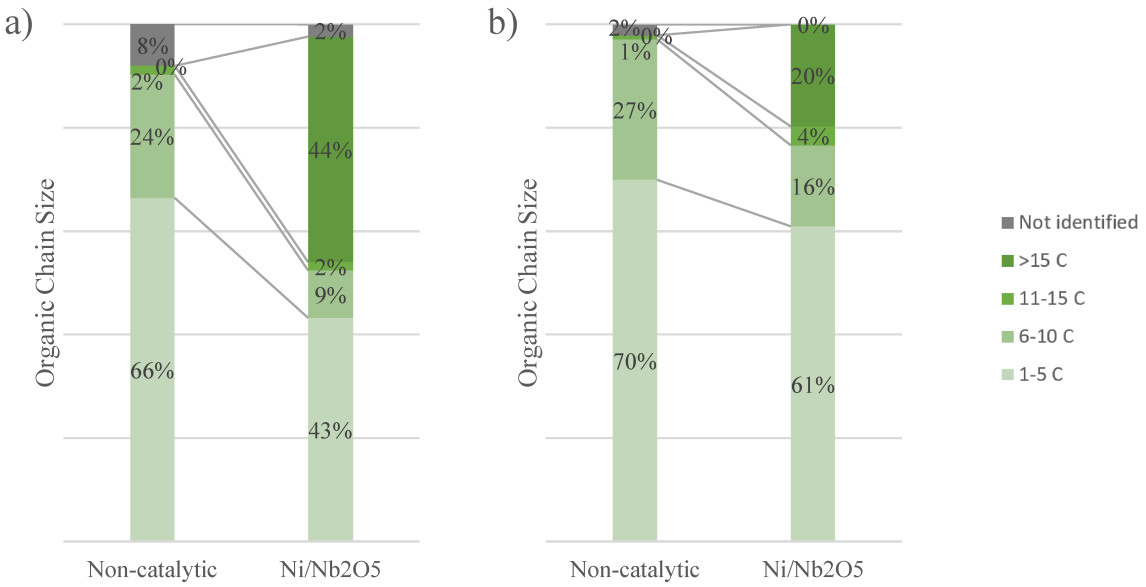


Figure 5.16. Size of chains based on number of carbons in the organic structure for the non-catalytic pyrolysis and pyrolysis with Ni/Nb_2O_5 of (a) SR and (b) CBS; temperature of 550°C and 3:1 catalyst proportion

Table 5.5. Main organic products from Catalytic pyrolysis with Ni/Nb_2O_5 at the temperature of 550°C and 3:1 catalyst proportion

Compound	Formula	Soybean Residue	Cocoa Bean Shell
Acetic acid	$C_2H_4O_2$	9.0%	18.5%
2-Propanone, 1-hydroxy-	$C_3H_6O_2$	0.8%	1.8%
Methanol	CH_4O	4.5%	6.7%
Acetaldehyde	C_2H_4O	3.6%	5.8%
Hydrocarbon Benzene Derivatives		2.6%	2.1%
Pyrrole	C_4H_5N	3.2%	3.5%
Acetonitrile	C_2H_3N	5.2%	0.0%
Methyl isocyanide	C_2H_3N	0.0%	4.8%
Heptadecanenitrile	$C_{17}H_{33}N$	10.2%	13.4%
9-Octadecynenitrile	$C_{18}H_{31}N$	8.1%	0.0%
Oleanitrile	$C_{18}H_{33}N$	18.0%	4.2%
1,8,11-Heptadecatriene	$C_{17}H_{30}$	3.6%	0.0%
Theobromine	$C_7H_8N_4O_2$	0.0%	5.1%
Caffeine	$C_8H_{10}N_4O_2$	0.0%	2.0%
Total		**69.0%**	**67.8%**

Another noteworthy aspect observed from Table 5.4. results is the discernible variation in acetic acid, methanol, and acetaldehyde compared to the non-catalytic pyrolysis results outlined in Table 5.1. This effect was particularly pronounced for SR, in which these compounds together were reduced by 20%.

In conclusion, the mechanisms of the two niobium-derived catalysts were notably similar, with the Ni-impregnated catalyst displaying a more pronounced impact on deoxygenation. Nickel catalysts can facilitate the removal of -OH groups, thereby enhancing the acylation of carboxylic acids, assisting in oxygen removal (Goh et al., 2008; Amani et al.,2017). It exhibited the ability to capture oxygen from aldehydes, acids, and alcohols, particularly for SR. This deoxygenation process was accompanied by polymerization and nitrogen capture, resulting in the formation of extended-chain nitriles.

5.1.6. Catalyst Effect Conclusions

Upon examining the outcomes for the four catalysts, catalytic pyrolysis with HTC resulted in a hydrocarbon production of approximately 30% for SR and CBS, whereas zeolite generated about 70% of hydrocarbons. The catalysts derived from niobium impregnated with Ni-Re and with Ni alone yielded less than 11% of hydrocarbons for both biomasses.

Both niobium-derived catalysts played a role in generating longer-chain organic compounds, which have the potential to enhance the quality of bio-oil and increase its calorific value, provided that nitrification of the new compounds did not occur, which, in this case, led to the formation of nitriles. The high concentration of nitrogen has a detrimental effect on the quality of the bio-oil, necessitating an additional denitrification step. This could be accomplished by introducing a second catalyst in series to facilitate nitrogen capture and the formation of long-chain hydrocarbons that may play a crucial role, as they have the potential to be miscible with the heavy fuels widely employed in maritime transport (Ampah et al., 2022). However, this falls beyond the scope of the current study.

Despite not being as efficient in deoxygenation, hydrotalcite demonstrated the ability to convert a significant portion of oxygenates into alcohols, thereby enhancing the overall product quality. These attributes encompass elevated calorific value, reduced acidity, enhanced stability

capable of delaying the aging and oxidation of bio-oil, and improved miscibility with other fuels (Bridgwater, 2018). This characteristic makes it an appealing option for further exploration.

In contrast, HZSM-5 exhibited remarkable efficiency in deoxygenation, with oxygenates reduced to 16% and 21% for SR and CBS, respectively. Additionally, it displayed selectivity for aromatic hydrocarbons, making it the most promising catalyst for producing higher-quality bio-oil.

Consequently, it was decided that the next stage of the experiment design would involve the employment of hydrotalcite and HZSM-5 zeolite as the catalysts. These catalysts have been identified as having the most significant potential to achieve the specific objective of this study, which is to maximize the production of hydrocarbon compounds. Thus, for the next stage of the experimental design, the impact of non-catalytic and catalytic pyrolysis temperatures will be assessed using these two catalysts.

5.2. Temperature Effect

The pyrolysis of biomass can be influenced by several factors, among which temperature is a crucial determinant in the pyrolysis process and the resulting product composition. Therefore, it is imperative to investigate the impact of temperature on pyrolysis product characteristics. Thus, following the previous stage's selection of catalysts, the influence of temperature on the non-catalytic pyrolysis of soybean residue (SR) and cocoa bean shell (CBS) was explored. Temperature ranging from 350°C to 750°C were considered, both for non-catalytic and catalytic processes using HZSM-5 Zeolite and Hydrotalcite (HTC) as catalysts. This temperature range was selected based on the decomposition stages identified through thermogravimetric analysis and pyrolysis studies documented in the literature (Xie et al., 2015; Ding et al., 2018; Guedes et al., 2018; Dai et al., 2020). Initially, thermogravimetric analysis results indicate that the active devolatilization or active pyrolysis phase might be finished around 350°C. Consequently, temperatures below 350°C are considered irrelevant. Given the focus on pyrolysis in this study, temperatures exceeding 750°C are deemed inappropriate, as they would fall into the category of gasification. Many pyrolysis studies maintain temperatures between 500 and 700°C (Borel et al., 2018; Ding et al., 2018; Rossi et al., 2023). Therefore, the 350 to 750°C temperature range was chosen to assess the variable's effects. For this stage, a fixed catalyst-to-biomass ratio of 3:1 was maintained.

The analysis involved categorizing the compounds into groups. These categories encompass aromatic and aliphatic hydrocarbons, nitrogen-containing compounds, as well as

oxygenated and nitrogenated compounds. Furthermore, the oxygenated were divided based on the number of oxygen atoms, distinguishing between those with one, two, and three or more oxygen atoms. In Figure 5.17, the results for SR are presented in (a) for non-catalytic pyrolysis, (b) for catalytic pyrolysis with HTC, and (c) for catalytic pyrolysis with HZSM-5. Similarly, the items (d), (e), and (f) depict the results for CBS in the same order.

At all examined temperature levels, it was confirmed the observed effect from the prior phase of this present study, where hydrotalcite and zeolites exhibited a significant capability to convert oxygenated compounds into hydrocarbons. Additionally, for non-catalytic pyrolysis, both biomass sources yielded similar results, demonstrating a tendency for an increase in hydrocarbons as temperatures escalated. Zhang et al. (2005), Silva (2020), Santana Júnior (2018), and Oliveira (2015) have also reported, for other biomasses, a decrease in oxygenated compounds content as the temperature rises, leading to an enhanced production of hydrocarbons. Regarding the catalytic experimental runs, the present study showed that pyrolysis using HTC catalyst increased hydrocarbons with the rising temperature, while HZM-5 maintained a stable hydrocarbon percentage across all temperature ranges. It is crucial to highlight that elevating temperatures on larger scale processes generally may reduce liquid yield despite improving bio-oil quality (Xie et al., 2015). This potential outcome may be one of the advantages of catalytic pyrolysis, which contributes to an overall enhancement in the system's energy efficiency.

Overall, the distinction between SR and CBS was striking due to the prevalence of nitrogenous compounds in all pyrolysis products derived from SR (designated as a, b, and c). In contrast, there was a significant prevalence of compounds containing oxygen and nitrogen in the same molecule for CBS pyrolysis products. This disparity might arise due to alkaloids present in the CBS, which are characteristic of this type of raw material (Vandenberghe et al., 2022). While both biomass samples demonstrated a satisfactory production of hydrocarbons, SR exhibited a higher hydrocarbon content, especially evident at the temperature of 750°C. This distinction can be recognized as another notable contrast between the two residues.

It can be highlighted that the majority of aliphatic compounds consisted of alkenes, accounting for over 80% of the products across almost all the experimental conditions. However, in the case of CBS with HTC, alkenes represented 60% of the compounds, signifying a notable difference. Another observation is the significant content of aromatic hydrocarbons in HZSM-5 pyrolysis, particularly at lower temperatures (450°C), being 68% of all compounds for SR and 69%

for CBS. This contrasts with the common trend in the literature, where most studies report an increase in aromatics under higher temperatures when using HZSM-5 as a catalyst in pyrolysis processes. Jin et al. (2022) witnessed an upsurge in aromatics during the pyrolysis of pinewood sawdust when conducting tests at 500, 600, and 700°C. They proposed that aliphatic hydrocarbons were undergoing conversion, a phenomenon not observed in the case of CBS and SR. Similarly, Sun et al. (2020) investigated HZSM-5 at various temperatures and conducted pyrolysis experiments on wood sawdust at 400, 500, 600, and 700°C. They also noticed an increase in aromatics with temperatures up to 600°C, followed by a decline at temperatures above 600°C, which they attributed to the decomposition of aromatics into smaller gas molecules. For the present study, it is hypothesized that this significant divergence is that wood-based biomass, rich in lignin, typically reacts at higher temperatures. Thus, for the SR and CBS, the temperature increment might have led to reactions favoring the formation of lighter aliphatic compounds.

Sun et al. (2021) investigated the non-catalytic pyrolysis of soybean residue at temperatures of 350, 500, and 600°C, observing an average of approximately 60% oxygenated compounds, while nitrogenated compounds remained consistently around 45%, regardless of temperature. Notably, the prominent generation of oxygen-containing compounds, particularly phenols, which increased with rising temperature, was observed. However, unlike the present study, no evidence of hydrocarbon formation was observed.

Conversely, Wijaya et al. (2020) conducted non-catalytic pyrolysis of cocoa shells. Their results indicated approximately 80% of oxygenated compounds, around 25% being acetic acid.

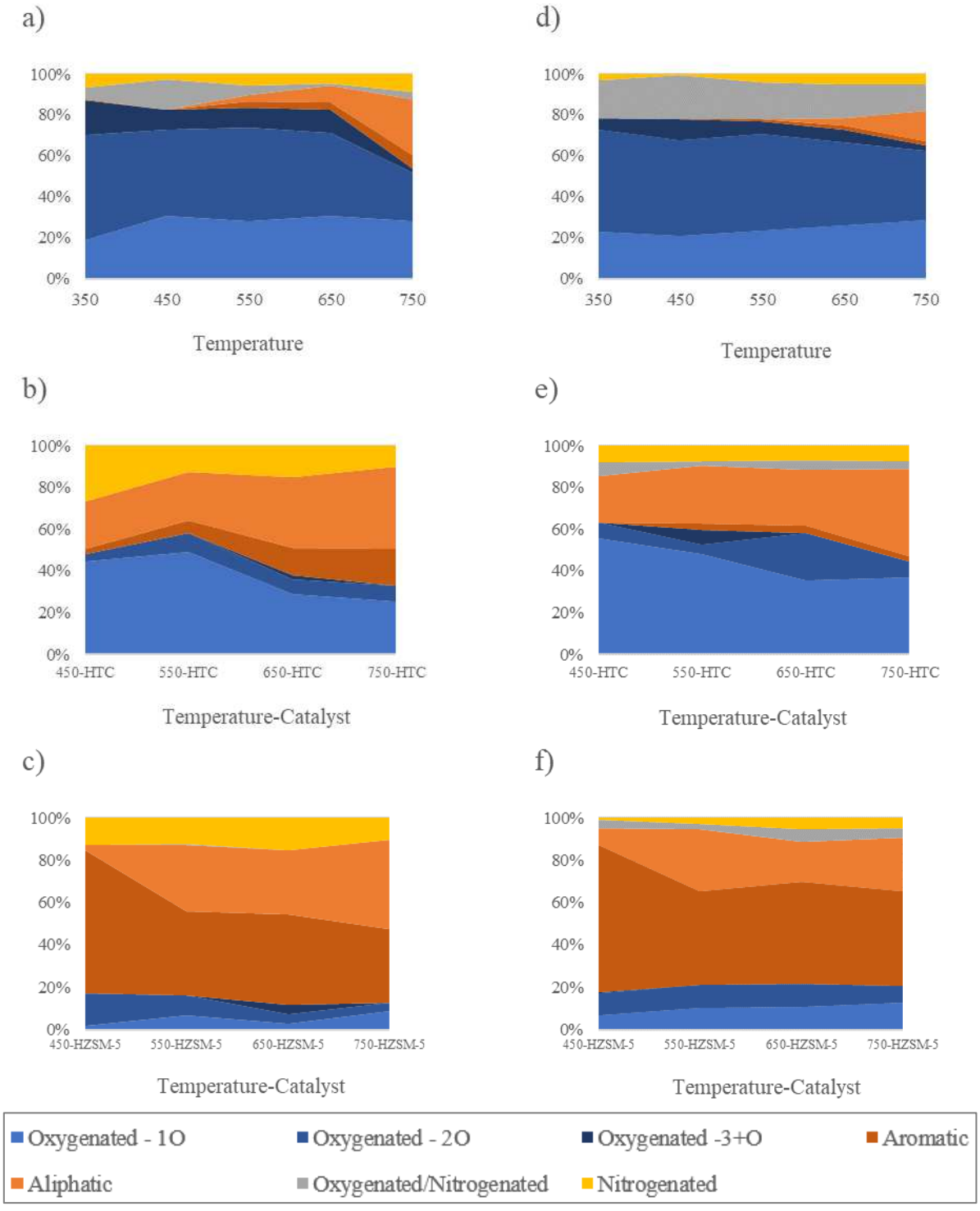


Figure 5.17. Categorization of pyrolysis products of SR for (a) non-catalytic, (b) catalytic with HTC, (c) HZSM-5; and of CBS for (d) non-catalytic, (e) catalytic with HTC, (f) HZSM-5

5.2.1. Non-Catalytic Pyrolysis with temperature variation from 350°C to 750°C

Regarding the non-catalytic pyrolysis, all the temperature levels revealed substantial heterogeneity, mirroring previous observations at 550°C (the chromatograms and compounds table can be found in Appendix A). Figure 5.18 analyses the resulting products, indicating that the primary constituents are acids, aldehydes, ketones, and alcohols. Interestingly, most of these components slightly declined with increasing temperature, coinciding with the increment in hydrocarbons. This trend was expected and confirmed for these two biomasses. Similar behavior has been reported in prior studies involving different residues (Wang et al., 2017a; Santana Júnior, 2018; Barbosa, 2020; Reis Filho, 2020; Silva, 2020).

Oliveira et al. (2015) studied the analytical pyrolysis of soybean hulls at 450, 550, 650, and 750°C. The primary compounds identified in the vapors generated during the analytical pyrolysis of soybean hulls at 450°C included carboxylic acids that were less prominent as the temperature rose. The more significant hydrocarbon content was found at 750°C. In agreement with the present study, high-temperature non-catalytic pyrolysis proved advantageous as it reduced the formation of acids, thereby contributing to the decreased acidity of bio-oil.

On the other hand, Grillo et al. (2019) conducted non-catalytic pyrolysis of cocoa bean shells at 500°C, revealing that alkaloids comprised 38% of the resulting pyrolytic products.

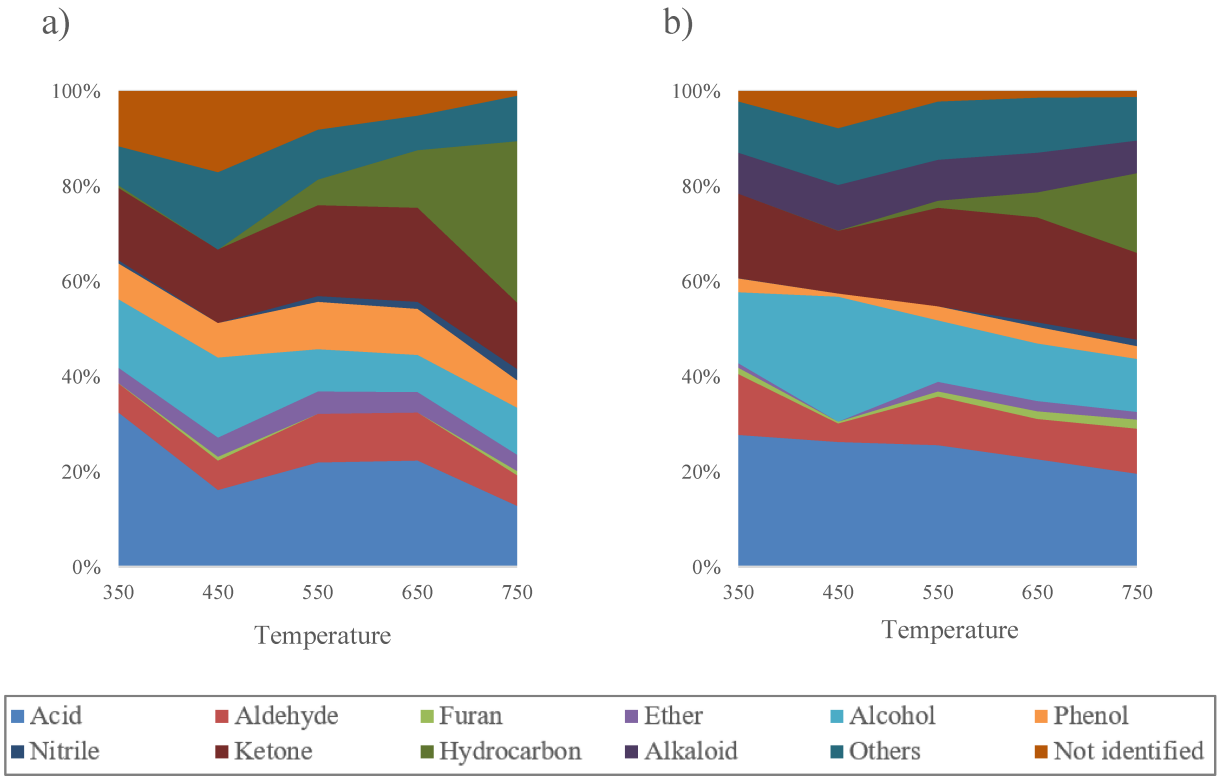


Figure 5.18. Categorization of non-catalytic pyrolysis products of (a) Soybean Residue and (b) Cocoa Bean Shell; temperature varying from 350 to 750°C

Another significant aspect of the temperature's influence on non-catalytic pyrolysis is the promotion of smaller molecules while the formation of larger compounds diminishes, a pattern previously elucidated by Alén et al. (1996). This trend is clearly illustrated when examining the distribution of carbon chain sizes, as shown in Figure 5.19. In both instances involving biomass, there was an increase in the composition of products characterized by organic molecules with five carbons or fewer in their structure. This proportion reached 68% for SR and 74% for CBS under the experimental conditions at 750°C.

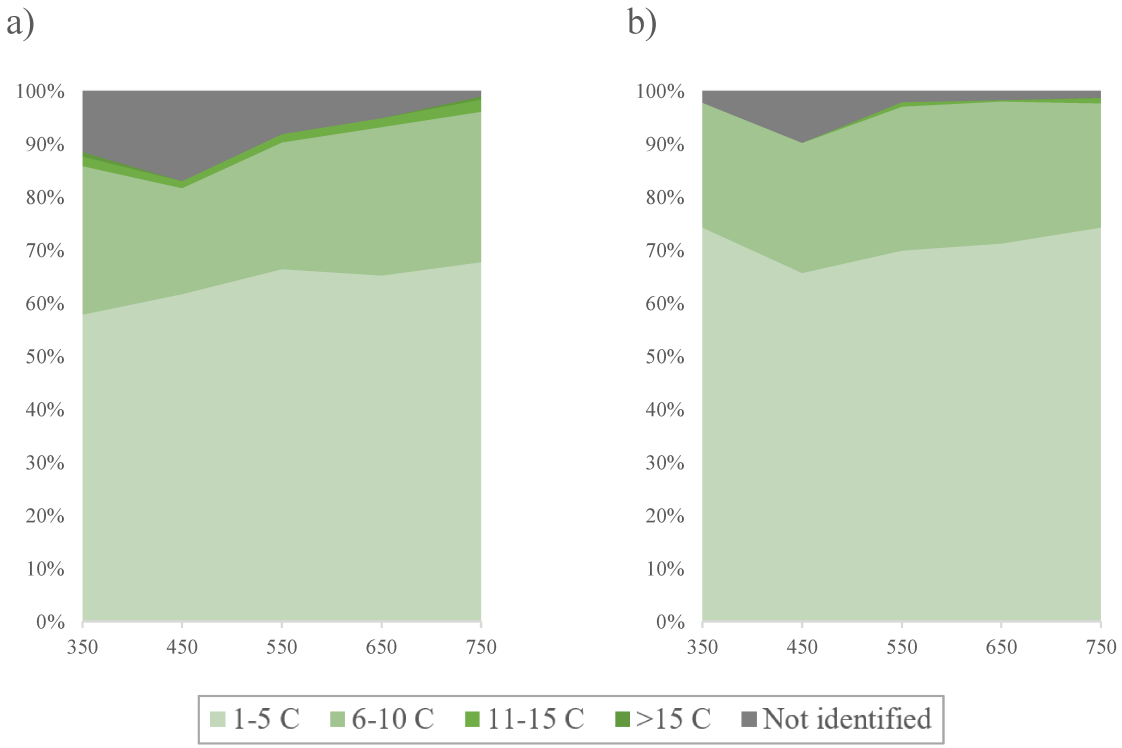


Figure 5.19. Size of chains based on number of carbons in the organic structure for the non-catalytic pyrolysis of (a) SR and (b) CBS; temperature varying from 350 to 750°C

The predominant compounds generated are delineated in Tables 5.6 and 5.7, accounting for at least 42% of the identified organic compounds in SR pyrolysis and 65% in CBS pyrolysis. This discrepancy may arise from CBS's purity (since it is a more well-benefited product), which resulted in more uniform product profiles.

Consistent with findings from previous research, non-catalytic pyrolysis of lignocellulosic biomasses typically generated acetic acid as a prominent product (Oliveira, 2015), a characteristic associated with hemicellulose. This imparts acidity to the bio-oil, which diminishes as temperatures rise due to the decrease in selectivity for forming acetic acid reactions, which become less competitive at higher temperatures. (Shen et al., 2010).

Another discernible temperature effect relates to phenolic compounds, which are inherent to the biomass's lignin content. This phenomenon aligns with the patterns reported in existing literature, wherein these compounds initially increase and subsequently decline with rising temperatures, most likely transforming into benzene-derived compounds that exhibit an uptrend with temperature escalation (Wang et al., 2017a).

Table 5.6. Main organic products from non-catalytic pyrolysis of the Soybean Residue with temperatures from 350°C to 750°C.

Compound	Formula	350	450	550	650	750
Acetic acid	$C_2H_4O_2$	13.4%	14.5%	18.0%	16.0%	10.6%
2-Propanone, 1-hydroxy-	$C_3H_6O_2$	9.5%	7.8%	9.4%	9.1%	7.8%
Methanol	CH_4O	4.5%	8.3%	7.5%	6.5%	6.7%
Acetaldehyde	C_2H_4O	3.8%	3.8%	5.0%	4.8%	4.4%
Hydrocarbon Benzene Derivatives		0.5%	1.0%	2.7%	3.4%	5.4%
Cyclic olefins and cyclic oxygenated derivatives	-	3.6%	14.9%	5.2%	5.5%	8.1%
Phenol Derivatives		3.1%	5.1%	7.1%	6.8%	3.4%
2,3,5-Trimethylanizole	$C_{10}H_{14}O$	2.6%	5.9%	1.9%	3.4%	0.0%
DL-Proline, 5-oxo-	$C_5H_7NO_3$	0.4%	4.6%	3.2%	2.1%	0.0%
L-Glutamine	$C_5H_{10}N_2O_3$	1.2%	8.3%	0.0%	0.0%	2.1%
Propene	C_3H_6	0.0%	0.0%	0.0%	0.0%	8.3%
Total		**42.7%**	**74.1%**	**60.1%**	**57.6%**	**56.6%**

At 750°C, the primary hydrocarbons comprised mainly propene and benzene derivative compounds. Anticipatedly, temperatures exceeding 650°C lead to elevated gas production, with the generation of non-condensable substances attributed to the secondary decomposition of components, resulting in the formation of more stable chemicals such as phenols and lightweight hydrocarbons (Conti et al., 1994; Encinar et al., 1998).

One particularity of the CBS noticed in the first stage of the experimental runs was the recurring presence of alkaloids, specifically Theobromine and Caffeine. Observing the consistent presence of these components at different temperatures, it is hypothesized that the presence of these alkaloids may be attributed to the challenge of cleavaging their structure through thermal heating alone. Islam et al. (2008) studied t-RNA binding by the cytotoxic protoberberine alkaloid coralyne, finding that the alkaloid enhanced the thermal stability of the t-RNA. Soltani et al. (2017) investigated the thermal stability of ionic liquids bearing quinoline alkaloids. Their findings indicate that ionic liquids of high thermal stability can be prepared and were found to be sensitive to the position of quinoline ring substitution.

Table 5.7. Main organic products from non-catalytic pyrolysis of the Cocoa Bean Shell with temperatures from 350°C to 750°C.

Compound	Formula	350	450	550	650	750
Acetic acid	$C_2H_4O_2$	24.2%	23.0%	22.8%	19.8%	17.0%
2-Propanone, 1-hydroxy-	$C_3H_6O_2$	8.7%	6.4%	8.5%	13.8%	7.0%
Methanol	CH_4O	7.4%	13.7%	6.3%	5.7%	6.0%
Acetaldehyde	C_2H_4O	3.2%	0.0%	3.7%	4.3%	4.8%
Hydrocarbon Benzene Derivatives		0.0%	0.0%	1.4%	1.9%	2.0%
Cyclic olefins and cyclic oxygenated derivatives	-	5.8%	4.6%	6.7%	6.7%	7.6%
Phenol Derivatives		2.8%	0.0%	3.0%	3.5%	2.7%
Theobromine	$C_7H_8N_4O_2$	14.0%	14.7%	13.6%	11.9%	9.7%
Caffeine	$C_8H_{10}N_4O_2$	2.5%	2.7%	2.4%	2.4%	1.7%
Pyrrole	C_4H_5N	2.0%	0.0%	3.7%	3.6%	3.6%
Acetone	C_3H_6O	1.3%	0.0%	2.4%	3.0%	2.9%
Acetaldehyde, hydroxy-	$C_2H_4O_2$	5.5%	0.0%	2.5%	1.4%	2.0%
Propene	C_3H_6	0.0%	0.0%	0.0%	0.0%	5.6%
Total		**77.4%**	**65.2%**	**77.0%**	**77.9%**	**72.7%**

5.2.2. Catalytic Pyrolysis with Hydrotalcite (HTC) with temperature variation from 450°C to 750°C

In the temperature assessment of catalytic pyrolysis using HTC, experiments were conducted across the temperature range of 450 to 750°C. Most of the catalyst's effects observed at 550 °C were replicated consistently at all temperature levels, as shown in Figure 5.20. Notably, at higher temperatures, there was a reduction in oxygenated compounds (aldehydes, acids, ethers, phenols, and ketones) alongside an increase in hydrocarbons. This trend resulted in hydrocarbon proportions of 54% and 43% for SR and CBS, respectively, primarily comprising aliphatics. These effects mirrored those observed in non-catalytic pyrolysis. Interestingly, the behavior of alcohols deviated from this pattern. While an increase was observed at 450 and 550°C, a decrease in alcohol compounds occurred at 650 and 750°C. Furthermore, it's worth noting that at lower temperatures, there was a notable rise in nitrile formation, particularly pronounced in SR due to its higher nitrogen content. Lastly, acid formation reduced across almost all temperatures, except at 650°C, where there was a peak in this group's formation, exemplified by the notable formation of acetic acid, as presented in Tables 5.8 and 5.9.

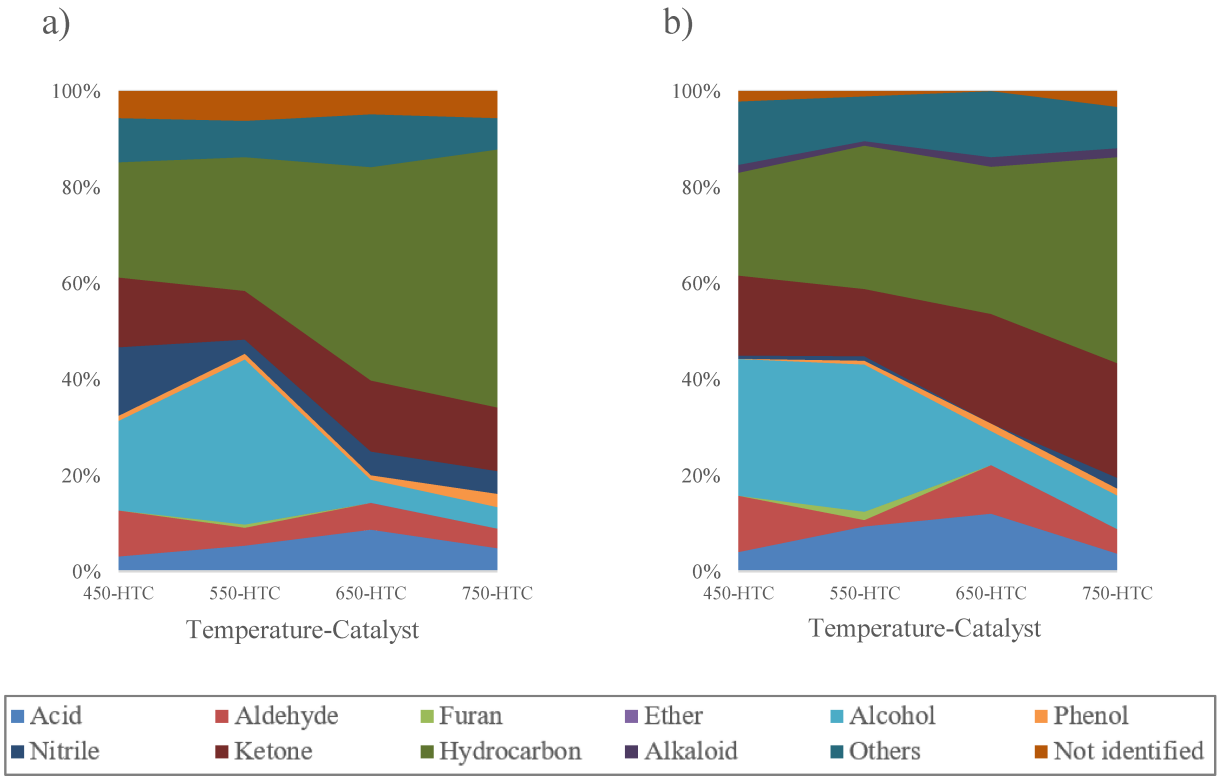


Figure 5.20. Categorization of HTC-catalytic pyrolysis products of (a) SR and (b) CBS; temperature varying from 450 to 750°C and 3:1 catalyst proportion

Figure 5.21 categorizes organic compounds into four distinct groups based on their carbon atom content. Upon analysis, it becomes evident that there is a temperature-dependent effect on the size of organic chains, most notably observable at 450°C. At this temperature, roughly 50% and 60% of the compounds in SR and CBS, respectively, consisted of structures with at least 11 carbons.

The breakage effect of the molecules exhibited more stability at higher temperatures, reaching approximately 85% at 650 and 750°C. This contrasts with non-catalytic pyrolysis, where the effect persisted within the temperature rise. In the case of soybean residues, there was a transitional point where the smaller group began to diminish, giving way to chains with 6 to 10 carbons. This change is more closely associated with the production of hydrocarbon benzene derivatives at higher temperatures, a phenomenon more pronounced in SR (14.8% at 750°C) than in CBS (4.8% at 750°C). The disparity between non-catalytic and catalytic processes primarily arises because the lighter compounds cracked due to the elevated temperature become more

accessible to the catalyst pores, facilitating oxygen capture and subsequent formation of aromatic and aliphatic compounds from these smaller molecules (Jin et al., 2022).

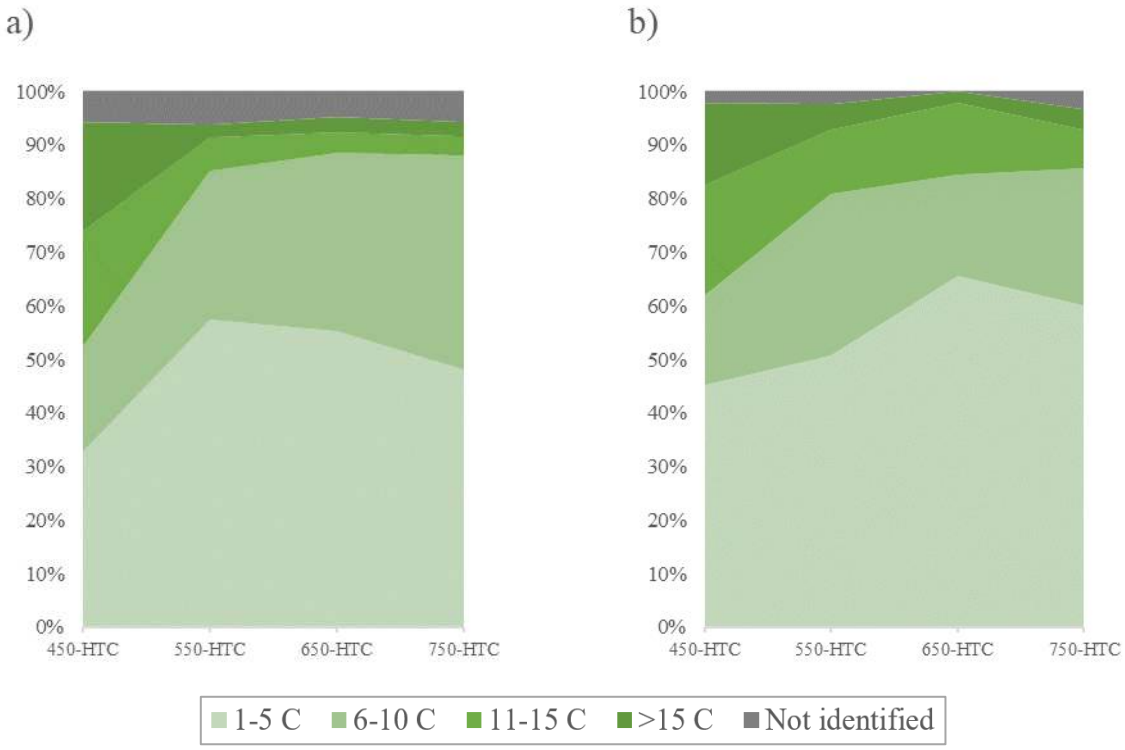


Figure 5.21. Size of chains based on number of carbons in the organic structure for the HTC-catalytic pyrolysis of (a) SR and (b) CBS; temperature varying from 450 to 750°C and 3:1 catalyst proportion

Tables 5.8 and 5.9 present the main products resulting from HTC catalytic pyrolysis at the four distinct temperatures examined. For SR, it's worth highlighting the remarkable presence of hydrocarbon benzene derivatives, reaching nearly 15% at 750°C. In contrast, CBS exhibited a more modest increase, at only 4.8%, but it did demonstrate the formation of 15% of cyclic products, including cyclic olefins and cyclic oxygenated compounds. These cyclic products possess the potential for further transformation into benzene through additional cyclization and dehydrogenation reactions (Yang et al., 2023).

Additionally, the production of acetonitrile, oleanitrile, and pyrrole is noteworthy for both biomasses. These compounds are products of protein-N decomposition and reactions with acids and ammonia, as proposed by Huang et al. (2023). The generation of ammonia and HCN was also

observed by Wang et al. (2013) during the pyrolysis of microalgae with a high N content, estimated at around 10%.

Table 5.8. Main organic products from catalytic pyrolysis with HTC of the Soybean Residue with temperatures from 450°C to 750°C and catalyst proportion of 3:1.

Compound	Formula	450	550	650	750
Acetic acid	$C_2H_4O_2$	0.0%	3.5%	4.8%	2.9%
2-Propanone, 1-hydroxy-	$C_3H_6O_2$	0.0%	2.3%	2.1%	1.9%
Methanol	CH_4O	7.6%	11.3%	2.6%	2.6%
Acetaldehyde	C_2H_4O	5.6%	0.0%	5.6%	4.1%
Hydrocarbon Benzene Derivatives		2.7%	4.9%	9.8%	14.8%
Cyclic olefins and cyclic oxygenated derivatives	-	9.0%	13.7%	4.3%	3.7%
Ethanol	C_2H_6O	5.2%	13.2%	2.2%	0.0%
1-Tridecene	$C_{13}H_{26}$	9.0%	0.0%	2.3%	0.8%
1-Pentene, 4-methyl-	C_6H_{12}	0.0%	5.8%	3.5%	4.3%
2-Butene	C_4H_8	0.0%	0.0%	8.8%	11.8%
1-Pentene	C_5H_{10}	0.0%	0.0%	2.4%	2.4%
Acetone	C_3H_6O	1.8%	2.3%	7.7%	5.5%
Acetonitrile	C_2H_3N	2.1%	2.2%	5.0%	4.7%
Oleanitrile	$C_{18}H_{33}N$	5.1%	0.0%	0.0%	0.0%
Pyrrole	C_4H_5N	3.1%	3.9%	4.1%	0.0%
Total		**51.2%**	**63.2%**	**65.2%**	**59.6%**

Table 5.9. Main organic products from catalytic pyrolysis with HTC of the Cocoa Bean Shell with temperatures from 450°C to 750°C and catalyst proportion of 3:1.

Compound	Formula	450	550	650	750
Acetic acid	$C_2H_4O_2$	2.3%	2.4%	12.0%	3.7%
2-Propanone, 1-hydroxy-	$C_3H_6O_2$	2.4%	1.8%	5.4%	2.5%
Methanol	CH_4O	10.9%	9.5%	3.1%	2.6%
Acetaldehyde	C_2H_4O	10.2%	0.0%	6.5%	5.1%
Hydrocarbon Benzene Derivatives		0.0%	2.8%	4.0%	4.8%
Cyclic olefins and cyclic oxygenated derivatives	-	9.1%	13.5%	10.7%	15.2%
Ethanol	C_2H_6O	6.7%	13.7%	2.7%	2.7%
1-Pentene, x-methyl-	C_6H_{12}	0.0%	4.5%	8.5%	4.0%
1-Heptene	C_7H_{14}	0.0%	3.5%	0.0%	2.3%
Acetone	C_3H_6O	3.1%	4.1%	4.7%	10.0%
Acetonitrile	C_2H_3N	0.0%	1.0%	0.0%	2.2%
Pyrrole	C_4H_5N	4.3%	4.6%	5.0%	3.9%
Theobromine	$C_7H_8N_4O_2$	3.5%	0.7%	2.0%	2.2%
Caffeine	$C_8H_{10}N_4O_2$	2.7%	1.4%	2.5%	1.4%
Total		**55.1%**	**63.5%**	**66.9%**	**62.7%**

5.2.3. Catalytic Pyrolysis with Zeolite HZSM-5 with temperature variation from 450°C to 750°C

Figure 5.22 shows the product variations across different temperature conditions in the catalytic pyrolysis using HZSM-5 catalyst, ranging from 450°C to 750°C. This figure mirrors the trends observed at 550°C in Figure 5.9, thus reinforcing the findings from the prior experiments performed in this study, as well as further studies involving various biomasses that, specifically, the addition of ZSM-5 results in enhanced dehydration, significantly reducing the oxygen content while increasing hydrocarbon content. It is noteworthy that different types of zeolites lead to varying effects on the distribution of pyrolysis products. This variance is attributed to the unique properties of the catalysts themselves and the distribution of components within the biomass (Silva, 2020; Sun et al., 2020; Wang et al., 2017a; Guedes et al., 2018). Furthermore, it is observed that hydrocarbon generation experienced a slight increase with temperature in SR pyrolysis, whereas a modest decrease was noted in the case of CBS. At larger scales, the temperature rise is likely to result in a decrease in liquid yield (Xie et al., 2015). Therefore, the application of catalysts, capable

of lowering the activation temperatures of the reactions, can contribute to enhanced energy efficiency. This allows for the attainment of satisfactory hydrocarbon values even at lower temperatures. Additionally, there was an increase in nitriles for both biomasses, a topic that will be further discussed in the subsequent section.

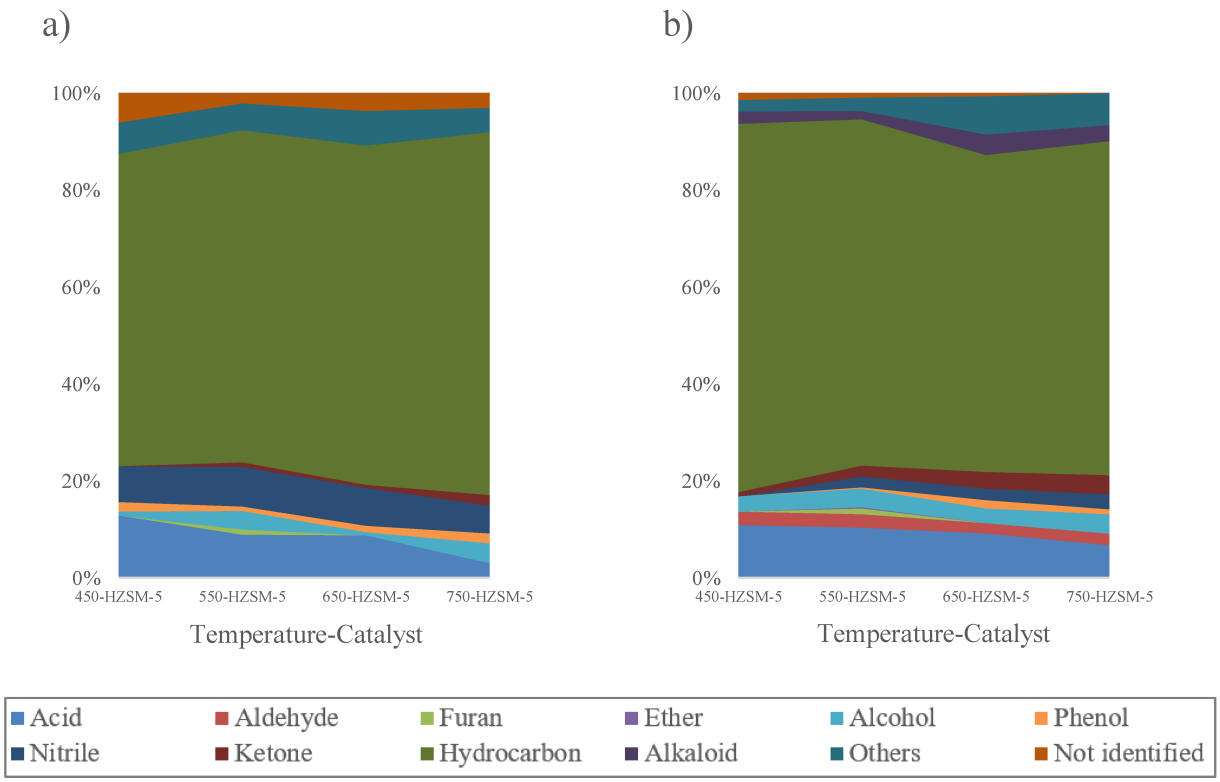


Figure 5.22. Categorization of HZSM-5 catalytic pyrolysis products of (a) Soybean Residue and (b) Cocoa Bean Shell; temperature varying from 450 to 750°C and 3:1 catalyst proportion

Figure 5.23 presents the compounds' categorization based on the number of carbons, exhibiting a similar trend to what was observed with the HTC catalyst. As the temperature increased from 450 to 750°C, there was a reduction in the proportion of compounds containing more than 10 carbons, decreasing from 11% to 4% for SR and from 18% to 5% for CBS. Notably, at 450°C, approximately 60% of the molecules contained 6 to 10 carbons, mainly comprising aromatic hydrocarbons. However, as the temperature increased, there was a decrease in these molecules, leading to the formation of smaller aliphatic hydrocarbons like propene and butene. These compounds are categorized as light olefins, and their production holds significance since they are fundamental components in the petrochemical and chemical industries. Their predominant

application involves producing polymers, synthetic fibers, rubbers, and plastic materials (Wang et al., 2020; Numpilai et al., 2021).

The formation of smaller aliphatic hydrocarbons becomes more evident when examining Tables 5.10 and 5.11, which delineate the primary substances generated in catalytic pyrolysis for SR and CBS. These results align with the proposed pathways by Wang et al. (2014) as depicted in Figure 5.12.

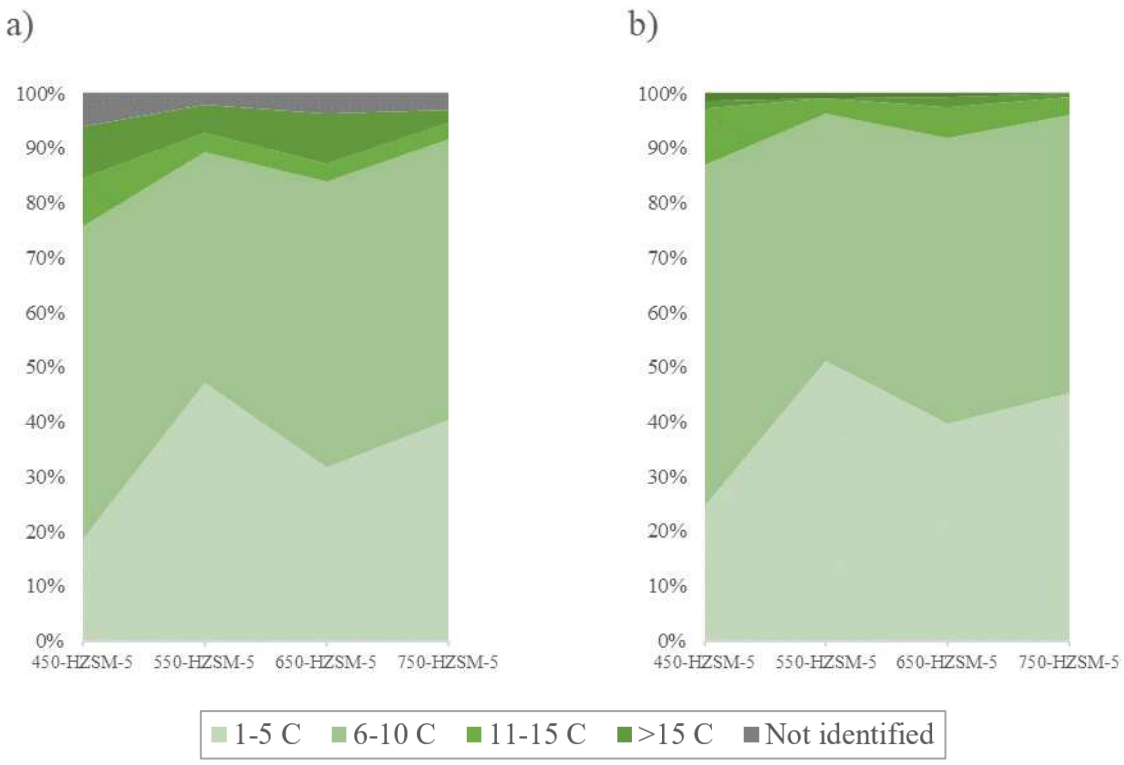


Figure 5.23. Size of chains based on number of carbons in the organic structure for the HZSM-5 catalytic pyrolysis of (a) SR and (b) CBS; temperature varying from 450 to 750°C and 3:1 catalyst proportion

A noteworthy observation is the comparison between Zeolites and HTC, wherein HZSM-5 proved significantly more effective in reducing most oxygenated organic groups, while HTC displayed greater effectiveness with acids, as shown in Figures 5.20 and 5.22. In addition, Tables 5.10 and 5.11 highlight this difference by showcasing the consistent presence of acetic acid in the products across all temperatures tested when using HZSM-5.

On the other hand, both catalysts presented nitrile formation when using SR, an N-rich biomass. With increasing temperature, there was a discernible impact on the type of nitriles formed. Lower temperatures favored the production of larger chain nitriles (hexadecanitriles, heptadecanitriles, and octadecanitriles), while higher temperatures led to the formation of smaller chain nitriles, primarily acetonitrile. The generation of these substantial chain nitriles may be attributed to a polymerization process, a possibility also suggested by Wang et al. (2014) as a plausible reaction pathway for HZSM-5 catalytic pyrolysis, as depicted in Figure 5.12.

Regarding the alkaloids specific to CBS, their quantities remained fairly consistent for both HZSM-5 and HTC, with no clear trend concerning temperature. This observation further substantiates the hypothesis presented in section 5.2.1 that temperature does not significantly impact the presence of this compound type.

Table 5.10. Main organic products from catalytic pyrolysis with HZSM-5 of the Soybean Residue with temperatures from 450°C to 750°C and catalyst proportion of 3:1.

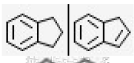
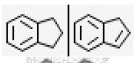
Compound	Formula	450	550	650	750
Acetic acid	$C_2H_4O_2$	10.8%	5.0%	3.2%	3.0%
2-Propanone, 1-hydroxy-	$C_3H_6O_2$	0.0%	0.0%	0.0%	0.7%
Methanol	CH_4O	0.0%	1.8%	0.7%	1.9%
Acetaldehyde	C_2H_4O	0.0%	0.0%	0.0%	0.0%
Hydrocarbon Benzene Derivatives		48.6%	30.6%	31.9%	31.3%
Cyclic olefins and cyclic oxygenated derivatives	-	0.0%	5.0%	4.5%	6.4%
Indan/Indene Derivatives		7.6%	2.6%	3.5%	3.8%
Naphtalene Derivatives		5.0%	3.8%	0.7%	3.7%
2-Butene	C_4H_8	0.0%	11.6%	9.0%	10.0%
Propene	C_3H_6	0.0%	10.0%	8.8%	10.8%
Acetonitrile	C_2H_3N	1.7%	3.8%	3.7%	4.2%
Big Chain Nitriles	$C_{16/17/18}H_xN$	5.6%	4.5%	4.2%	1.5%
Total		**79.5%**	**78.7%**	**70.2%**	**77.4%**

Table 5.11. Main organic products from catalytic pyrolysis with HZSM-5 of the Cocoa Bean Shell with temperatures from 450°C to 750°C and catalyst proportion of 3:1.

Compound	Formula	450	550	650	750
Acetic acid	$C_2H_4O_2$	8.8%	8.4%	7.7%	5.3%
2-Propanone, 1-hydroxy-	$C_3H_6O_2$	0.0%	0.2%	0.7%	0.5%
Methanol	CH_4O	1.1%	2.0%	0.9%	1.1%
Acetaldehyde	C_2H_4O	2.7%	2.8%	2.2%	2.4%
Hydrocarbon Benzene Derivatives		47.1%	36.7%	36.9%	35.4%
Cyclic olefins and cyclic oxygenated derivatives	-	0.8%	2.6%	1.8%	14.3%
Indan/Indene Derivatives		9.3%	4.6%	6.9%	4.2%
Naphtalene Derivatives		8.3%	2.7%	5.9%	3.3%
2-Butene	C_4H_8	6.9%	8.7%	6.6%	8.6%
Propene	C_3H_6	0.0%	14.0%	8.5%	0.0%
Theobromine	$C_7H_8N_4O_2$	2.9%	1.9%	4.9%	3.6%
Caffeine	$C_8H_{10}N_4O_2$	1.3%	0.5%	1.1%	0.9%
Ethanol	C_2H_6O	2.0%	1.8%	0.9%	1.2%
Acetonitrile	C_2H_3N	0.0%	2.2%	2.3%	2.5%
Big Chain Nitriles	$C_{16/17/18}H_xN$	0.0%	0.0%	0.0%	0.6%
Total		**91.2%**	**88.9%**	**87.4%**	**83.7%**

5.2.4. Temperature Effect Conclusions

Upon assessing the results obtained from a range of temperature conditions for both non-catalytic and catalytic pyrolysis employing hydrotalcite (HTC) and zeolite HZSM-5, it becomes evident that temperature had a noticeable impact on the selectivity of hydrocarbon formation in the pyrolysis reactions. In non-catalytic pyrolysis, a modest temperature effect was observed, resulting in hydrocarbon contents of 34% and 17% at 750°C for SR and CBS, respectively. In contrast, HTC displayed improved selectivity, reaching 54% and 43% for the same temperature conditions, using SR and CBS biomasses, respectively. HZSM-5 exhibited the most impressive performance, with hydrocarbon content reaching 75% at 750°C for SR and 76% at 450°C for CBS. While hydrotalcite demonstrated enhanced capability in converting a substantial portion of oxygenated compounds into hydrocarbons and other higher-quality oxygenated products, it still presented a variety of substances and greater heterogeneity when compared to pyrolysis with HZSM-5. HZSM-5, aside

from significantly increasing hydrocarbon production, also exhibited over 40% aromatic components, rendering it a satisfactory option for further exploration.

Consequently, it was decided that the next phase of the experimental design would entail utilizing HZSM-5 zeolite as the catalyst at different proportions and two distinct temperature settings (550 and 750°C) to delve into the catalyst's effects on the selectivity of hydrocarbon compounds. The selection of the highest temperature, 750°C, was based on its promising outcomes in catalytic and non-catalytic reactions, demonstrating a more substantial generation of the targeted products. Additionally, to explore the catalyst's potential in generating satisfactory quantities of hydrocarbons, even comparable to those at 750°C, a lower temperature of 550°C was included in the experimental design. This choice of 550°C, as opposed to 350 and 450°C, was determined due to the thermogravimetric analysis, which indicated that both biomasses at temperatures lower than 450°C might still be in the stages of decomposition, potentially hindering the cleavage of certain molecules. Consequently, temperatures around 450°C or lower were deemed less meaningful. The decision to examine various catalyst proportions at the temperatures of 550 and 750°C was considered an interesting path for new experimental runs.

5.3. Catalyst-to-biomass Ratio (C:B) Effect

When performing catalytic pyrolysis, another critical factor to be evaluated is the catalyst-to-biomass ratio (C:B) and its influence on the pyrolysis reaction. Thus, pursuing the objective of maximizing the hydrocarbon content in the organic products, zeolite HZSM-5 was utilized in different proportions: 0:1 (non-catalytic), 1:1, 3:1, and 5:1. These experiments were conducted at two different temperatures, 550 and 750°C, for both types of biomasses. The outcomes were analyzed and categorized consistently with the previous sections and are presented in Figures 5.24, 5.25, and 5.26.

Figure 5.24 shows the impact of the catalyst on the deoxygenation of the compounds in the pyrolysis process across the four distinct analyses (considering two types of biomasses and two different temperatures). It is evident that the catalyst plays a crucial role in reducing oxygen content and transforming it into hydrocarbons. Furthermore, an increasing proportion of the catalyst demonstrates the potential to enhance the aromatic content in the product. The highest hydrocarbon content was achieved at 96% for SR biomass (comprising 74% aromatics and 22% aliphatic) under

the conditions of 550°C and a C:B ratio of 5:1. For CBS biomass, the best outcome was observed at the same conditions, with a hydrocarbon generation of 90% (consisting of 82% aromatics and 8% aliphatic).

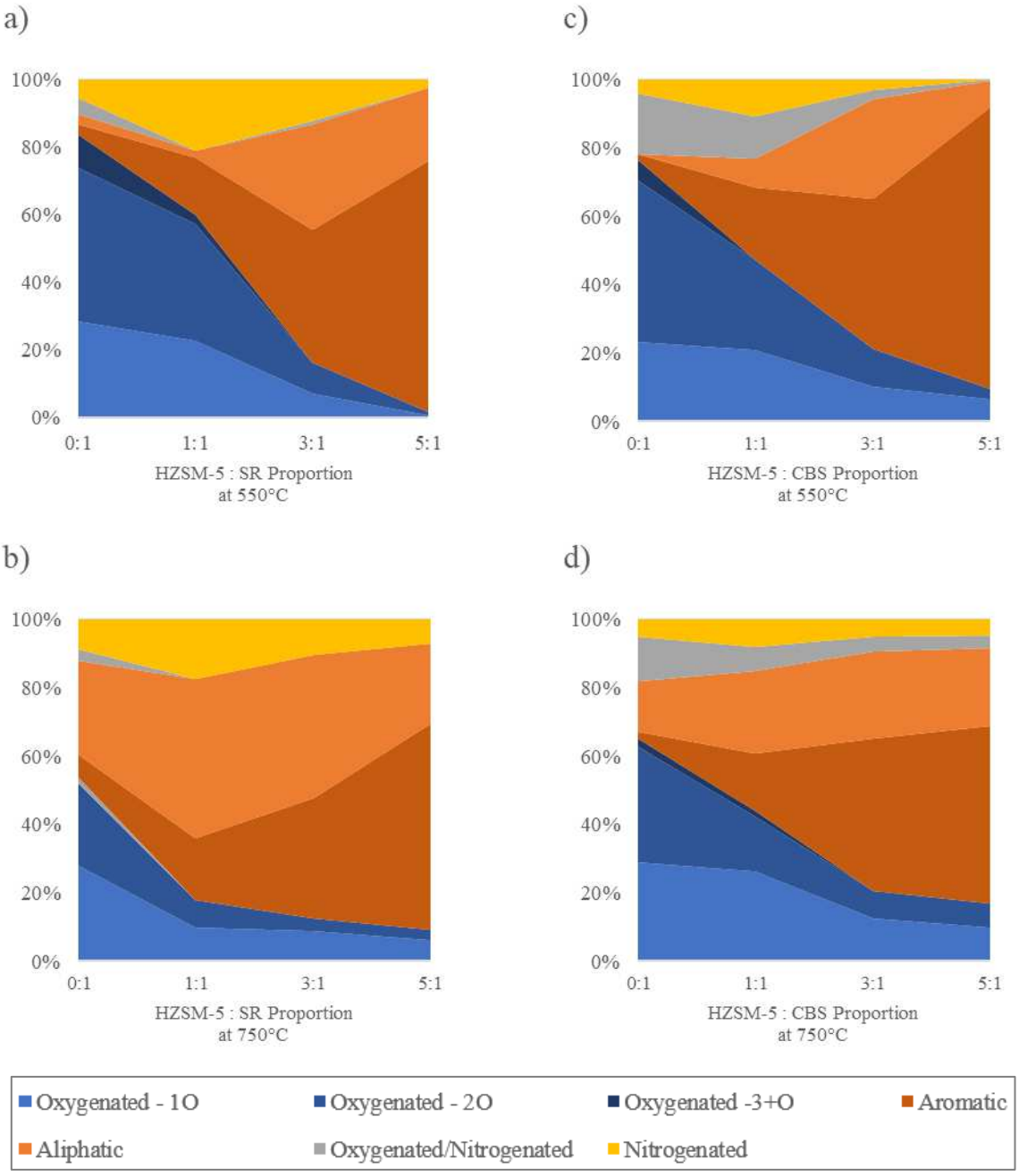


Figure 5.24. Categorization of pyrolysis products at different catalyst:biomass proportion for (a) SR at 550°C, (b) SR at 750°C, (c) CBS at 550°C and (d) CBS at 750°C

The presence of nitrogenated compounds reached its maximum when employing C:B ratios of 1:1 and lower temperatures, achieving 21% in the case of SR and 11% for CBS during pyrolysis at 550°C. This represents a substantial increase compared to non-catalytic pyrolysis at the same temperature, which yielded 6% for SR and 4% for CBS. Conversely, the lowest nitrogen content was observed using the highest C:B ratio at 550°C, dropping to 2% for SR and 0% for CBS. As previously discussed, SR consistently exhibited higher nitrogen content compared to CBS.

A possible explanation for this behavior is that zeolite HZSM-5 primarily captures available oxygen and will only interact with nitrogen if unoccupied sites exist. Consequently, when the catalyst proportion is lower, complete deoxygenation is not achieved due to catalyst saturation, allowing compounds with removed oxygen to react with available nitrogen during the reaction phase. Wang et al. (2013) observed that at higher temperatures, there is an increase in ammonia production, which can potentially react with other compounds to form nitriles. This observation could elucidate why, even with an optimal C:B ratio, nitriles became the predominant group alongside hydrocarbons at 750°C with a C:B ratio of 5:1, as shown in Figure 5.25 (b) and (d).

Both biomass sources exhibited similar trends with varying C:B ratios. Silva (2020) conducted experiments using corn cob as the biomass, employing the same proportions as in this study. The findings were consistent, with a comparable trend observed in hydrocarbon generation, reaching 92% with a C:B ratio of 5:1. Silva suggested that the catalyst's primary influence was acidity. Likewise, Promsampao et al. (2022) explored various C:B ratios in eucalyptus pyrolysis and achieved a remarkable 98% aromatics yield with the highest C:B ratio, further confirming this common trend. Conversely, Toro-Trochez et al. (2022) conducted catalytic pyrolysis of soybean residue at 500°C with a biomass-to-catalyst (HZSM-5) ratio of 50:1. The outcomes indicated that the proportions of acids, ketones, and phenols remained approximately at 20% each, while hydrocarbon generation was around 10%.

One distinctive feature specific to CBS is the presence of oxygenated/nitrogenated compounds, primarily alkaloids. As previously discussed, temperature exerted minimal effects on the reaction of these components. Conversely, the catalyst appeared to facilitate the conversion of these components into hydrocarbons, as shown in Figure 5.25 (c) and (d). This is evident in the reduced alkaloid content with increasing C:B ratios, reaching a minimum value of 0.4% at 550°C with a C:B ratio of 5:1 (the chromatograms and compounds table can be found in Appendix A).

The escalation in catalyst load might enhance the residence time between the catalyst and the pyrolytic vapors and the number of available catalyst sites (Dai et al., 2020). This improved interaction between pyrolytic vapors and catalyst likely favored reactions, leading to increased formation of the product of interest. Gopakumara et al. (2012) similarly observed increased hydrocarbon content in pyrolysis products with increased catalyst load.

Additionally, zeolites may exhibit enhanced selectivity for oxygenated compounds, as demonstrated by Hasegawa et al. (2002) and Gu et al. (2005). However, this does not imply its inability to react with nitrogenated molecules. Nazir et al. (2020) reported a variability in zeolite membrane selectivity for CO_2/N_2 ranging from approximately 10 to 35. The present study hypothesizes that zeolites can retain nitrogen in the presence of an increased number of free active sites. Hence, adding an appropriate quantity of HZSM-5 molecular sieve catalyst can substantially enhance aromatic selectivity and reduce nitrogen compound levels in the oil, promoting the facilitation of subsequent bio-oil processing and utilization.

Furthermore, Qi et al. (2018) documented a transformation in the nitrogen compound proportion, decreasing from 18.37% to 0.59% as the catalyst/feedstock mass ratio ranged from 0:1 to 10:1. They explain that this shift occurred because, with the introduction of an optimal amount of HZSM-5, the pyrolytic vapors effectively reached the surface of zeolite catalysts. Consequently, the nitrogen-containing functional group underwent degradation and elimination, producing more hydrocarbons and other nonpolar compounds, thereby diminishing the nitrogen compound content.

Ansah et al. (2018) observed a decrease in the nitrogen (N) content of *C. debaryana* from 9.5 to 5.2 wt.% during hydrothermal carbonization. Rahman et al. (2018) conducted pyrolysis of *Isochrysis sp*. using a commercial Li-LSX zeolite, resulting in bio-oil with 23.1% aliphatic hydrocarbons and 11.8% aromatic compounds, achieved through the expediting denitrogenation of pyrolytic products. Lee et al. (2020) proposed that a potential pathway for nitrogen removal using zeolites involves protein cracking and deamination.

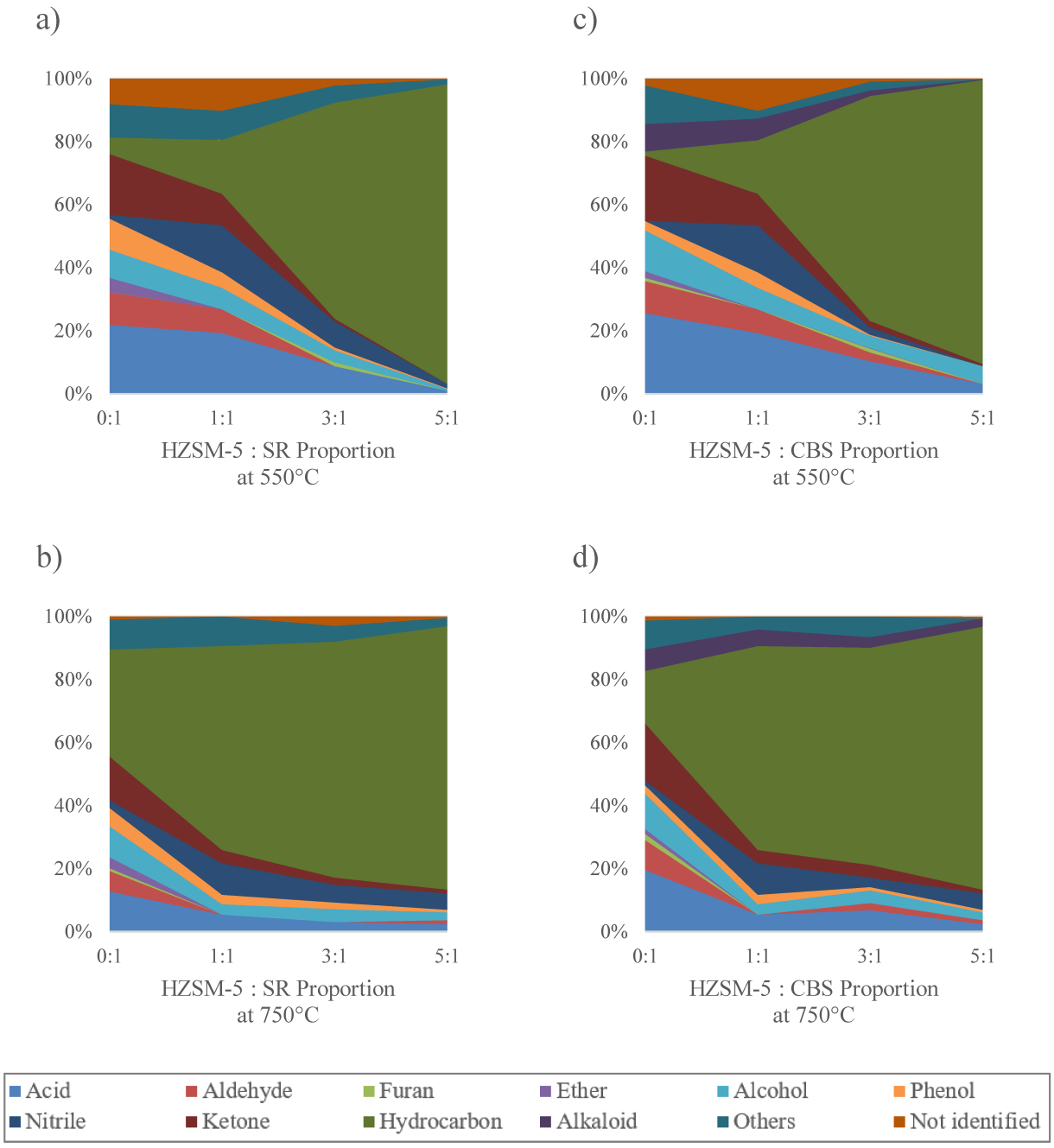


Figure 5.25. Organic groups categorization of pyrolysis products at different catalyst:biomass proportion for (a) SR at 550°C, (b) SR at 750°C, (c) CBS at 550°C and (d) CBS at 750°C

Analyzing Figure 5.26, a notable observation is the uptrend of long-chain compounds when employing a C:B ratio of 1:1 for both biomasses. This phenomenon is closely associated with the formation of nitriles, particularly evident at 550°C, where predominantly large-chain nitriles such as hexadecanitrile, heptadecanitrile, and octadecanitrile were identified. These findings are also

corroborated in Tables 5.12 and 5.13, which summarize the main compounds generated during the pyrolysis reaction.

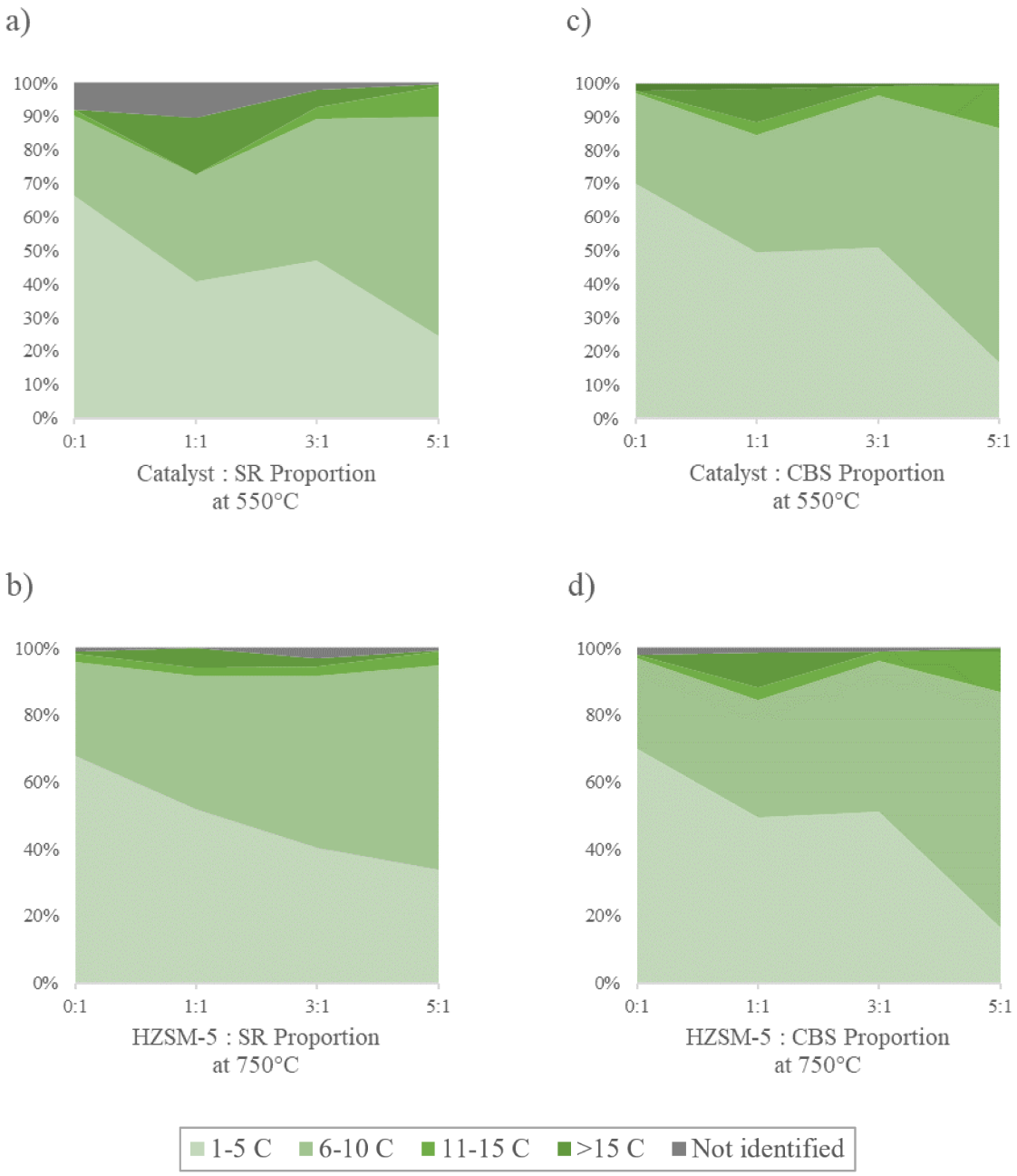
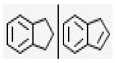


Figure 5.26. Size of chains based on number of carbons in the organic structure for the pyrolysis products at different catalyst:biomass proportion for (a) SR at 550°C, (b) SR at 750°C, (c) CBS at 550°C and (d) CBS at 750°C

Another notable effect observed is the rise in organic compounds containing 6 to 10 carbon atoms, likely attributed to the increased presence of aromatic compounds, predominantly benzene derivatives. This is further detailed in the tables below.

Table 5.12. Main organic products from catalytic pyrolysis with HZSM-5 of the SR with temperatures of 550°C and 750°C and catalyst:biomass proportion varying from 0:1 to 5:1.

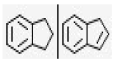
Compound	Formula	Temperature of 550°C				Temperature of 750°C			
		0:1	1:1	3:1	5:1	0:1	1:1	3:1	5:1
Acetic acid	$C_2H_4O_2$	18.0%	14.9%	5.0%	1.0%	10.6%	5.4%	3.0%	2.4%
2-Propanone,1-hydroxy-	$C_3H_6O_2$	9.4%	3.7%	0.0%	0.0%	7.8%	1.8%	0.7%	0.5%
Methanol	CH_4O	7.5%	2.1%	1.8%	0.0%	6.7%	0.0%	1.9%	0.5%
Acetaldehyde	C_2H_4O	5.0%	4.1%	0.0%	0.0%	4.4%	0.0%	0.0%	1.2%
Hydrocarbon Benzene Derivatives		2.7%	14.1%	30.6%	58.0%	5.4%	12.8%	31.3%	48.7%
Cyclic olefins and cyclic oxygenated derivatives	-	5.2%	6.3%	5.0%	3.7%	8.1%	22.5%	6.4%	2.0%
Indan/Indene Derivatives		0.0%	0.0%	2.6%	6.3%	0.0%	0.9%	3.8%	3.0%
Naphthalene Derivatives		0.0%	1.3%	3.8%	7.9%	0.0%	3,2%	3.7%	7.0%
Phenol Derivatives		7.1%	2.5%	1.0%	0.2%	3.4%	2,2%	1.4%	0.8%
2-Butene	C_4H_8	0.0%	0.0%	11.6%	10.2%	0.0%	0,0%	10.0%	7.6%
Propene	C_3H_6	0.0%	0.0%	10.0%	8.5%	8.3%	8,8%	10.8%	11.9%
Acetonitrile	C_2H_3N	0.0%	0.0%	3.8%	1.5%	0.0%	3,2%	4.2%	4.2%
Big Chain Nitriles	C_yH_xN	0.0%	14.9%	4.5%	0.0%	0.0%	5,9%	1.5%	0.6%
Total		**54.9%**	**61.4%**	**78.7%**	**97.2%**	**54.7%**	**69.1%**	**77.4%**	**89.6%**

Tables 5.12. and 5.13 reveals a noticeable increase in the production of indan/indenes and naphthalene derivatives among the aromatic compounds as the C:B ratio rises. This cumulative effect led to a combined percentage of 14.2% for SR and 10.0% for CB.

Furthermore, a noteworthy observation is the prevalence of acetic acid among the oxygenated compounds formed with a C:B ratio of 5:1, regardless of temperature and biomass type. This suggests that acetic acid may be one of the more stable components generated during this pyrolysis reaction.

Lastly, it is worth highlighting that with a C:B ratio of 5:1, approximately 80% of the aliphatic compounds were identified as butene and propene, the most relevant olefins produced when using the HZSM 5 as the catalyst.

Table 5.13. Main organic products from catalytic pyrolysis with HZSM-5 of the CBS with temperatures of 500°C and 750°C and catalyst:biomass proportion varying from 0:1 to 5:1.

Compound	Formula	Temperature of 550°C				Temperature of 750°C			
		0:1	1:1	3:1	5:1	0:1	1:1	3:1	5:1
Acetic acid	$C_2H_4O_2$	22.8%	18.5%	8.4%	3.1%	17.0%	8.0%	5.3%	4.1%
2-Propanone,1-hydroxy-	$C_3H_6O_2$	8.5%	2.2%	0.2%	0.0%	7.0%	1.9%	0.5%	0.8%
Methanol	CH_4O	6.3%	1.7%	2.0%	4.1%	6.0%	1.9%	1.1%	1.1%
Acetaldehyde	C_2H_4O	3.7%	4.4%	2.8%	0.0%	4.8%	3.6%	2.4%	2.3%
Hydrocarbon Benzene Derivatives		1.4%	17.0%	36.7%	59.6%	2.0%	13.0%	35.4%	39.5%
Cyclic olefins and cyclic oxygenated derivatives	-	6.7%	3.2%	2.6%	0.5%	7.6%	16.6%	14.3%	1.7%
Indan/Indene Derivatives		0.0%	1.8%	4.6%	9.4%	0.0%	0.9%	4.2%	2.3%
Naphthalene Derivatives		0.0%	3.0%	2.7%	10.7%	0.0%	0.7%	3.3%	6.8%
Phenol Derivatives		3.0%	3.3%	0.4%	0.0%	2.7%	0.0%	1.0%	0.8%
2-Butene	C_4H_8	0.0%	5.9%	8.7%	6.6%	0.0%	3.9%	8.6%	6.8%
Propene	C_3H_6	0.0%	0.0%	14.0%	0.0%	5.6%	0.0%	0.0%	11.1%
Ethanol	C_2H_6O	0.0%	1.3%	1.8%	1.6%	0.0%	10.0%	1.2%	0.7%
Acetone	C_3H_6O	2.4%	0.0%	0.0%	0.0%	2.9%	0.0%	0.0%	0.0%
Pyrrole	C_4H_5N	3.7%	0.0%	0.0%	0.0%	3.6%	0.0%	0.0%	0.0%
Theobromine	$C_7H_8N_4O_2$	13.6%	10.0%	1.9%	0.2%	9.7%	5.8%	3.6%	2.8%
Caffeine	$C_8H_{10}N_4O_2$	2.4%	2.0%	0.5%	0.2%	1.7%	1.1%	0.9%	0.7%
Acetonitrile	C_2H_3N	0.0%	0.0%	2.2%	0.0%	0.0%	1.7%	2.5%	3.2%
Big Chain Nitriles	C_yH_xN	0.0%	8.5%	0.0%	0.0%	0.0%	3.7%	0.6%	3.2%
Total		**74.5%**	**83.0%**	**89.3%**	**96.2%**	**70.6%**	**72.9%**	**84.7%**	**88.1%**

Upon analyzing the catalytic pyrolysis process of biomasses and examining the results from various aggregated groups in Table 5.13, a suggestion was made to adapt the reaction mechanism proposed by Yang et al. (2023). This adaptation involves the inclusion of cyclic olefins and indan/indenes groups as intermediates in the pathway, leading to the formation of polyaromatic compounds when HZSM-5 is used as the catalyst.

The reaction pathway proposed is shown in Figure 5.27. It assumes that the primary compounds generated in the non-catalytic process, which are predominantly oxygenated, undergo a series of transformation pathways after the primary pyrolysis when in contact with HZSM-5. These pathways include decarbonylation, decarboxylation, and dehydration reactions, forming

alkenes and alkanes. Subsequently, these compounds undergo cyclization and Diels-Alder reactions, ultimately resulting in the formation of cyclic substances. These cyclic compounds then experience further dehydrogenation processes, culminating in the production of monoaromatic substances. These monoaromatics can, in turn, engage in subsequent reactions, eventually generating indan, indene, and further polyaromatic compounds. It is important to note that these reactions are influenced by factors such as temperature, the nature of the raw material, and the C:B ratio (Guedes et al., 2018), which can lead to distinct vapor products of pyrolysis in each stage presented in this work.

For instance, in the case of SR at 550°C with a C:B ratio of 5:1, the resulting products comprised 1.8% oxygenated compounds, 15.9% alkanes and alkenes, 3.7% cyclic olefins, 59.6% benzene derivatives (monoaromatics), 6.3% indan and indene derivatives, and 7.9% naphthalene compounds (polyaromatics).

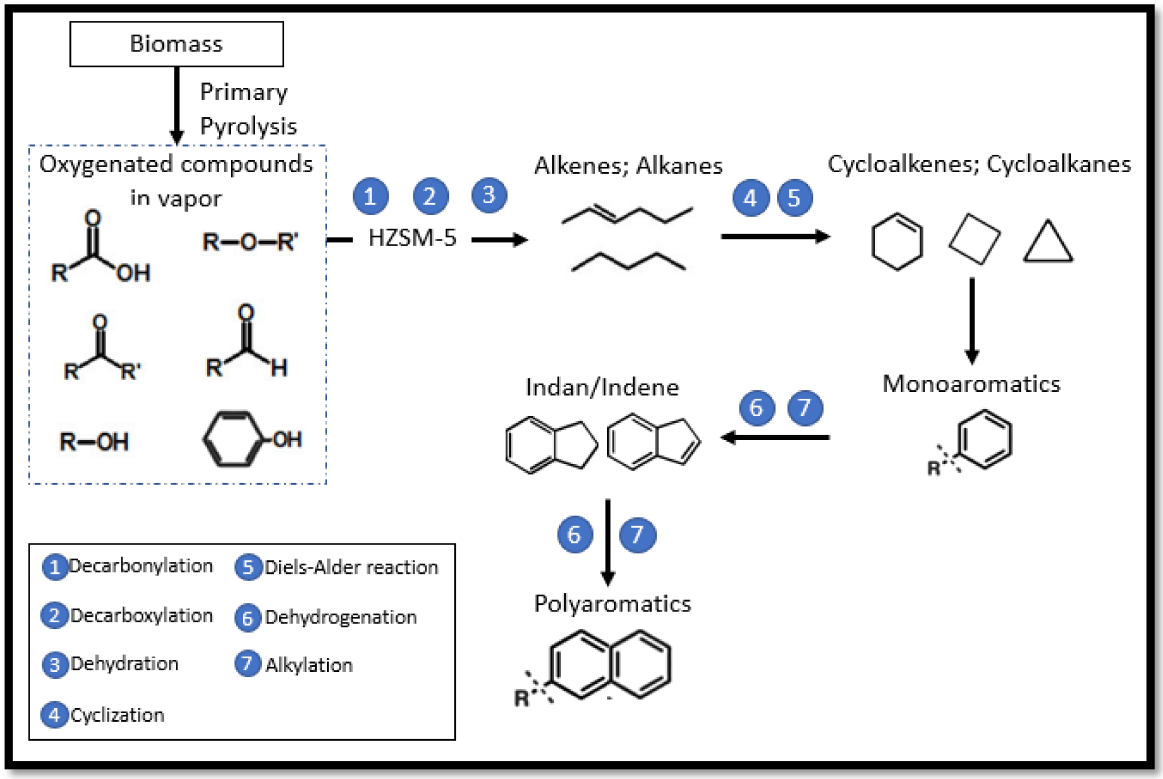


Figure 5.27. Reaction pathways for the catalytic pyrolysis of SR and CCBS with HZSM-5 (adapted from Yang et al., 2023)

5.4. References

Abelló, S.; Medina, F.; Tichit, D.; Pérez-Ramírez, J.; Sueiras, J.E.; Salagre, P.; Cesteros, Y. (2007). Aldol condensation of campholenic aldehyde and MEK over activated hydrotalcites. Applied Catalysis B: Environmental, 70, 577–584. https://doi.org/10.1016/j.apcatb.2006.01.021

Aleem, S. A., Asikin-Mijan, N., Hussain, A. S., Voon, C. H., Dolfi, A., Sivasangar, S., & Taufiq-Yap, Y. H. (2021). Catalytic ketonization of palmitic acid over a series of transition metal oxides supported on zirconia oxide-based catalysts. RSC Advances, 11(51), 31972–31982. https://doi.org/10.1039/d0ra10963k

Alén, R., Kuoppala, E., Oesch, P. (1996). Formation of the main degradation compound groups from wood and its components during pyrolysis. Journal of Analytical and Applied Pyrolysis, 36 (2), 137–148. https://doi.org/10.1016/0165-2370(96)00932-1

Ampah, J.D., Liu, X., Sun, X., Pan, X., Xu, L., Jin, C., Sun, T., Geng, Z., Afrane, S., Liu, H. (2022). Study on characteristics of marine heavy fuel oil and low carbon alcohol blended fuels at different temperatures. Fuel, 310, 122307. https://doi.org/10.1016/j.fuel.2021.122307

Amani, J.; Molander, G.A. (2017). Direct Conversion of Carboxylic Acids to Alkyl Ketones, Organic Letters, 19 (13), 3612–3615. https://doi.org/10.1021/acs.orglett.7b01588

Andrade, L.A.; Barbosa, J.M.; Barrozo, M.A.S.; Vieira, L.G.M. (2020). A comparative study of the behavior of Chlamydomonas reinhardtii and Spirulina platensis in solar catalytic pyrolysis. Energy Research, 1–15. https://doi.org/10.1002/er.5289

Ansah, E., Wang, L., Zhang, B., Shahbazi, A. (2018). Catalytic pyrolysis of raw and hydrothermally carbonized Chlamydomonas debaryana microalgae for denitrogenation and production of aromatic hydrocarbons. Fuel, 228, 234–242. https://doi.org/10.1016/j.fuel.2018.04.163

Azreena, I.N.; Lau, H.L.N.; Asikin-Mijan, N.; Izham, S.M.; Hassan, M.A.; Kennedy, E.; Stockenhuber, M.; Taufiq-Yap, Y.H. (2021). Hydrodeoxygenation of oleic acid for effective diesel-like hydrocarbon production using zeolite-based catalysts. Reaction Kinetics. Mechanisms and Catalysis, 134 (2), 1069–1083. https://doi.org/10.1007/s11144-021-02082-w

Barbosa, J.M. (2020). Pirólise solar catalítica ex-situ da microalga Chlamydomonas reinhardtii. Faculdade de Engenharia Química, Universidade Federal de Uberlândia, Tese de Doutorado.

Borel, L.D.M.S., Lira, T.S., Ribeiro, J.A., Ataíde, C.H., Barrozo, M.A.S. (2018). Pyrolysis of brewe 's spent grain: Kinetic study and products identification,). Industrial Crops & Products, 121, 388–395. https://doi.org/10.1016/j.indcrop.2018.05.051

Bridgwater, B.T. (2018), Challenges and Opportunities in Fast Pyrolysis of Biomass: Part I, Johnson Matthey Technology Review, 62, 118–130. https://doi.org/10.1595/205651318X696693

Chang, C.C., Je Cho, H., Yu, J., Gorte, R. J., Gulbinski, J., Dauenhauer, P., Fan, W. (2016). Lewis acid zeolites for tandem Diels-Alder cycloaddition and dehydration of biomass-derived dimethylfuran and ethylene to renewable p-xylene. Green Chemistry, 18(5), 1368–1376. https://doi.org/10.1039/c5gc02164b

Cinar, Z.Ö., Atanassova, M., Tumer, T.B., Caruso, G., Antika, G., Sharma, S., Sharifi-Rad, J., Pezzani, R. (2021). Cocoa and cocoa bean shells role in human health: An updated review. Journal of Food Composition and Analysis, 103(August). https://doi.org/10.1016/j.jfca.2021.104115

Conti, L., Scano, G., Boufala, J. (1994). Bio-oils from arid land plants: Flash pyrolysis of Euphorbia characias bagasse. Biomass and Bioenergy, 7 (1–6), 291–296. https://doi.org/10.1016/0961-9534(94)00071-Z

Dai, L.; Wang, Y.; Liu, Y.; He, C.; Ruan, R.; Yu, Z.; Jiang, L.; Zeng, Z.; Wu, Q. (2020). A review on selective production of value-added chemicals via catalytic pyrolysis of lignocellulosic biomass. Science of the Total Environment, 749, 142386. https://doi.org/10.1016/j.scitotenv.2020.142386

Dai, L.; Wang, Y.; Liu, Y.; Ruan, R.; Duan, D.; Zhao, Y.; Yu, Z.; Jiang, L. (2019). Catalytic fast pyrolysis of torrefied corn cob to aromatic hydrocarbons over Ni-modified hierarchical ZSM-5 catalyst. Bioresource Technology, 272, 407–414. https://doi.org/10.1016/j.biortech.2018.10.062

Danilina, N., Payrer, E. L., Troussard, E., & Van Bokhoven, J. A. (2011). Selective production of 2-phenylhexane from benzene and n-hexane over Pt- and Ga-modified zeolites. Catalysis Letters, 141(3), 391–399. https://doi.org/10.1007/s10562-010-0511-0

Ding, K., Zhong, Z., Wang, J., Zhang, B., Fan, L., Liu, S., Wang, Y., Liu, Y., Zhong, D., Chen, P., Ruan, R. (2018). Improving hydrocarbon yield from catalytic fast co-pyrolysis of hemicellulose and plastic in the dual-catalyst bed of CaO and HZSM-5. Bioresource Technology, 261, 86-92. https://doi.org/10.1016/j.biortech.2018.03.138

Domínguez, A.; Menéndez, J.A.; Inguanzo, M.; Bernad, P.L.; Pis, J.J. (2003). Gas chromatographic-mass spectrometric study of the oil fractions produced by microwave-assisted pyrolysis of different sewage sludges. Journal of Chromatography A, 101, 193–206. https://doi.org/10.1016/S0021-9673(03)01176-2

Encinar, J.M., Beltrán, F.J., Ramiro, A., González, J.F. (1998). Pyrolysis/gasification of agricultural residues by carbon dioxide in the presence of different additives: Influence of variables. Fuel Processing Technology, 55 (3), 219–233. https://doi.org/10.1016/S0378-3820(98)00052-6

Evans, D. G., & Slade, R. C. T. (2005). Structural aspects of layered double hydroxides. Structure and Bonding, 119(December 2005), 1–87. https://doi.org/10.1007/430_005

Fan, Y., Zhang, D., Zheng, A., Zhao, Z., Li, H., & Yang, T. (2019). Selective production of anhydrosugars and furfural from fast pyrolysis of corncobs using sulfuric acid as an inhibitor and catalyst. Chemical Engineering Journal, 358, 743–751. https://doi.org/10.1016/j.cej.2018.10.014

Gholami, Z., Tišler, Z., Velvarská, R., & Kocík, J. (2020). Comn catalysts derived from hydrotalcite-like precursors for direct conversion of syngas to fuel range hydrocarbons. Catalysts, 10(8). https://doi.org/10.3390/catal10080813

Goh, K.H.; Lim, T.T.; Dong, Z. (2008). Application of layered double hydroxides for the removal of oxyanions. Water Res. 42, 1343-1368, 2008. https://doi.org/10.1016/j.watres.2007.10.043

Gopakumara, S.T., Sushil, A.S.A. (2012). Catalytic pyrolysis of green microalgae for hydrocarbon production using HZSM-5 catalyst. Bioresource Technology, 118, 150-157. https://doi.org/10.1016/j.biortech.2012.05.080

Grillo, G., Boffa, L., Binello, A., Mantegna, S., Cravotto, G., Chemat, F., Dizhbite, T., Lauberte, L., Telysheva, G. (2019). Cocoa bean shell waste valorisation; extraction from lab to pilot-scale cavitational reactors. Food Research International, 115, 200–208. https://doi.org/10.1016/j.foodres.2018.08.057

Gu, X., Dong, J., Nenoff, T.M. (2005). Synthesis of defect-free FAU-type zeolite membranes and separation for dry and moist CO2/N2 mixtures. Industrial and Engineering Chemistry Research, 44 (4), 937–944. https://doi.org/10.1021/ie049263i

Guedes, R.E., Luna, A.S., Torres, A.R. (2018), Journal of analytical and applied pyrolysis operating parameters for bio-oil production in biomass pyrolysis: a review, J. Anal. Appl. Pyrol., 129, 134-149, https://doi.org/10.1016/j.jaap.2017.11.019

Güllü, D., & Demirbaş, A. (2001). Biomass to methanol via pyrolysis process. Energy Conversion and Management, 42(11), 1349–1356. https://doi.org/10.1016/S0196-8904(00)00126-6

Handbook of Biomass Downdraft Gasifier Engine Systems, Solar Technical Information Program. (1988). U.S. Government Printing Office Washington, DC 20402. Chapter 5.

Hasegawa, Y., Watanabe, K., Kusakabe, K., Morooka, S. (2002). Influence of alkali cations on permeation properties of Y-type zeolite membranes. Journal of Membrane Science, 208 (1–2), 415–418. https://doi.org/10.1016/S0376-7388(01)00694-9

Higginbotham, C. (2021). Introductory Organic Chemistry, https://openoregon.pressbooks.pub/introductoryorganic/chapter/heteroatoms-and-functional-groups/, [on-line accessed 26-10-2023, 17:30h].

Huang, D., Song, G., Li, R., Han, H., He, L., Jiang, L., Wang, Y., Su, S., Hu, S., Xiang, J. (2023). Evolution mechanisms of bio-oil from conventional and nitrogen-rich biomass during photo-thermal pyrolysis. Energy, 282, 128813. https://doi.org/10.1016/j.energy.2023.128813

Islam, M. M., Pandya, P., Kumar, S., & Kumar, G. S. (2009). RNA targeting through binding of small molecules: Studies on t-RNA binding by the cytotoxic protoberberine alkaloid coralyne. Molecular BioSystems, 5(3), 244–254. https://doi.org/10.1039/b816480k

Jin, X., Lee, J.H., Choi, J.W. (2022). Catalytic co-pyrolysis of woody biomass with waste plastics: Effects of HZSM-5 and pyrolysis temperature on producing high-value pyrolytic products and reducing wax formation. Energy, 239, 121739. https://doi.org/10.1016/j.energy.2021.121739

Kumar, R., Enjamuri, N., Shah, S., Al-Fatesh, A. S., Bravo-Suárez, J. J., & Chowdhury, B. (2018). Ketonization of oxygenated hydrocarbons on metal oxide based catalysts. Catalysis Today, 302(December 2016), 16–49. https://doi.org/10.1016/j.cattod.2017.09.044

Lee, D., Nam, H.; Won Seo, M., Hoon Lee, S., Tokmurzin, D.; Wang, S., Park, Y.K. (2022). Recent progress in the catalytic thermochemical conversion process of biomass for biofuels. Chemical Engineering Journal, 447, 137501. https://doi.org/10.1016/j.cej.2022.137501

Lee, J., Kwon, E. E., Park, Y.K. (2020). Recent advances in the catalytic pyrolysis of microalgae. Catalysis Today, 355, 263–271. https://doi.org/10.1016/j.cattod.2019.03.010

Li, F., Srivatsa, S.C., Bhattacharya, S. (2019). A review on catalytic pyrolysis of microalgae to high-quality bio-oil with low oxygeneous and nitrogenous compounds. Renewable and Sustainable Energy Reviews, 108, 481-497. https://doi.org/10.1016/j.rser.2019.03.026

Liang, J., Morgan, H.M., Liu, Y., Shi, A., Lei, H., Mao, H., Bu, Q. (2017). Enhancement of bio-oil yield and selectivity and kinetic study of catalytic pyrolysis of rice straw over transition metal modified ZSM-5 catalyst. Journal of Analytical and Applied Pyrolysis, 128, 324–334. https://doi.org/10.1016/j.jaap.2017.09.018

Lin, Y. L., Zheng, N.Y., Hsu, C.H. (2021). Torrefaction of fruit peel waste to produce environmentally friendly biofuel. Journal of Cleaner Production, 284(xxxx), 124676. https://doi.org/10.1016/j.jclepro.2020.124676

Liu, H., Zhang, F., Liu, H., Ma, C., Hu, J., Zhong, W., Wang, H. (2023). Comprehensive investigation on fast pyrolysis of waste Lotus shells to produce valuable products: Pyrolysis

characteristics, reaction mechanism and economic analysis. Journal of Environmental Chemical Engineering, 11(6), 111172. https://doi.org/10.1016/j.jece.2023.111172

Moogi, S., Pyo, S., Farooq, A., Valizadeh, S., Jun Choi, Y., Hoon Rhee, G., Lee, J., Jae, J., Hussain, M., Ali Khan, M., Jeon, B.H., Andrew, L.K.Y., Chen, W.H., Park, Y.K. (2022). Enhancement of bioaromatics production from food waste through catalytic pyrolysis over Zn and Mo-loaded HZSM-5 under an environment of decomposed methane. Chemical Engineering Journal, 446, 137215. https://doi.org/10.1016/j.cej.2022.137215

Morris, M.A. (2011). Production of bio-oils via catalytic pyrolysis. In Handbook of Biofuels Production: Processes and Technologies. Woodhead Publishing Limited. https://doi.org/10.1533/9780857090492.3.349

Moujahid, E. M., Dubois, M., Besse, J. P., Leroux, F. (2002). Role of atmospheric oxygen for the polymerization of interleaved aniline sulfonic acid in LDH. Chemistry of Materials, 14(9), 3799–3807. https://doi.org/10.1021/cm0211094

Moura, L.G. (2022). Study of hydrodeoxygenation reaction of phenolic compounds using niobium-based catalysts. Universidade Federal de Uberlândia, Faculdade De Engenharia Química Programa De Pós-Graduação Em Engenharia Química – Tese de Doutorado.

Navarro, R.M., Guil-Lopez, R., Fierro, J.G., Mota, N., Jiménez, S., Pizarro, P., Coronado, J.M., Serrano, D.P. (2018). Catalytic fast pyrolysis of biomass over Mg-Al mixed oxides derived from hydrotalcite-like precursors: Influence of Mg/Al ratio. Journal of Analytical and Applied Pyrolysis, 1–9. https://doi.org/10.1016/j.jaap.2018.07.001

Nazir, L.S.M., Yeong, Y.F., Chew, T.L. (2020). Methods and synthesis parameters affecting the formation of FAU type zeolite membrane and its separation performance: a review. Journal of Asian Ceramic Societies, 8 (3), 553–571. https://doi.org/10.1080/21870764.2020.1769816

Newman, S. P., & Jones, W. (1998). Synthesis, characterization and applications of layered double hydroxides containing organic guests. New Journal of Chemistry, 22(2), 105–115. https://doi.org/10.1039/a708319j

Numpilai, T., Cheng, C.K., Limtrakul, J., Witoon, T. (2021). Recent advances in light olefins production from catalytic hydrogenation of carbon dioxide. Process Safety and Environmental Protection, 151, 401–427. https://doi.org/10.1016/j.psep.2021.05.025

Oliveira, T.J.P., Cardoso, C.R., Ataíde, C.H. (2015). Fast pyrolysis of soybean hulls: Analysis of bio-oil produced in a fluidized bed reactor and of vapor obtained in analytical pyrolysis. Journal of Thermal Analysis and Calorimetry, 120 (1), 427–438. https://doi.org/10.1007/s10973-015-4600-6

Oliveira, T.J.P. (2015). Pirólise rápida de casca de soja: desenvolvimento do reator de leito fluidizado, análise do bio-óleo produzido e do vapor obtido na pirólise analítica. Faculdade de Engenharia Química, Universidade Federal de Uberlândia, Tese de Doutorado.

Patwardhan, P. R., Brown, R. C., & Shanks, B. H. (2011). Product distribution from the fast pyrolysis of hemicellulose. ChemSusChem, 4(5), 636–643. https://doi.org/10.1002/cssc.201000425

Porto de Souza Vandenberghe, L., Kley Valladares-Diestra, K., Amaro Bittencourt, G., Fátima Murawski de Mello, A., Sarmiento Vásquez, Z., Zwiercheczewski de Oliveira, P., Vinícius de Melo Pereira, G., Ricardo, C. (2022), Added-value biomolecules' production from cocoa pod husks: A review, Bioresource Technology, 344. https://doi.org/10.1016/j.biortech.2021.126252

Prabhakara, H.M.; Bramer, E.A.; Brem, G. (2022). Hydrotalcite as a deoxygenation catalyst in fast pyrolysis of biomass for the production of high quality bio-oil. Journal of Analytical and Applied Pyrolysis, 161, 105431. https://doi.org/10.1016/j.jaap.2022.105431

Promsampao, N., Chollacoop, N., & Pattiya, A. (2022). Effect of low-temperature hydrothermal treatment of HZSM-5 extrudates on the production of deeply-deoxygenated bio-oil via ex-situ catalytic fast pyrolysis of biomass. Fuel, 324(PB), 124627. https://doi.org/10.1016/j.fuel.2022.124627

Prusova, B., Humaj, J., Sochor, J., & Baron, M. (2022). Formation, Losses, Preservation and Recovery of Aroma Compounds in the Winemaking Process. Fermentation, 8(3). https://doi.org/10.3390/fermentation8030093

Qi, P., Chang, G., Wang, H., Zhang, X., Guo, Q. (2018). Production of aromatic hydrocarbons by catalytic co-pyrolysis of microalgae and polypropylene using HZSM-5. Journal of Analytical and Applied Pyrolysis, 136, 178–185. https://doi.org/10.1016/j.jaap.2018.10.007

Rahman, N.A.A., Fermoso, J., Sanna, A. (2018). Effect of Li-LSX-zeolite on the in-situ catalytic deoxygenation and denitrogenation of Isochrysis sp. Microalgae pyrolysis vapours. Fuel Process. Technol. 173, 253–261. https://doi.org/10.1016/j.fuproc.2018.01.020

Reis Filho, A.M. (2020). Pirólise rápida de bagaço de malte em leito de jorro: otimização, caracterização dos produtos e melhoramento do bio-óleo. Faculdade de Engenharia Química, Universidade Federal de Uberlândia, Dissertação de Mestrado.

Rossi, R.A.S., Dai, L., Barrozo, M.A.S., Vieira, L.G.M., Hori, C.E., Cobb, K., Chen, P., Ruan, R. (2023). Bio-fuel production from catalytic microwave-assisted pyrolysis of the microalgae Schizochytrium limacinum in a tandem catalytic bed. Chemical Engineering Journal, 478, 147223. https://doi.org/10.1016/j.cej.2023.147223

Santana Júnior, J.A. (2018). Efeito catalítico de zeólita ZSM-5 e ácido nióbico HY-340 na pirólise e hidropirólise de ligninas KRAFT industriais. Faculdade de Engenharia Química, Universidade Federal de Uberlândia, Tese de Doutorado.

Shen, D. K., Gu, S., & Bridgwater, A. V. (2010). Study on the pyrolytic behaviour of xylan-based hemicellulose using TG-FTIR and Py-GC-FTIR. Journal of Analytical and Applied Pyrolysis, 87(2), 199–206. https://doi.org/10.1016/j.jaap.2009.12.001

Shen, D.K., Gu, S., Bridgwater, A.V. (2010). Study on the pyrolytic behaviour of xylan-based hemicellulose using TG-FTIR and Py-GC-FTIR. Journal of Analytical and Applied Pyrolysis, 87(2), 199–206. https://doi.org/10.1016/j.jaap.2009.12.001

Silva, A.C.R. (2020). Pirólise Rápida Catalítica de Sabugo De Milho: Seletividade dos Catalisadores HZSM-5 e Hβ para a Produção de Hidrocarbonetos Aromáticos, Faculdade de Engenharia Química, Universidade Federal de Uberlândia, Dissertação de Mestrado.

Simão, B.L.; Santana Júnior, J.A.; Chagas, B.M.E.; Cardoso, C.R.; Ataíde, C.H. Pyrolysis of Spirulina maxima: Kinetic modeling and selectivity for aromatic hydrocarbons. Algal Research, v. 32, p. 221–232, 2018. https://doi.org/10.1016/j.algal.2018.04.007

Soltani, M., Siu, B., Salter, E. A., Wierzbicki, A., West, K. N., & Davis, J. H. (2017). Synthesis, thermal stability, and computed bond dissociation energies of tetraarylphosphonium-based mesothermal ionic liquids bearing a quinoline ring system. Tetrahedron Letters, 58(49), 4628–4631. https://doi.org/10.1016/j.tetlet.2017.10.073

Sun, L., Wang, Z., Chen, L., Yang, S., Xie, X., Gao, M., Zhao, B., Si, H., Li, J., Hua, D. (2020). Catalytic fast pyrolysis of biomass into aromatic hydrocarbons over Mo-modified ZSM-5 catalysts. Catalysts, 10 (9), 1–10. https://doi.org/10.3390/catal10091051

Sun, Y., Li, C., Zhang, S., Li, Q., Gholizadeh, M., Wang, Y., Hu, S., Xiang, J., Hu, X. (2021), Pyrolysis of soybean residue: Understanding characteristics of the products, Renewable Energy, 174, 487–500. https://doi.org/10.1016/j.renene.2021.04.063

Taarning, E., Osmundsen, C. M., Yang, X., Voss, B., Andersen, S. I., & Christensen, C. H. (2011). Zeolite-catalyzed biomass conversion to fuels and chemicals. Energy and Environmental Science, 4(3), 793–804. https://doi.org/10.1039/c004518g

To, A. T., & Resasco, D. E. (2014). Role of a phenolic pool in the conversion of m-cresol to aromatics over HY and HZSM-5 zeolites. Applied Catalysis A: General, 487, 62–71. https://doi.org/10.1016/j.apcata.2014.09.006

Toro-Trochez, J.L., Haro Del Río, D.A., Sandoval-Rangel, L., Bustos-Martínez, D., García-Mateos, F.J., Ruiz-Rosas, R., Rodríguez-Mirasol, J., Cordero, T., Carrilo-Pedraza, E.S. (2022). Catalytic fast pyrolysis of soybean hulls: Focus on the products. Journal of Analytical and Applied Pyrolysis, 163. https://doi.org/10.1016/j.jaap.2022.105492

Thompson, N.S. (2000). Hemicellulose. Kirk-Othmer Encyclopedia of Chemical Technology, 1. https://doi.org/10.1002/0471238961.0805130920081513.a01

Väisänen, S., Ajdary, R., Altgen, M., Nieminen, K., Kesari, K.K., Ruokolainen, J., Rojas, O.J., Vuorinen, T. (2021). Cellulose dissolution in aqueous NaOH–ZnO: cellulose reactivity and the role of ZnO. Cellulose, 28 (3), 1267–1281. https://doi.org/10.1007/s10570-020-03621-9

Valle, B., Gayubo, A. G., Aguayo, A. T., Olazar, M., & Bilbao, J. (2010). Selective production of aromatics by crude bio-oil valorization with a nickel-modified HZSM-5 zeolite catalyst. Energy and Fuels, 24(3), 2060–2070. https://doi.org/10.1021/ef901231j

Wang, H.; Liu, W.; Wang, Y.; Tao, N.; Cai, H.; Liu, J.; Liv, J. (2020). Mg-Al Mixed Oxide Derived from Hydrotalcites Prepared Using the Solvent-Free Method: A Stable Acid-Base Bifunctional Catalyst for Continuous-Flow Transesterification of Dimethyl Carbonate and Ethanol. Industrial and Engineering Chemistry Research, 59 (13), 5591–5600. https://doi.org/10.1021/acs.iecr.9b06303

Wang, K. Brown, R.C. (2013). Catalytic pyrolysis of microalgae for production of aromatics and ammonia, Green Chemistry, 1-20, https://doi.org/10.1039/C3GC00031A

Wang, K., Kim, K. H., Brown, R.C. (2014). Catalytic pyrolysis of individual components of lignocellulosic biomass. Green Chemistry, 16(2), 727–735. https://doi.org/10.1039/c3gc41288a

Wang, S., Dai, G., Yang, H., Luo, Z. (2017b). Lignocellulosic biomass pyrolysis mechanism: A state-of-the-art review. Progress in Energy and Combustion Science, 62, 33–86. https://doi.org/10.1016/j.pecs.2017.05.004

Wang, S., Luo, Z. (2017a). Pyrolysis of Biomass, China Science Publishing & Media Ltd. Vol.1, Alternative Energy Resources. https://doi.org/10.1515/9783110369632

Wang, S., Ru, B., Lin, H., & Sun, W. (2015). Pyrolysis behaviors of four O-acetyl-preserved hemicelluloses isolated from hardwoods and softwoods. Fuel, 150, 243–251. https://doi.org/10.1016/j.fuel.2015.02.045

Wang, S., Zhang, L., Zhang, W., Wang, P., Qin, Z., Yan, W., Dong, M., Li, J., Wang, J., He, L., Olsbye, U., Fan, W. (2020). Selective Conversion of CO2 into Propene and Butene. Chem, 6 (12), 3344–3363. https://doi.org/10.1016/j.chempr.2020.09.025

White, J.L. (2011). Methanol-to-hydrocarbon chemistry: The carbon pool (r)evolution. Catalysis Science and Technology, 1(9), 1630–1635. https://doi.org/10.1039/c1cy00197c

Wijaya, M., Wiharto, M. (2020). Synthesis and characterization of bioactive compound from Cocoa fruit shell by pyrolysis process. Journal of Physics: Conference Series, 1567 (2). https://doi.org/10.1088/1742-6596/1567/2/022025

Wu, Y. M., Zhao, Z. L., Li, H. Bin, & He, F. (2009). Low temperature pyrolysis characteristics of major components of biomass. Ranliao Huaxue Xuebao/Journal of Fuel Chemistry and Technology, 37(4), 427–432. https://doi.org/10.1016/s1872-5813(10)60002-3

Xie, Q., Addy, M., Liu, S., Zhang, B., Cheng, Y., Wan, Y., Li, Y., Liu, Y., Lin, X., Chen, P., Ruan, R. (2015), Fast microwave-assisted catalytic co-pyrolysis of microalgae and scum for bio-oil production. Fuel, 160, 577–582. https://doi.org/10.1016/j.fuel.2015.08.020

Yang, Q., Wu, Q., Zhou, N., Ke, L., Fan, L., Zeng, Y., Xu, C., Liu, Y., Ruan, R., Wang, Y. (2023). Continuous catalytic pyrolysis of waste oil to aromatics: Exploring the structure-performance relations of ZSM-5 based on different scale-up forms. Chemical Engineering Journal, 475, 146259. https://doi.org/10.1016/j.cej.2023.146259

Zhang, J., Fan, Z.L., Lin, X.F. (2005) Online measurement of products during fast pyrolysis of biomass. Journal of Southeast University (Natural Science Edition), 35 (1), 16–19.l

Zhou, G., Jensen, P. A., Le, D. M., Knudsen, N. O., & Jensen, A. D. (2016). Direct upgrading of fast pyrolysis lignin vapor over the HZSM-5 catalyst. Green Chemistry, 18(7), 1965–1975. https://doi.org/10.1039/c5gc01976a

Zhou, X., Li, W., Mabon, R., & Broadbelt, L. J. (2018). A mechanistic model of fast pyrolysis of hemicellulose. Energy and Environmental Science, 11(5), 1240–1260. https://doi.org/10.1039/c7ee03208k

CHAPTER 6

6. CONCLUSIONS

The production of bio-oil using the pyrolysis process offers a promising alternative for generating renewable products, which currently require improvements in terms of product quality. Thus, this study focused on two agricultural residues with the potential to be converted into bio-oil for energy purposes, serving as a renewable energy alternative. To achieve this goal, it was essential to comprehensively understand the characteristics of each biomass and its reaction products through non and catalytic pyrolysis. Distinct catalysts were tested to identify the most effective one among the options analyzed for producing high-quality products suitable as a renewable fuel source. Consequently, an increased hydrocarbon content was pursued. The primary findings are summarized as follows.

The characteristics of biomass make it well-suited for the pyrolysis process, with a substantial volatile content of 78% and 88%, and most weight loss occurring at temperatures around 450°C. One potential challenge is the presence of ashes, which may pose difficulties in industrial combustion processes, but these issues can be managed. The effective management can be achieved using specific equipment in response to regulated limits on particulate emissions and the imperative for proper ash disposal. This technology is already well-established and widely adopted by industries.

Notably, the soybean residue contains a higher nitrogen content at 6%, which has a noticeable impact on the formation of nitrogenated compounds compared to the cocoa bean shell with a nitrogen content of 3%.

The results of non-catalytic pyrolysis, as anticipated, yielded a wide array of compounds with insufficient quality for consideration as a fuel source. The most favorable outcomes, regarding the non-catalytic process, were observed at a temperature of 750°C, with oxygenates comprising 54% and 65% for soybean residue and cocoa bean shell, respectively. Hydrocarbon content reached 34% and 17%, predominantly composed of propene and benzene derivatives. The oxygenated compounds were generally a mixture of carboxylic acids, ketones, phenol, alcohol, and aldehydes. These compounds introduce undesirable attributes to the bio-oil, and many possess a polar nature, making them unsuitable for blending with petroleum-derived fuels. Another notable result from non-catalytic pyrolysis was the presence of alkaloids

in the CBS products, which exhibited limited reactivity during pyrolysis, persisting in the vapors even at temperatures as high as 750°C, comprising 11.4% of the compounds generated.

All catalysts demonstrated deoxygenation capabilities. The niobium-derived catalysts, in particular, played a significant role in generating longer-chain organic compounds but mainly transformed them into nitrogenated substances, achieving levels of 42% and 24% for soybean residue (SR) and cocoa bean shells (CBS), respectively, when employing the Ni/Nb2O5 catalyst. This approach may require additional steps for further quality enhancement, such as denitrification.

Conversely, hydrotalcite, studied across various temperatures, generated 33% and 45% oxygenated products. Despite its effective deoxygenation and conversion to hydrocarbons, along with the ability to enhance overall product quality, it fell short of the potential offered by HZSM-5 zeolite in generating higher-quality products focused on bio-fuel production.

The use of HZSM-5 zeolite as the catalyst for micro-pyrolysis was extensively explored, not only at different temperatures but also with varying catalyst-to-biomass ratios (C:B). In its most successful trial, it achieved remarkable results: 95.1% of hydrocarbons, 1.8% of oxygenated compounds, and 1.4% of nitrogenated compounds for soybean residue (SY), and 90.1%, 9.5%, and 0.2% for cocoa bean shells (CBS). These outcomes were attained at a temperature of 550°C and a C:B ratio of 5:1. The catalyst proved highly effective across a range of temperatures with a C:B ratio of 3:1 or higher, consistently generating hydrocarbon contents exceeding 68% for both biomasses. Another noteworthy result was the substantial aromatic production, which reached 74% for SR and 82% for CBS, using the parameters from the optimal run test at 550°C with a C:B ratio of 5:1.

This study's results confirm that using HZSM-5 as a catalyst for the pyrolysis of soybean residue and cocoa bean shells offers a promising alternative for selectively generating hydrocarbon products. Furthermore, a potential reaction pathway was considered for catalytic pyrolysis with HZSM-5.

6.1. Recommendations for Future Work

In order to improve the process studied and further explore alternatives, below are some suggestions for future work:

- perform Hydropyrolysis with HZSM-5 as the catalyst to enhance aromatic formation;

- combine a second catalyst with the niobium-derived catalysts to enhance long-chain hydrocarbon formation;
- perform catalytic pyrolysis with HZSM-5 in a pilot scale unit to find the best energy-efficient operation parameters.

APPENDIX A
ANALYTICAL PYROLYSIS CHROMATOGRAMS AND COMPOUNDS' TABLES

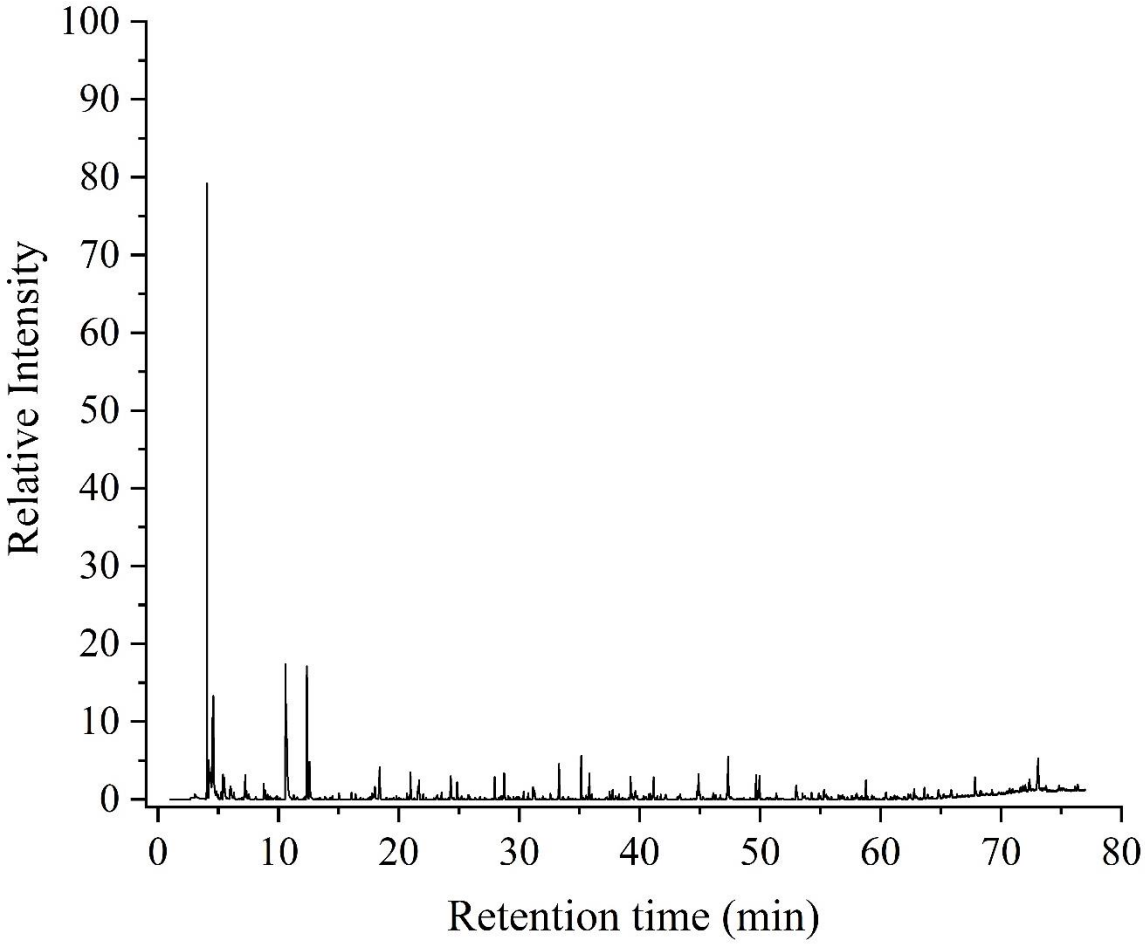


Fig. A1. Chromatogram for the non-catalytic analytical pyrolysis of SR at 550 °C.

Table A1. Compounds identified in the test non-catalytic analytical pyrolysis of SR at 550 °C.

Retention time (min)	Compound	Area
4.332	1-Propene, 2-methyl-	619980
4.502	Acetaldehyde	850309
4.603	Methyl Alcohol	1261272
4.867	Cyclopropane, 1,2-dimethyl-, trans-	114599
5.398	Acetone	279454
5.509	Propane, 1,1'-sulfonylbis-	269233
6.011	Acetonitrile	161350
7.244	Acetic acid ethenyl ester	243189
8.792	Acetaldehyde, hydroxy-	162387
10.588	Acetic acid	3018293
12.370	2-Propanone, 1-hydroxy-	1506131
12.587	Toluene	513655
18.018	1-Hydroxy-2-butanone	116890
18.417	Pyrrole	578427
20.974	Propanoic acid, 2-oxo-, methyl ester	294964
21.599	2-Cyclopenten-1-one	139828
21.686	Furfural	217893
24.849	2-Propanone, 1-(acetyloxy)-	227428
27.967	2-Cyclopenten-1-one, 2-hydroxy-	264392
28.756	Diisoamyl ether	357838
31.267	2(5H)-Furanone	114403
33.310	1,2-Cyclopentanedione, 3-methyl-	405099
35.154	Phenol	486186
35.828	Phenol, 2-methoxy-	299241
39.254	p-Cresol	230011
39.652	2-Pyrrolidinone	124335
41.169	Pentanal	274544
47.350	Benzene, 2-methoxy-1,3,5-trimethyl-	607745
49.672	Phenol, 2,6-dimethoxy-	262133
49.961	Indole	287725
52.997	Phenol, 2-methoxy-4-(1-propenyl)-, (Z)-	149442
55.319	1-Pyrrolidinebutyronitrile	113604
62.803	Beta.-D-Glucopyranose, 1,6-anhydro-	142792
64.816	2,4-Imidazolidinedione, 5-(2-methylpropyl)-, (S)-	144434
67.857	4-((1E)-3-Hydroxy-1-propenyl)-2-methoxyphenol	221057
73.101	DL-Proline, 5-oxo-	650386

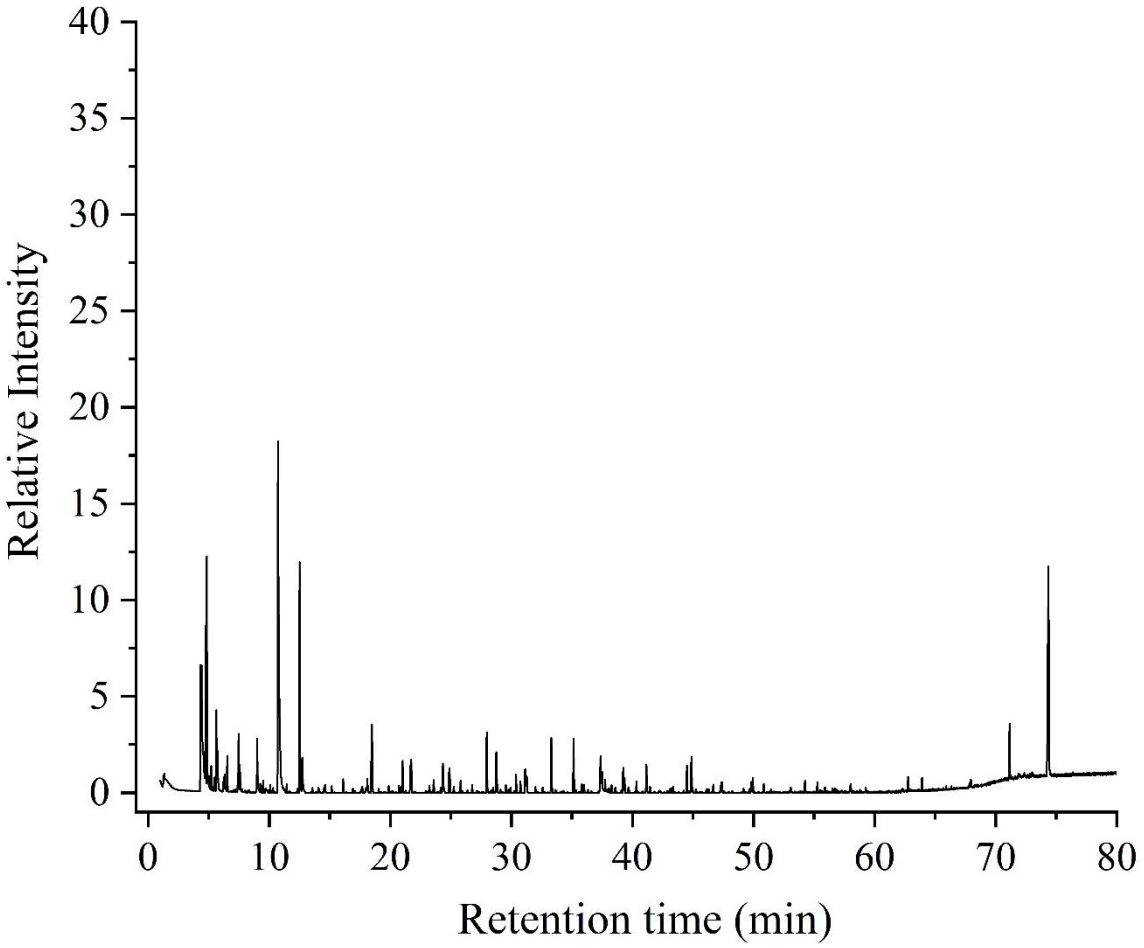


Fig. A2. Chromatogram for the non-catalytic analytical pyrolysis of CBS at 550 °C.

Table A2. Compounds identified in the test non-catalytic analytical pyrolysis of CBS at 550 °C.

Retention time (min)	Compound	Area
4.744	Acetaldehyde	593049
4.847	Methyl Alcohol	1073090
5.213	Furan	111407
5.639	Acetone	395159
5.746	Methyl glyoxal	227308
6.540	Furan, 2-methyl-	154923
7.476	Acetic acid ethenyl ester	256563
7.576	2-Butanone	149355
9.010	Acetaldehyde, hydroxy-	294118
10.727	Acetic acid	3580612
12.521	2-Propanone, 1-hydroxy-	1307535
12.735	Toluene	240850
18.490	Pyrrole	568879
21.029	Propanoic acid, 2-oxo-, methyl ester	173975
21.659	2-Cyclopenten-1-one	154822
21.738	3-Furaldehyde	193719
24.358	2-Furanmethanol	195167
24.883	2-Propanone, 1-(acetyloxy)-	198748
27.976	2-Cyclopenten-1-one, 2-hydroxy-	368972
28.768	Diisoamyl ether	298192
30.394	2-Cyclopenten-1-one, 3-methyl-	103133
31.283	2(5H)-Furanone	109048
33.309	1,2-Cyclopentanedione, 3-methyl-	361754
35.148	Phenol	307999
37.374	Glycerin	289703
37.507	1,2-Ethanediol, 1,2-diphenyl-, [R-(R*,R*)]-	132433
39.248	p-Cresol	134253
41.163	Pentanal	177696
44.513	Isosorbide	160734
44.808	3-Pyridinol	235068
62.782	Beta.-D-Glucopyranose, 1,6-anhydro-	100326
71.157	Caffeine	349340
74.369	Theobromine	2068425

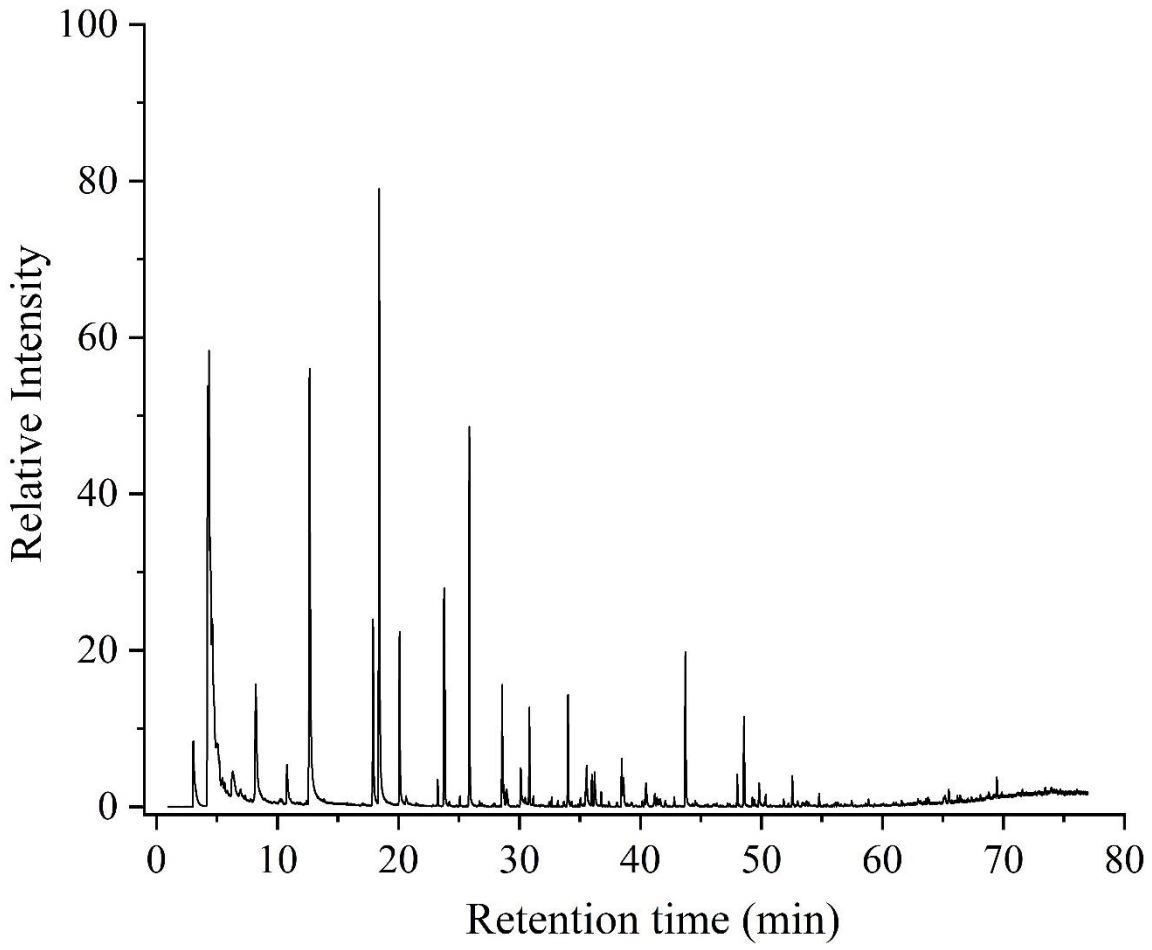


Fig. A3. Chromatogram for the catalytic analytical pyrolysis of SR at 550 °C. Performed using HZSM-5 at a catalyst-to-biomass ratio of 5:1.

Table A3. Compounds identified in the catalytic analytical pyrolysis of SR at 550 °C. Performed using HZSM-5 at a catalyst-to-biomass ratio of 5:1.

Retention time (min)	Compound	Area
4.441	Propene	2295180
4.611	2-Butene	1558312
5.049	Cyclopropane, 1,1-dimethyl-	407801
5.205	Ethanol	253843
6.316	Acetonitrile	193165
8.223	Benzene	982791
10.794	Acetic acid	320331
12.668	Toluene	3771849
17.914	Ethylbenzene	1595116
18.420	p-Xylene	5317621
20.104	o-Xylene	1487526
23.258	Benzene, propyl-	227766
23.784	Benzene, 1-ethyl-3-methyl-	1890042
25.876	Mesitylene	3273481
28.584	Indane	1052663
28.722	Benzene, 1-methyl-3-propyl-	181220
28.898	Benzene, 1-methyl-4-propyl-	118536
28.969	Benzene, 1,4-diethyl-	137825
30.123	1H-Indene, 1-chloro-2,3-dihydro-	318398
30.835	Benzene, 1-methyl-2-(2-propenyl)-	832660
34.026	1H-Indene, 2,3-dihydro-5-methyl-	954613
35.058	Phenol	72444
35.452	2-Methylindene	106643
35.568	Benzene, (1-methyl-2-cyclopropen-1-yl)-	319928
35.996	1H-Indene, 2,3-dihydro-4,7-dimethyl-	268440
36.229	Cycloprop[a]indene, 1,1a,6,6a-tetrahydro-	285205
36.774	2-Ethyl-2,3-dihydro-1H-indene	121083
38.471	Naphthalene	404790
38.624	2-Ethyl-2,3-dihydro-1H-indene	216428
40.467	Naphthalene, 1,2,3,4-tetrahydro-1-methyl-	185683
40.545	1H-Indene, 1,3-dimethyl-	89108
41.222	1H-Indene, 1,3-dimethyl-	96233
43.727	Naphthalene, 2-methyl-	1327848
48.021	Naphthalene, 2-ethyl-	268652
48.577	Naphthalene, 1,6-dimethyl-	767024
49.826	Indole	196664
50.361	Naphthalene, 1,2-dimethyl-	93740
52.567	Naphthalene, 2-(1-methylethyl)-	259295
54.783	Naphthalene, 2,3,6-trimethyl-	106985
65.504	Dibenzo[b,e]7,8-diazabicyclo[2.2.2]octa-2,5-diene	110159
69.472	Anthracene, 9-methyl-	167411

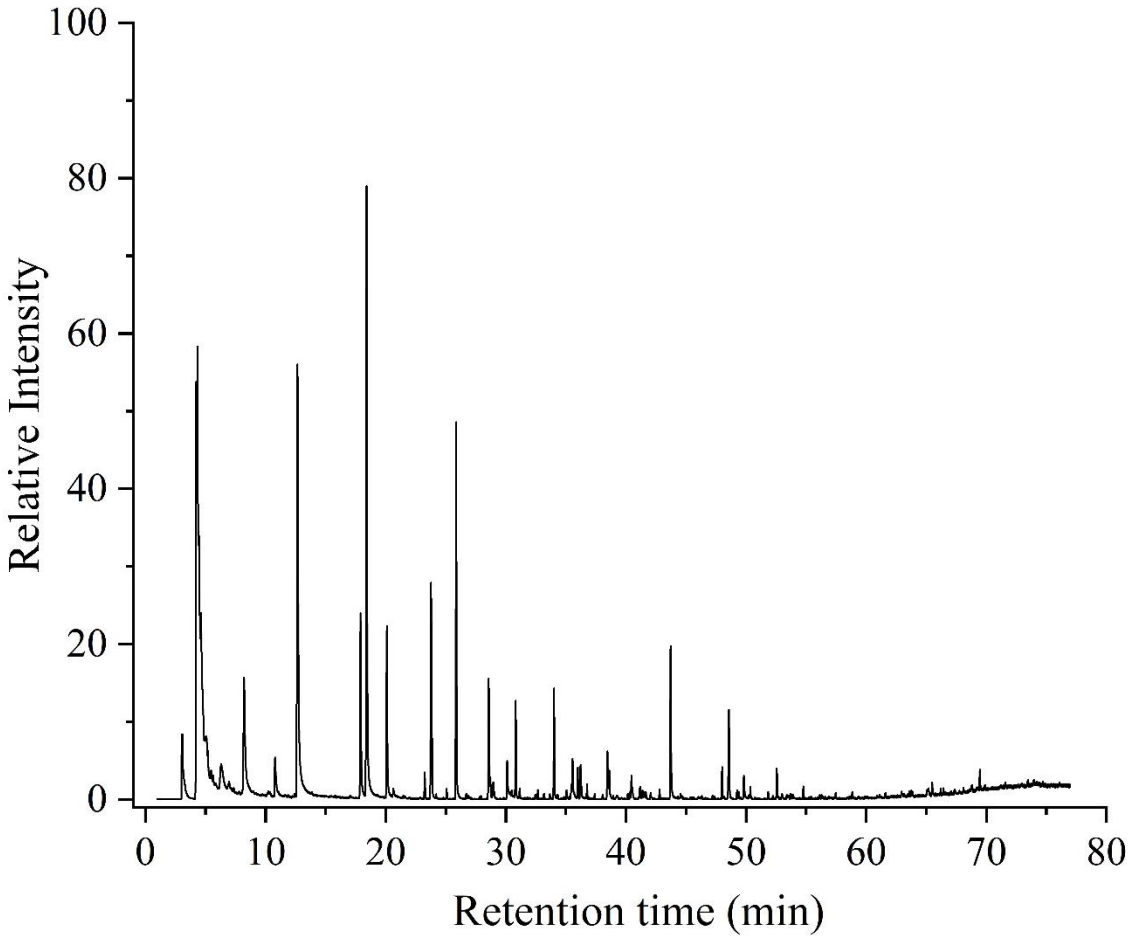


Fig. A4. Chromatogram for the catalytic analytical pyrolysis of CBS at 550 °C. Performed using HZSM-5 at a catalyst-to-biomass ratio of 5:1.

Table A4. Compounds identified in the catalytic analytical pyrolysis of CBS at 550 °C. Performed using HZSM-5 at a catalyst-to-biomass ratio of 5:1.

Retention time (min)	Compound	Area
4.572	2-Butene	8420064
4.728	Methyl Alcohol	5203669
5.008	Oxetane, 3-(1-methylethyl)-	865392
5.082	Cyclopropane, 1,1-dimethyl-	685435
5.173	Ethanol	2025781
5.605	Acetone	847678
8.193	Benzene	5090744
10.724	Acetic acid	3972696
12.654	Toluene	19957490
17.913	Ethylbenzene	4261927
18.417	Benzene, 1,3-dimethyl-	21751598
20.110	o-Xylene	5658236
23.269	Benzene, propyl-	276078
23.788	Benzene, 1-ethyl-3-methyl-	6893422
25.096	Benzene, (1-methylethyl)-	226250
25.886	Benzene, 1,2,3-trimethyl-	9908214
28.598	Indane	3706177
28.742	Benzene, 1-methyl-2-propyl-	262567
30.136	Indene	1054078
30.845	1-Phenyl-1-butene	1898635
32.694	Benzene, 1,2,3,4-tetramethyl-	260515
34.039	1H-Indene, 2,3-dihydro-5-methyl-	3169423
35.480	2-Methylindene	365425
35.587	Benzene, (1-methyl-2-cyclopropen-1-yl)-	1188200
36.015	1H-Indene, 2,3-dihydro-4,7-dimethyl-	878176
36.244	2-Methylindene	1045288
38.489	Naphthalene	1876770
38.640	2-Ethyl-2,3-dihydro-1H-indene	586129
40.489	1H-Indene, 2,3-dihydro-4,7-dimethyl-	494899
40.561	1H-Indene, 1,3-dimethyl-	333130
41.232	1H-Indene, 1,3-dimethyl-	324294
43.744	Naphthalene, 2-methyl-	5464926
44.570	Naphthalene, 2-methyl-	451332
48.036	Naphthalene, 1-ethyl-	766409
48.599	Naphthalene, 1,6-dimethyl-	3110396
49.278	Naphthalene, 2,6-dimethyl-	704379
49.427	Naphthalene, 1,5-dimethyl-	563185
52.589	Naphthalene, 2-(1-methylethyl)-	705070
65.534	9H-Fluorene, 9-methylene-	410421
69.504	Anthracene, 2-methyl-	601364
69.919	Anthracene, 2-methyl-	262188
71.007	Caffeine	273002